



COMPLEX GEOLOGICAL–GEOPHYSICAL 3D MODEL OF THE CRUST IN THE SOUTHEASTERN FENNOSCANDIAN SHIELD: NATURE OF DENSITY LAYERING OF THE CRUST AND THE CRUST–MANTLE BOUNDARY

V. N. Glaznev¹, M. V. Mints², O. M. Muravina¹, A. B. Raevsky³, L. G. Osipenko³

¹ Voronezh State University, Voronezh, Russia

² Geological Institute of RAS, Moscow, Russia

³ Geological Institute, Kola Science Center of RAS, Apatity, Russia

Abstract: The complex geophysical 3D model of the Earth's crust and the upper mantle is created for the Archaean Karelian Craton and the Late Palaeoproterozoic accretionary Svecofennian Orogen of the southeastern Fennoscandian Shield with the use of methods of complex inversion of geophysical data based on stochastic description of interrelations of physical properties of the medium (density, P-wave velocity, and heat generation). To develop the model, we use results of deep seismic studies, gravity and surficial heat flow data on the studied region. Numerical solutions of 3D problems are obtained in the spherical setting with an allowance for the Earth's surface topography. The geophysical model is correlated with the regional geological data on the surface and results of seismic CMP studies along 4B, FIRE-1 and FIRE-3-3A profiles. Based on results of complex geophysical simulation and geological interpretation of the 3D model, the following conclusions are drawn. (1) The nearly horizontal density layering of the continental crust is superimposed on the previously formed geological structure; rock differentiation by density is decreasing with depth; the density layering is controlled by the recent and near-recent state of the crust, but can be disturbed by the latest deformations. (2) Temperature variations at the Moho are partially determined by local variations of heat generation in the mantle, which, in turn, are related to local features of its origin and transformation. (3) The concept of the lower continental crust being a reflectivity zone and the concept of the lower continental crust being a layer of high density and velocity are not equivalent: the lower crust is the deepest, high-density element of near-horizontal layering, whereas the seismic image of the reflectivity zone is primarily related to transformation of the crust as a result of magmatic under- and intraplating under conditions of extension and mantle-plume activity. (4) At certain combinations of crustal thickness and temperature at the level of Moho discontinuity, the crust in a platform region can be transformed into eclogites. In this case, the crust–mantle boundary is determined by quantitative proportions of the rocks that underwent eclogitization or escaped this process and by corresponding density and velocity values. (5) High compaction of rocks in the crust under lithostatic loading cannot be explained by «simple» concepts of metamorphism and/or rock compaction, which are based on laboratory studies of rock samples and mathematical simulations; this is an evidence of the existence of additional, quite strong mechanisms providing for reversible changes of the rocks.

Key words: geophysical simulation, complex inversion, thermal model, density model, CMP seismic profiling, crustal–mantle boundary, velocity–density Moho discontinuity, Karelian Craton, Svecofennian Orogen.

Recommended by E.V. Sklyarov

For citation: Glaznev V.N., Mints M.V., Muravina O.M., Raevsky A.B., Osipenko L.G. 2015. Complex geological–geophysical 3D model of the crust in the southeastern Fennoscandian Shield: Nature of density layering of the crust and the crust–mantle boundary. *Geodynamics & Tectonophysics* 6 (2), 133–170. doi:10.5800/GT-2015-6-2-0176.

КОМПЛЕКСНАЯ 3-МЕРНАЯ ГЕОЛОГО-ГЕОФИЗИЧЕСКАЯ МОДЕЛЬ КОРЫ НА ЮГО-ВОСТОКЕ ФЕННОСКАНДИНАВСКОГО ЩИТА: ПРИРОДА ПЛОТНОСТНОЙ РАССЛОЕННОСТИ КОРЫ И КОРОМАНТИЙНОЙ ГРАНИЦЫ

В. Н. Глазнев¹, М. В. Минц², О. М. Муравина¹, А. Б. Раевский³, Л. Г. Осипенко³

¹ Воронежский государственный университет, Воронеж, Россия

² Геологический институт РАН, Москва, Россия

³ Геологический институт КНЦ РАН, Анатиты, Россия

Аннотация: Трехмерная комплексная геофизическая модель земной коры и верхней части мантии архейско-Карельского кратона и позднепалеопротерозойского Свекофеннского аккреционного орогена на юго-востоке Фенноскандинавского щита получена с использованием методов комплексной инверсии геофизических данных, основанных на стохастическом описании взаимосвязей физических свойств среды: плотности, скорости продольных волн и теплогенерации пород. Для построения модели использованы результаты глубоких сейсмических исследований, данные о гравитационном поле и поверхностном тепловом потоке изучаемого региона. Численные схемы решения трехмерных задач реализованы в сферической постановке с учетом реального рельефа Земли. Методика достаточно универсальна и перспективна при исследовании строения коры и литосферы крупных регионов. Геофизическая модель сопоставлена с региональными поверхностными геологическими данными и результатами сейсмических исследований МОГТ по профилям 4В, FIRE-1 и FIRE-3-ЗА. По результатам комплексного геофизического моделирования и геологической интерпретации особенностей полученной объемной модели показано: (1) субгоризонтальная плотностная расслоенность континентальной коры накладывается на ранее сформированную геологическую структуру, плотностная дифференциация пород с глубиной уменьшается; особенности плотностной расслоенности в преобладающей степени определяются современным и относительно недавним состоянием коры, но могут быть нарушены в результате наиболее поздних деформаций; (2) температурные вариации на разделе Мохо частично определяются «локальными» изменениями теплогенерации мантии, которые обусловлены особенностями ее формирования и преобразования; (3) представления о нижней коре континентов как о «зоне рефлексивити» и как о слое значительно повышенной плотности и скорости не являются эквивалентными: нижняя кора – это наиболее глубокий и наиболее высокоплотный элемент субгоризонтальной плотностной расслоенности, в свою очередь, сейсмический образ «зоны рефлексивити» преимущественно связан с процессами преобразования коры в результате магматического андерплейтинга и интерплейтинга в обстановках рифтогенного растяжения и мантийно-плюмовой активности; (4) при определенных сочетаниях мощности коры и температурного режима на уровне раздела Мохо породы коры платформенных областей могут быть преобразованы в эклогиты – в этом случае граница коры и мантии определяется количественными соотношениями пород, подвергшихся и не подвергшихся эклогитизации, и соответствующими значениями плотностных и скоростных характеристик; (5) высокий уровень уплотнения пород в коре под воздействием литостатической нагрузки невозможно объяснить на уровне «простых» представлений о метаморфизме и/или об уплотнении и компактизации пород, базирующихся на лабораторных исследованиях образцов и расчетных моделях, что свидетельствует о существовании дополнительных и весьма мощных механизмов, которые обеспечивают обратимые изменения горных пород.

Ключевые слова: геофизическое моделирование, комплексная инверсия, термическая модель, плотностная модель, сейсмопрофилирование МОГТ, граница кора-мантия, сейсмopлотностной раздел Мохо, Карельский кратон, Свекофеннский ороген.

CONTENTS

| | |
|--|-----|
| 1. Introduction | 135 |
| 2. Principles and methods of complex interpretation | 136 |
| 3. Geological overview | 140 |
| 4. Complex geophysical model | 142 |
| 4.1. Thermal model of the Earth's crust and upper mantle | 143 |
| 4.2. Density model of the Earth's crust and upper mantle | 145 |
| 5. Deep structure: Geological model based on interpretation of seismic crustal images in sections along CMP seismic profiles | 149 |
| 5.1. Archaean tectonic units | 150 |
| 5.2. Palaeoproterozoic tectonic units | 150 |

| | |
|--|-----|
| 6. Comparison of the density and geological models of the crust | 154 |
| 6.1. Density layering and structural geological characterization of the crust | 154 |
| 6.2. Velocity–density Moho discontinuity and crust–mantle boundary | 155 |
| 7. Thermodynamic conditions and metamorphism in the zone of crustal–mantle boundary | 155 |
| 8. Discussion | 158 |
| 8.1. Density heterogeneity and nature of density layering of the crust | 158 |
| 8.2. Nature of the lower crust, the crust–mantle boundary and the velocity–density Moho discontinuity beneath the Karelian Craton | 159 |
| 8.3. Nature of the lower crust, the crustal–mantle boundary, and the velocity–density Moho discontinuity beneath the accretionary Svecofennian Orogen | 161 |
| 9. Conclusions | 163 |
| 10. Acknowledgments | 164 |
| 11. References | 165 |

1. INTRODUCTION

In studies of deep structure of the crust and upper mantle, the most appropriate approach is using a complex of geophysical methods [Glaznev, 2003]. Meanwhile, some properties of the geological medium, which are determined by different geophysical methods cannot be successfully combined under the common framework of complex models. It is thus required to examine two or more independent models. In particular, it is well known that images of the crust–mantle boundary and structural–compositional layering established by refraction seismic methods (including the models, where velocity characteristics of the medium are interpreted in combination with gravity data) differ in principle from those based on reflection seismic methods.

Although the Moho discontinuity has been known for more than a century, determining the origin and formation conditions of the Moho, as well as crust–mantle boundary remains one of the main problems in studying the lithosphere [Carbonell et al., 2013; Prodehl et al., 2013]. Historically, many authors consider terms *crust–mantle boundary* and *Moho discontinuity* as synonyms. With enhancement of our knowledge on the transitional zone and the crust–mantle boundary proper, it has become evident that these notions do not coincide completely. The Moho is a geophysical image of the smoothly curving surface of the planetary rank, at intersection of which P-wave velocity increases more or less abruptly from 6.9–7.4 to 8.0–8.2 km/s. This surface is approximately following the lower boundary of the Earth's crust. The crust–mantle boundary is a complex geological phenomenon characterized by a combination of data on composition, metamorphic grade, and mechanical properties of the crust, mantle and transitional zone, as well as on structural features of the crust–mantle boundary. Further in the text, we use term *Moho boundary or discontinuity* for notation of the velocity boundary in the transitional crust–mantle zone. In

discussion of structural and compositional features of the boundary and/or the transitional zone between the crust and the mantle, we use geological terms *crust–mantle boundary / interface*. In general, the Moho discontinuity and the crust–mantle boundary may be not coincident [O'Reilly, Griffin, 2013].

The geological structure of the crust–mantle boundary can be characterized, in particular, by patterns of seismic reflections (seismic images). The Moho discontinuity may be situated both above and below this boundary. In some cases, the crust–mantle boundary remains unchanged from the time of crust formation, whereas in other cases, it is younger than the major part of the overlying crust [Braile, Chiangl, 1986; Mereu et al., 1989; Mooney, Meissner, 1992; Berzin et al., 2002; Cook et al., 2010; Mints, 2011].

Reflection seismic methods yield widely variable seismic images of the crust–mantle boundary at the base of Precambrian crust, and specific features of such images suggest a dependence on structure and formation history of the crust [BABEL Working Group, 1990; Abramovitz et al., 1997; White et al., 2000; Van der Velden, Cook, 2005; Kukkonen, Lahtinen, 2006; Mints et al., 2009, 2015; Cook et al., 2010; Hammer et al., 2010; Mints, 2011]. It is assumed that beneath the Precambrian cratons, as a rule, this boundary is rather distinctly expressed in the replacement of the moderately or intensely reflecting lower crust by the mantle domain that is acoustically transparent. To determine a true vertical depth of the crust–mantle boundary, the crustal velocity structure should be known. If the CMP profiles are not accompanied by refraction seismic studies, uncertainty in determination of depth can reach 5–6 % [Holbrook et al., 1992].

The studies of P-wave velocities with application of refraction seismic methods have shown that the Earth's crust is subdivided in several «layers» that differ in velocities of acoustic signal propagation and are separated by distinct and, in other cases, vague boundaries or diffuse gradient zones. Statistically persistent corre-

lations between density and velocity parameters of rocks make it possible to jointly discuss velocity layering and density layering of the crust [Christensen, Mooney, 1995]. As a rule, velocity (V_p) and density (ρ) progressively increase with depth.

Velocity and density layering of the crust in the central Fennoscandian Shield was described in [Korsman et al., 1999; Kozlovskaya et al., 2004; Kuusisto et al., 2006; Silvennoinen et al., 2014]. In particular, these authors established gradual variations of velocity and density within the crustal «layers», which number may amount to six according to [Kuusisto et al., 2006].

In this paper, we focus on the key region located at the junction of two tectonic units differing in structure and age, the Archaean Karelian Craton and the Late Palaeoproterozoic accretionary Svecofennian Orogen. Our study is aimed at establishing structural and compositional layering of the crust, nature of crust–mantle boundary, and the present-day thermodynamic state of the boundary zone between the crust and the upper mantle.

A fragment of the 3D complex geophysical model of the Fennoscandian crust and upper mantle is used as the major tool. It characterizes relationships between P-wave velocity, density, heat generation, and thermal conductivity of rocks, which determine gravity field, surficial heat flow, and internal fields of temperature and lithostatic pressure [Glaznev et al., 1996; Glaznev,

2003]. Seismic images of the crust along detailed 4B, FIRE-1, FIRE-3-3A CMP profiles and corresponding geological interpretation sections [Kukkonen, Lahtinen, 2006; Mints et al., 2009, 2015; Mints, 2011] are used as the second independent model.

The efficient modern methods for 3D geophysical (petrophysical) modeling of the Earth's crust are based on the criteria–target–oriented approach [Strakhov, Romanyuk, 1984; Golizdra, 1988], which assumes a combination of the solutions obtained using a complex of geophysical methods within a certain coherent presentation of interpretational petrophysical parameters characterizing the geological medium [Glaznev, 1987, 2003; Glaznev et al., 1989, 1996, 2008; Buyanov et al., 1995; Romanyuk, 1995; Romanyuk et al., 2001; Tiberi et al., 2003; Kozlovskaya et al., 2004; Artemieva et al., 2006; Kobrunov, 2008; Tikhotsky, Achauer, 2008]. Nevertheless, issues of adequacy of the mathematical tool used for compilation of coordinated complex geophysical models of the medium in various situations has not been scrutinized yet to a sufficiently detailed level. This especially concerns identification of non-horizontal layering of the Earth's crust, which is only partly reflected in the available models. It is also evident that the criteria–target–oriented approach leads to a certain generalization of the studied medium structure that depends on discreteness of the network representation of relevant physical properties.

2. PRINCIPLES AND METHODS OF COMPLEX INTERPRETATION

The technique of complex geophysical simulation of the crust was considered in detail in [Glaznev et al., 1996; Glaznev, 2003]. This paper is confined only to the description of the main principles and justification of this technique.

Let us consider statement of certain principal elements of the technique aimed at complex geophysical inversion of gravimetric and geothermal data on the basis of seismic data on structure of the crust and stochastic descriptions of interrelations between physical properties of rocks in the studied medium. The proposed algorithms to solve 3D complex inverse problem are considered in a spherical setting, taking into account a real surface of the Earth, because of significant dimensions (i.e. area and depth) of the simulated region. As a result of complex inverse problem solution, 3D thermal and density models are proposed for the crust and the upper mantle of the Karelian Craton and the adjacent territories of Fennoscandia. These models reflect the main features of the deep structure of the studied region.

The crustal rocks are characterized by velocity of P-waves V , density ρ , heat generation q , and heat conductivity λ , which generate the external observable gravity field $\Delta g(x)$ and the field of surficial heat flow $Q(x)$ as well as the internal fields of temperature $T(\xi)$ and lithostatic pressure $P(\xi)$ in the medium. It is assumed that the sought physical properties of the medium (V, ρ, q) are characterized by stochastic interrelations, which can be described by certain sets of statistic parameters.

Taking into account the availability of a priory velocity model, the problem of complex interpretation is defined as a calculation of 3D thermal and density models on the basis of inverse problem solutions of geothermal and gravimetric data. Following the principle described in [Strakhov, Romanyuk, 1984; Glaznev, 1987] for selection of solutions that can ensure (within the given confidence interval) the correspondence of solutions to the accepted law of relationships between parameters, the procedure of complex interpretation is stated as follows:

$$\|A_{\Delta g}\{p(\xi), p_N(\xi)\} - \Delta g(x)\| = \delta_{\Delta g}, \quad (1)$$

$$\|A_Q\{q(\xi), \lambda(\xi)\} - Q(x)\| = \delta_Q, \tag{2}$$

where $A_{\Delta g}\{\}$ and $A_Q\{\}$ are operators of the corresponding direct problems; $\rho(\xi)$ and $q(\xi)$ are the sought density and heat generation values; $\rho_N(\xi)$ is the one-dimensional normal density in medium; $\lambda(\xi)$, thermal conductivity of medium; $\Delta g(x)$ and $Q(x)$ are observed gravity field and field of surficial heat flow; ξ and x are integrated coordinates of field sources and observation points; $\delta_{\Delta g}$ and δ_Q are discrepancies of fields. Solution quality functionals based on stochastic descriptions of the relationship between density, heat generation, and velocity in medium [Glaznev, 2003] are defined as follows:

$$\int_v W_\rho(\xi) \cdot (\rho(\xi) - \rho_{ini}(\xi))^2 dv = \min, \tag{3}$$

$$\int_v W_q(\xi) \cdot (q(\xi) - q_{ini}(\xi))^2 dv = \min, \tag{4}$$

where $W_\rho(\xi)$ and $W_q(\xi)$ are weight functions for density and heat generation models of medium expressed via entropic characteristics of density–velocity and heat generation–density distributions; $\rho_{ini}(\xi)$ and $q_{ini}(\xi)$ are initial approximations of density and heat generation models based on initial velocity model of the medium. According to [Strakhov, 1990], smallness of solution fluctuation versus initial approximation, as well as limitation of $W_\rho(\xi)$ and $W_q(\xi)$ weight function are assumed.

Initial approximations $\rho_{ini}(\xi)$ and $q_{ini}(\xi)$ for models of the medium can be expressed through velocity $V(\xi)$ based on approximation density–velocity $\rho=f_\rho(V)$ and heat generation–density $q=f_q(\rho)$ relationships. The dependence of these physical properties on thermodynamic conditions in the medium should be taken into account:

$$\rho_{ini}(\xi) = f_\rho \left(V(\xi) - \int (dV/dP)_T dP - \int (dV/dT)_P dT \right) + \int (d\rho/dP)_T dP + \int (d\rho/dT)_P dT, \tag{5}$$

$$q_{ini}(\xi) = f_q \left(\rho(\xi) - \int (d\rho/dP)_T dP - \int (d\rho/dT)_P dT \right), \tag{6}$$

where $(dV/dP)_T$ and $(dV/dT)_P$ are isothermal and isobaric corrections to velocity; $(d\rho/dP)_T$ and $(d\rho/dT)_P$ are similar corrections to density established from results of integration of experimental data on rock samples from the lithosphere [Glaznev et al., 1996; Glaznev, 2003].

The critical aspect in the problem of complex inversion is the use of limitations on values of sought solutions:

$$\rho_{j \min} \leq \rho(\xi_j) \leq \rho_{j \max}, \tag{7}$$

$$q_{j \min} \leq q(\xi_j) \leq q_{j \max}, \tag{8}$$

where $j \in [1, M]$ are corresponding minimum and maximum values set for certain finite subregions of medium j . Such limitations need to be taken due to geological reasoning and on the basis of a priori classification requirements [Buyanov et al., 1989]. In addition, solution of inverse problems takes into account the data obtained from petrophysical (density) regional mapping [Galitchanina et al., 1995] and estimations of heat generation of the rocks occurring at the surface, which are a priori boundary values for density $\rho_S(\xi)$ and heat generation $q_S(\xi)$ of the rocks occurring at the surface $h(x)$ of the studied medium:

$$\rho(\xi)|_{\xi=h(x)} = \rho_S(h), \tag{9}$$

$$q(\xi)|_{\xi=h(x)} = q_S(h). \tag{10}$$

The computation algorithm of complex interpretation in the setting (Eqs. 1–10) is determined by the initial velocity model of the medium, which is considered to be the constant basis. This model corresponds to a certain initial distribution of density $\rho^{(0)}(\xi)$ and heat generation $q^{(0)}(\xi)$ in the studied medium. At the first step of complex interpretation, the 3D thermal model $T^{(1)}(\xi)$ is computed and heat generation $q^{(1)}(\xi)$ is specified from

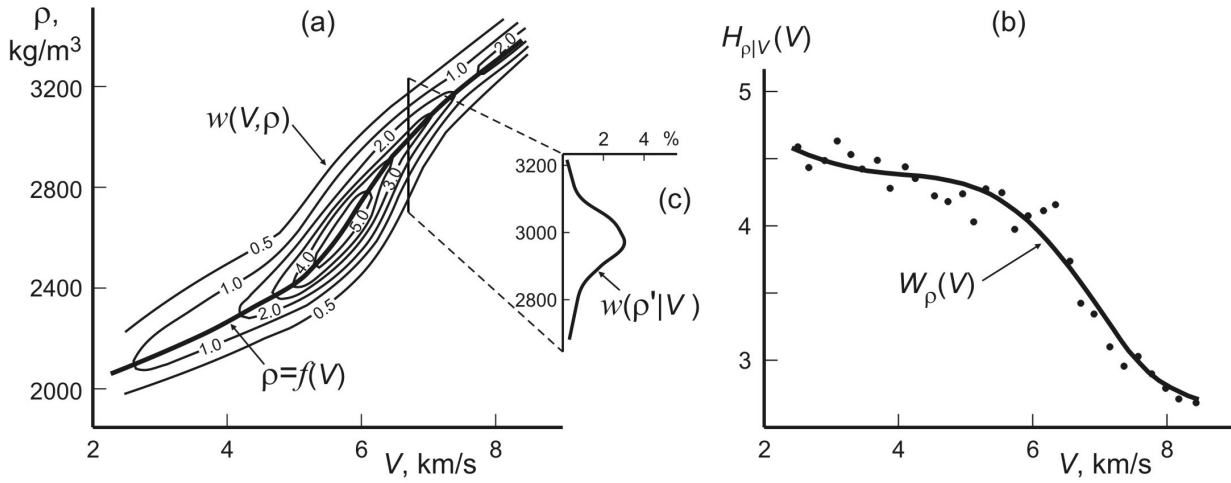


Fig. 1. (a) Stochastic interrelations between P-wave velocity (V) and density (ρ) of crustal rocks in form of 2D probability distribution (contour lines, %) and approximation graph $\rho=f(V)$ (Eq. 11). (b) Conditional probability density $w(\rho|V)$ in a section of 2D process $w=w(V,\rho)$. (c) Calculated entropy $H_{\rho|V}(V)$ and approximation of weight function $W_{\rho}(V)$ (Eq. 13).

Рис. 1. (a) Стохастическая взаимосвязь между скоростью и плотностью пород земной коры в виде двумерного распределения вероятности (изолинии в процентах) и график аппроксимации $\rho=f(V)$ в форме (11). (b) Условная плотность вероятности $w(\rho|V)$ по некоторому сечению двумерного процесса $w=w(V,\rho)$. (c) Вычисленные значения энтропии $H_{\rho|V}(V)$ и аппроксимация весовой функции $W_{\rho}(V)$ в форме (13).

the solution of the inverse geothermal problem (Eqs. 2, 4, 6, 8, 10). At the second step, medium density $\rho^{(1)}(\xi)$ is computed and lithostatic pressure $P^{(1)}(\xi)$ is specified from the solution of the inverse gravimetric problem (Eqs. 1, 3, 5, 7, 9). The obtained coordinated model of temperature, heat generation, and density is further specified at the next steps of iteration cycle to ensure more accurate correspondence of models to one another on the basis of a priori accepted stochastic interrelations of the physical properties.

The important aspect of this simulation is establishing interrelations between P-wave velocity, density, and heat generation. The stochastic interrelations between velocity and density under normal thermodynamic conditions have been revealed for typical lithospheric rocks [Glaznev et al., 1996; Glaznev, 2003]. As a function of mutual density–velocity transition, the following approximation is proposed:

$$\rho = f(V) = a + b \cdot \ln(|V + c|), \quad (11)$$

where a , b , and c coefficients determined for two velocity ranges: (1) $a=2933$, $b=-518$, and $c=-7.985$ at $V \leq 5.5$ km/s; (2) $a=1656$, $b=1068$, and $c=-3.181$ at $V > 5.5$ km/s. Dimensions of velocity and density in Eq. 11 are given in km/s and kg/m³, respectively. Graphs of $\rho = f(V)$ in corresponding velocity ranges are shown in Fig. 1, a. It is noteworthy that Eq. 11 coincides with known density–velocity relationships [Birch, 1961; Ludwig et al., 1970; Barton, 1986; Sobolev, Babeyko, 1994] for sedimentary and crystalline rocks and was efficiently used for development of geophysical models of the Earth's crust in various regions [Vernant et al., 2002; Miksat et al., 2010].

The stochastic character of transition from P-wave velocity to density can be expressed via entropy of conditional density probability of 2D accidental process $w(\rho|V)$ shown in Fig. 1, b. From definition of conditional entropy

$$H_{\rho|V}(V) = - \int_{-\infty}^{+\infty} w(\rho'|V) \cdot \log_2 w(\rho'|V) \cdot d\rho', \quad (12)$$

one can calculate a weight function that characterizes ambiguity of relationship between velocity and density. Approximation of calculated entropy values shown in Fig. 1, c is given by equation

$$W_{\rho}(V) = H_{\rho|V}(V) = \sum_{n=0}^4 d_n \cdot (V)^n, \quad (13)$$

where constants $d_0=10.365$, $d_1=-5.195$, $d_2=1.637$, $d_3=-0.2173$, and $d_4=-0.0099$; velocity dimension is km/s. A graph of approximation $W_p(V)$ is shown in Fig. 1, c. The equations shown in Figs. 11 and 13 describe empirical statistical density vs. velocity under normal thermodynamic conditions and also characterize a measure of its uncertainty.

The relationships between density and heat generation for typical rocks in the lithosphere were introduced in the same way [Glaznev, 2003] and used for development of the thermal model of the region under consideration. In addition, an integrated relationship of thermal conductivity versus temperature figuring in Eq. 2 was introduced into the thermal model in form

$$\lambda(T) = \lambda_0(1 + c \cdot T)^{-1}, \quad (14)$$

where constant λ_0 and c for crystalline crustal rocks were chosen for two temperature intervals. In the range up to 900 K, $\lambda_0=3.5$ W/m·K and $c=1.2 \cdot 10^3$ K⁻¹. In the range from 900 to 1200 K, $\lambda_0=0.8$ W/m·K and $c=-5.8 \cdot 10^{-4}$ K⁻¹. The relationship of thermal conductivity versus pressure was taken in linear approximation after [Seipold, 1998].

The methods of direct gravimetry problem solution are of substantial importance for procedure of complex simulation. In our case, they are realized in the 3D spherical setting [Glaznev, Raevsky, 1991] based on precise expressions for gravity field from a spherical disc in its polar point. The calculation of anomalous fields is based on the radial-ring overlay grid for a set of thin spherical rectangular sheets. For Δg field of thin spherical rectangle with constant $\Delta \rho$ density, we have

$$\Delta g(r, 0, 0) = \gamma \Psi_m \Delta \rho \frac{R^2}{r^2} \left(\frac{R - r \cos \theta_{m+1}}{r_{m+1}} + \frac{R - r \cos \theta_m}{r_m} \right) dR, \quad (15)$$

where

$$\begin{aligned} r_m^2 &= R^2 + r^2 - 2Rr \cos \theta_m, & r_{m+1}^2 &= R^2 + r^2 - 2Rr \cos \theta_{m+1}, \\ r &= R_0 + h, & R &= R_0 - z, \end{aligned}$$

in which R_0 is the Earth's radius and h is the height of field calculation point. For the rectangle: $\Psi_m = (\varphi_{n+1} = \varphi_n)$ in longitude and $(\theta_{m+1} - \theta_m)$ in latitude, optimal angular sizes are determined from conditions of field calculation accuracy and the requirement of approximate isometry of the spherical element of the network. The total gravitational effect from approximation of the medium by such elements is given as follows:

$$\Delta g(h, \phi, \theta) = \left(\sum_{k=0}^K \sum_{m=0}^M \sum_{n=0}^{N_m} C_{kmn} \cdot \Delta \rho(k, m, n) + \sum_{k=0}^K C'_k \cdot \Delta \bar{\rho}_M(k) \right) dR, \quad (16)$$

where variable indices k , m , and n operate in local polar coordinates, and C_{kmn} coefficients are calculated for a single element from the formula given above (C'_k are coefficients taking into account the effect of the far spherical zone).

The 3D inversion of gravimetric data is stated as a problem of finding such a distribution of density $\Delta \rho(r, \varphi, \theta)$, which satisfies a minimum of discrepancy (Eq. 1) for Δg field and minimizes solution quality functional (Eq. 3). The inverse problem in that setting was considered in various aspects by many authors [Kobrunov, 1982, 2008; Dolgal, 2002; Pedersen, 1991; Tarantola, Valette, 1982]. However, in our case, the weight functions $W(r, \varphi, \theta)$ for the density model of the medium are determined through entropic characteristics of velocity–density interrelations (Eq. 13).

For practical realization of the iteration algorithm of inversion, two stages are distinguished in the solution of inverse problem: calculation of the simple layer density, and its equivalent redistribution over the mass-carrier region. Calculation of the equivalent layer density can be regarded as a certain approximate solution of the inverse problem for the given set of discrete elements of the medium approximation [Aleksidze, 1987]. In the spherical setting, coefficients of the approximate inverse operator of determining the equivalent density of the simple spherical layer were obtained [Glaznev, 2003]. These coefficients are used in specific computational schemes.

The equivalent rearrangement from a thin layer (thickness Δh) into the model layer (thickness $N\Delta h$) is performed following the iteration scheme, and the following equation is obtained for density in layer n :

$$\Delta \rho^{(i+1)}(n, \varphi, \theta) = \Delta \rho^{(i)}(n, \varphi, \theta) + W_p(n) \cdot \left(\Delta \rho_e^{(i)}(\varphi, \theta) D(n, \varphi', \theta') \right), \quad (17)$$

where $\Delta\rho_e(\varphi, \theta)$ is the equivalent density for approximation $\Delta\rho(\varphi, \theta) - \Delta\rho^{(i)}(\varphi, \theta)$, and redistribution operator $D(n, \varphi, \theta)$ in spectral form assumes explicit presentation in form of binomial series of analytical continuations for the potential field. For the central point of the local polar spherical system of coordinates, with a limited number of members in this series, the second item in the right part of Eq. 17 is given as follows:

$$\Delta\rho(n, 0, 0) = \frac{1}{2} \sum_{m=0}^M C(n, m)_D \cdot (\Delta\bar{\rho}_e(R, \theta'_m) + \Delta\bar{\rho}_e(R, \theta'_{m+1})), \quad (18)$$

where equivalent density values are taken as average values at the circumferences. The cubature coefficients are

$$C_{(n,m)_D} = \sum_{p=0}^3 (-1)^p R \int_{\theta'_m}^{\theta'_{m+1}} \frac{(R^2 - r^2(n, p)) \cdot \sin(p + 1 - n) \cdot \sin \theta'}{(R^2 + r^2(n, p) \cdot 2Rr(n, p) \cdot \cos \theta')^{3/2}} d\theta', \quad (19)$$

where $r(n, p) = R - (p + 1 - n)\Delta h$. The choice of a small number of members in series (Eqs. 18, 19) actually realizes the method of local redistribution of corrections [Martushko, Prutkin, 2003] in the problem of model layer density calculation.

The above-described technology of complex geophysical simulation was efficiently used for creation of the Earth's crust models under various conditions [Buyanov et al., 1989, 1995; Glaznev et al., 1996, 2008]. The same technology of inversion of 3D gravimetric and geothermal data in the spherical setting is applied for complex geophysical simulation of the Earth's crust in the Karelian Craton.

3. GEOLOGICAL OVERVIEW

The studied area is situated in the southeastern Fennoscandian Shield in the territories of Russia and Finland (Fig. 2, a, b). The Karelian Craton and the Belomorian Province, that extends along the craton's eastern boundary, embrace the major in size and geological significance domains of the continental crust in the Fennoscandian Shield [Mints et al., 2015]. The crust was largely formed by the onset of the Neoproterozoic and then underwent tectonic and metamorphic reworking during the Neoproterozoic and Palaeoproterozoic. The volcanic–sedimentary and volcanic–plutonic associations of the Late Palaeoproterozoic Svecofennian Accretionary Orogen are bordering on the Karelian Craton in the southeast. The Archaean crustal granite–greenstone domains (GGD) making up the Late Palaeoproterozoic Karelian Craton are regarded as fragments of ancient microcontinents somewhat different in age. The Ranua, Iisalmi and Vodlozero GGDs are composed of the oldest granitoids dated at 3.14–2.82 Ga. The age of their protoliths reaches 3.5–3.7 Ga. The Kianta and Kuhmo–Segozero complexes mainly consist of tonalite–trondhjemite gneisses dated at 2.89–2.72 Ga.

The Archaean greenstone belts are subdivided into two groups. Mafic and ultramafic volcanic rocks play a significant role or are predominant in the first group. The extended linear belts of this group are considered as palaeosutures corresponding to collision events between the Segozero–Vedlozero, Central Belomorian,

and Tipasjärvi–Kuhmo–Suomussalmi microcontinents (Fig. 2, b).

The Segozero–Vedlozero and Central Belomorian sutures arose 3.05–2.82 Ga ago. Rocks of the Tipasjärvi–Kuhmo–Suomussalmi suture are dated at 2.81–2.74 Ga. According to geological data and interpretation of seismic crustal images along CMP profiles 1-EU, 4B, FIRE-1 and FIRE-3-3A, all the three sutures plunge in the eastern and northeastern directions and are traced down to the crust–mantle boundary [Mints et al., 2009, 2015]. The younger belts of the second group, which are primarily composed of epicontinental metasedimentary and metavolcanic rocks, are dated at 2.75–2.73 Ga. These rocks are close in density to TTG and GG gneisses, do not reveal density anomalies, and thus are not shown in Fig. 2, b.

The Karelian Craton and Belomorian Province completed to evolve in the Neoproterozoic (2.75–2.73 Ga ago). Later on, the crust was built up and reworked primarily in the intracontinental setting. The Varpasjärvi and Chupa synforms composed of granulite–gneiss complexes appeared in the framework of the Karelian Craton 2.74–2.70 Ga ago as a result of mantle–plume activity. The granite–greenstone crust in the basement of these synforms was also affected by high-temperature granulite-facies metamorphism.

In the Early Palaeoproterozoic (~2.5–2.3 Ga ago), significant bodies of mafic igneous rocks, mainly of gabbroanorthosite composition, were accommodated at the base of the Archaean crust, which thickness

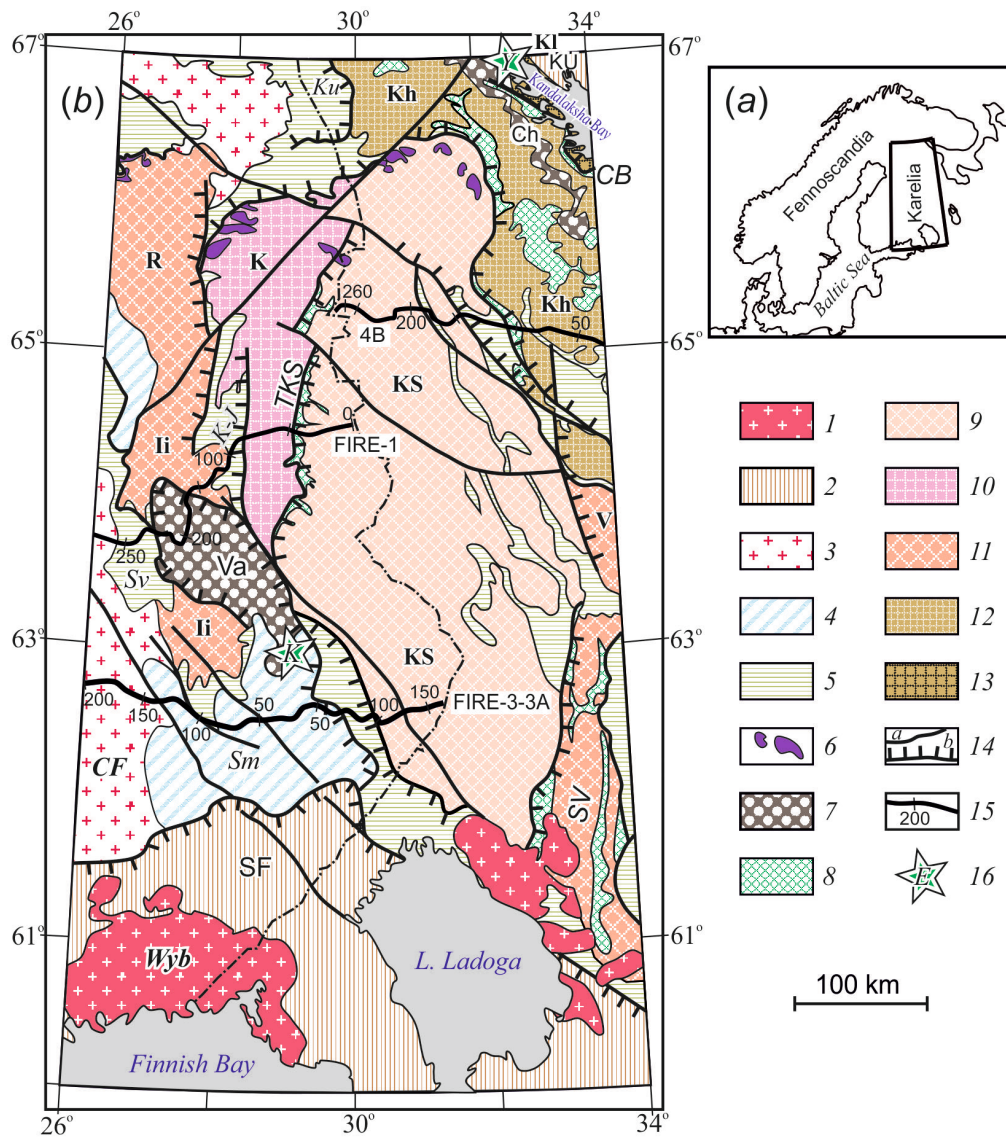


Fig. 2. (a) The geographical position of the area of effective integrated geophysical modeling. (b) Main tectonic units in the southeastern Fennoscandian Shield, simplified after [Mints et al., 2015].

1 – Mesoproterozoic rapakivi granites (Wyb, Wyborg pluton); 2–6 – Palaeoproterozoic: 2 – granulite-gneiss belts (SF – South Finland and KU – Kolvitsa–Umba); 3–4 – Svecofennian Orogen: 3 – granitoids (CF, Central Finland pluton), 4 – accretionary complex (Sv – Savo and Sm – Saimaa belts); 5 – volcanic-sedimentary belts (K–J – Kainuu volcanic-sedimentary belt containing Jormua ophiolite complex; Ku – Kuolajärvi structure); 6 – North Karelian belt, layered mafic-ultramafic intrusions; 7–12 – Archaean: 7 – granulite-gneiss belts (Va, Varpaisjärvi and Ch, Chupa), 8 – greenstone belts, inferred sutures (TKS, Tipasjärvi–Kuhmo–Suomussalmi, SV, Segozero–Vedlozero, and CB, Central Belomorian), 9–11 – Karelian Craton, granite-greenstone domains: 9 – Kuhmo–Segozero (KS), 10 – Kianta (Ki), 11 – Ranua (R), Iisalmi (Ii) and Vodlozero (V), 12 – Belomorian Province, Khetolambina granite-greenstone domain (Kh); 13 – Kola Craton (Kl); 14 – tectonic boundary: (a) normal–strike-slip fault, (b) thrust fault (ticks indicate direction of fault-plane plunging); 15 – 4B, FIRE-1 and FIRE-3-3A CMP seismic profiles; 16 – kimberlite pipes containing deep xenoliths (Y, Yelovy Island and K, Kaavi–Kuopio).

Рис. 2. (a) Географическое положение результирующей области комплексного геофизического моделирования. (b) Главные тектонические структуры на юго-востоке Фенноскандинавского щита (упрощенно по [Mints et al., 2015]).

1 – мезопротерозой, граниты рапакиви (Wyb – Выборгский массив); 2–6 – палеопротерозой: 2 – гранулитогнейсовые пояса (SF – Южно-Финляндский, KU – Колвица-Умбинский); 3–4 – Свекоефенский аккреционный ороген: 3 – гранитоиды (CF – Центрально-Финляндский плутон), 4 – аккреционный комплекс (пояса: Sv – Саво, Sm – Сaimaa); 5 – осадочно-вулканогенные пояса (K–J – пояс Кайнуу, вмещающий офиолитовый комплекс Йормуа; Ku – Куолаярвинская структура); 6 – раннепалеопротерозойский Северо-Карельский пояс, расслоенные массивы мафит-ультрамафитов; 7–12 – архей: 7 – гранулитогнейсовые пояса (Va – Варпайсъярви, Ch – Чупинский), 8 – зеленокаменные пояса – предполагаемые палеосутуры (TKS – Типасъярви-Кухмо-Суомуссалми, SV – Сегозеро-Ведлозеро, CB – Центрально-Беломорский), 9–11 – Карельский кратон, террейны (гранит-зеленокаменные области): 9 – Кухмо-Сегозерский (KS), 10 – Кьянта (Ki), 11 – Рануа-Иисалми (R), Водлозерский (V), 12 – Беломорская провинция, Хетоламбинская гранит-зеленокаменная область (Kh); 13 – Кольский кратон (Kl); 14 – тектонические границы (а – сбросо-сдвиги, б – надвиги, штрихи указывают направление погружения сместителя); 15 – сейсмические профили МОГТ: 4В и FIRE-1; 16 – кимберлитовые трубки с глубинными ксенолитами (Y – Кандалакшский залив, остров Еловый, K – район Каави-Куопио).

reached 60–70 km at that time as a result of resumed mantle-plume activity. The intrusive bodies were subject to granulite-facies metamorphism along with the Archaean country rocks [Mints et al., 2009, 2015]. In the course of the Late Palaeoproterozoic tectonic compression, fragments of gabbroanorthosite bodies were transferred to the upper crust and accommodated at the base of tectono-stratigraphic sections of granulite-gneiss belts, mostly in the Lapland and Kolvitsa–Umba belts in the Kola Peninsula [Mints et al., 1996], whereas the predominant mass of gabbroanorthosites remained at the level of the crust–mantle boundary. Almost synchronously with accommodation of gabbroanorthosites, mafic–ultramafic magmas were emplaced into the upper crust along the northern boundary of the Karelian Craton to form the North Karelian belt of layered intrusions. At the same time, the middle part of the crust in the Belomorian Province was intensely impregnated by small portions of mafic and ultramafic magma to form minor intrusions known as «drusites» (local name). At present, some of these intrusions are exposed at the surface.

The peak of rifting controlled by mantle-plume processes is most probably related to division of the large Archaean Lauroscandia continent (supercontinent) into the North American and East European parts and to opening of the Svecofennian paleocean [Mints, Konilov, 2004; Mints, 2007]. In the same period of time, extended rifts filled with sediments, basalts and basaltic andesites were formed in the inner domain of the Karelian Craton. Rifting and related volcanic activity developed with breaks up to the end of the Palaeoproterozoic. The second peak of mantle-plume magmatism is dated at the Late Palaeoproterozoic, 2.2–1.8 Ga. The stage was accompanied by local transition of rifting to spreading and partial rupture of the continental lithosphere, in particular, within the Kainuu Belt along the boundary between the Kuhmo–Segozero and Kianta GGDs (Fig. 2, b). The Jormua ophiolite complex retained in the present-day structure marks the rupture of the continental crust ~1.95 Ga ago and short-term existence of the oceanic structure of the Red Sea type [Peltonen et al., 1998]. The spatial distribution of Palaeoproterozoic mafic–ultramafic igneous rocks and the lower crustal reflectivity zone in the seismic images of the crust along the CMP seismic profiles allows us to consider the reflectivity zone as a manifestation of underplating [Mints, 2011; Thybo, Artemieva, 2013, and references therein].

In the Late Palaeoproterozoic history of the composite East European Craton, the final event was formation of the arcuate intracontinental Lapland–Mid-Russia–South Baltica Collisional Orogen that surrounds the Karelian Craton in north, east, south, and southwest and the Svecofennian Orogen along the western margin of the Karelian Orogen 1.93–1.87 Ga ago [Mints et al.,

2015; Mints, 2011]. The evolution of the Svecofennian paleocean was completed by eastward subduction of the oceanic lithosphere and accretion of island-arc complexes and rocks of inter-arc basins to the margin of the Karelian Craton. In the course of accretion, most of these complexes were thrust under the continental margin, whereas others, conversely, were thrust over the margin. These movements resulted in the formation of a crocodile-type structure [Abramovitz et al., 1997; Mints et al., 2009] that is characteristic of marginal continental and collisional orogens. Scrutiny of the seismic crustal image along the FIRE-1 profile [Kukkonen, Lahtinen, 2006] makes it possible to trace tectonic sheets composed of accreted volcanic–plutonic complexes beneath the Archaean crust of the Karelian Craton.

The thrust–nappe ensembles of granulite-gneiss belts were formed by ~1.87 Ga in the setting of overall collisional compression. The tectonic sheets making up the South Finland Belt were thrust from the south over the Svecofennian Orogen almost immediately after its formation [Mints et al., 2015]. These events completed the Palaeoproterozoic history.

A new stage in evolution of the crust (the last in the considered time interval) was related to formation of the Mesoproterozoic rapakivi granite pluton in the eastern part of the Russian Platform. The 3D model of deep structure of the Early Precambrian crust based on geological evidence and interpretation of CMP seismic profiles demonstrates an image of the tectonically delaminated crust with predominance of low-angle boundaries between the main tectonic units and shows complex structure of the crust–mantle boundary [Mints, 2011].

4. COMPLEX GEOPHYSICAL MODEL

The complex interpretation of gravimetric and geothermal data is based on the results of regional seismic DSS studies and CMP profiling of the sedimentary cover of the adjacent platform, as well as seismic estimation of the crust thickness. This heterogeneous information described in [Glaznev, 2003; Grad et al., 2009] were used for creation of the initial seismogeological model of the crust for the territory much larger than the area of the eventual 3D complex model of the lithosphere (Fig. 3) in order to take into account the influence of marginal zones when solving direct and inverse problems related to thermal and density simulation.

Statistical analysis of the seismic data allowed us to recognize four layers with characteristic velocities, which correspond to the integrated models of the continental crust [Christensen, Mooney, 1995]. The estimates of the total thickness of the crust based on CMP profiling, which generally coincide with results of DSS

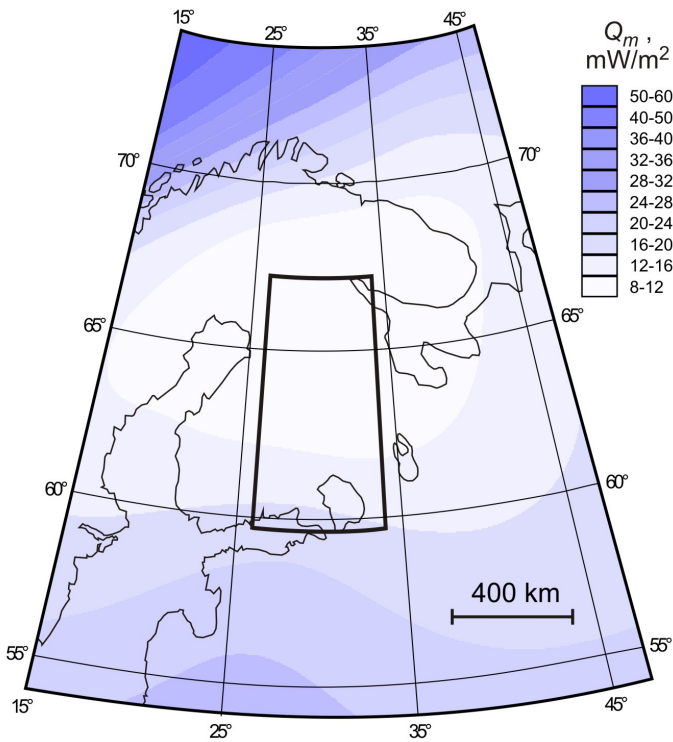


Fig. 3. Smoothed mantle heat flow in the eastern Fennoscandian Shield and the adjacent part of the Russian Plate. The area of simulation is shown.

Рис. 3. Схема сглаженного мантийного теплового потока (в мВт/м²) для восточной части Фенноскандинавского щита и сопредельной части Русской платформы. Показан контур результирующей области моделирования.

[Berzin *et al.*, 2002], were also used as initial data for complex geophysical simulation.

4.1. THERMAL MODEL OF THE EARTH'S CRUST AND UPPER MANTLE

At the first stage of simulation, the 3D stationary thermal model of the lithosphere is created on the basis of the data on the regional surface heat flow, thermal conductivity and heat generation in the crust [Glaznev, 2003], according to the initial seismogeological model of the crust, and the data on the upper mantle of the studied region. The 3D thermal model is calculated in spherical coordinates with spacing of 0.25° in latitude, 0.5° in longitude, and 5 km along radius down to a depth of 65 km. The model combines distribution of temperature and heat generation in the Earth's crust plus estimation of the deep (mantle) heat flow currently supplied from the mantle to the lower edge of the model.

The mantle-derived heat flow appreciably affects temperature distribution in the studied medium. Therefore, estimation of this boundary condition is

crucial for all the subsequent procedures developing of the model. The initial data used for estimation of the mantle heat flow are based on the classification of the studied territory by thickness of crustal layers, which was carried out on the basis of the seismogeological model of the region. As a result, the region is subdivided into a number of large blocks, each having its relatively homogeneous seismic structure, and the mantle heat flow is estimated for each of the blocks [Glaznev, 2003].

The smoothed calculated values of the mantle heat flow (Fig. 3) are consistent with the estimates previously obtained for particular areas of the Fennoscandian Shield [Balling, 1995; Pasquale *et al.*, 1991]. These values make it possible to differentiate the recent thermal activity of the mantle. The lowest mantle heat flow values (no higher than 8–10 mW/m²) are estimated for the Karelian Craton, the Belomorian and Kola Provinces, which are typical of domains that underwent the Archaean consolidation [Nyblade, Pollack, 1993]. The low mantle heat flow in these areas was partly caused by the effect of paleoclimatic processes on the recent surface heat flow [Kukkonen *et al.*, 1998; Glaznev *et al.*, 2004]. In the adjacent Russian Platform and the Barents Sea Plate that were also impacted by the last glaciation, the minimum mantle heat flow is evidently local against the background of relatively high values (up to 16–24 mW/m²) and probably reflects a level of recent thermal activity of the upper mantle in the eastern Fennoscandian Shield.

Based on the solution of the 3D inverse problem of geothermics in the setting (Eqs. 2, 4, 6, 8, 10) with an allowance for the estimated mantle heat flow, a correct stationary temperature model of the medium is created. A discrepancy of the eventual thermal model (Eq. 2) is ±3.7 mW/m², and this value is commensurable with the uncertainty of the initial geothermal data. For the deep levels, the accuracy of temperature calculation from the stochastic simulation results is estimated at ±40 °C.

Temperature values at various depth levels of the 3D model are shown in Fig. 4. The temperature distribution pattern in the crust demonstrates an isometric area of relatively low temperatures in the northern Karelian Craton and the southwestern Belomorian Province. Along with relatively homogeneous distribution of radiogenic chemical elements in the Earth's crust [Glaznev, Skopenko, 1991], such an anomalous temperature area is indicative of the heterogeneous mantle heat flow in the crust of the region. A potential increase in the horizontal temperature gradient is revealed at the lower levels of the thermal model (40–60 km) in the southwestern part of the studied region; it may be caused by substantially increased surface and mantle heat flows in the zone of transition to the South Baltica segment of the intracontinental Late Palaeoproterozoic

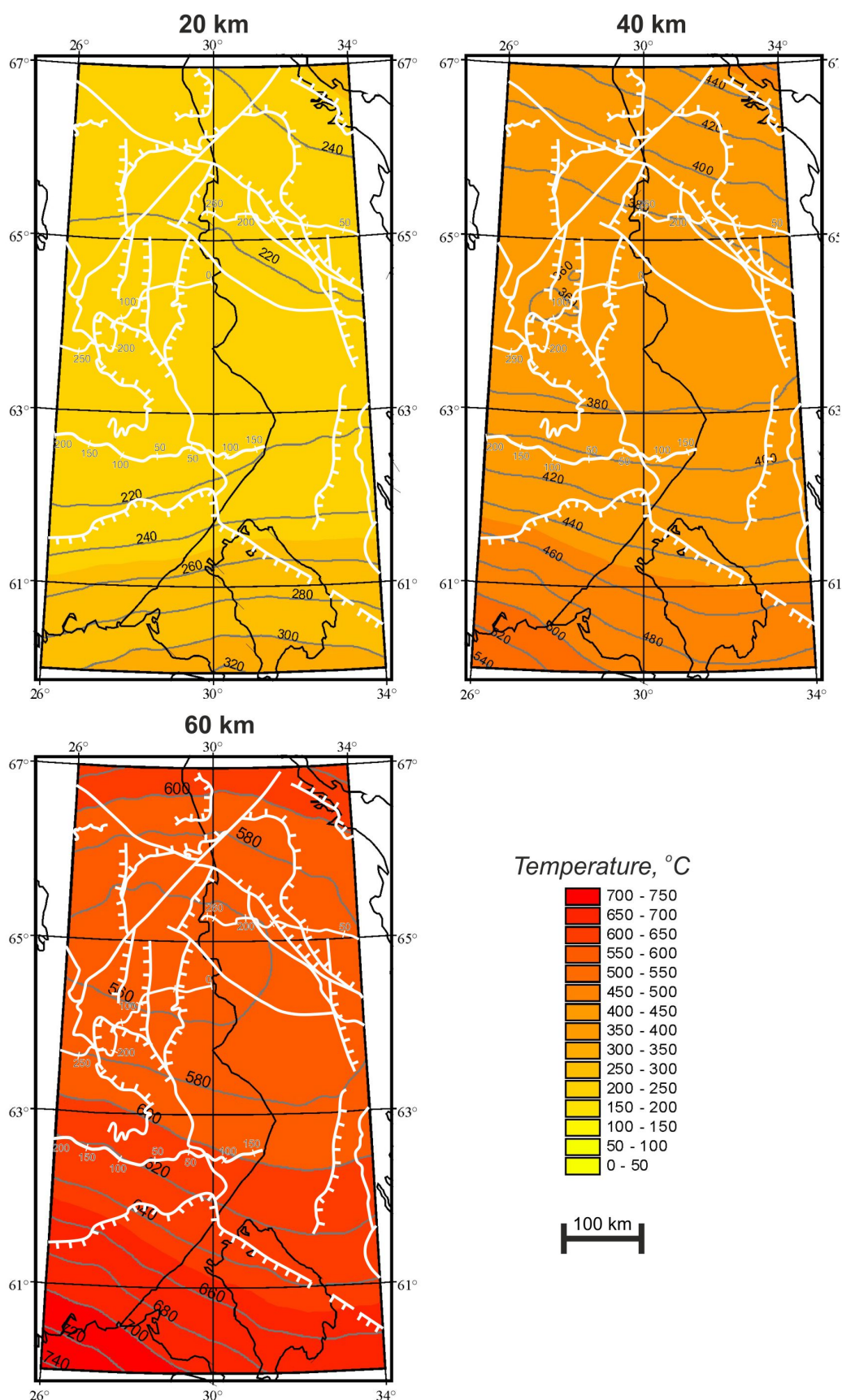


Fig. 4. Temperature distribution in the Earth's crust at depths of 20, 40, and 60 km. In Figs. 4–7 and 12, white lines show contours of geological structures at the surface and seismic CMP profiles (see Fig. 2).

Рис. 4. Распределение температур в земной коре на глубинах 20, 40 и 60 км (в °C). На рис. 4–7 и 12 белыми линиями показаны контуры геологических структур на дневной поверхности и профилей МОГТ, представленных на рис. 2.

Lapland–Mid-Russia–South Baltica Collisional Orogen overlain by the sedimentary cover of the Russian Platform [Mints *et al.*, 2015; Mints, 2011]. The map of the surface heat flow in Europe [Artemieva *et al.*, 2006] (Fig. 3) shows similar regular patterns of heat flow distribution in the Karelian Craton and the surrounding arcuate orogen at the regional level.

The 3D model of temperature distribution is a necessary element of the complex velocity–density model of the crust, which provides insights into the nature of deep-seated geophysical boundaries.

4.2. DENSITY MODEL OF THE EARTH'S CRUST AND UPPER MANTLE

At the second stage of simulation, an initial density model of the crust is created on the basis of velocity and thermal models. Validation with gravity data makes it possible to estimate discrepancy between the observed gravity field and the estimated effect of the initial model. The direct problem for the upper crust is solved with account of the available data on density of the near-surface rocks in the studied region [Galitshanina *et al.*, 1995] and stochastic estimations of thickness of the ‘gravity active layer’ in the range from 2.5 to 14 km [Glaznev, 2003]. When the gravity field is computed from the initial approximation, densities of the near-surface rocks are extrapolated only over the gravity active layer, while densities corresponding to the initial velocity model are taken into account for the deeper layers. Such an approach is dictated by the necessity to take into account, at least, roughly the data on shallow-seated rock complexes in initial approximation of the model, and specific features of such an approach make a certain impact on the resultant density model (this issue is discussed below).

For solving direct and inverse problems of gravimetry, the planetary density model of the Earth's crust and its gravity field [Kartvelishvili, 1983] is used as a normal density model. Our model is based on the solution of the inverse 3D problem of gravimetry in the spherical setting with account of the actual topography. The initial data include the difference gravity field of initial approximation of the model and the initial density model of the crust. The network 0.25° in latitude, 0.25° in longitude, and 5 km in depth is used in solution of inverse problem. The eventual discrepancy of density model determined by Eq. 1 is ± 2.4 mGal. The accuracy of calculated density in network elements of model is ± 0.02 g/cm³.

The eventual density model is isostatically compensated owing to special constraints placed into the algorithm of inverse problem solution, which ensure the absence of significant mass forces at the lower edge of model. The final 3D density model is presented in Figs. 5–7 as a series of horizontal slices.

It has been repeatedly shown that the crust models

characterizing distribution of P-wave velocities correspond to density layering of the crust. The boundaries of layers are fragmentary fixed by abrupt variations of velocity and density. With rare exception, these parameters regularly increase with depth and from top to bottom of particular layers [Christensen, Mooney, 1995; Korsman *et al.*, 1999; Kuusisto *et al.*, 2006]. The obtained model also demonstrates that density of the crust increases with depth, however, the layer boundaries remain vague.

At the uppermost level of the model (Fig. 5), the density of rocks is 2.52–2.88 g/cm³ (2.69 g/cm³, on average). These values are consistent with the regional petrophysical data [Galitshanina *et al.*, 1995]. Against the background of the average values, clearly detectable are anomalies caused by the presence of high-density gabbroanorthosites and granulites of the Kolvitsa–Umba Belt, layered mafic–ultramafic intrusions, the Palaeoproterozoic volcanic–sedimentary and the Archaean greenstone belts. Anomalies related to the rocks of the Svecofennian accretionary complex are not so contrasting. It should be noted that configurations and sizes of the high-density anomalies are mainly associated with the initial density model as objects smaller than 20–25 km cannot be reliably reflected in its discrete representation within the given network. Nevertheless, a certain increase in density is revealed for narrow, sufficiently long high-density objects.

Low-density anomalies at the upper level of the model reliably mark the spatial position of rapakivi granite in the southeast and granitic rocks of the Central Lapland Complex in the northwest. The area of the lower density in the southeast corresponds to the platform sedimentary cover and partly to rapakivi granite.

At depths of 5–10 km, which, in fact, are near-surface and occupy two upper layers in the model network, density varies from 2.62 to 2.88 g/cm³ (2.75 g/cm³ on average). The domain of elevated values up to 2.82–2.86 g/cm³ is located in the southwestern Karelian Craton and the adjacent Svecofennian Orogen. In contrast, the eastern Karelian region at depths of 5–10 km differs in lower density (up to 2.68–2.72 g/cm³). The low-density crust apparently underlies Palaeoproterozoic volcanic–sedimentary belts. Large dimensions of the anomaly with relatively low density give evidence of its existence in reality and reflect internal features of the upper crust of the Karelian Craton. With sinking to deeper levels, the density contour lines shift to the east, indicating a gentle slope of isodensity surfaces in the eastern and northeastern directions.

It is noteworthy that a negative anomaly of density at depths of 5–10 km is located near the northern boundary of the model beneath the central part of the Palaeoproterozoic Kuolajärvi structure (Fig. 2, *b*) filled largely with mafic metavolcanics. It is suggested that this anomaly is compensating, i.e. arising by solution of

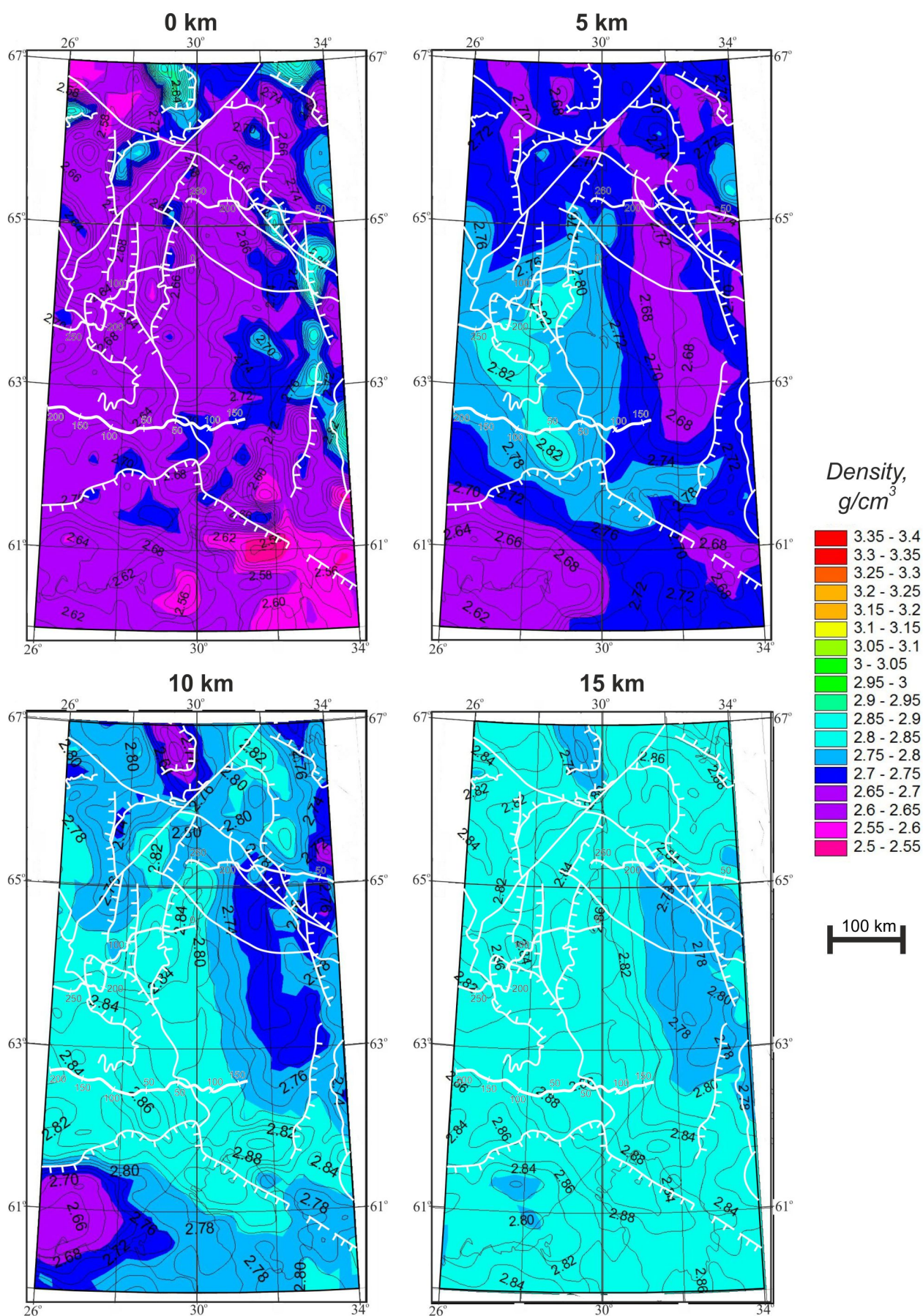


Fig. 5. Density distribution in the Earth's crust at depths of 0, 5, 10, and 15 km.

Рис. 5. Распределение плотности в земной коре на глубинах 0, 5, 10 и 15 км (значения плотности в г/см^3).

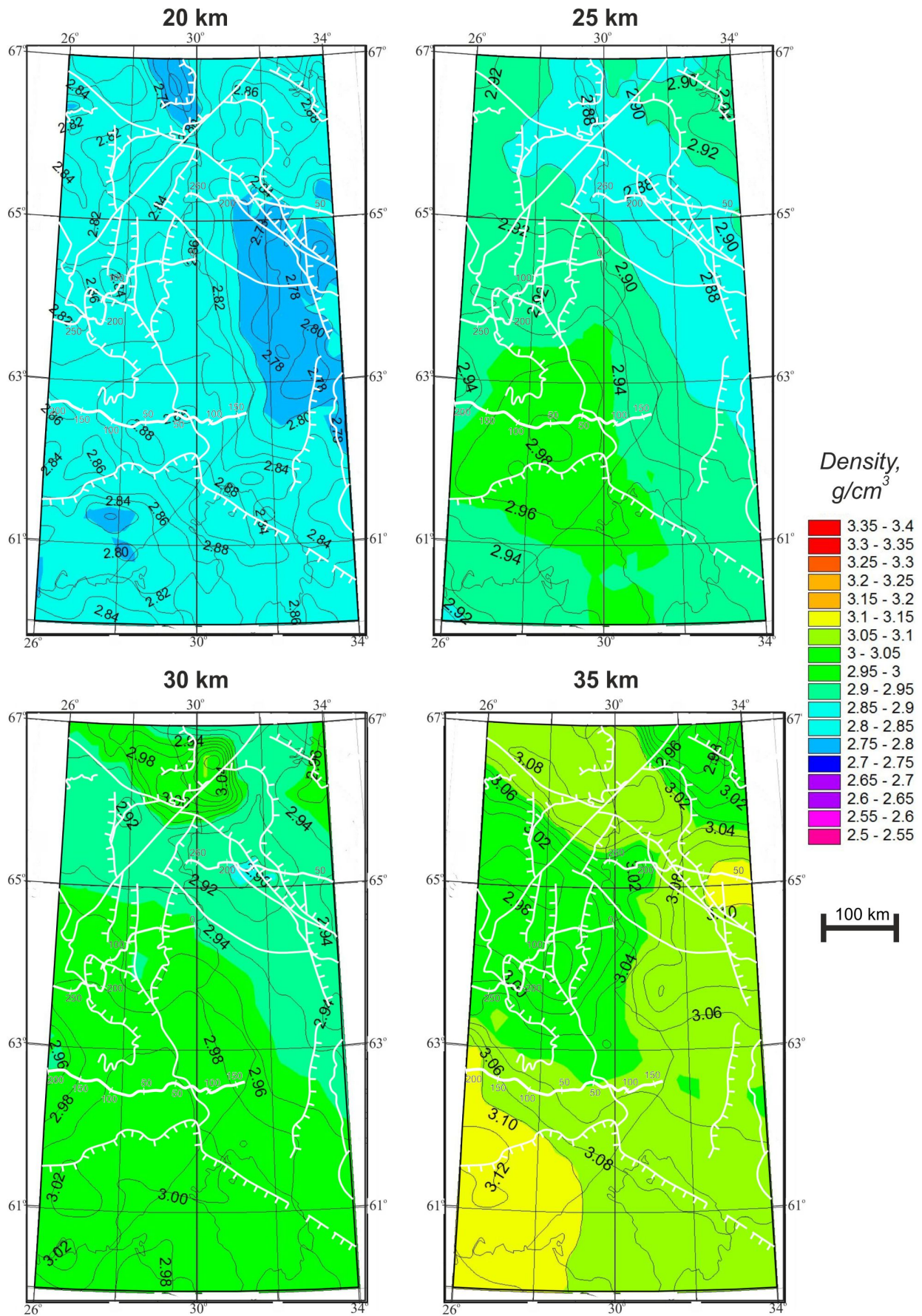


Fig. 6. Density distribution in the Earth's crust at depths of 20, 25, 30, and 35 km.

Рис. 6. Распределение плотности в земной коре на глубинах 20, 25, 30 и 35 км (значения плотности в г/см³).

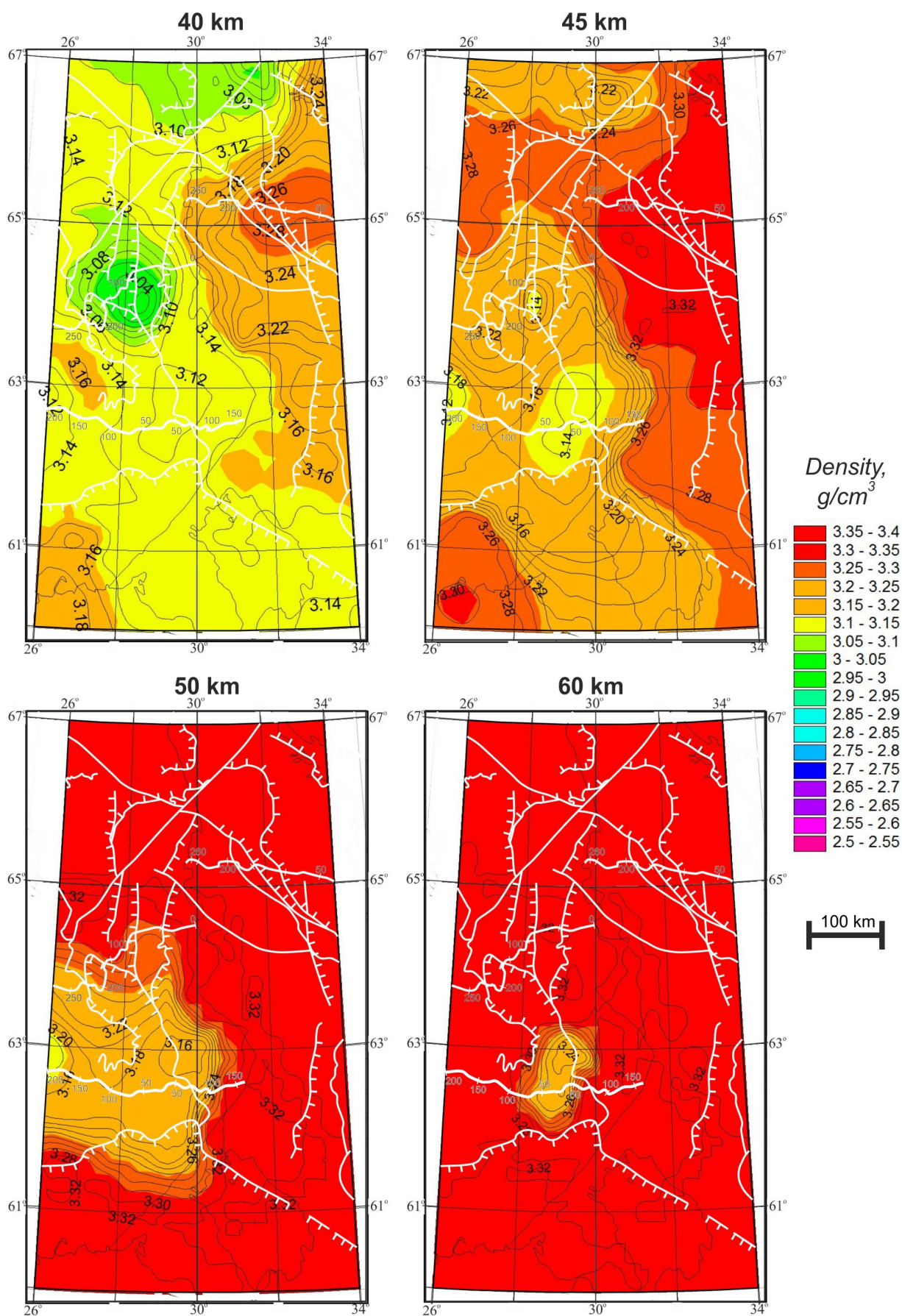


Fig. 7. Density distribution in the Earth's crust at depths of 40, 45, 50, and 60 km.

Рис. 7. Распределение плотности в земной коре на глубинах 40, 45, 50 и 60 км (значения плотности в г/см³).

the inverse problem of gravimetry as a result of overestimation of thickness of the volcanic–sedimentary complex in the initial density model. The vertical section of the Kuolajärvi structure is apparently smaller than its estimate from the averaged thickness of the gravity active layer, and the total vertical thickness of metavolcanic rocks does not exceed 2–3 km.

In the southwestern part of the region, an anomaly of relatively low density (2.60–2.68 g/cm³) is distinctly revealed at the same depth in the upper crust. This anomaly is related to the deep portion of the Wyborg rapakivi granite pluton (Fig. 2, b).

The upper crust at depths of 15–20 km is distinguished by relatively weak differentiation of the medium in the lateral direction within a density range of 2.78 to 2.92 g/cm³. The vertical gradient of rock density is also insignificant. At the levels of 15 and 20 km, the average density is 2.83 and 2.87 g/cm³, respectively. Nevertheless, the crust density of the Karelian Craton decreases from the southwest to the northeast. This is especially appreciable at the level of 20 km, where relatively low-density rocks occupy almost the entire area of the Karelian Craton. The rocks of relatively elevated density in the west are related to the Svecofennian Orogen.

In the middle crust of the Karelian Craton at depth levels of 25 and 30 km (Fig. 6), the rock density varies from 2.88 to 3.04 g/cm³ with a tendency to decrease in the northeastern direction to 2.88–2.94 g/cm³. The rocks of the Belomorian Province adjoining the Karelian Craton in the east are characterized by increase in density up to 2.96–3.02 g/cm³. In general, the distribution of density at depths of 25–30 km suggests that the contour lines of rock density at 2.93–2.95 g/cm³ beneath the central part of the Karelian Craton depict the eastern boundary of the Svecofennian Orogen plunging eastward.

At the level of the lower crust (35–45 km), rock densities vary within a range of 2.98–3.26 g/cm³ (Figs. 6, 7). The highest density values are characteristic of the transitional crust–mantle zone approximately at the level of Moho discontinuity. The density model of the lower crust is distinguished by an anomalous domain of low density (2.98–3.02 g/cm³) at a depth of 35 km beneath the western part of the Karelian Craton. At the level of 40 km, this anomaly is significantly reduced in dimensions. Similar relationships are also noted at deeper slices of the model and thus bear systematic character.

In the lowermost crust at depths of 40–45 km (Fig. 7), the rocks with density ranging from 3.10 to 3.30 g/cm³ are related to the transitional crust–mantle zone (crust–mantle mixture?). At depths of 50–60 km, the mantle rocks occupy almost the entire domain of simulation. The only exception is the region of the anomalously deep Moho discontinuity at the boundary

between the Karelian Craton and the Svecofennian Orogen [Grad *et al.*, 2009; Kozlovskaya *et al.*, 2004].

The vertical step of the network is 5 km in the accepted discretization of the model and thus does not allow us to determine unambiguously a position of the Moho boundary. Densities exceeding 3.30 g/cm³ are reliably related to the mantle rocks, whereas densities below 3.20 g/cm³ are typical of the lowermost crustal rocks. The density of 3.24 g/cm³ approximately corresponds to the Moho discontinuity. The contour lines of this density depict a surface, which coincides with the Moho discontinuity interpolated on the basis of the initial seismic data. The calculated average depths are 45.5 and 45.3 km, respectively, and the mean square difference of these depths (± 2.1 km) is minimal as compared with all other isodensity surfaces. The obtained mean square discrepancy corresponds to accuracy of initial data on the Moho depth in the studied region [Grad *et al.*, 2009] and allows us to consider the isodensity surface of 3.24 g/cm³ as an analog of Moho discontinuity in the density model (velocity–density Moho discontinuity). The use of this image of Moho discontinuity coinciding in accuracy with the DSS data seems to be more correct, because the density model is fully agreed with the observed gravity field. A maximal discrepancy between depths of the isodensity surface and the seismic Moho boundary exceeding 4 km is noted in the southeastern region of simulation, where DSS data are absent and the initial seismogeological model of the crust was created as interpolation of the data on converted waves [Sharov *et al.*, 2005] of low accuracy.

The depth and topography of the velocity–density Moho discontinuity are shown in Fig. 8, where the isodensity surface of 2.9 g/cm³ is also given for comparison. The relationship of the depths of these boundaries demonstrates an approximate isostatic compensation of the density model: decrease in thickness of the upper low-density part of the Earth's crust is compensated by significant increase in thickness of the lower high-density part of the crust. In the domain of the anomalously deep position of the velocity–density Moho discontinuity at a depth of ~ 63 km, the compensation is partly supplemented by increase in density of the lowermost Earth's crust (Fig. 7). The plunging velocity–density Moho discontinuity (Fig. 8) is spatially coincident with a «Moho depression» earlier recognized on the basis of seismic data and density simulation [Kozlovskaya *et al.*, 2004].

5. DEEP STRUCTURE: GEOLOGICAL MODEL BASED ON INTERPRETATION OF SEISMIC CRUSTAL IMAGES IN SECTIONS ALONG CMP SEISMIC PROFILES

Information on deep geological structure of the region is based on results of geological mapping and

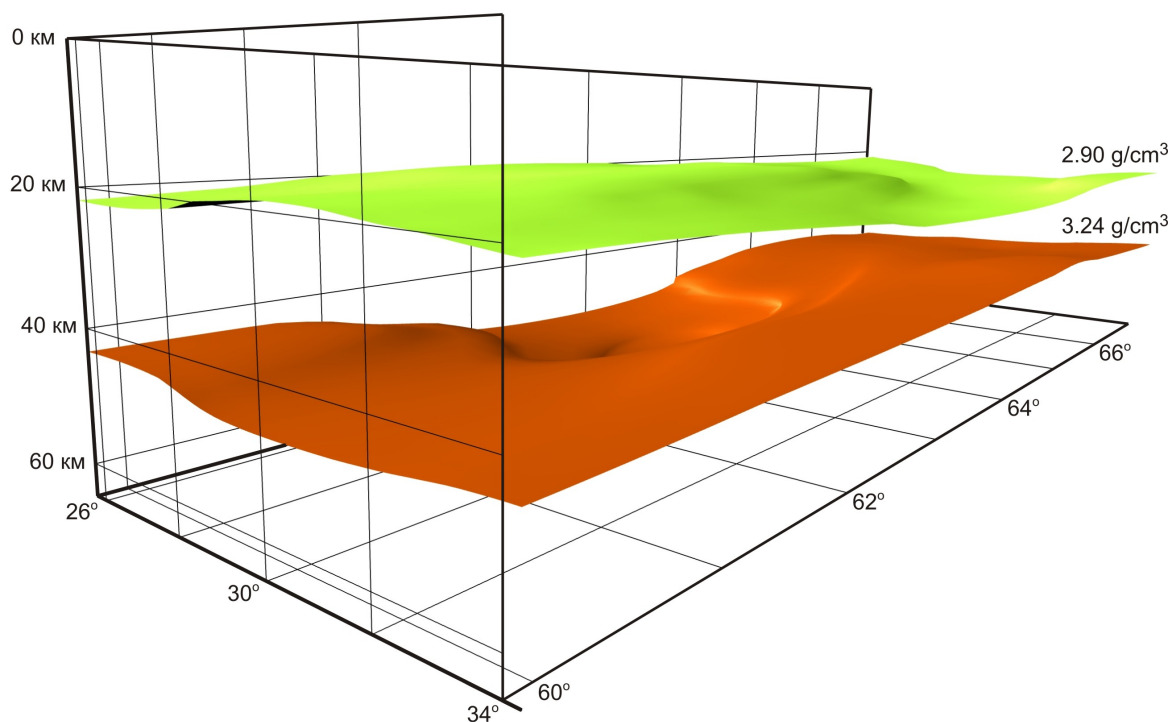


Fig. 8. Smoothed isodensity surfaces separating the middle and lower crust (2.90 g/cm^3), the lower crust and the upper mantle (3.24 g/cm^3), and the velocity–density Moho discontinuity.

Рис. 8. Положение и морфология сглаженных изоплотностных поверхностей, разделяющих: 2.90 г/см^3 – среднюю и нижнюю кору, 3.24 г/см^3 – нижнюю кору и мантию (сейсмоплотностной раздел Мохо).

studies along CMP seismic profiles: 4B (Fig. 9), FIRE-1 (Fig. 10), and FIRE-3-3A (Fig. 11) [Kukkonen, Lahtinen, 2006; Mints et al., 2009, 2015; Mints, 2011].

Careful correlation of geological structural units at the surface and geological interpretation of seismic crustal images along 1-EU and 4B CMP profiles has provided for creation of a 3D model of geological structure of the crust and upper mantle in the studied region. The geological interpretation of seismic images of the crust along the FIRE-1 and FIRE-3-3A profiles in Finland carried out by M.V. Mints serves as an additional support of the western part of the 3D model and allows us to provide insights into the structure of the Svecofennian Orogen and to characterize its boundary with the Karelian Craton [Mints et al., 2009, 2015].

5.1. ARCHAEOAN TECTONIC UNITS

In the vertical section along 4B profile (Fig. 9), the sheet-like wedge-shaped domain represents the Archaean granite–greenstone crust of the Kuhmo–Segozero microcontinent, which is the main constituent of the Karelian Craton. The maximum thickness of the sheet amounts to almost 30 km near the western and southwestern margins of the microcontinent, and the sheet gradually becomes thinner while plunging

eastward beneath the Khetolambina microcontinent. The southeastern margin of the Kuhmo–Segozero microcontinent plunges beneath the Vodlozero microcontinent. The section along 4B profile indicates that the tectonic sheet of Kuhmo–Segozero microcontinent overlying the lower crust underwent tectonic displacements and became slanted after formation of isometric acoustically transparent domains, i.e. large granitic plutons in our interpretation. Their formation can be logically attributed to the completion of the Neoproterozoic evolution.

5.2. PALAEOPROTEROZOIC TECTONIC UNITS

The boundary zone of the Lapland sector of the Palaeoproterozoic intracontinental orogen is located at the eastern part of the studied region, which is intersected by 4B profile. This zone is represented by the structural ensemble of the imbricate East Karelian Thrust Belt composed of alternating tectonic sheets of the Archaean granite–greenstone and Palaeoproterozoic volcanic–sedimentary associations.

The lower crustal layer with intense seismic reflections stands out at the base of the Karelian Craton. The overlying gently dipping geological bodies gradually flatten when approaching the upper boundary of this

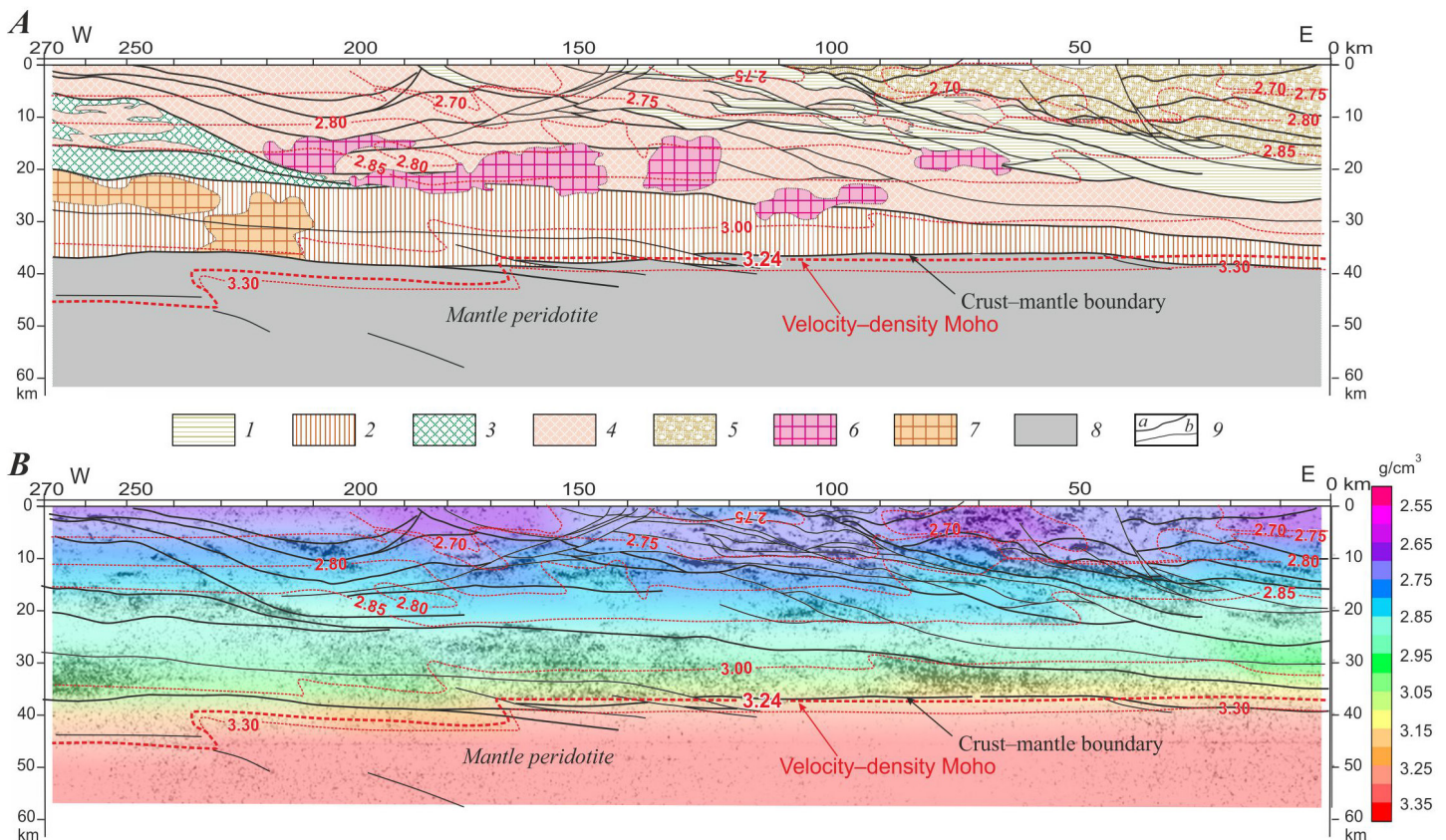


Fig. 9. Sections of the crust and the upper mantle along 4B profile: (A) geological section obtained as a result of geological interpretation of the seismic crustal image [Mints *et al.*, 2009, 2015]; (B) density section (section of 3D crust model). Main tectonic boundaries and certain isodensity contours (including the velocity-density Moho discontinuity, 3.24 g/cm³) are shown.

1–2 – Palaeoproterozoic: 1 – volcanic-sedimentary belt, 2 – lower crustal granulite-basic complex; 3–5 – Archaean: 3 – rocks of greenstone belts, mainly basic volcanics, 4 – Kuhmo-Segozero TTG gneiss complex with inclusions of metavolcanic and metasedimentary rocks, 5 – Khetolambina granite-greenstone complex; 6–7 – plutons: 6 – in the middle crust, mainly granitoids, 7 – in the lower crust, mainly gabbro and gabbroanorthosite; 8 – mantle peridotite; 9 – faults, mainly of reverse-thrust type: (a) major and (b) subordinate.

Рис. 9. Разрезы коры и верхней части мантии по профилю 4В: (А) геологический, полученный в результате геологической интерпретации сейсмического образа коры [Mints *et al.*, 2009, 2015]; (В) плотностной – сечение трехмерной модели коры; показаны главные тектонические границы и некоторые изолинии плотности (в том числе сейсмоденситивной Мохо – 3.24 г/см³).

1–2 – палеопротерозой: 1 – осадочно-вулканогенные пояса, 2 – гранулит-базитовый комплекс пород нижней коры; 3–5 – архей: 3 – породы зеленокаменных поясов, преимущественно вулканиты основного состава, 4 – Кухмо-Сегозерский гранитогнейсовый комплекс с включениями метавулканитов и метаосадков, 5 – Хетоламбинский гранит-зеленокаменный комплекс; 6–7 – плутоны: 6 – в средней коре, предположительно гранитоиды, 7 – в нижней коре, предположительно габбро и габбро-анортозиты; 8 – мантия (мантийные перидотиты); 9 – разломы, преимущественно взбросо-надвигового типа: главные (a) и второстепенные (b).

layer. The determinant role in origin and composition of this layer belongs to the Palaeoproterozoic under- and intraplating by the mantle-derived mafic magmas, which underlie the Archaean crust of the Karelian Craton [Kempton *et al.*, 2001; Mints *et al.*, 2009, 2015; Mints, 2011, and references therein].

In the southwestern part of the region crossed by FIRE-1 and FIRE-3-3A profiles, tectonic sheets composed of island-arc and back-arc complexes of the Svecofennian Orogen are traced from the surface to the

crust-mantle boundary and plunge further as if «dissolving» in the mantle. The total thickness of the accretionary complex exceeds 30 km. As shown in the geological section along FIRE-1 seismic profile (Fig. 10), starting from stake 230 km and further southeastward, the profile crosses the Svecofennian Orogen and Central Finland granitoid pluton, one of the largest in the Fennoscandian Shield. It is evident from the seismic profile that this pluton is a nearly horizontal layered sheet, which maximum thickness does not exceed

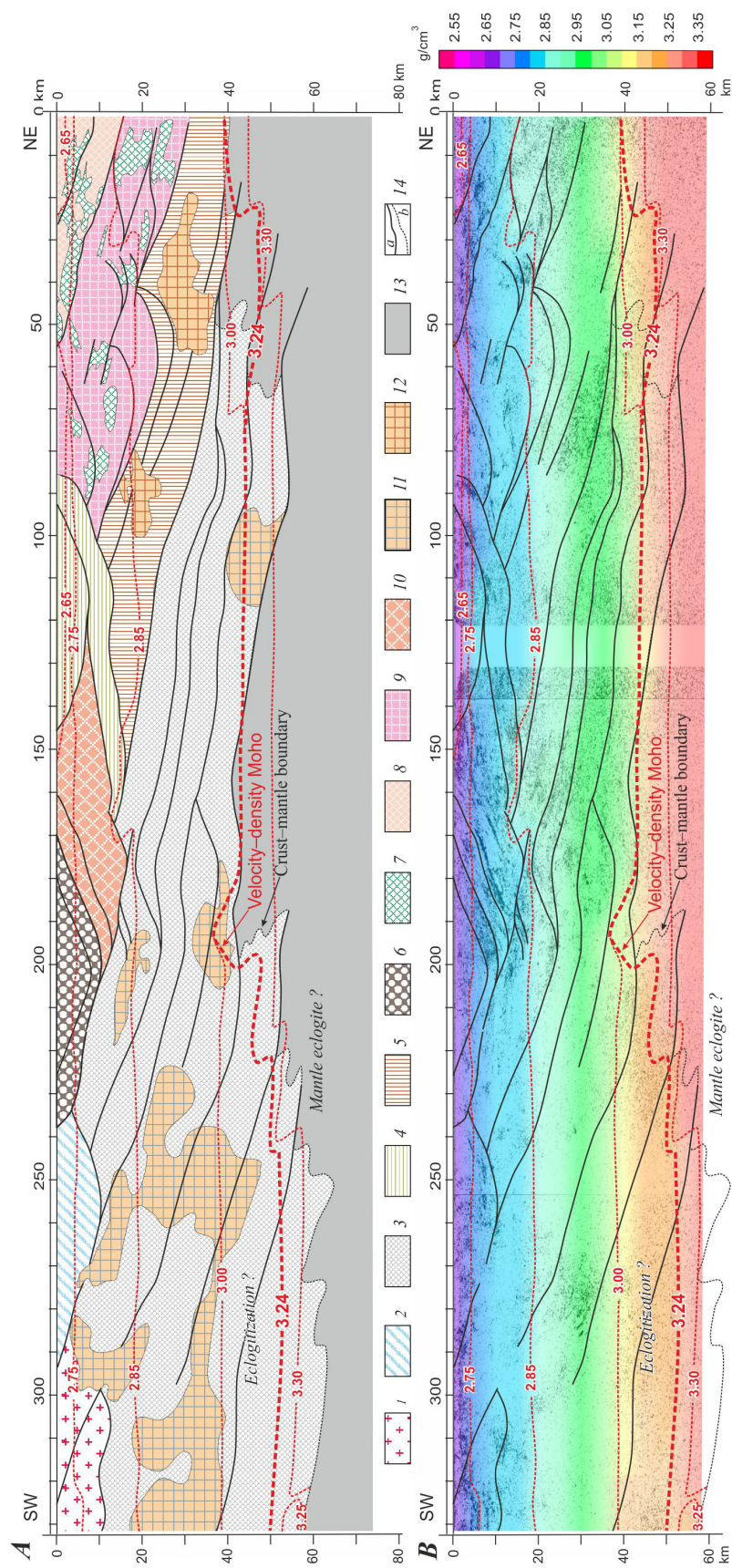


Fig. 10. Sections of the crust and the upper mantle along FIRE-1 profile: (A) geological interpretation of the seismic crustal image [Mints et al., 2015]; (B) density section (section of 3D crust model). Main tectonic boundaries and certain isodensity contours (including the velocity–density Moho discontinuity, 3.24 g/cm³) are shown.

1–5 – Palaeoproterozoic: 1–3 – Svecofennian Orogen; 2 – Savo Accretionary Belt, 3 – tectonic sheets overlain by granitoids of Central Finland pluton, 4 – volcanic–sedimentary complex of Kainuu Belt, 5 – lower crustal granulite–basic complex; 6–9 – Archaean: 6 – Varpaisjärvi granulite–gneiss complex, including diaphthorites, 7 – rocks of greenstone belts, mainly basic volcanics, 8 – Kuhmo–Segozero, 9 – Kianta, 10 – Iisalmi TTG complex; 11–12 – plutons: 11 – presumably granitoids in accretionary complex, 12 – presumably gabbro and gabbroanorthosite in Palaeoproterozoic lower crustal complex; 13 – mantle rocks with significant or predominant participation of eclogites; 14 – geological boundaries: (a) reverse–thrust and over- and underthrust faults; (b) diffuse crust–mantle boundary.

Рис. 10. Разрезы коры и верхней части мантии по профилю FIRE-1: (A) геологический, полученный в результате геологической интерпретации сейсмического образа коры [Mints et al., 2015]; (B) плотностной – сечение трёхмерной модели – сечение трёхмерной модели коры; показаны главные тектонические границы и некоторые изолинии плотности (в том числе сейсмоплотностной Мохо – 3.24 г/см³).

1–5 – палеопротерозой: 1–3 – Свекофенский аккреционный ороген; 2–3 – аккреционный пояс Саво (2), тектонические пластины, перекрытые гранитоидами Центрально-Финляндского плутона, погружающиеся под окраину Карельского кратона (3), 4 – осадочно-вулканогенный комплекс пояса Кайнуу, 5 – гранулит-базитовый комплекс пород нижней коры; 6–9 – архей: 6 – гранулитогнейсовый комплекс Варпайсъярви (в том числе диафторированные разновидности гранулитов), 7 – породы зеленокаменные поясов, преимущественно вулканиты основного состава, 8–10 – гранитоидные комплексы: Кухмо-Сегозерский (8), Кьянта (9), Рануа-Иисалми (10); 11–12 – плутоны: 11 – в аккреционном комплексе, предпочтительно гранитоиды, 12 – в палеопротерозойском нижнекоревом комплексе, предпочтительно габбро и габбро-анортозиты; 13 – мантия (предположительно со значительным или преобладающим участием эклогитов); 14 – главные геологические границы: разломы, преимущественно взбросо-надвигового и надвиго-поддвигового типа (a), диффузная граница между корой и мантией (b).

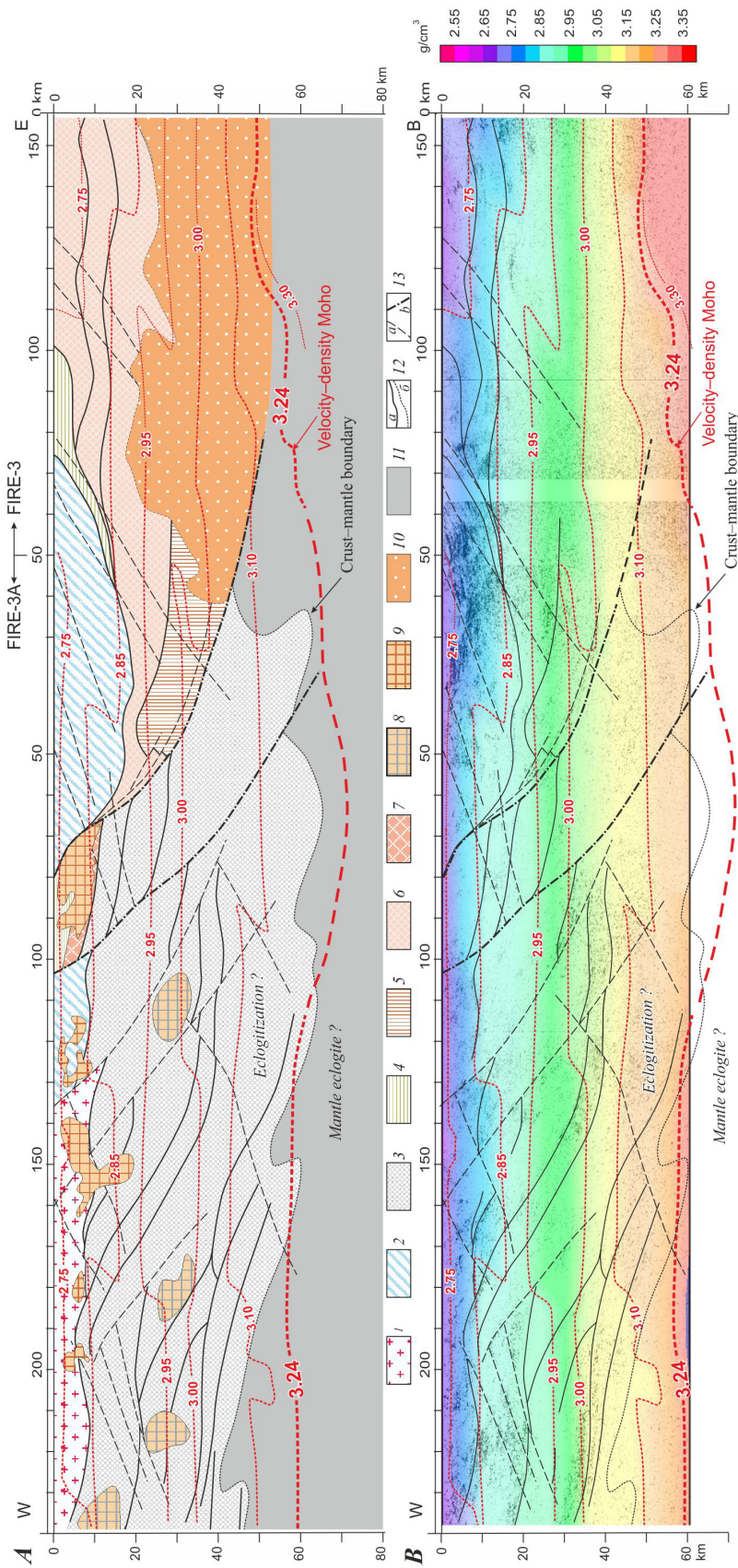


Fig. 11. Sections of the crust and the upper mantle along FIRE-3-3A profile: (A) geological section obtained as a result of geological interpretation of the seismic crustal image; (B) density section (section of the 3D crust model). Main tectonic boundaries and certain isodensity contours (including the velocity–density Moho discontinuity, 3.24 g/cm³) are shown.

1–5 – Palaeoproterozoic; 1–3 – Svecofennian Orogen; 1 – granitoids of Central Finland pluton, 2 – Saimaa Accretionary Belt, 3 – tectonic sheets plunging beneath margin of Karelian Craton and overlain by granitoids of Central Finland pluton, 4 – volcanic–sedimentary complex of passive margin, 5 – lower crustal granulite–basic complex; 6–9 – Archaean; 6 – Kuhmo–Segozero and 7 – Iisalmi TTG gneiss complex; 8–9 – plutons presumably granitoid in accretionary complex (8) and upper crust (9); 10 – acoustically transparent domain in middle–lower crust presumably homogenized as a result of high-temperature metamorphism; 11 – mantle rocks with significant or predominant participation of eclogites; 12 – geological boundaries: (a) reverse–thrust and over- and underthrust faults, (b) diffuse crust–mantle boundary; 13 – normal–strike-slip (a) and inferred transform strike-slip (b) faults.

Рис. 11. Разрезы коры и верхней части мантии по профилю FIRE-3-3A: (A) геологический, полученный в результате геологической интерпретации сейсмического образа коры; (B) плотностной – сечение трехмерной модели коры; показаны главные тектонические границы и некоторые изолинии плотности (в том числе сейсмоплотностной Мохо – 3.24 г/см³).

1–5 – палеопротерозой: 1–3 – Свеккофенский аккреционный ороген; 1 – гранитоиды Центрально-Финляндского плутона, 2–3 – аккреционный комплекс: пояс Саймаа (2), тектонические пластины, перекрытые гранитоидами Центрально-Финляндского плутона, погружающиеся под окраину Карельского кратона (3), 4 – осадочно-вулканогенный комплекс пассивной окраины, 5 – гранулит-базитовый комплекс пород нижней коры; 6–7 – архей, гранитогнейсовые комплексы: Кухмо-Сегозерский (6), Рануа-Иисалми (7); 8–9 – плутоны, предположительно гранитоиды: в аккреционном комплексе (8), в верхней части коры (9); 10 – акустически прозрачная область в средней-нижней коре, предположительно гомогенизированная в результате высокотемпературного метаморфизма; 11 – мантия (предположительно со значительным или преобладающим участием эклогитов); 12 – главные геологические границы: разломы, преимущественно взбросо-надвиговые и надвиго-поддвиговые и (a) диффузная граница между корой и мантией (b); 13 – разломы: сбросо-сдвиги (a), предполагаемые трансформные сдвиги (b).

10–12 km in FIRE-1 and FIRE-3-3A sections. This conclusion agrees with interpretations in [Kontinen, Paavola, 2006; Korja et al., 2006]. The massif overlies the accretionary complex proper represented by the sequence of 10–20 km thick tectonic sheets that consecutively plunge northeastward at angles of 10–12° and make up the crustal section down to the crust–mantle boundary at a depth of more than 60 km. The accretionary complex is traced beneath the margin of the Karelian Craton for more than 150 km.

The subsidence of the tectonic sheets beneath the margin of the Karelian Craton is the main structural feature of the boundary between the Palaeoproterozoic orogen and the Archaean Kola–Karelia continent. It is noteworthy that plunging of the large tectonic sheets is accompanied by thrusting of small fragments of the Svecofennian Orogen over the active margin of the Archaean continent. In particular, the Savo Belt, judging by its position in the section, is the sedimentary fill of the back-arc basin squeezed out on the northeastern and southwestern walls of this basin. The sections along FIRE-1 and FIRE-3-3A seismic profiles show clearly that the margin of the Karelian Craton is broken, and the craton's fragments, including the Ranua and Iisalmi microcontinents and the Palaeoproterozoic Kainuu Belt, are displaced in the northeastern direction and form a crocodile-shaped structure. A similar structure of the boundary between the Svecofennian Orogen and the Karelian Craton was established in the section along BABEL profile [BABEL Working Group, 1990, 1993; Abramovitz et al., 1997; Lahtinen et al., 2009].

6. COMPARISON OF THE DENSITY AND GEOLOGICAL MODELS OF THE CRUST

The complex model of the crust and upper lithospheric mantle in the studied region demonstrates a generalized pattern of rock density distribution because the 3D network used for solution of the inverse gravity problem has low spatial resolution. Nevertheless, this model makes it possible to characterize the crucial spatial and structural relationships of the geological objects localized at various depth levels in the Earth's crust.

It is challenging to compare parameters of the density model with results of the geological interpretation of seismic images of the crust along CMP profiles: 4B [Mints et al., 2009, 2015], FIRE-1 and FIRE-3-3A [Kukkonen, Lahtinen, 2006; Mints et al., 2015].

6.1. DENSITY LAYERING AND STRUCTURAL GEOLOGICAL CHARACTERIZATION OF THE CRUST

The rock density values for the upper part of the 3D model of the Earth's crust (Fig. 5), which are obtained

by simulation with an allowance for relationships between density and velocity (Fig. 1), are consistent with the laboratory measurement results for corresponding rocks. Even objects of the real geological medium, which are insignificant in size and comparable in dimensions to a cell in the modeling network, find their mediated inference in the anomalies of density in the upper level of the model. The geological structures formed by rocks variable in density, which make up the upper crust along CMP seismic profiles (Figs. 9–11), are reliably identified by density simulation. In general, there are sufficient grounds to state that the 3D model of the regional deep geological structure discussed in this paper also reflects real density heterogeneities at deeper levels of the crust and upper mantle on a scale of the used network of discretization. It should be noted that by virtue of the known resolution of gravimetric problems [Aleksidze, 1987; Glaznev, 1999], which substantially depends on spatial positions of field sources, it is unlikely that in the network assigned for solving inverse problem at the lower levels of the section, decreasing the size of cells may lead to any appreciable increase in minuteness of density models or any closer coincidence of simulation results with CMP models.

The heterogeneities of the crust generalized on a scale of simulation show systematic increase in density with depth along with leveling of lateral variations in density, while the main structural features of the medium are maintained (Figs. 5–7). The sections of the 3D density model along 4B (Fig. 9), FIRE-1 (Fig. 10) and FIRE-3-3A CMP profiles also demonstrate density layering in agreement with general trends. The smoothly bending sections of isodensity surfaces are generally near-horizontally oriented.

At first glance, comparison of the density and geological sections demonstrates that coordination is lacking between the density boundaries (and, correspondingly, the velocity boundaries) and the geological and tectonic boundaries separating the rock complexes differing in composition and age. Such relationships between the images of the crust obtained with refraction and reflection seismic methods were established in various geological situations [Glaznev et al., 1989; Mitrofanov et al., 1998; White et al., 2000; Kuusisto et al., 2006; Cook et al., 2010]. Therefore, especially important are evidences for partial coordination of the boundaries of density /velocity layering in the crust, on the one hand, and the geological boundaries identified in CMP profiles, on the other hand.

We have revealed a number of specific structural relationships between density anomalies in the crust and geological boundaries in the section along 4B profile (Fig. 9):

- within intervals of 0–25 km and 50–90 km along the profile in the upper crust, boundaries of areas with

low-density rocks ($< 2.70 \text{ g/cm}^3$) approximately follow geological boundaries identified in the seismic image of the crust;

- in the middle crust within the interval of 55–195 km along the strike, the isodensity contour of 2.85 g/cm^3 plunges from a depth of ~ 15 km down to 20–25 km, wherein acoustically transparent oval domains interpreted as granitoid plutons in [Mints *et al.*, 2009, 2015] are localized;

- abrupt vertical displacement of isodensity contours within intervals of 60–65, 100–110, and 170–180 km along the profiles, where reverse–thrust faults are identified.

In the section along FIRE-1 profile (Fig. 10), the general near-horizontal attitude of isodensity contours is combined with similarity between density anomalies and boundaries of geological bodies:

- at intersections of over- and underthrust dislocations in the crust [Mints *et al.*, 2009, 2015] at various depths, the insignificant in amplitude but rather sharp vertical shifts of isodensity contours mimic in a smoothed form the main structural lines in the crust within intervals of 25–35, 45–75, 115–125, 165–175, 215–225, and 320–330 km along the profile.

Similar relationships between the boundaries of density layering, emphasized by the isodensity contours, and the geological boundaries are noted in the section along FIRE-3-3A profile (Fig. 11). Noteworthy is local sinking of the isodensity contour of 2.85 g/cm^3 within intervals of 0–50 km and 130–180 km along FIRE-3 profile due to accommodation of relatively low-density rocks close to the surface.

6.2. VELOCITY–DENSITY MOHO DISCONTINUITY AND CRUST–MANTLE BOUNDARY

As follows from comparison of density and geological sections along 4B, FIRE-1, and FIRE-3-3A profiles, the morphology of the density image of the crust–mantle boundary depends, to a certain degree, on geological structure of the crust in the boundary zone and the crust–mantle boundary proper.

In 4B profile (Fig. 9), where the crustal base is clearly traced as the lower crustal layer (reflectivity zone), an abrupt increase in density to mantle values ($3.24\text{--}3.30 \text{ g/cm}^3$) is noted at the bottom of this level at a depth of 40 km; the crust–mantle boundary and Moho discontinuity are coordinated and have flat outlines. In the interval of 160–270 km along the profile, where the mantle is enriched in reflecting elements immediately close to the crust, isodensity contours of 3.00 and 3.24 g/cm^3 plunge from a depth of 38 km to 40–45 km. The increase in the depth of Moho discontinuity in the western segment of the profile is apparently caused by approaching the Svecofennian Orogen.

In the geological section along FIRE-1 profile (Fig.

10), the diffuse crust–mantle boundary has complex indented outlines controlled by consecutive plunging of tectonic elements pertaining to the accretionary complex into the mantle and disappearance of their seismic image in the mantle. The velocity–density Moho discontinuity related to the isodensity contour of 3.24 g/cm^3 is characterized by a flat shape complicated by a series of stepwise bends. The localization of the most distinctly curved isodensity contour is directly related to subsidence of the sheets pertaining to the accretionary complex into the mantle. In the southwestern segment of FIRE-1 profile within the interval of 215–335 km, where the seismic CMP image of these sheets gives evidence of their penetration below the 60-km depth, the isodensity contours of 3.24 and 3.30 g/cm^3 also reach a depth of about 60 km.

A similar pattern is observed along FIRE-3-3A profile (Fig. 11), and the following relationships are observed:

- Moho discontinuity marked by the isodensity contour of 3.24 g/cm^3 plunges to a depth of about 70 km within the interval of 60 km along FIRE-3A profile to 110 km along FIRE-3 profile, where the plunging tectonic sheets also reach a maximum depth;

- the isodensity contour of 3.24 g/cm^3 ascends by 15–20 km at the intersection of the boundary between the Svecofennian Orogen and the Karelian Craton.

In the sections along 4B and FIRE-1 profiles, the density boundaries are ascending to the east, while the tectonic sheets are plunging in this direction. This is especially evident in FIRE-1 profile. In other words, in the region adjoining the boundary between the Karelian Craton and the Svecofennian Orogen, the tectonic sheets comprising the accretionary complex are traced to a greater depth than at a distance from this boundary. As shown below, «dissolution» of the crustal sheets can be explained by transformation of the rocks composing such sheets under conditions of eclogite facies.

7. THERMODYNAMIC CONDITIONS AND METAMORPHISM IN THE ZONE OF THE CRUSTAL–MANTLE BOUNDARY

The 3D thermal and density models of the regional lithosphere make it possible to conduct spatial analyses of thermodynamic conditions at the crustal–mantle boundary. For this purpose, the 3D models are transformed into 2D curves of temperature and pressure variations corresponding to Moho discontinuity. As mentioned above, the isodensity surface of 3.24 g/cm^3 satisfies this discontinuity. The spatial distribution of lithostatic pressure at the level of this surface is shown in Fig. 12, *a*. The lithostatic pressure is computed from the real density of the medium with account of the real topography of the studied area. The

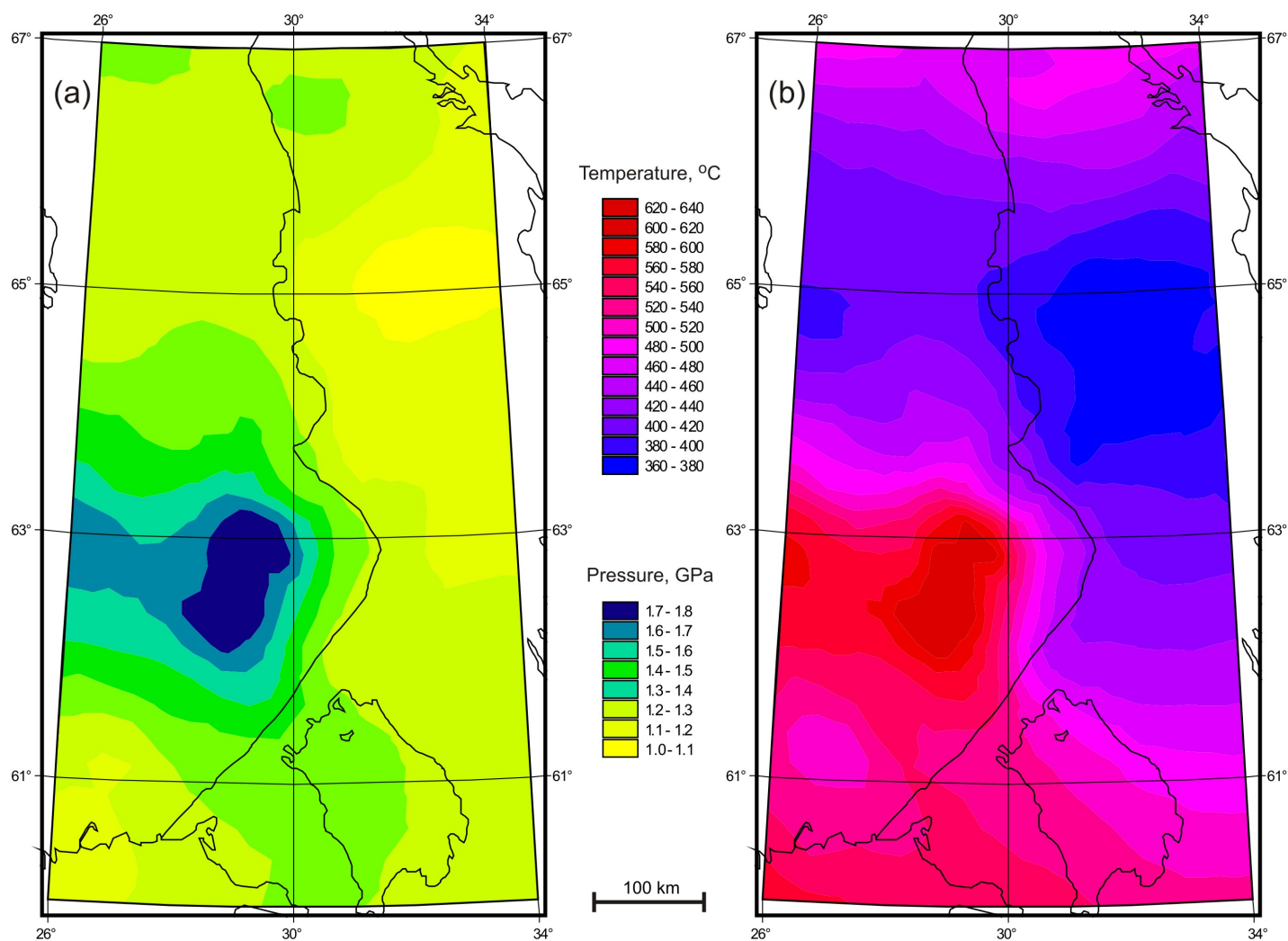


Fig. 12. Distribution of lithostatic pressure (in hPa) (a) and temperature (in °C) (b) at the level of the velocity–density Moho discontinuity.

Рис. 12. Термодинамические характеристики сейсмоплотностного раздела Мохо: (a) Распределение литостатического давления (в ГПа); (b) Распределение температуры (в °C).

estimated lithostatic pressure values range from 1.0 to 1.8 GPa, and this variation is only partly caused by the density anomalies in the middle and lower crust (Figs. 6, 7) and primarily related to significant variations of depth of the velocity–density Moho discontinuity (Fig. 8). In gravity field inversion calculations, pressure determination errors do not exceed ± 0.01 GPa.

Spatial distribution of temperature at Moho discontinuity (Fig. 12, b) is estimated by interpolation of 3D temperature characteristics of the model at the given depths corresponding to the isodensity surface of 3.24 g/cm^3 . Temperatures at this surface range from 360 to 640 °C due to variations of the Moho depth (Fig. 8) and spatial temperature variations in the model (Fig. 4). The temperature determination error is below ± 40 °C at the lower levels of the model, which is signifi-

cantly smaller than the temperature range at the level of the velocity–density Moho discontinuity.

For classification of the obtained estimates of the thermodynamic state of Moho discontinuity, we use the method of group account of arguments [Ivakhnenko, Yurachkovsky, 1987; Muravina, 2012] with application of the synergetic approach to establishment of homogeneous groups by model values. According to the pattern of discrete PT estimates at the level of the velocity–density Moho discontinuity (Fig. 13, a), it is possible to reliably distinguish seven large simply connected spatial domains belonging to six relatively homogeneous physical groups. The same estimates plotted on the PT diagram of metamorphic facies are shown in Fig. 13, b. The points corresponding to the selected groups are concentrated in the PT diagram within two linear belts and two isometric–oval clusters. A regular

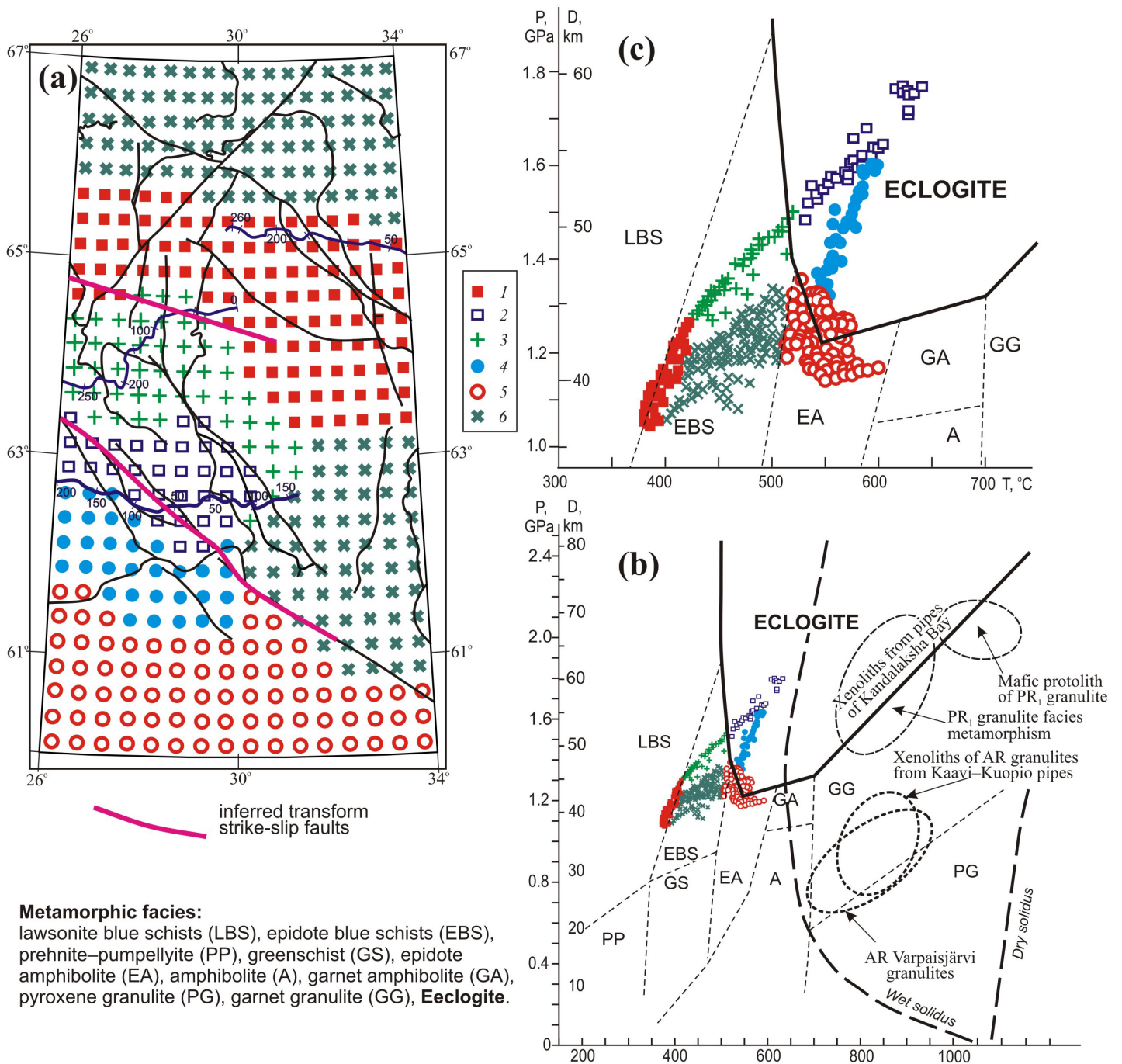


Fig. 13. (a) Spatial classification of thermodynamic conditions at the level of the velocity–density Moho discontinuity; (b) groups of points for spatial classification of thermodynamic conditions at the level of the velocity–density Moho discontinuity plotted on the PT diagram of metamorphic facies, after [Peacock *et al.*, 1994]; (c) enlarged fragment of the PT diagram.

1–6 – groups of points for spatial classification of thermodynamic conditions at the level of the velocity–density Moho discontinuity (explanations are given in the text). Estimates of PT parameters for rocks of deep crustal xenoliths: Palaeoproterozoic metagabbroanorthosite and mafic granulites from pipes of Kandalaksha Bay [Vetrin *et al.*, 2009]; Archaean granulites from pipes of Kaavi–Kuopio district [Hölttä *et al.*, 2000b] and Varpaisjärvi granulites [Hölttä *et al.*, 2000a].

Рис. 13. (a) Пространственная классификация термодинамических условий на уровне сейсмоплотностного раздела Мохо. (b) Положение групп точек пространственной классификации термодинамических условий на уровне сейсмоплотностного раздела Мохо на PT -диаграмме метаморфических фаций по [Peacock *et al.*, 1994]. (c) Увеличенный фрагмент PT -диаграммы.

1–6 – группы точек пространственной классификации термодинамических условий на уровне сейсмоплотностного раздела Мохо (пояснения в тексте). Оценки вариаций PT -параметров в породах глубинных коровых ксенолитов: палеопротерозойских метагаббро-анортозитов и мафитовых гранулитов из трубок Кандалакшского залива по [Vetrin *et al.*, 2009], архейских гранулитов из трубок района Каави-Куопио по [Hölttä *et al.*, 2000b]; то же для архейских гранулитов Варпаисъярви по [Hölttä *et al.*, 2000a].

distribution of the data points in space and in PT coordinates convincingly indicate that the revealed regularities are of real geological significance, as considered below in more details.

(1) Beneath the central part of the Karelian Craton to the north and northeast of the Moho depression, the velocity–density Moho discontinuity is characterized by the group 1 of data points (Fig. 13, *a*) corresponding to the most shallow and colder part of this discontinuity (Fig. 12). In the PT diagram, this group is represented by a compact swarm of points, which extends along the boundary between facies of lawsonite and epidote blue schists (Fig. 13, *b*). The swarm is bounded by $T=370\text{--}420\text{ }^{\circ}\text{C}$ and $P=1.08\text{--}1.30\text{ GPa}$, which correspond to the depth of Moho discontinuity from 36 to 45 km. The minimal depth of Moho discontinuity is established beneath the eastern Karelian Craton (Fig. 13, *a*).

(2) A relatively high-pressure deep linear swarm is represented in the PT diagram (Fig. 13, *b*) by groups 2 and 3, which occupy the field corresponding to $T=410\text{--}620\text{ }^{\circ}\text{C}$ and $P=1.3\text{--}1.8\text{ GPa}$ (45–60 km). Groups 2 and 3 characterize the maximal depth of Moho discontinuity (Fig. 12, *a*) related to plunging of the Svecofennian Orogen beneath the western margin of the Karelian Craton (Figs. 7, 10, 11). In the PT diagram, this swarm of points is subdivided into two clusters by the boundary of metamorphic eclogite facies at the level of $510\text{--}520\text{ }^{\circ}\text{C}$ and 1.55 GPa ($\sim 52\text{ km}$) (Fig. 13, *b*). The high-temperature and high-pressure part of the swarm is located in the field of eclogite facies and represented by group 2 in the diagram; it characterizes the deepest position of the velocity–density Moho discontinuity (52–60 km) (Fig. 12). The second part of the swarm is located in the region of lower temperature and pressure (group 3) and corresponds to facies of epidote blue schists; it characterizes a shallower and less heated part of the velocity–density Moho discontinuity which is located further northward (Fig. 12).

(3) Another high-temperature linear swarm of data points is represented in the PT diagram by group 4 (Fig. 13, *b*). It occupies the field corresponding to $T=530\text{--}600\text{ }^{\circ}\text{C}$ and $P=1.35\text{--}1.65\text{ GPa}$ (46–56 km), i.e. the field of eclogite metamorphic facies. The spatial position of the velocity–density Moho discontinuity characterized by this group of data points (Fig. 13, *a*) fits the southern slope of Moho depression (Fig. 8) distinguished by relatively high temperature values (Fig. 12).

To the south and southeast of this region, parameters of the velocity–density Moho discontinuity are characterized by compact group 5 of data points (Fig. 13, *a*). In the PT diagrams, this group makes up an isometric oval swarm of points bounded by $T=500\text{--}590\text{ }^{\circ}\text{C}$ and $P=1.18\text{--}1.39\text{ GPa}$ (41–47 km) in the boundary zone between eclogite and epidote-amphibolite facies (Fig. 13, *b*). In geological terms, this field charac-

terizes the Mid-Russia sector of the intracontinental Palaeoproterozoic collision orogen (Fig. 2, *b*) [Mints, 2007, 2011].

(4) Group 6 of data points occupies a special position in space. In the PT diagram, this swarm is represented by a wide belt of points in temperature and pressure ranges of $380\text{--}500\text{ }^{\circ}\text{C}$ and $1.00\text{--}1.38\text{ GPa}$, respectively, which corresponds to the field of epidote blue schists. The Moho discontinuity of this type underlies the northern part of the Karelian Craton and the Belomorian Province, as well as the region to the east of Moho depression (Fig. 13, *a*). The Archaean crust of these tectonic units underwent tectonic and thermal transformation in the Palaeoproterozoic [Bibikova et al., 2001; Mints et al., 2015].

8. DISCUSSION

The thermal and density models compared with the geological interpretation of the seismic CMP profiles allow us to provide further insight into the structure and physical parameters of the crust and the upper lithospheric mantle of the southeastern Fennoscandian Shield. The seismic sections along the CMP profiles show conventional character of subdivision of the continental crust into the upper, middle, and lower «layers» (Figs. 9–11). Nevertheless, these terms are still in use as being convenient for description of different levels of the crust.

In further discussion, we will focus on consideration of two regions contrasting in their structure and geological history, which are comprehensively presented by the proposed model, specifically the central and eastern parts of the Karelian Craton and the Svecofennian Orogen together with the adjacent margin of the Karelian Craton.

8.1. DENSITY HETEROGENEITY AND NATURE OF DENSITY LAYERING OF THE CRUST

According to the density model, the regional structure of the crust is determined largely by the nearly horizontal boundaries (Figs. 5–7, 9–11), which reflect gradient variations of rock densities with depth. The crustal layers bounded by isodensity surfaces are, as a rule, discordant with respect to the inclined boundaries of geological complexes in seismic images of the crust (Figs. 9–11). As noted above, the density heterogeneities (crustal layers) reveal only local and incomplete interrelations with localization and morphology of the geological bodies.

The isodensity contours in the crustal sections are oriented largely near-horizontally and approximately parallel to the present-day topography, and this is also valid for other Archaean terrestrial cratons [Abbott et

al., 2013]. It is evident that only the regional lithostatic pressure remains to be a crucial factor of variations in density of the rocks at the upper and middle crustal levels, where metamorphism is blocked by low temperature (~400 °C in the lower crust and no higher than 300 °C in the middle crust). Density is changing under the lithostatic pressure, while structure of the medium remains intact as formed earlier in the course of sedimentation, magmatic activity, metamorphism, and tectonic reworking. Local factors may include variable crustal and mantle heat flows [Glaznev, 2003; Glaznev *et al.*, 2004], zones of stress relaxation [Lyakhovskiy, Ben-Zion, 2009], and tectonic stresses resulting from interaction of density heterogeneities [Glaznev *et al.*, 1991; Rebetsky, 2007]. Rock density increases with increasing depth, while the density differentiation between rocks that differ in compositions is appreciably decreasing [Glaznev, 2003].

For long, it has been suggested that the increase in density of the continental crust with increasing depth is determined by variations in composition of the rocks. These ideas were highlighted by the assumption that «granitic» and «basaltic» geophysical layers are separated by Conrad surface in the crust [Conrad, 1925]. Despite the fact that conditionality of these terms was always emphasized afterward, the idea of density layering of the continental crust with direct change of its bulk composition has retained its appeal [Christensen, Mooney, 1995]. According to [Kuusisto *et al.*, 2006], the available information on the crust in the predominant part of the Fennoscandian Shield (including the data discussed in this paper) shows that the layers with different velocities participate in crustal complexes. In the model proposed by M. Kuusisto and co-authors, a contribution of mafic rocks increases with increasing depth; the upper crust consists primarily of gneisses in combination with granite and granodiorite; amphibolite and quartzite are subordinate in abundance; role of amphibolite increases in the middle crust.

We believe, however, that this model cannot represent the structure of the accretionary complex of the Svecofennian Orogen which comprises tectonic sheets plunging beneath the margin of the Karelian Craton and underlying the Archaean rocks of the craton over a significant distance (Fig. 9–11) hardly can be represented. On the contrary, it can be stated that quantitative ratios of different rocks in the plunging tectonic sheets do not undergo any systematic variations either in each particular sheet or in the accretionary ensemble as a whole.

The nature of rock compaction under lithostatic pressure, which is the most important factor determining the state of the continental crust, has been studied insufficiently so far. Since compaction of ancient rocks is controlled by the recent or close-to-recent state of

the crust at least for the upper and middle crust, metamorphism (often mentioned as a factor of compaction) should be excluded from the list of potential causes. Undoubtedly important factors are closure of fractures and pores and release of solutions and fluids contained therein. However, all by themselves, such factors are not able to provide for the observed compaction of rocks which is significantly exceeding the results of laboratory experiments on rock samples under elevated pressure (for example, from 2.80–2.85 to 3.0–3.1 g/cm³ in the case of sedimentary and volcanic rocks of the Svecofennian accretionary complex). It is also noteworthy that the discussed variation in density of rocks is apparently reversible, because the boundaries of the crustal layers with different densities, except for the uppermost ones, are not cut by the erosion topography features, and the density layering pattern is similar for young orogens, undergoing the stage of growth and intense denudation, and for equilibrated isostatic platform regions. Further studies are needed to clarify of the nature of global compaction of the crust.

8.2. NATURE OF THE LOWER CRUST, THE CRUST–MANTLE BOUNDARY AND THE VELOCITY–DENSITY MOHO DISCONTINUITY BENEATH THE KARELIAN CRATON

In seismic CMP sections, the lower crust is commonly identified with a reflectivity zone localized immediately above the crust–mantle boundary, in other words, with a zone of intense seismic reflections that occupy either the entire zone or its major part and depict an image of the layered lower crust [Mooney, Meissner, 1992]. Such a reflectivity zone (7–12 km thick) continuously underlies the Archaean crust in the eastern Fennoscandian Shield, including the Karelian and Kola Cratons and the Belomorian Province [Mints *et al.*, 2009; Mints, 2011].

In the region considered in this paper, the lower crust of this type is observed in the section along 4B profile (Fig. 9). The pattern of seismic reflections in this section demonstrates an almost horizontal smooth crust–mantle boundary lying at a depth of 37–39 km. In the major segment of 4B profile, the crust–mantle boundary practically coincides with the velocity–density Moho discontinuity (represented by the isodensity contour (surface) of 3.24 g/cm³) of the similar morphology. In the central part of the Karelian Craton, the Moho depth varies from 38 to 45 km (Fig. 12, *a*). Depths of 42–45 km, which are more significant than those in 4B profile, are characteristic of the Kianta and Iisalmi terranes in the western part of the craton. It should be noted that the depth of Moho in this region is 46–52 km according to the models described in [Tesauro *et al.*, 2008] and [Grad *et al.*, 2009] or 48–52 km according to [Kozlovskaya *et al.*, 2004]. Even a

greater depth of Moho discontinuity is suggested in [Silvennoinen et al., 2014]. At the Moho discontinuity of this type, temperature varies in a narrow range from 370 to 420 °C (Fig. 13, b, group 1), and such a variation is the lowest as compared to values for other Moho segments. These parameters are consistent with minimal values of heat flow (8 ± 10 mW/m²) which are typical of the studied region.

In the eastern Fennoscandian Shield, the lower crust (5–15 km thick) is bounded by the crust–mantle boundary of this type [Mints et al., 2009; Mints, 2011]. The increase in thickness of the lower crustal layer is related to hummocking (over- and underthrusting) of tectonic sheets at the crust bottom. In particular, a significant increase of the lower crust thickness (up to 20 km) is noted at the western and southwestern margins of the Karelian Craton along its boundary with the Svecofennian Orogen (Figs. 9, 10). In this region, the lower crustal layer is not only characterized by larger thickness values but is also uplifted due to the mutual over- and underthrusting of the rock complexes pertaining to the Karelian Craton and the Svecofennian Orogen. Two important features should be emphasized. First, the lower crustal layer is cut off by the Palaeoproterozoic volcanic–plutonic associations belonging to the Late Palaeoproterozoic Kainuu Belt. Second, this layer is underlain by tectonic sheets of the Svecofennian accretionary complex. The above implies that the lower crustal layer of the Karelian Craton was formed before the Late Palaeoproterozoic collisional events. Thus, the geological data and the seismic images show that formation of the lower crustal complex was related to under- and intraplating by mantle-derived mafic magmas in connection with development of the Palaeoproterozoic large igneous province in the eastern part of Fennoscandian Shield and the adjacent basement of the Russian Platform [Mints, 2011].

The lower crust and underlying upper mantle at the boundary between the Kola Craton and the Belomorian Province are cut through by the Devonian kimberlite and lamproite pipes and dikes outcropped at the coast and on islands of the Kandalaksha Bay (Fig. 2). Among lower crustal xenoliths, garnet granulite is dominant; it is identical to mafic granulites and metagabbro-anorthosites of the Lapland and Kolvitsa–Umba granulite-gneiss belts. Peak parameters of granulite-facies metamorphism of rocks from xenoliths are estimated at 800–950 °C and 14–18 kbar and correspond to depths from 50 to 70 km (Fig. 13, b) [Mints et al., 2007]. In the present-day structure, these rocks belong to the lower crust and occur at a depth of ~ 45 km [Mints et al., 2009]. Zircons from garnet granulite range in age from 2.84 to 0.26 Ga and are concentrated within four discrete time intervals as follows: Neoproterozoic (2.84–2.74 Ga), Palaeoproterozoic (2.47–2.41) and (1.83–1.75 Ga), and Palaeozoic (0.33–0.26) [Vetrin, 2006; Ve-

trin et al., 2009; Downes et al., 2002, and references therein]. These dates correspond to the main events in the long history of formation and transformation of the crust. The ages of Early Palaeoproterozoic zircons coincide with ages of the known manifestations of magmatism and high-temperature metamorphism of granulite and eclogite facies [Mints et al., 2007], which gave start for the Palaeoproterozoic evolution initiated by mantle plumes responsible for formation of the lower crustal «granulite–mafic» layer. A model of the «layered lower crust», that is formed under extension accompanied by sheetlike intrusions of mafic mantle-derived magma, is described in [Hollinger, Levander, 1994]. Similar conclusions concerning the origin of the lower crustal reflectivity zone are stated in [McBride et al., 2004; Meissner et al., 2006].

Thus, we have sufficient grounds to infer that the lower crust, underlying the Archaean Karelian Craton and represented by a reflectivity zone bounded by the smooth nearly horizontal crust–mantle boundary combined with the velocity–density Moho discontinuity of the first type, was formed in the Palaeoproterozoic as a result of tectonothermal and magmatic processes of plume type.

Correspondingly, the Archaean lithospheric mantle of the Karelian Craton was intensely transformed under the impact of the Palaeoproterozoic plumes. Minimal temperature values at the present-day Moho discontinuity indicate that the heat flow generated by this mantle is minimal too, which is believed typical of the domains of the Archaean consolidation [Nyblade, Pollack, 1993].

The crust of the western Karelian Craton in the Iisalmi terrane immediately bordering on the Svecofennian Orogen is also characterized by deep xenoliths carried up by the Late Neoproterozoic kimberlite pipes in the Kaavi–Kuopio area (Fig. 2). The kimberlite pipes are located between FIRE-1 and FIRE-3-3A seismic profiles. As can be seen from the section along FIRE-1 seismic profile, a reflectivity zone is absent at the base of the Iisalmi terrane (Fig. 10). The sole of the Archaean complex of rocks in this terrain is located at a depth of no more than 20 km. In the Kaavi–Kuopio area, the thickness of the lower crustal layer and depth of its sole are significantly reduced in comparison with those in the section along FIRE-1 profile. The Archaean crust is underlain by a thick (> 40 km) packet of tectonic sheets pertaining to the Svecofennian accretionary complex, which plunge eastward beneath the Karelian Craton. The high-density (up to 3.0–3.24 g/cm³) rocks at the base of the crust are conjugated with the Palaeoproterozoic rocks of this complex. Any reader can make the same conclusion by analyzing the geological map (Fig. 2) with respect to the geological sections along FIRE-1 and FIRE-3-3A seismic profiles (Figs. 10, 11).

Deep xenoliths are mainly composed of the Archaean and Palaeoproterozoic mafic granulites; the age of their protoliths reaches 3.7–3.5 Ga [Peltonen *et al.*, 2006]. Summing up geochronological data on granulites from xenoliths and the Varpaisjärvi Complex exposed nearby [Hölttä *et al.*, 2000a] shows that the age of Archaean granulite-facies metamorphism ranges from 2.7 to 2.6 Ga. The peak parameters of granulite-facies metamorphism estimated from the data on xenoliths are 800–930 °C and 8.4–12.5 kbar (depths of 30–45 km) [Hölttä *et al.*, 2000b]. For the Varpaisjärvi Complex, the peak parameters are 800–900 °C and 9–11 kbar (depths of 32–39 km) [Hölttä, Paavola, 2006]. An evidence for superposition of the Palaeoproterozoic granulite-facies metamorphism on the Archaean rocks of the Varpaisjärvi Complex in the time interval of 2.5–1.7 Ga was obtained only for xenoliths and was not supported by rocks from the Varpaisjärvi Complex [Hölttä *et al.*, 2000a; Peltonen *et al.*, 2006]. In addition, zircons younger 1.85 Ga, which crystallized under the thermal impact following the Svecofennian orogeny, were found in xenoliths.

It is quite evident that xenoliths of granulites from the Kaavi–Kuopio pipes and the Varpaisjärvi granulites belong to the same rock complex, which is occurring now at a relatively high level in the crust and at a significant distance from the crust–mantle boundary. Most likely, these xenoliths should be regarded as relics of the Neoarchaean lower crust rather than fragments of the recent lower crust as suggested in [Kuusisto *et al.*, 2006; Peltonen *et al.*, 2006].

8.3. NATURE OF THE LOWER CRUST, THE CRUSTAL–MANTLE BOUNDARY, AND THE VELOCITY–DENSITY MOHO DISCONTINUITY BENEATH THE ACCRETIONARY SVECOFENNIAN OROGEN

In the part of the Svecofennian Orogen, which is neighboring the Karelian Craton, the reflectivity zone is absent, while on the contrary, the lower crust is acoustically transparent and characterized by vaguely oriented dispersed reflections. In [Korsman *et al.*, 1999], based on seismic wave velocities, the lower crustal complex is represented by the layer with P-wave velocities ranging from 7.0 to 7.45 km/s, which is presumably composed of anorthosites, mafic and metapelitic granulites, and pyroxenite in the highest-velocity areas. According to calculations based on the model proposed in [Kuusisto *et al.*, 2006], the upper part of the lower crust (25–40 km) consists of tonalitic gneiss, amphibolite, mafic garnet granulite and pyroxenite, whereas the lower part of the lower crust is mainly composed of hornblendite, mafic garnet granulite, pyroxenite and mafic eclogite. The authors find a confirmation of their model in the fact that all the above-mentioned rocks, except for eclogite, are identified

among deep xenoliths in the Kaavi–Kuopio kimberlite pipes. In our turn, we have to remind that in the preceding section we have tried to show that it is hardly valid to compare the recent high-velocity lower crust with these xenoliths.

In [Lahtinen *et al.*, 2009], based on paleogeodynamic reconstruction of the Svecofennian Orogen's history, it is assumed that the acoustically transparent region in the lower part of the crust, which is separated by a diffuse boundary from the accretionary complex (Fig. 10, 11), is primarily composed of mafic granulites, formerly making up a hypothetical Keitele microcontinent, which fragments remain unidentified at the surface. A smaller part of this region is occupied by the oceanic crust that was also metamorphosed under conditions of granulite facies. The inferred situation is comparable with the section of the Trans-Hudson Orogen in North America, where the Archaean crust of the Sask Craton is overlapped almost entirely by tectonic nappes of island-arc complexes [Baird *et al.*, 1996; Hammer *et al.*, 2010]. However, the rocks of the Sask Craton are rarely found at the present-day surface; in the seismic section, such rocks are characterized by a complex reflection pattern inherent to the Archaean granite–greenstone domains down to the crust–mantle boundary coinciding with Moho discontinuity.

In our view, the structure of the crust established by geological mapping and recorded in the seismic images is a crucial evidence for reconstruction of the lower crust in the Svecofennian Orogen. The ensemble of the inclined tectonic sheets playing the determinant role in structure of the Svecofennian Orogen is limited from below by the uneven boundary that is serrate in many cases. When approaching the mantle, the image of the sheets becomes diffuse and disappears (as if the sheets are dissolved in the mantle), and the serrate shape of the boundary is generally diffusive. In agreement with the above observations, the calculations of the lower crust and upper mantle densities do not show any significant jump of density at the crust–mantle transition. The same was emphasized in [Kuusisto *et al.*, 2006].

The Moho discontinuity at the base of Svecofennian Orogen is classified into two subtypes that are distinctly separated in both the *PT* plot and the geological space. The minimal depth of Moho is estimated at 45 km for both subtypes, wherein the difference in temperature is 90 °C. Obviously, the two subtypes are represented by two independent packets of tectonic sheets that plunge (subduct) eastward beneath the Archaean crust of the Karelian Craton (Fig. 13, *a*). It is also evident that the mantle domains directly underlying these ensembles are characterized by different heat flow values. At a depth of 45 km, the temperature of 410 °C is typical of the colder subtype, whereas 500 °C is typical of the warmer subtype. At a maximal depth

(~60 km), the temperature is estimated at 600–630 °C for both subtypes. The Moho of the hot packet entirely falls in the *PT* field of eclogitic facies, whereas beneath the colder subtype, the Moho is split approximately in twain by the boundary of *PT* field of eclogitic facies: the deeper and more heated part of the Moho surface is characterized by temperature and pressure of eclogite facies, while the other half is under conditions of epidote blue schists (Fig. 13, *b*).

Considering high densities of rocks in the lower crust and the underlying mantle along with the diffusive boundary between them, there are grounds to suggest that similar high-density eclogites participate in either of them.

The limits of corresponding parts of the Moho surface projected on the surface show boundaries of the plunging packets of tectonic sheets. Judging by the configuration of the boundaries, the packets are separated by a transform fault zone striking in the SE direction (Fig. 13, *a*). The width of the northern colder packet amounts to 250 km. The width of the southern warmer packet exceeds 100 km. The maximal depth of the velocity–density Moho discontinuity is somewhat greater than 60 km.

It is noteworthy that the contours of the plunging tectonic ensembles are advanced far away from the boundary between the Svecofennian Orogen and the Karelian Craton, which is observed at the surface. This fact is fully in accordance with the suggested subduction of island-arc, backarc, and interarc basins of the Svecofennian Orogen beneath the margin of the Karelian Craton. It should be specially noted that in regard to subduction, both methods based on refraction and reflection seismic profiling have given strikingly consistent results.

Generally, one of the most plausible scenarios of the Moho discontinuity formation is represented by the model of the crust–mantle boundary assuming transformation of the lower crustal rocks, largely gabbro and basalt (density of 2.8–3.2 g/cm³) into eclogite (3.3–3.7 g/cm³), as reviewed in [Mjelde et al., 2013]. The model envisages that the Moho boundary separates differently metamorphosed mafic rocks, and eclogites, being the crustal rocks by their chemical composition, are referred to as the mantle rocks by their elastic properties. As a rule, the gabbro–eclogite model of Moho discontinuity is considered in specific geodynamic settings, including continental domains and rift zones, suture zones, and bottom of high-pressure granulite complexes [Mareschal et al., 1982; Brown, 2009; Mjelde et al., 2013].

It has been repeatedly noted that the reflection packets plunging into the mantle (similar to those observed along FIRE-1 and FIRE-3-3A profiles, see Figs. 10 and 11) are intersected by Moho discontinuity. This specific feature of the Moho boundary was noted in

studies of the Palaeoproterozoic structural units of the Bothnian Bay along BABEL profile [BABEL Working Group, 1990] and the Trans-Hudson Orogen along COCORP profiles [Baird et al., 1995, 1996], and interpreted as a result of a supra-regional mantle event that occurred after formation of the collision orogen. A partial removal of the eclogitized keel is commonly explained by its subsequent delamination and subsidence into the mantle.

The thorough study of deep xenoliths in the Late Neoproterozoic kimberlite (500–600 Ma) from the Kaavi–Kuopio pipes, however, did not reveal any fragments of crustal eclogites [Peltonen et al., 2006]. This fact can be interpreted equivocally. According to the model described in [Kukkonen et al., 2008], eclogites were formed at the base of the Late Palaeoproterozoic Svecofennian accretionary complex during subduction and collision with the Karelian Craton. Later on, the lower crust of accretionary complex was subject to delamination; the majority of fragments of the eclogite layer subsided into the mantle, while others were partly disintegrated and thus ‘missed’ when xenoliths were trapped by the kimberlitic magma. Alternatively, it can be assumed that the lower crust and upper mantle were devoid of eclogites during the period of kimberlite magmatism.

Based on our results of complex 3D simulation, we can pioneer in characterizing the temperature distribution pattern along the Moho surface at the bottom of the crust in the Svecofennian Orogen, including the region of its plunging beneath the continental margin of Karelian Craton. The results of computation (Figs. 12, 13) indicate that the boundary of thermodynamic conditions corresponding to eclogite facies is approximately coincident with the present-day position of the crust–mantle boundary in the Moho depression. Therefore, it can be concluded that eclogite-facies metamorphism may be related to the recent thermal state of the regional lithosphere. At the same time, it should be kept in mind that in the absence of fluid, these conditions are insufficient for the metamorphic reactions to proceed. With account of the fact that the eclogitic model provides explanations for both the high density of the lower crust composed of the accretionary complex, and the diffuse character of the boundaries between the accretionary complex, the lower crust and the mantle, such a model seems quite plausible, yet remains hypothetical. Moreover, differences in the mantle heat flows in the two separate parts of the accretionary complex give evidence in favor of the eclogitic model of the lower crust of the Svecofennian Orogen.

Thus, the complex geophysical 3D model discussed in this paper allows us to suggest that transformation of the volcanic and sedimentary rocks of the lower part of the accretionary complex into eclogites have taken

place in the recent or relatively recent past. In terms of this interpretation, the upper part of the nonuniformly eclogitized rock sequence is represented by acoustically translucent high-velocity and high-density rocks that are regarded as the lower crust, whereas its denser bottom part of the lower crust with predominant eclogite-facies rocks is pertaining to the mantle.

Taking into account the technique of model calculations, it can be assumed that variations in temperature at the level of the velocity–density Moho discontinuity are directly dependent on variations in heat flow from the underlying mantle. With account of specific features of the geological history of the region, it can be suggested that the mantle underlying the Karelian Craton beyond the boundary zone with the Svecofennian Orogen had originated during growth of the continental «nucleus». It was transformed by subduction 3.0–2.8 Ga ago (which has not been reliably characterized yet), modified by high-temperature mantle plumes about 2.7 Ga ago and minimum twice (2.5–2.3 and 2.2–1.8 Ga) in the Palaeoproterozoic.

The mantle underlying the Svecofennian Orogen and its boundary zone with the Karelian Craton was formed at the end of the Palaeoproterozoic during subduction and accretion of island-arc complexes and rocks of back-arc basins. It is evident that this mantle differs from the mantle of the Karelian Craton. Judging by the higher heat flow, the content of heat-generating radioactive elements in the Svecofennian mantle is higher than that in the mantle underlying the Karelian Craton. It is noteworthy that the specific features of the model provide for identification of local differences in heat generation in various part of the Svecofennian mantle.

9. CONCLUSION

The paper presents results of complex geophysical 3D modelling of the Earth's crust in the Karelian Craton and adjacent regions in the southeastern Fennoscandian Shield. The model is developed with the use of complex inversion of the geophysical data based on the stochastic description of interrelated physical properties of the medium, including density, P-wave velocity and heat generation. For the studied region, the model provides the most comprehensive characteristics of the crust and the upper part of the lithospheric mantle for the Archaean Karelian Craton and Late Palaeoproterozoic Svecofennian Orogen.

The model analyses provide for transition from the averaged characteristics of the temperature field at the Moho that is variable in depth to the 3D representation of temperature variations therein. This, in turn, allows us to characterize regularities in temperature variations at the Moho, separately reconstruct the nature of

the Moho for different tectonic units, estimate variations of the mantle heat flow, and consider geodynamic and tectonic causes of the variations.

Based on results of our studies, we make a number of important conclusions concerning both regional and fundamental problems of deep structure of the Precambrian lithosphere:

(1) The seismic–geological models of the crust and the upper mantle, which are based on the results of geological mapping and interpretation of the seismic reflection patterns, demonstrate associations of geological bodies differing in morphology, such as inclined and horizontal layers and tectonic sheets, as well as nearly isometric bodies. The velocity and density models, that are developed by methods of refraction seismic profiling in combination with gravity measurements, demonstrate near-horizontal layering of the geological medium, which formation is directly related to the recent state of the crust, including distribution of lithostatic loading, heat flow, tectonic stresses etc.

(2) Due to lithostatic loading through geological time, rock density progressively increases with depth. Rock density variability decreases with compaction. A high level of rock compaction cannot be explained by 'simple' concepts of metamorphism and/or rock compaction, which are based on results of laboratory studies of samples and relevant computer models. This implies the existence of additional vigorous mechanisms providing for reversible alteration of rocks.

The detailed pattern of density layering indicates displacements in the crust, which deform isodensity surfaces, including the surface of the velocity–density Moho discontinuity. Stepwise bends of the isodensity surfaces are distinctly related to the previously formed zones of tectonic deformations. These bends apparently arose after termination of lithostatic compaction of rocks. The arrangement of dislocations shows that relaxation of recent stresses in the crust occurs as a result of remobilization of older tectonic zones.

(3) Considering the structural–geological and thermodynamic characteristics of the geological boundary between the crust and the mantle and those of the velocity–density Moho discontinuity at the base of the Archaean Karelian Craton and the Palaeoproterozoic accretionary complex of the Svecofennian Orogen, it is revealed that such characteristics are variable, and their spatial relationships differ significantly.

(3.1) The Archaean crust of the Karelian Craton is underlain by the Palaeoproterozoic lower crustal complex of the mantle-plume origin. This complex consists of the Archaean and Palaeoproterozoic mafic intrusive rocks and gabbroanorthosites metamorphosed in the Palaeoproterozoic under granulite-facies conditions. The reflectivity zone corresponding to this complex is separated from the mantle by the near-horizontal flat boundary that is distinctly expressed in the pattern of

seismic reflections. By its position in the section, the crust–mantle boundary is partly coincident with the velocity–density Moho discontinuity; both boundaries are morphologically similar. The depth of the crust–mantle boundary along 4B seismic profile is 38–39 km and varies elsewhere within a relatively narrow interval (38–45 km). Temperatures at the Moho (370 °C and 410 °C at the depth of 38 km and 45 km, respectively) are the lowest in the studied region.

(3.2) In the pattern of seismic reflections, the Late Palaeoproterozoic accretionary complex of the Svecofennian Orogen is separated from the mantle by a wide translucent domain. According to its density of 3.0–3.24 g/cm³, this domain is regarded as the lower crust, which is separated from the ensemble of inclined tectonic sheets and, from below, from the mantle by the diffuse transitional zone with serrate outlines. The velocity–density Moho discontinuity is generally following the morphology of the crust–mantle boundary in a smoothed form.

(3.3) The well-known «Moho depression» corresponds to the area of subsidence of the Svecofennian accretionary complex in the boundary zone with the Karelian Craton and further beneath its margin. In this area, the accretionary complex comprises two packets of tectonic sheets that are plunging to the east and divided by the SE-trending transform strike-slip fault. The width of the northern packet is 250 km; the width of the southern packet exceeds 100 km. The depth of the velocity–density Moho discontinuity varies from 45 to 60 km in the region of plunging of both packets. The contours of plunging tectonic ensembles advance far to the east relative to the boundary between Svecofennian Orogen and Karelian Craton, and this fact is fully compliant with the concept assuming subduction of the island-arc, back-arc, and inter-arc basins of the Svecofennian Orogen beneath the margin of the Karelian Craton. In regard to evidences of Svecofennian subduction, both methods based on refraction and reflection seismic profiling have given strikingly consistent results.

(3.4) The complex geophysical model of the geological medium reveals fine temperature distinctions for the identified packets of tectonic sheets at the level of the velocity–density Moho discontinuity. At a depth of 45 km, temperatures of 410 °C and 500 °C correspond to the colder and warmer packets, respectively. At the maximal depth for both packets, temperatures amount to 600–630 °C. The relationships between temperature and pressure at the Moho and the lack of eclogites among deep xenoliths in the Late Neoproterozoic kimberlite pipes allow us to suggest a recent age of transformation of volcanic–sedimentary rocks into eclogites in the lower part of accretionary complex. The upper part of the sequence of nonuniformly eclogitized rocks can be regarded as the lower crust, whereas its denser

bottom part with predominant eclogite-facies rocks is pertaining to the mantle.

Based on the complex geophysical simulation results and geological interpretation of the obtained 3D model of the crust and the upper mantle in the south-eastern Fennoscandian Shield, we arrive at conclusions of the supraregional level:

- Near-horizontal density layering of the continental crust is superposed on the older geological structure, and the features of such layering are primarily controlled by the recent and near-recent state of the crust and may be disturbed by the youngest deformations;

- Fine temperature variations at Moho discontinuity are determined by local variations of heat generation in the mantle, which, in turn, are related to local features of its origin and transformation;

- Interpretations of the lower continental crust as a «reflectivity zone» and as a layer of high density are not completely equivalent. The lower crust occurs everywhere as the deepest and densest element of near-horizontal density layering of the continental crust; within its limits, the degree of compaction can cardinaly differ from laboratory estimates based on relationships between rock composition, density and velocity. Conversely, the seismic image of the reflectivity zone is related to quite definite geological phenomena, that are more or less constrained in space, i.e. mainly to magmatic under- and intraplate under conditions of extensional rifting and ascent of mantle plumes, which form the lower crust of granulite–basic type;

- Rocks of platform domains can be transformed into eclogites at certain combinations of the crust thickness and temperature regime at the level of Moho discontinuity. In this case, the crust–mantle boundary is determined by quantitative proportions of rocks that underwent eclogitization or remained unchanged with corresponding shifts of density and velocity;

- A high level of rock compaction in the crust under lithostatic loading cannot be explained in terms of «simple» concepts of metamorphism and/or rock compaction, which are based on results of laboratory studies of samples and relevant computer models. This implies the existence of very powerful additional mechanisms providing for reversible alteration of rocks. Special studies are needed to clarify their nature.

10. ACKNOWLEDGEMENTS

This study was supported by the Russian Foundation for Basic Research (Projects Nos. 11-05-00110, 11-05-00492 and 15-05-01214) and the Division of Earth Sciences, Russian Academy of Sciences (Program No. 6). The authors thank Victor Popov and Olga Baksheeva who translated the manuscript in English.

11. REFERENCES

- Abbott D.H., Mooney W.D., Van Tongeren J.A., 2013. The character of the Moho and lower crust within Archean cratons and the tectonic implications. *Tectonophysics* 609, 690–705. <http://dx.doi.org/10.1016/j.tecto.2013.09.014>.
- Abramovitz T., Thybo H., Berthelsen A., 1997. Proterozoic sutures and terranes in the southeastern Baltic Shield interpreted from BABEL deep seismic data. *Tectonophysics* 270 (3–4), 259–277. [http://dx.doi.org/10.1016/S0040-1951\(96\)00213-2](http://dx.doi.org/10.1016/S0040-1951(96)00213-2).
- Aleksidze M.A., 1987. Approximate Methods of Solution of Direct and Inverse Gravimetric Problems. Nauka, Moscow, 336 p. (in Russian) [Алекси́дзе М.А. Приближенные методы решения прямых и обратных задач гравиметрии. М.: Наука, 1987. 336 с.].
- Artemieva I.M., Thybo H., Kaban M.K., 2006. Deep Europe today: geophysical synthesis of the upper mantle structure and lithospheric processes over 3.5 Ga. In: D.G. Gee, R.A. Stephenson (Eds.), European lithosphere dynamics. Geological Society London Memoirs, vol. 32, p. 11–41. <http://dx.doi.org/10.1144/GSL.MEM.2006.032.01.02>
- BABEL Working Group, 1990. Evidence for early Proterozoic plate tectonics from seismic reflection profiles in the Baltic shield. *Nature* 348 (6296), 34–38. <http://dx.doi.org/10.1038/348034a0>.
- BABEL Working Group, 1993. Deep seismic reflection/refraction interpretation of crustal structure along BABEL profiles A and B in the Southern Baltic Sea. *Geophysical Journal International* 112 (3), 325–343. <http://dx.doi.org/10.1111/j.1365-246X.1993.tb01173.x>.
- Baird D.J., Knapp J.H., Steer D.N., Brown L.D., Nelson K.D., 1995. Upper mantle reflectivity beneath the Williston basin, phase-change Moho and the origin of intracratonic basins. *Geology* 23 (5), 431–434. [http://dx.doi.org/10.1130/0091-7613\(1995\)023<0431:UMRBTW>2.3.CO;2](http://dx.doi.org/10.1130/0091-7613(1995)023<0431:UMRBTW>2.3.CO;2).
- Baird D.J., Nelson K.D., Knapp J.H., Walters J.J., Brown L.D., 1996. Crustal structure and evolution of the Trans-Hudson orogen: Results from seismic reflection profiling. *Tectonics* 15 (2), 416–426. <http://dx.doi.org/10.1029/95TC02425>.
- Balling N., 1995. Heat flow and thermal structure of the lithosphere across the Baltic Shield and northern Tornquist Zone. *Tectonophysics* 244 (1–3), 13–50. [http://dx.doi.org/10.1016/0040-1951\(94\)00215-U](http://dx.doi.org/10.1016/0040-1951(94)00215-U).
- Barton P.J., 1986. The relationship between seismic velocity and density in the continental crust – a useful constraint? *Geophysical Journal of the Royal Astronomical Society* 87 (1), 195–208. <http://dx.doi.org/10.1111/j.1365-246X.1986.tb04553.x>.
- Berzin R.G., Yurov Y.G., Pavlenkova N.I., 2002. CDP and DSS data along the Uchta–Kem profile (the Baltic Shield). *Tectonophysics* 355 (1–4), 187–200. [http://dx.doi.org/10.1016/S0040-1951\(02\)00141-5](http://dx.doi.org/10.1016/S0040-1951(02)00141-5).
- Bibikova E., Skiöld T., Bogdanova S., Gorbatshev R., Slabunov A., 2001. Titanite-rutile thermochronometry across the boundary between the Archaean Craton in Karelia and the Belomorian Mobile Belt, eastern Baltic Shield. *Precambrian Research* 105 (2–4), 315–330. [http://dx.doi.org/10.1016/S0301-9268\(00\)00117-0](http://dx.doi.org/10.1016/S0301-9268(00)00117-0).
- Birch F., 1961. The velocity of compressional waves in rocks to 10 kilobars: 2. *Journal of Geophysical Research* 66 (7), 2199–2224. <http://dx.doi.org/10.1029/JZ066i007p02199>.
- Braile L.W., Chiang C.S., 1986. The Continental Mohorovičić Discontinuity: Results from Near-Vertical and Wide-Angle Seismic Reflection Studies. In: M. Barazangi, L. Brown (Eds.), Reflection seismology: a global perspective. AGU Geodynamics Series, vol. 13, p. 257–272.
- Brown M., 2009. Metamorphic patterns in orogenic systems and the geological record. In: P.A. Cawood, A. Kröner (Eds.), Earth accretionary systems in space and time. Geological Society London Special Publications, vol. 318, p. 37–74. <http://dx.doi.org/doi:10.1144/SP318.2>.
- Buyanov A.F., Glaznev V.N., Mitrofanov F.P., Raevsky A.B., 1995. Three-dimensional modelling of the Lapland Granulite Belt and adjacent structures of the Baltic Shield from geophysical data. In: D. Roberts, N. Nordgulen (Eds.), Geology of the eastern Finnmark – western Kola peninsula region. Geological Survey of Norway, Special Publication, vol. 7, p. 167–178.
- Buyanov A.F., Glaznev V.N., Raevsky A.B., Skopenko G.B., 1989. Integrated interpretation of gravity, seismic and geothermal data. *Geofizicheskiy Zhurnal (Geophysical Journal)* 11 (2), 30–39 (in Russian) [Буянов А.Ф., Глазнев В.Н., Раевский А.Б., Скопенко Г.Б. Комплексная интерпретация данных гравиметрии, сейсмометрии и геотермии // Геофизический журнал. 1989. Т. 11. № 2. С. 30–39].
- Carbonell R., Levander A., Kind R., 2013. The Mohorovičić discontinuity beneath the continental crust: An overview of seismic constraints. *Tectonophysics* 609, 353–376. <http://dx.doi.org/10.1016/j.tecto.2013.08.037>.
- Christensen N.I., Mooney W.D., 1995. Seismic velocity structure and composition of the continental crust: A global view. *Journal of Geophysical Research* 100 (B6), 9761–9788. <http://dx.doi.org/10.1029/95JB00259>.
- Conrad V., 1925. Laufzeitkurven des Tauernbebens vom 28. November, 1923. Mitteilungen der Erdbeben-Kommission der Akademie der Wissenschaften in Wien, Neue Folge, 59 p.
- Cook F.A., White D.J., Jones A.G., Eaton D.W.S., Hall J., Clowes R.M., 2010. How the crust meets the mantle: Lithoprobe perspectives on the Mohorovičić discontinuity and crust–mantle transition. *Canadian Journal of Earth Sciences* 47 (4), 315–351. <http://dx.doi.org/10.1139/E09-076>.

- Dolgal A.S., 2002. Computer Technology of Gravity and Magnetic Surveys Data Processing and Interpretation in Mountainous Areas. Mart Publishing House, Abakan, 187 p. (in Russian) [Долгаль А.С. Компьютерные технологии обработки и интерпретации данных гравиметрической и магнитной съемок в горной местности. Абакан: ООО "Фирма Март", 2002. 188 с.].
- Downes H., Peltonen P., Mänttari I., Sharkov E.V., 2002. Proterozoic zircon ages from crustal granulite xenoliths, Kola Peninsula, Russia: evidence for crustal growth and reworking. *Journal of the Geological Society, London* 159 (5), 485–488. <http://dx.doi.org/doi:10.1144/0016-764901-162>.
- Galitchanina L.D., Glaznev V.N., Mitrofanov F.P., Olesen O., Henkel H., 1995. Surface density characteristics of the Baltic Shield and adjacent territories. In: D. Roberts, N. Nordgulen (Eds.), *Geology of the Eastern Finnmark–Western Kola Peninsula Region*. Geological Survey of Norway, Special Publication, vol. 7, p. 349–354.
- Glaznev V.N., 1987. About one approach to construction of a consistent model of the Earth's crust. In: V.I. Starostenko (Ed.), *Studies of the lithosphere by geophysical methods*. Naukova Dumka, Kiev, p. 228–235 (in Russian) [Глазнев В.Н. Об одном подходе к построению согласованной модели земной коры // Изучение литосферы геофизическими методами / Ред. В.И. Старостенко. Киев: Наукова думка, 1987. С. 228–235].
- Glaznev V.N., 1999. Evaluation of the limits of applicability of stochastic models of potential fields. *Vestnik VSU, Seriya Geologiya (Bulletin of Voronezh State University, Geology Series)* (8), 153–156 (in Russian) [Глазнев В.Н. Оценка границ применимости стохастических моделей потенциальных полей // Вестник Воронежского государственного университета, серия Геология. 1999. № 8. С. 153–156].
- Glaznev V.N., 2003. *Complex Geophysical Models of the Fennoscandian Lithosphere*. K&M Publishing House, Apatity, 252 p. (in Russian) [Глазнев В.Н. Комплексные геофизические модели литосферы Фенноскандии. Апатиты: Каэм, 2003. 252 с.].
- Glaznev V.N., Kukkonen I.T., Raevsky A.B., Ekkinen J., 2004. New data on thermal flow in the central part of the Kola Peninsula. *Doklady Earth Sciences* 396 (4), 512–514.
- Glaznev V.N., Raevsky A.B., 1991. About the decision of direct tasks of gravimetry on the spherical Earth for gradient-layered models. In: N.V. Sharov, V.A. Glebovitskiy (Eds.), *Problems of integrated interpretation of geological and geophysical data*. Nauka, Leningrad, p. 183–188 (in Russian) [Глазнев В.Н., Раевский А.Б. О решении прямой задачи гравиметрии на сфере для градиентно-слоистых моделей среды // Проблемы комплексной интерпретации геолого-геофизических данных / Ред. Н.В. Шаров, В.А. Глебовицкий. Л.: Наука, 1991. С. 183–188].
- Glaznev V.N., Raevsky A.B., Sharov N.V., 1989. A model of the deep structure of the north-eastern part of the Baltic Shield based on joint interpretation of seismic, gravity, magnetic and heat flow data. *Tectonophysics* 162 (1–2), 151–164. [http://dx.doi.org/10.1016/0040-1951\(89\)90361-2](http://dx.doi.org/10.1016/0040-1951(89)90361-2).
- Glaznev V.N., Raevsky A.B., Skopenko G.B., 1996. A three-dimensional integrated density and thermal model of the Fennoscandian lithosphere. *Tectonophysics* 258 (1–4), 15–33. [http://dx.doi.org/10.1016/0040-1951\(95\)00147-6](http://dx.doi.org/10.1016/0040-1951(95)00147-6).
- Glaznev V.N., Skopenko G.B., 1991. Thermal model of lithosphere along the European geotranssect 3. In: U.I. Moiseenko, V.V. Gordienko (Eds.), *Geothermal models of geological structures*. VSEGEI, St. Petersburg, p. 25–31 (in Russian) [Глазнев В.Н., Скопенко Г.Б. Термическая модель литосферы вдоль европейского геотрансекта 3 // Гео-термические модели геологических структур / Ред. У.И. Моисеенко, В.В. Гордиенко. СПб.: ВСЕГЕИ, 1991. С. 25–31].
- Glaznev V., Skopenko G., Smolyaninova E., Lyakhovsky V., 1991. Complex geophysical model of the crust for the Baltic profile. Institute of Seismology University of Helsinki, Report S-25, 107–113.
- Glaznev V.N., Zhironova A.M., Raevsky A.B., 2008. New data on the deep structure of the Khibiny and Lovozero massifs, Kola Peninsula. *Doklady Earth Sciences* 422 (1), 1150–1152. <http://dx.doi.org/10.1134/S1028334X08070349>.
- Golizdra G.J., 1988. *Complex Interpretation of Geophysical Fields in Studying of Deep Structure of the Earth's Crust*. Nedra, Moscow, 212 p. (in Russian) [Голыздра Г.Я. Комплексная интерпретация геофизических полей при изучении глубинного строения земной коры. М.: Недра, 1988. 212 с.].
- Grad M., Tiira T., ESC Working Group., 2009. The Moho depth map of the European Plate. *Geophysical Journal International* 176 (1), 279–292. <http://dx.doi.org/10.1111/j.1365-246X.2008.03919.x>.
- Hammer P.T.C., Clowes R.M., Cook F.A., Van der Velden A.J., Vasudevan K., 2010. The lithoprobe trans-continental lithospheric cross sections: imaging the internal structure of the North American continent. *Canadian Journal Earth Sciences* 47 (5), 821–857. <http://dx.doi.org/10.1139/E10-036>.
- Holbrook W.S., Purdy G.M., Collins J.A., Sheridan R.E., Musser D.L., Glover L., Talwani M., Ewing J.I., Hawman R., Smithson S.B., 1992. Deep velocity structure of rifted continental crust, U.S. Mid-Atlantic Margin, from wide-angle reflection / refraction data. *Geophysical Research Letters* 19 (16), 1699–1702. <http://dx.doi.org/10.1029/92GL01799>.
- Holliger K., Levander A., 1994. Lower crustal reflectivity modeled by rheological controls on mafic intrusions. *Geology* 22 (4), 367–370. [http://dx.doi.org/10.1130/0091-7613\(1994\)022<0367:LCRMBR>2.3.CO;2](http://dx.doi.org/10.1130/0091-7613(1994)022<0367:LCRMBR>2.3.CO;2).
- Hölttä P., Huhma H., Mänttari I., Paavola J., 2000a. P-T-t development of Archaean granulites in Varpaisjärvi area, Central Finland. II. Dating of high-grade metamorphism with the U-Pb and Sm-Nd methods. *Lithos* 50 (1–3), 121–136. [http://dx.doi.org/10.1016/S0024-4937\(99\)00055-9](http://dx.doi.org/10.1016/S0024-4937(99)00055-9).

- Hölttä P., Huhma H., Mänttari I., Peltonen P., Juhanaja J., 2000b. Petrology and geochemistry of mafic granulite xenoliths from the Lahtojoki kimberlite pipe, eastern Finland. *Lithos* 51 (1–2), 109–133. [http://dx.doi.org/10.1016/S0024-4937\(99\)00077-8](http://dx.doi.org/10.1016/S0024-4937(99)00077-8).
- Hölttä P., Paavola J., 2000. P-T-t development of Archaean granulites in Varpaisjärvi area, Central Finland. I. Effects of multiple metamorphism on the reaction history of mafic rocks. *Lithos* 50 (1–3), 97–120. [http://dx.doi.org/10.1016/S0024-4937\(99\)00056-0](http://dx.doi.org/10.1016/S0024-4937(99)00056-0).
- Ivakhnenko A.G., Yurachkovsky J.P., 1987. Modeling of Complex Systems by Experimental Data. Radio i Svyaz Publishing House, Moscow, 120 p. (in Russian) [Ивахненко А.Г., Юрачковский Ю.П. Моделирование сложных систем по экспериментальным данным. М.: Радио и связь, 1987. 120 с.].
- Kartvelishvili K.M., 1983. Planetary Density Model and the Normal Gravitational Field of the Earth. Nauka, Moscow, 93 p. (in Russian) [Картвелишвили К.М. Планетарная плотностная модель и нормальное гравитационное поле Земли. М.: Наука, 1983. 93 с.].
- Kempton P.D., Downes H., Neymark L.A., Warty J.A., Zartman R.E., Sharkov E.V., 2001. Garnet granulite xenoliths from the northern Baltic Shield – the underplated lower crust of a Paleoproterozoic large igneous province? *Journal of Petrology* 42 (4), 731–763. <http://dx.doi.org/10.1093/petrology/42.4.731>.
- Kobrunov A.I., 1982. About best value solutions to the inverse problem of gravity. *Izvestiya AN SSSR, Seriya Fizika Zemli* (2), 100–107 (in Russian) [Кобрунов А.И. О классах оптимальности решений обратной задачи гравиразведки // Известия АН СССР, серия Физика Земли. 1982. № 2. С. 100–107].
- Kobrunov A.I., 2008. Mathematical Foundations of the Theory of Interpretation of Geophysical Data. ChentrLitNeftGaz Publishing House, Moscow, 288 p. (in Russian) [Кобрунов А.И. Математические основы теории интерпретации геофизических данных. М.: ЦентрЛитНефтеГаз, 2008. 286 с.].
- Kontinen A., Paavola J., 2006. A preliminary model of the crustal structure of the eastern Finland Archaean complex between Vartiuss and Vieremä, based on constraints from surface geology and FIRE 1 seismic survey. In: I.T. Kukkonen, R. Lahtinen (Eds.), Finnish Reflection Experiment FIRE 2001–2005. Geological Survey of Finland Special Paper, vol. 43, p. 223–240.
- Korja A., Lahtinen R., Heikkinen P., Kukkonen I.N., and FIRE Working Group, 2006. A geological interpretation of the upper crust along FIRE-1. In: I.T. Kukkonen, R. Lahtinen (Eds.), Finnish Reflection Experiment FIRE 2001–2005. Geological Survey of Finland Special Paper, vol. 43, p. 45–76.
- Korsman K., Korja T., Pajunen M., Virransalo P., GGT/SVEKA Working Group, 1999. The GGT/SVEKA transect: structure and evolution of the continental crust in the Palaeoproterozoic Svecofennian orogen in Finland. *International Geology Review* 41 (4), 287–333. <http://dx.doi.org/10.1080/00206819909465144>.
- Kozlovskaya E., Elo S., Hjelt S.-E., Yliniemi J., Pirttijärvi M., SVEKALAPKO Seismic Tomography Working Group, 2004. 3-D density model of the crust of southern and central Finland obtained from joint interpretation of the SVEKALAPKO crustal P-wave velocity models and gravity data. *Geophysical Journal International* 158 (3), 827–848. <http://dx.doi.org/10.1111/j.1365-246X.2004.02363.x>.
- Kukkonen I.T., Gosnold W.D., Šafanda J., 1998. Anomalously low heat flow density in eastern Karelia, Baltic Shield: a possible palaeoclimatic signature. *Tectonophysics* 291 (1–4), 235–249. [http://dx.doi.org/10.1016/S0040-1951\(98\)00043-2](http://dx.doi.org/10.1016/S0040-1951(98)00043-2).
- Kukkonen I.T., Kuusisto M., Lehtonen M., Peltonen P., 2008. Layering of eclogitized lower crust: Control on the crust–mantle boundary in the central Fennoscandian shield. *Tectonophysics* 457 (3–4), 111–127. <http://dx.doi.org/10.1016/j.tecto.2008.04.029>.
- Kukkonen I.T., Lahtinen R. (Eds.), 2006. Finnish Reflection Experiment FIRE 2001–2005. Geological Survey of Finland Special Paper, vol. 43, Helsinki, 247 p.
- Kuusisto M., Kukkonen I.T., Heikkinen P., Pesonen L.J., 2006. Lithological interpretation of crustal composition in the Fennoscandian Shield with seismic velocity data. *Tectonophysics* 420 (1–2), 283–299. <http://dx.doi.org/10.1016/j.tecto.2006.01.014>.
- Lahtinen R., Korja A., Nironen M., Heikkinen P., 2009. Palaeoproterozoic accretionary processes in Fennoscandia. In: P.A. Cawood, A. Kröner (Eds.), Earth accretionary systems in space and time. The Geological Society, London, Special Publications, vol. 318, p. 237–256. <http://dx.doi.org/10.1144/SP318.8>.
- Ludwig J.W., Nafe J.E., Drake C.L., 1970. Seismic refraction. In: A.E. Waxwell (Ed.), The Sea, vol. 4. Wiley, New York, p. 53–84.
- Lyakhovskiy V., Ben-Zion Y., 2009. Evolving geometrical and material properties of fault zones in a damage rheology model. *Geochemistry Geophysics Geosystems* 10 (11), Q11011. <http://dx.doi.org/10.1029/2009GC002543>.
- Mareschal J.-C., Gangi A.F., Lamping N.L., 1982. The Moho as a phase change: a test of the hypothesis. *Journal of Geophysical Research* 87 (6), 4723–4730. <http://dx.doi.org/10.1029/JB087iB06p04723>.
- Martushko P.S., Prutkin I.L., 2003. Technology of division of the gravitational field sources in depth. *Geofizicheskiy Zhurnal (Geophysical Journal)* 25 (3), 30–34 (in Russian) [Мартышко П.С., Пруткин И.Л. Технология разделения источников гравитационного поля по глубине // Геофизический журнал. 2003. Т. 25. № 3. С. 30–34.].

- McBride J.H., White R.S., Smallwood J.R., England R.W., 2004. Must magmatic intrusion in the lower crust produce reflectivity? *Tectonophysics* 388 (1–4), 271–297. <http://dx.doi.org/10.1016/j.tecto.2004.07.055>.
- Meissner R., Rabbel W., Kern H., 2006. Seismic lamination and anisotropy of the Lower Continental Crust. *Tectonophysics* 416 (1–4), 81–99. <http://dx.doi.org/10.1016/j.tecto.2005.11.013>.
- Mereu, R.F., Baerg, J., Wu, J., 1989. The complexity of the continental lower crust and Moho from PmP data: results from COCRUST experiments. In: R.F. Mereu, S. Mueller, D.M. Fountain (Eds.), *Properties and Processes of Earth's Lower Crust*. AGU Geophysical Monograph, vol. 51, p. 103–119.
- Miksat J., Wen K.-L., Wenzel F., Sokolov V., Chen C.-T., 2010. Numerical modelling of ground motion in the Taipei Basin: basin and source effects. *Geophysical Journal International* 183 (3), 1633–1647. <http://dx.doi.org/10.1111/j.1365-246X.2010.04818.x>.
- Mints M.V., 2007. Paleoproterozoic supercontinent: Origin and evolution of accretionary and collisional orogens exemplified in northern cratons. *Geotectonics* 41 (4), 257–280. <http://dx.doi.org/10.1134/S0016852107040012>.
- Mints M.V., 2011. 3D model of deep structure of the Early Precambrian crust in the East European Craton and paleogeodynamic implications. *Geotectonics* 45 (4), 267–290. <http://dx.doi.org/10.1134/S0016852111040054>.
- Mints M.V., Dokukina K.A., Konilov A.N., Philippova I.B., Zlobin V.L., Babayants P.S., Belousova E.A., Blokh Yu.I., Bogina M.M., Bush W.A., Dokukin P.A., Kaulina T.V., Natapov L.M., Piip V.B., Stupak V.M., Suleimanov A.K., Trusov A.A., Van K.V., Zamozhniaya N.G., 2015. East European Craton: Early Precambrian history and 3D models of deep crustal structure. *Geological Society of America Special Paper*, vol. 510, 433 p. <http://dx.doi.org/10.1130/2015.2510>.
- Mints M.V., Glaznev V.N., Konilov A.N., Kunina N.M., Nikitichev A.P., Raevskiy A.B., Sedykh J.N., Stupak V.M., Fonarev V.I., 1996. Early Precambrian of the North-East of the Baltic Shield: Paleogeodynamics, Structure and Evolution of the Continental Crust. Nauchnyi Mir, Moscow, 287 p. (in Russian) [Миц М.В., Глазнев В.Н., Кониров А.Н., Кунина Н.М., Никитичев А.П., Раевский А.Б., Седых Ю.Н., Ступак В.М., Фонарев В.И. Ранний докембрий северо-востока Балтийского щита: палеогеодинамика, строение и эволюция континентальной коры. М.: Научный мир, 1996. 287 с.].
- Mints M.V., Kaulina T.V., Konilov A.N., Krotov A.V., Stupak V.M., 2007. The thermal and geodynamic evolution of the Lapland granulite belt: implications for the thermal structure of the lower crust during granulite-facies metamorphism. *Gondwana Research* 12 (3), 252–267. <http://dx.doi.org/10.1016/j.gr.2006.10.007>.
- Mints M.V., Konilov A.N., 2004. Geodynamic crustal evolution and long-lived supercontinents during the Palaeoproterozoic: Evidence from granulite-gneisses belts, collisional and accretionary orogens. In: P.G. Eriksson, W. Altermann, D.R. Nelson, W.U. Mueller, O. Catuneanu (Eds.), *The Precambrian Earth: Tempos and Events*. Elsevier, p. 223–239.
- Mints M., Suleimanov A., Zamozhniaya N., Stupak V., 2009. A 3-D model of the Early Precambrian crust under the southeastern Fennoscandian Shield: Karelia Craton and Belomorian tectonic province. *Tectonophysics* 472 (1–4), 323–339. <http://dx.doi.org/10.1016/j.tecto.2008.12.008>.
- Mitrofanov F.P., Sharov N.V., Zagorodny V.G., Glaznev V.N., Korja A., 1998. Crustal structure of the Baltic shield along the Pechenga – Kostomuksha – Lovisa geotraverse. *International Geology Review* 40 (11), 990–997. <http://dx.doi.org/10.1080/00206819809465250>.
- Mjelde M., Goncharov A., Müller R.D., 2013. The Moho: Boundary above upper mantle peridotites or lower crustal eclogites? A global review and new interpretations for passive margins. *Tectonophysics* 609, 636–650. <http://dx.doi.org/10.1016/j.tecto.2012.03.001>.
- Mooney W.D., Meissner R., 1992. Multi-genetic origin of crustal reflectivity: a review of seismic reflection profiling of the continental lower crust and Moho. In: D.M. Fountain, R. Arculus, R.W. Kay (Eds.), *Continental Lower Crust*. Elsevier, Amsterdam, p. 45–79.
- Muravina O.M., 2012. The method of the group account of arguments in the analysis of geophysical data. *Geofizika (Geophysics)* (6), 16–20 (in Russian) [Муравина О.М. Метод группового учета аргументов при анализе геофизических данных // Геофизика. 2012. № 6. С. 16–20].
- Nyblade A.A., Pollack H.N., 1993. A global analysis of heat flow from Precambrian terrains: implications for the thermal structure of Archean and Proterozoic lithosphere. *Journal of Geophysical Research* 98 (B7), 12207–12218. <http://dx.doi.org/10.1029/93JB00521>.
- O'Reilly S.Y., Griffin W.L., 2013. Moho vs crust–mantle boundary: Evolution of an idea. *Tectonophysics* 609, 535–546. <http://dx.doi.org/10.1016/j.tecto.2012.12.031>.
- Pasquale V., Verdoya M., Chiozzi P., 1991. Lithospheric thermal structure in the Baltic Shield. *Geophysical Journal International* 106 (3), 611–620. <http://dx.doi.org/10.1111/j.1365-246X.1991.tb06333.x>.
- Peacock S.M., Rushmer T., Thompson A.B., 1994. Partial melting of subducting oceanic crust. *Earth and Planetary Science Letters* 121 (1–2), 227–244. [http://dx.doi.org/10.1016/0012-821X\(94\)90042-6](http://dx.doi.org/10.1016/0012-821X(94)90042-6).
- Pedersen L.B., 1991. Relations between potential fields and some equivalent sources. *Geophysics* 56 (7), 961–971. <http://dx.doi.org/10.1190/1.1443129>.

- Peltonen P., Kontinen A., Huhma H., 1998. Petrogenesis of the mantle sequence of the Jormua Ophiolite (Finland): Melt migration in the upper mantle during Palaeoproterozoic continental break-up. *Journal of Petrology* 39 (2), 297–329. <http://dx.doi.org/10.1093/ptro/39.2.297>.
- Peltonen P., Mänttari I., Huhma H., Whitehouse M.J., 2006. Multi-stage origin of the lower crust of the Karelian craton from 3.5 to 1.7 Ga based on isotopic ages of kimberlite-derived mafic granulite xenoliths. *Precambrian Research* 147 (1–2), 107–123. <http://dx.doi.org/10.1016/j.precamres.2006.02.008>.
- Prodehl C., Kennett B., Artemieva I., Thybo H., 2013. 100 years of seismic research on the Moho. *Tectonophysics* 609, 9–44. <http://dx.doi.org/10.1016/j.tecto.2013.05.036>.
- Rebetsky Yu.L., 2007. Tectonic Stresses and Strength of Natural Massive. Akademkniga Publishing House, Moscow, 406 p. (in Russian) [Ребецкий Ю.Л. Тектонические напряжения и прочность природных горных массивов. М.: ИКЦ «Академкнига», 2007. 406 с.].
- Romanyuk T.V., 1995. Seismo-density modelling of the crust and upper mantle along geotranssect Quartz. *Fizika Zemli* (9), 11–23 (in Russian) [Романюк Т.В. Сейсмоплотностное моделирование коры и верхней части мантии вдоль геотравверса "Кварц" // *Физика Земли*. 1995. № 9. С. 11–23].
- Romanyuk T.V., Mooney W.D., Blakely R.J., 2001. Density model of the Cascadia subduction zone. *Izvestiya, Physics of the Solid Earth* 37 (8), 617–635.
- Seipold U., 1998. Temperature dependence of thermal transport properties of crystalline rocks – a general law. *Tectonophysics* 291 (1–4), 161–172. [http://dx.doi.org/10.1016/S0040-1951\(98\)00037-7](http://dx.doi.org/10.1016/S0040-1951(98)00037-7).
- Silvennoinen H., Kozlovskaya E., Kissling E., Kosarev G., POLENET/LAPNET Working Group, 2014. A new Moho boundary map for the northern Fennoscandian Shield based on combined controlled-source seismic and receiver function data. *GeoResJ* 1–2, 19–32. <http://dx.doi.org/10.1016/j.grj.2014.03.001>.
- Sharov N.V., Mitrofanov F.P., Verba M.L., Gillen K. (Eds.), 2005. Lithospheric Structure of the Russian Barents Region. Karelian Research Centre RAS, Petrozavodsk, 318 p. (in Russian) [Строение литосферы российской части Баренц-региона / Ред. Н.В. Шаров, Ф.П. Митрофанов, М.Л. Верба, К. Гиллен. Петрозаводск: КНЦ РАН, 2005. 318 с.].
- Sobolev S.V., Babeyko A.Y., 1994. Modelling of mineralogical composition, density and elastic wave velocities in anhydrous magmatic rocks. *Surveys in Geophysics* 15 (5), 515–544. <http://dx.doi.org/10.1007/BF00690173>.
- Strakhov V.N., 1990. On linear inverse problems of gravimetry and magnetometry. *Doklady AN SSSR* 311 (6), 1348–1352 (in Russian) [Страхов В.Н. О решении линейных обратных задач гравиметрии и магнитометрии // Доклады АН СССР. 1990. Т. 311. № 6. С. 1348–1352].
- Strakhov V.N., Romanyuk T.V., 1984. Restoration of the density of the Earth's crust and upper mantle according to the DSS and gravimetry I. *Fizika Zemli* (6), 44–63 (in Russian) [Страхов В.Н., Романюк Т.В. Восстановление плотностей земной коры и верхней мантии по данным ГСЗ и гравиметрии I. *Физика Земли*. 1984. № 6. С. 44–63].
- Tarantola A., Valette B., 1982. Generalized nonlinear inverse problems solved using the least square criterion. *Review of Geophysics and Space Physics* 20 (2), 219–232. <http://dx.doi.org/10.1029/RG020i002p00219>.
- Tesauro M., Kaban M., Cloetingh S., 2008. EuCRUST-07: A new reference model for the European crust. *Geophysical Research Letters* 35 (5), L05313. <http://dx.doi.org/10.1029/2007GL032244>.
- Thybo H., Artemieva I.M., 2013. Moho and magmatic underplating in continental lithosphere. *Tectonophysics* 609, 605–619. <http://dx.doi.org/10.1016/j.tecto.2013.05.032>.
- Tiberi C., Diament M., Déverchère J., Petit-Mariani C., Mikhailov V., Tikhotsky S., Achauer U., 2003. Deep structure of the Baikal rift zone revealed by joint inversion of gravity and seismological data. *Journal of Geophysical Research* 108 (B3), 2133. <http://dx.doi.org/10.1029/2002JB001880>.
- Tikhotsky S., Achauer U., 2008. Inversion of controlled-source seismic tomography and gravity data with the self-adaptive wavelet parametrization of velocities and interfaces. *Geophysical Journal International* 172 (2), 619–630. <http://dx.doi.org/10.1111/j.1365-246X.2007.03648.x>.
- Van der Velden A.J., Cook F.A., 2005. Relict subduction zones in Canada. *Journal of Geophysical Research* 110 (B8), B08403. <http://dx.doi.org/10.1029/2004JB003333>.
- Vernant P., Masson F., Bayer R., Paul A., 2002. Sequential inversion of local earthquake traveltimes and gravity anomaly – the example of the western Alps. *Geophysical Journal International* 150 (1), 79–90. <http://dx.doi.org/10.1046/j.1365-246X.2002.01694.x>.
- Vetrin V.R., 2006. Composition and structure of the lower crust of the Belomorian Mobile Belt, Baltic Shield. *Petrology* 14 (4), 415–438. <http://dx.doi.org/10.1134/S0869591106040047>.
- Vetrin V.R., Lepikhina E.N., Paderin I.P., Rodionov N.V., 2009. Stages of the lower crust formation of the Belomorian mobile belt, Kola Peninsula. *Doklady Earth Sciences* 425 (1), 269–273. <http://dx.doi.org/10.1134/S1028334X09020214>.
- White D.J., Forsyth D.A., Asudeh I., Carr S.D., Wu H., Easton R.M., Mereu R.F., 2000. A seismic-based cross-section of the Grenville Orogen in southern Ontario and western Quebec. *Canadian Journal of Earth Sciences* 37 (2–3), 183–192. <http://dx.doi.org/10.1139/e99-074>.



Glaznev, Victor N., Doctor of Physics and Mathematics, Head of the Chair of Geophysics
Voronezh State University
1 Universitetskaya pl., Voronezh 394006, Russia
✉ e-mail: glaznev@geol.vsu.ru

Глазнев Виктор Николаевич, докт. физ.-мат. наук, заведующий кафедрой геофизики
Воронежский государственный университет
394006, Воронеж, Университетская площадь, 1, Россия
✉ e-mail: glaznev@geol.vsu.ru



Mints, Mikhail V., Doctor of Geology and Mineralogy, Head of laboratory
Geological Institute of RAS
7 Pyzhevsky lane, Moscow 119017, Russia
e-mail: michael-mints@yandex.ru

Мицн Михаил Вениаминович, докт. геол.-мин. наук, зав. лабораторией
Геологический институт РАН
119016, Москва, Пыжевский пер., 7, Россия
e-mail: michael-mints@yandex.ru



Muravina, Olga M., Candidate of Geology and Mineralogy, Associate Professor
Voronezh State University
1 Universitetskaya pl., Voronezh 394006, Russia
e-mail: muravina@geol.vsu.ru

Муравина Ольга Михайловна, канд. геол.-мин. наук, доцент
Воронежский государственный университет
394006, Воронеж, Университетская площадь, 1, Россия
e-mail: muravina@geol.vsu.ru



Raevsky, Aleksei B., Candidate of Physics and Mathematics, Lead Researcher
Geological Institute, Kola Science Center of RAS
14 Fersman street, Apatity 184200, Russia
e-mail: raevsky@geoksc.apatity.ru

Раевский Алексей Борисович, канд. физ.-мат. наук, в.н.с.
Геологический институт КНЦ РАН
184200, Апатиты, ул. Ферсмана, 14, Россия
e-mail: raevsky@geoksc.apatity.ru



Osipenko, Lyudmila G., Researcher
Geological Institute, Kola Science Center of RAS
14 Fersman street, Apatity 184200, Russia
e-mail: osipenko@geoksc.apatity.ru

Осипенко Людмила Григорьевна, н.с.
Геологический институт КНЦ РАН
184200, Апатиты, ул. Ферсмана, 14, Россия
e-mail: osipenko@geoksc.apatity.ru



CRYOGENESIS AND GEODYNAMICS OF ICING VALLEYS

V. R. Alekseyev

Melnikov Permafrost Institute, Siberian Branch of RAS, Yakutsk, Russia
Sochava Institute of Geography, Siberian Branch of RAS, Irkutsk, Russia

Abstract: Due to local groundwater seeping and freezing in layers that accumulate over each other and create large ice clusters on the ground surface, specific conditions of energy and mass transfer are created in the atmosphere–soil–lithosphere system. In winter, the vertical temperature distribution curve is significantly deformed due to heat emission from the water layer above the ice cover during its freezing, and a thermocline is thus formed. Deformation of the temperature curve is gradually decreasing in size downward the profile and decays at the interface of frozen and thaw rocks. Values and numbers of temperature deviations from a 'normal' value depend on heat reserves of aufeis water and the number of water seeps/discharges at a given location. The production of the thermocline alters freezing conditions for underlying ground layers and changes the mechanism of ice saturation, thus leading to formation of two-layer ice-ground complexes (IGC). IGCs are drastically different from cryogenic formations in the neighbouring sections of the river valley. Based on genetic characteristics and the ratios of components in the surface and subsurface layers, seven types of aufeis IGCs are distinguished: massive-segregation, cement-basal, layered-segregation, basal-segregation, vacuum-filtration, pressure-injection, and fissure-vein. Annual processes of surface and subsurface icing and ice ablation are accompanied by highly hazardous geodynamic phenomena, such as winter flooding, layered water freezing, soil heaving/pingo, thermokarst and thermal erosion. Combined, these processes lead to rapid and often incidental reconfigurations of the surface and subsurface runoff channels, abrupt uplifting and subsiding of the ground surface, decompaction and 'shaking-up' of seasonally freezing/thawing rocks, thereby producing exceptionally unfavourable conditions for construction and operation of engineering structures.

Formation and development of river networks are heavily influenced by aufeis deposits and processes taking place at the aufeis surfaces, especially in areas of discontinuous and continuous permafrost where an average thickness of the ice cover on rivers ranges from 1.0 to 2.5 m, and the major part of the ice cover is accumulated layer by layer due to freezing of discharged groundwater. In the permafrost zone, the intensity of cryogenic channelling is clearly cyclical, and the cycles depend on accumulation of aufeis ice above the river level during the autumn low-water period. Five stages of cryogenic channelling are distinguished: I – pre-glacial development, II – transgression, III – stabilization, IV – regression, and V – post-glacial development. Each stage is characterised by a specific glaciological regime of runoff channels and their specific shapes, sizes and spatial patterns.

The channel network is subject to the maximum transformation in aufeis development stages III and IV, when the transit flow channel is split into several shallow-water branches, producing a complicated plan pattern of the terrain. In the mature aufeis glades, there are sites undergoing various development stages, which gives evidence that aufeis channelling is variable in a wide range in both space and time. With respect to sizes of aufeis glades, river flow capacities and geological, geomorphological, cryo-hydrogeological conditions, aufeis patterns of the channel network are classified into five types as follows: fan-shaped, cone-shaped, treelike, reticular, and longitudinal-insular types. The aufeis channel network is a reliable indicator of intensity of both recent and ancient geodynamic processes in the cryolithozone.

In Siberia and the Far East, the aufeis deposits are much larger, more numerous and more important in terms of morpholithology in comparison with the 'classical' (sedimentary metamorphic) icing structures. The more contrasting is the terrain, the more active are neotectonic movements, the lower is the mean annual air temperature, and the higher is the annual percentage of the territory covered by aufeis ice. The aufeis ratio of the permafrost zone is determined from parameters of over 10000 ice fields and amounts to 0.66 % (50000 km²). In mountains and tablelands, the total area of aufeis deposits amounts to 40000 km², and the number of ice clusters (0.77 km² in average) exceeds 60000. On the rivers up to 500 km long, the aufeis size depends on the stream rank. In all the natural zones, the majority of gigantic aufeis spots produced by groundwater are located in river valleys of ranks 3 and 4. The square area of aufeis deposits of mixed feed, i.e. produced by river water and groundwater, which occupy the entire river channel, yet do not go beyond the floodplain, amounts to 68000 km², i.e. by a factor of 1.7 larger than the area of all the aufeis deposits (taryns). The cumulative channel-forming effect of aufeis phenomena is expressed by an increment in the channel network relative to characteristics of the river segments located upstream and downstream of the aufeis

glade. This indicator is well correlated with the aufeis ratios of the river basins, morphostructural and cryo-hydro-meteorological conditions of the territory under study. The incremental length of the channel network, ρ_n per one groundwater aufeis deposit is increased, in average, from 3.5 km in mountains in the southern regions of East Siberia to 23 km in the Verkhoyansk-Kolyma mountain system and Chukotka. The value of ρ_n is decreased to 2.2 km in the plains and intermountain depressions of the Baikal rift system where the average dimensions of the ice fields are smaller. An average incremental length of the channel network per one large groundwater aufeis deposit amounts to 12.2 km, and the total incremental length in continuous and discontinuous permafrost areas ($F=7.6$ mln km²) is estimated at 690000 km.

Combined impacts of aufeis and icing processes on underlying rocks and the channel network is a specific (aufeis) form of cryogenic morpholithogenesis that is typical of regions with inclement climate and harsh environment. A more detailed research of these processes is required, including large-scale aerospace surveys, monitoring and observations on special aufeis polygons.

Key words: cryogenic phenomena, subsurface ice, aufeis, icing, naled, aufeis processes, aufeis channeling, channel networks, cryogenic movement of soil, ground heaving, pingo, mound, thermokarst.

Recommended by V.S. Imaev

For citation: Alekseyev V.R. 2015. Cryogenesis and geodynamics of icing valleys. *Geodynamics & Tectonophysics* 6 (2), 171–224. doi:10.5800/GT-2015-6-2-0177.

КРИОГЕНЕЗ И ГЕОДИНАМИКА НАЛЕДНЫХ УЧАСТКОВ РЕЧНЫХ ДОЛИН

В. Р. Алексеев

*Институт мерзлотоведения им. П.И. Мельникова СО РАН, Якутск, Россия
Институт географии им. В.Б. Сочавы СО РАН, Иркутск, Россия*

Аннотация: Локализованный выход подземных вод на поверхности земли, их намораживание в виде крупных ледяных массивов создают специфические условия энерго- и массообмена в системе атмосфера – почва – литосфера. Зимой кривая вертикального распределения температур существенно деформируется за счет выделения тепла наледным слоем воды при его промерзании, при этом образуется своеобразный термоклин. Деформация температурной кривой, постепенно уменьшаясь в размерах, смещается вниз по разрезу и затухает на границе мерзлых и талых горных пород. Величина и количество отклонений температуры от «нормального» положения зависят от теплозапаса наледобразующих вод и числа излияний в заданной точке пространства. Появление термоклина изменяет условия промерзания подстилающих грунтов и механизм их льдонасыщения, приводит к формированию двухъярусных ледогрунтовых комплексов (ЛГК), резко отличных от криогенных отложений смежных участков долины. По генетическим особенностям и соотношению составных частей наземного и подземного ярусов описано семь типов наледных ЛГК – массивно-сегрегационный, цементно-базальный, слоисто-сегрегационный, базально-сегрегационный, вакуум-фильтрационный, напорно-инъекционный и трещинно-жильный. Ежегодное формирование и разрушение наледей и подземных льдов сопровождается чередой особо опасных геодинамических явлений, среди которых ведущее место занимают зимнее затопление территории, намораживание воды, пучение грунтов, термокарст и термоэрозия. Совокупность этих процессов приводит к быстрому, часто неожиданному переформированию каналов поверхностного и подземного стока, резкому поднятию и опусканию земной поверхности, разуплотнению и «перетряхиванию» сезоннопротаивающих и сезоннопромерзающих горных пород, что создает крайне неблагоприятные условия для строительства и эксплуатации инженерных сооружений.

Наледеи и наледные процессы оказывают влияние на формирование и развитие речной сети. Наиболее широко оно проявляется в областях прерывистого и сплошного распространения вечной мерзлоты, где средняя толщина льда на реках колеблется в пределах 1.0–2.5 м, а основная часть ледяного покрова формируется за счет намораживания излившихся подземных вод. Интенсивность криогенного руслообразования в криолитозоне носит ярко выраженный циклический характер, зависящий от превышения наледного льда над урезом реки в осеннюю межень. Описаны пять стадий криогенного руслогенеза: 1) предгляциальная, 2) трансгрессивная, 3) стабилизационная, 4) регрессивная и 5) постгляциальная. Каждой стадии соответствует определенный гляциогидрологический режим каналов стока, их форма, размеры и пространственное распределение.

Максимальная трансформация русловой сети происходит в третью и четвертую стадию развития наледных долин, когда русло транзитного потока разбивается на ряд мелководных рукавов, создающих сложный плановый рисунок местности. На зрелых наледных полях выделяются участки, находящиеся на разных стадиях развития, что свидетельствует о широком диапазоне изменчивости наледного руслогенеза в про-

странстве и времени. В зависимости от размеров наледей, водности реки, геолого-геоморфологических и мерзлотно-гидрогеологических условий выделено пять видов наледной структуры русловой сети: веерообразная, конусовидная, древовидная, сетчатая и продольно-островная. Наледная русловая сеть может служить надежным показателем интенсивности геодинамических процессов в криолитозоне, как современных, так и древних.

По количеству, размерам и морфолитогенетическому значению наледи Сибири и Дальнего Востока многократно превышают «классическую» (осадочно-метаморфическую) форму оледенения. Чем контрастнее рельеф местности, активнее неотектонические движения и ниже среднегодовая температура воздуха, тем выше процент территории, ежегодно занимаемой наледным льдом. Относительная наледность криолитозоны, определенная с учетом параметров более 10000 ледяных полей составляет 0.66 % (50000 км²). В горах и на плоскогорьях суммарная площадь наледей равна 40000 км², а число ледяных массивов со средней площадью 0.770 км² превышает 60000. На реках длиной до 500 км размеры наледей зависят от порядка водоотков. Наибольшее количество гигантских наледей подземных вод во всех природных зонах располагается в долинах рек 3–4-го порядка. Площадь наледей смешанного питания (речных и подземных вод), занимающих все русло реки, но не выходящих за границу обычной поймы, составляет 68000 км² – в 1.7 раза больше, чем все наледи-тарыны. Кумулятивный руслообразующий эффект наледных явлений выражается величиной прироста русловой сети по отношению к участкам реки выше и ниже наледной поляны. Этот показатель находится в хорошей корреляционной связи с наледностью речных бассейнов, морфоструктурными и мерзлотно-гидрогеологическими условиями территории. Прирост русловой сети ρ_n , приходящийся на одну наледь подземных вод, в среднем увеличивается от 3.5 км в горах юга Восточной Сибири до 23 км в Верхояно-Колымской горной стране и на Чукотке. На равнинах и в пределах межгорных котловин Байкальской рифтовой системы величина ρ_n снижается до 2.2 км, что связано с уменьшением средних размеров ледяных полей. В среднем прирост русловой сети на одну крупную наледь подземных вод составляет 12.2 км, а общий прирост в области сплошной и прерывистой вечной мерзлоты ($F=7.6$ млн км²) оценивается в 690 тыс. км.

Совокупность воздействия наледей и наледных процессов на подстилающие горные породы и русловую сеть есть особая (наледная) форма криогенного морфолитогенеза, характерная для регионов с суровыми природно-климатическими условиями. Дальнейшее ее изучение требует крупномасштабных аэрокосмических съемок и режимных наблюдений на специальных наледных полигонах.

Ключевые слова: криогенные явления, подземные льды, наледи, наледные процессы, наледный руслогенез, русловая сеть, криогенное движение грунтов, бугры пучения, термокарст.

1. INTRODUCTION

Generally, a large aufeis deposit (taryn) is clearly visible in the terrain. In winter, even when frosts are severe, the taryn is typically marked by 'streaming' at groundwater seeping spots or evidenced by ice-covered surfaces extending for many kilometres. In summer, remarkable features are fresh green meadows located between sparkling white or emerald-green ice slabs. The 'exotic' shapes, puzzles and conundrums of aufeis deposits and ice-covered terrains have always been attractive for scientists, fishermen and hunters, as well as other nature enthusiasts. Only in the past 50–60 years, the secret of aufeis has been unveiled, and explanations were found for a number of once mysterious phenomena, such as explosive failure of heaving mounds, migration and decomposition of ice fields, feed and persistent variability of aufeis-generating sources etc.

Based on data collected in long-term studies, it is established that groundwater aufeis is a specific indicator of thermal conditions of the permafrost zone, as well as

a powerful factor controlling surface and underground runoff and causing changes in the microclimate, landscape, composition and structure of loose sediments and cryogenic terrains in general [Åkerman, 1982; Alekseyev, 1968, 1997, 2005, 2013; Baranowski, 1982; Carey, 1973; Sloan et al., 1976; Clark, Lauriol, 1997; Deikin, 1985; Fotiev, 1964; French, 1976; Froehlich, Slupik, 1982; Gorbunov, Ermolin, 1981; Harden et al., 1977; Heldmann et al., 2005; Hu, Pollard, 1997; Kolosov, 1938; Olszewski, 1982; Pollard, Franch, 1983; Priesnitz, Schunke, 2002; Romanovsky, 1972, 1973, 1974, 1993, 1997; Veillette, Thomas, 1979; Yoshikawa et al., 2007]. However, many aspects of aufeis and icing processes have still remained outside the scope of studies: heat interaction between ice clusters and underlying rock layers, specific features of underground icing, regularities of development of hazardous geodynamic phenomena, such as soil heaving, thermal erosion, thermokarst, suffusion etc. The information available from publications is mainly based on visual observations during short-term field studies; geocryological profiles, special maps and instrumental measurement data are quite rare.

2. REGIONS UNDER STUDY. INPUT DATA

This publication is based on data collected by the author in long-term field studies in Yakutia, Transbaikalia, Pribaikalia and East Sayan mountains and surface and aerial surveys of aufeis and icing processes on the Charskie Peski and Eden polygons, as well as on published data on other permafrost regions (Fig. 1), including remote sounding materials and satellite data available in Google.

The Charskie Peski polygon (15 km²) is located at the elevation of 710–750 m in the central part of the Upper Chara depression in the Stanovoe upland. Its major area is occupied by the right-side floodplain of the Middle Sakukan river, the wide boggy valley of the Bolotny brook, which is neighbouring the floodplain at the west, and valleys of the Kholodny and Alyonushka brooks, both going across the mass of drift sands. In this territory, the total thickness of the permafrost bed, including sand, sandy clay, boulder-pebble deposits, and peat, ranges from 300 to 350 m. It is cut by narrow thawing lenses of complicated shapes and ascending flows of artesian groundwater. In winter, the entire polygon is covered by the aufeis deposit which thickness ranges from 3.0 to 3.5 m. The soil under the ice cover is penetrated by the network of recurrent-vein ice, injected ice bands and lenses. Seasonal and perennial heaving mounds, thermokarst holes and small lakes are abundant. The snow cover is rarely thicker than 15–20 cm. In these regions, natural icing and vertical movement of the crust were studied from 1976 to 1980. The studies were combined with other geocryological, geographical and landscape surveys. For monitoring purposes, 330 reference points were established along 54 profiles [Alekseyev, 2005]. Simultaneously with research on the polygon, studies of aufeis and subsurface ice were conducted on routes in the Lower Ingamakit, Cheena, Apsat, Middle and Upper Sakukan river valleys and at the Chara river head.

The Eden polygon (1250 km²) is located at the border between Tofalaria and Tuva in the upper part of the Uda river basin at elevations from 1300 to 2000 m. It includes two basins of the Egegi and Eden rivers of ranks 3 and 4 and a part of the sublatitudinal segment of the Uda river valley of the glacial-tectonic origin. The territory is characterized by the strongly dissected relief, discontinuous and continuous permafrost (50 to 200 m thick), and irregular snow cover patterns (10 to 15 cm in the taiga belt; 50 to 80 cm in the sub-goltsy and taiga belts). From 1983 to 1992, the dynamics of cryogenic events was studied by methods of instrumental landscape profiling, field and remote mapping. Glaciation, hydrogeological and meteorological conditions were monitored at reference stations and points. The landscape profiles were constructed across the river/stream valleys at 0.1–0.5 km intervals. In total,

there were 142 landscape-glaciological profiles in the river valleys (Uda – 21, Bolshoy Eden – 51, Maly Eden – 30, and Egegi – 40). Five temporary meteorological stations operated in the region under study. Aerial photos and land survey data were consolidated in a database for mapping, and 13 large-scale landscape-glaciological maps covered sites located in the mountain-taiga belt (9 maps), sub-goltsy (2 maps) and goltsy belts (2 maps) [Alekseyev, 2005].

3. SPECIFIC FEATURES OF SUBSURFACE ICING IN AUFEIS SECTIONS OF RIVER VALLEYS

Aufeis and icing processes significantly affect the intensity of seasonal freezing and thawing of rocks, thermal modes and phase transitions of water in the soil layers. In some cases, subsurface icing may become more active and result in larger reserves of subsurface ice, or sometimes, the volume of subsurface ice may be reduced and its depths may be more shallow. On some sites, ice masses are buried and classified as aufeis deposits or snow patches in terms of their origin and viewed as subsurface ice with respect to their bedding and positions relative to the day surface.

During formation of aufeis deposits, specific conditions are created for subsurface icing, and such conditions differ from those in the neighbouring areas of the river valleys [Alekseyev, 1989, 2005; Boitsov, 1979; Klimovsky, 1978; Koloskov, Koreisha, 1975; Romanovsky et al., 1973, 1978; Shvetsov, Sedov, 1941]. In winter, the vertical temperature distribution curve is significantly disrupted due to heat emission from the water layer above the ice cover during its freezing, and a thermocline is thus formed (Fig. 2). Deformation of the temperature curve is gradually decreasing in size downward the profile and generally decays at the interface of frozen and thawed rocks. Values of temperature deviations from a 'normal' value depend on heat reserves of aufeis water. The number of cases when a thermocline is formed corresponds to the number of water seep cases, which is reflected in the total number of primary aufeis layers at the given point of the profile.

Sometime after the occurrence of water above ice, the frozen soil is partially thawing at the bottom due to 'sinking' of the heat wave. As a result of the phase transition of water, vacuum at the bottom of the frozen layer causes infiltration of ground water from the neighbouring horizons and sidewise inflow. After the water layer freezes above the ice, the temperature distribution curve straightens, and the thermocline disappears. At this time, a horizontal ice schlier is formed, and freezing of the underlying wet rock mass is ongoing. Such cycles of heterogeneous icing are repeated many times (Fig. 2). Therefore, on the one side, the ice thickness on the ground surface is increasing, and, on the other side,

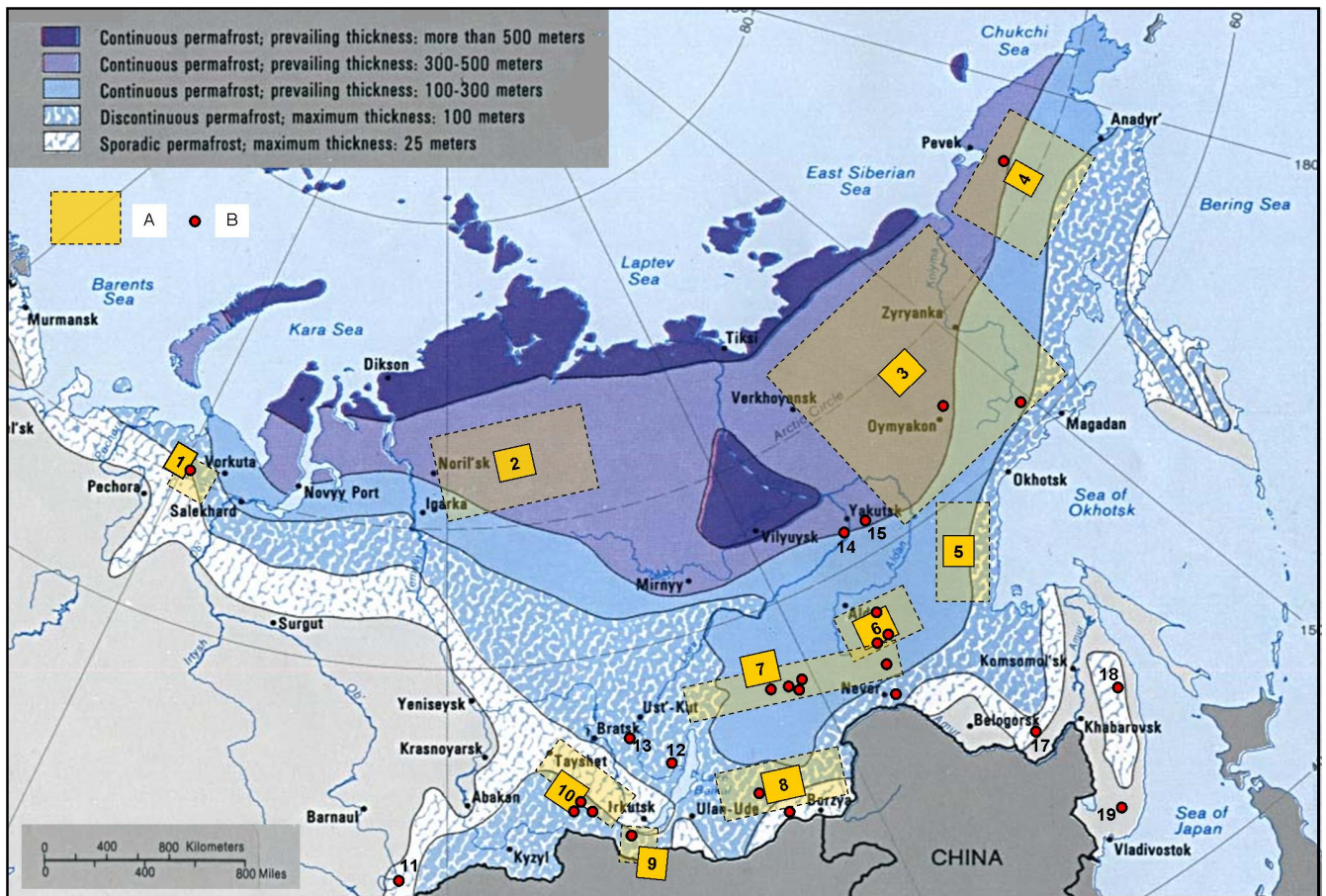


Fig. 1. The map showing surveyed locations and main observation points for studying aufeis phenomena in the territory of Russia.

Territories covered by remote ground-based and routine surveys with catalogued data on aufeis deposits (the routine survey sites are marked): 1 – Polar Ural [Oberman, 1985, 1989]; 2 – Putorana plateau [Aleksyeyev, Gienko, 2002]; 3 – Tikhon-Yuryakh and Anmangynda aufeis polygons in the north-eastern regions of Russia [Aleksyeyev et al., 2012; Lebedev, 1969; Simakov, 1959, 1961; Sokolov, 1975; Tolstikhin, 1974]; 4 – Kookvyn aufeis polygon in North Chukotka [Aleksyeyev et al., 2011]; 5 – Priokhotie [Shmatkov, Kozlov, 1994]; 6 – Samokit, Leglier, Chulman, Lokuchakit, and Iengra aufeis polygons on the Aldan upland [Aleksyeyev, 1973, 1975, 2005; Topchiev, 1979; Topchiev, Gavrilov, 1981; Sokolov, 1975; Boitsov, 1979]; 7 – Lower Ingamakit, Charskie Peski, Middle Sakukan, Mururin, Chutkanda, and Shakhtaum aufeis polygons in the Baikal-Amur Railroad zone [Aleksyeyev, 1975, 2005; Aleksyeyev, Kirichenko, 1997; Aleksyeyev, Furman, 1976; Deikin, Abakumenko, 1986; Deikin, Markov, 1983, 1985; Catalogue..., 1980, 1981, 1982; Prokacheva et al., 1982; Shesternev, Verkhoturov, 2006]; 8 – Ingoda aufeis polygon in Transbaikalie [Aleksyeyev, 1975; Shesternev, Verkhoturov, 2006; Chernyavskaya, 1973]; 9 – Tumusum, Khangarul, and Dabady aufeis polygons in the south-western Pribaikalie [Aleksyeyev, 1976]; 10 – Blue Rock, Shamanka, and Eden aufeis polygons in East Sayan [Aleksyeyev, 2005; Aleksyeyev, Kovalchuk, 2004; Kravchenko, 1985a]. Routine observations on polygons to study the dynamics of individual aufeis deposits: 11 – Aktru aufeis polygon in Altai [Revyakin, 1981]; 12 – Ilikta [Berkin, 1964]; 13 – Polovinka [Kazakov, 1976]; 14 and 15 – Ulaخان Taryn, Bulus [Piguzova, Shepelev, 1972, 1975; Tolstikhin, 1974]; 16 – Kerak [Rumyantsev, 1964, 1991]; 17 – Kuldur [Chekotillo et al., 1960]; 18 – Plastun [Tsvid, Khomichuk, 1981]; 19 – Southern mine [Tsvid, 1957].

Рис. 1. Карта расположения съемочных работ и основных пунктов режимных наблюдений за динамикой наледных явлений на территории России.

Территория, в пределах которой проведены наземные дистанционные и режимные съемочные работы, составлены каталоги наледей (места режимных наблюдений выделены пунсоном): 1 – Полярный Урал [Oberman, 1985, 1989]; 2 – плато Путорана [Aleksyeyev, Gienko, 2002]; 3 – Северо-Восток России; наледные полигоны Тихон-Юрях, Анмангында [Aleksyeyev et al., 2012; Lebedev, 1969; Simakov, 1959, 1961; Sokolov, 1975; Tolstikhin, 1974]; 4 – Северная Чукотка; наледный полигон Кооквын [Aleksyeyev et al., 2011]; 5 – Приохотье [Shmatkov, Kozlov, 1994]; 6 – Алданское нагорье; наледные полигоны Самокит, Леглиер, Чульман, Локучакит, Иенгра [Aleksyeyev, 1973, 1975, 2005; Topchiev, 1979; Topchiev, Gavrilov, 1981; Sokolov, 1975; Boitsov, 1979]; 7 – зона БАМ; наледные полигоны Нижний Ингамakit, Чарские Пески, Средний Сакукан, Мурурин, Читканда, Шахтаум [Aleksyeyev, 1975, 2005; Aleksyeyev, Kirichenko, 1997; Aleksyeyev, Furman, 1976; Deikin, Abakumenko, 1986; Deikin, Markov, 1983, 1985; Catalogue..., 1980, 1981, 1982; Prokacheva et al., 1982; Shesternev, Verkhoturov, 2006]; 8 – Забайкалье; наледный полигон Ингода [Aleksyeyev, 1975; Shesternev, Verkhoturov, 2006; Chernyavskaya, 1973]; 9 – Юго-Западное Прибайкалье; наледные полигоны Тумусун, Хангарул, Дабады [Aleksyeyev, 1976]; 10 – Восточные Саяны; наледные полигоны Синий Камень, Шаманка, Эден [Aleksyeyev, 2005; Aleksyeyev, Kovalchuk, 2004; Kravchenko, 1985a]. Режимные наблюдения на полигонах за динамикой отдельных наледей: 11 – Алтай; наледный полигон Актру [Revyakin, 1981]; 12 – Иликта [Berkin, 1964]; 13 – Половинка [Kazakov, 1976]; 14, 15 – Улахан-Тарын, Булус [Piguzova, Shepelev, 1972, 1975; Tolstikhin, 1974]; 16 – Керак [Rumyantsev, 1964, 1991]; 17 – Кульдур [Chekotillo et al., 1960]; 18 – Пластун [Tsvid, Khomichuk, 1981]; 19 – Южный рудник [Tsvid, 1957].

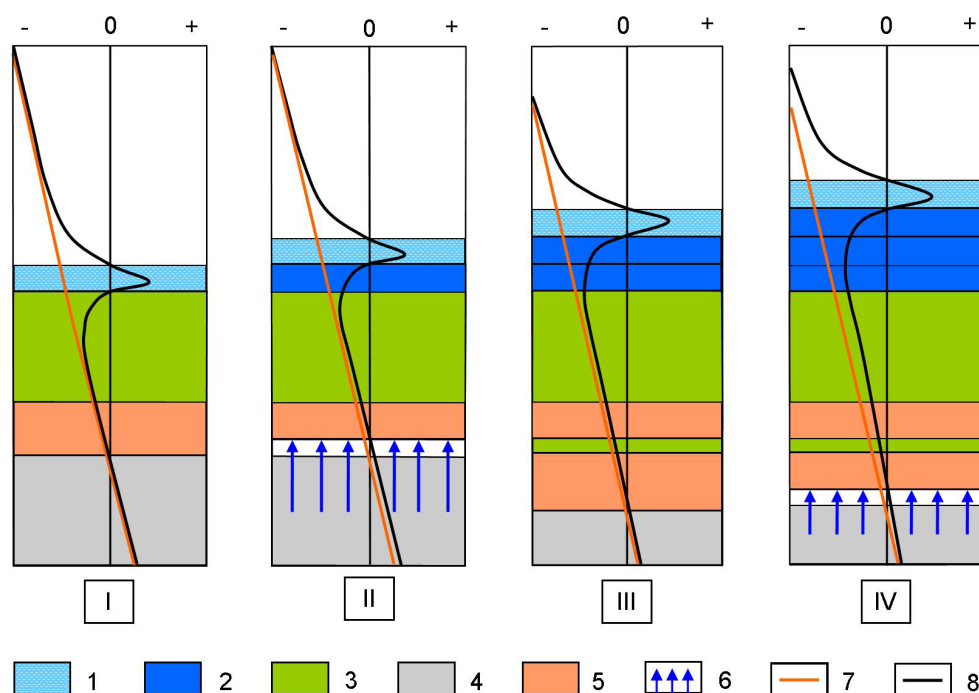


Fig. 2. Schemes of joint surface and subsurface icing.

Icing stages: *I* – freezing-through of the aufeis bed, and formation of the first aufeis-forming layer of water; *II* – vacuum in the rock layer as a result of partial thawing of ground ice, infiltration of water from below, and formation of the second aufeis-forming layer of water; *III* – alignment of the temperature distribution curve, increment in the thickness of the ground-ice layer, and formation of the third aufeis-forming layer of water; *IV* – melting of the ground ice from below, vacuum at its lower surface, another infiltration of water, and formation of the next aufeis-forming layer. 1 – water; 2 – aufeis ice; 3 – frozen soil; 4 – thawed soil; 5 – ground ice; 6 – direction of cryogenic filtration of groundwater; 7 – temperature distribution curve between aufeis formation periods; 8 – temperature distribution curve at the period of formation and crystallization of the water layer on the ice.

Рис. 2. Схемы сопряженного формирования наледи и подземного льда.

Стадии льдобразования: *I* – промораживание наледного ложа и формирование первого наледнеобразующего слоя воды; *II* – образование вакуума в толще горных пород в результате частичного таяния подземного льда и подсос воды снизу; формирование второго наледнеобразующего слоя воды; *III* – выравнивание кривой распределения температуры, прирост толщины слоя подземного льда; формирование третьего наледнеобразующего слоя воды; *IV* – подтаивание подземного льда снизу, образование вакуума у его нижней поверхности, новый подсос воды, формирование очередного наледнеобразующего слоя. 1 – вода; 2 – наледный лед; 3 – мерзлый грунт; 4 – талый грунт; 5 – подземный лед; 6 – направление криогенной фильтрации подземных вод; 7 – кривая распределения температуры между периодами наледнеобразования; 8 – кривая распределения температуры в период образования и кристаллизации слоя воды на льду.

the thickness of frozen soil with the clearly layered cryogenic structure is also increasing.

Observations on the Charskie Peski polygon show that ice schlier stacks are most often oriented parallel to the icing surface and composed of pure transparent ice of prismatic or granular structures [Alekseyev, 2007; Sannikov, 1988]. In the layers composed of sand and sandy clay, the schlier thickness generally ranges from 2 to 50 mm; the layers maintain the strike and are limited by the plane surface of the host soil mass (Fig. 3, a). Distances between neighbouring ice inclusions can range from a few millimetres to 8–10 cm. The thickness of the soil layer between ice layers depends on the duration of the period of repeated icing: the longer is the time from water discharge to complete crystallization of the aufeis layer, the more lasting is freezing of the

underlying rocks and, correspondingly, the larger is the distance between the ice schlieren. The regular pattern is disturbed in soils of inhomogeneous composition, and frequent squeeze-out and wedging of ice inclusions result from irregular freezing of the soil layers as they differ in thermal characteristics and moisture contents. However, downward the profile, rhythmical icing patterns are sustained and generally correspond to the number of icing water outflow cycles. In analyses of cryogenic permafrost, this indicator may serve as a marker of potential development of aufeis.

Laminated cryogenic textures are lacking in clastic rocks and well-washed boulder-gravel beds. In rocks with a water-cut, which are not under pressure during freezing, a basic cryogenic texture is formed, and the 'free' space is completely occupied by ice. In such cases,

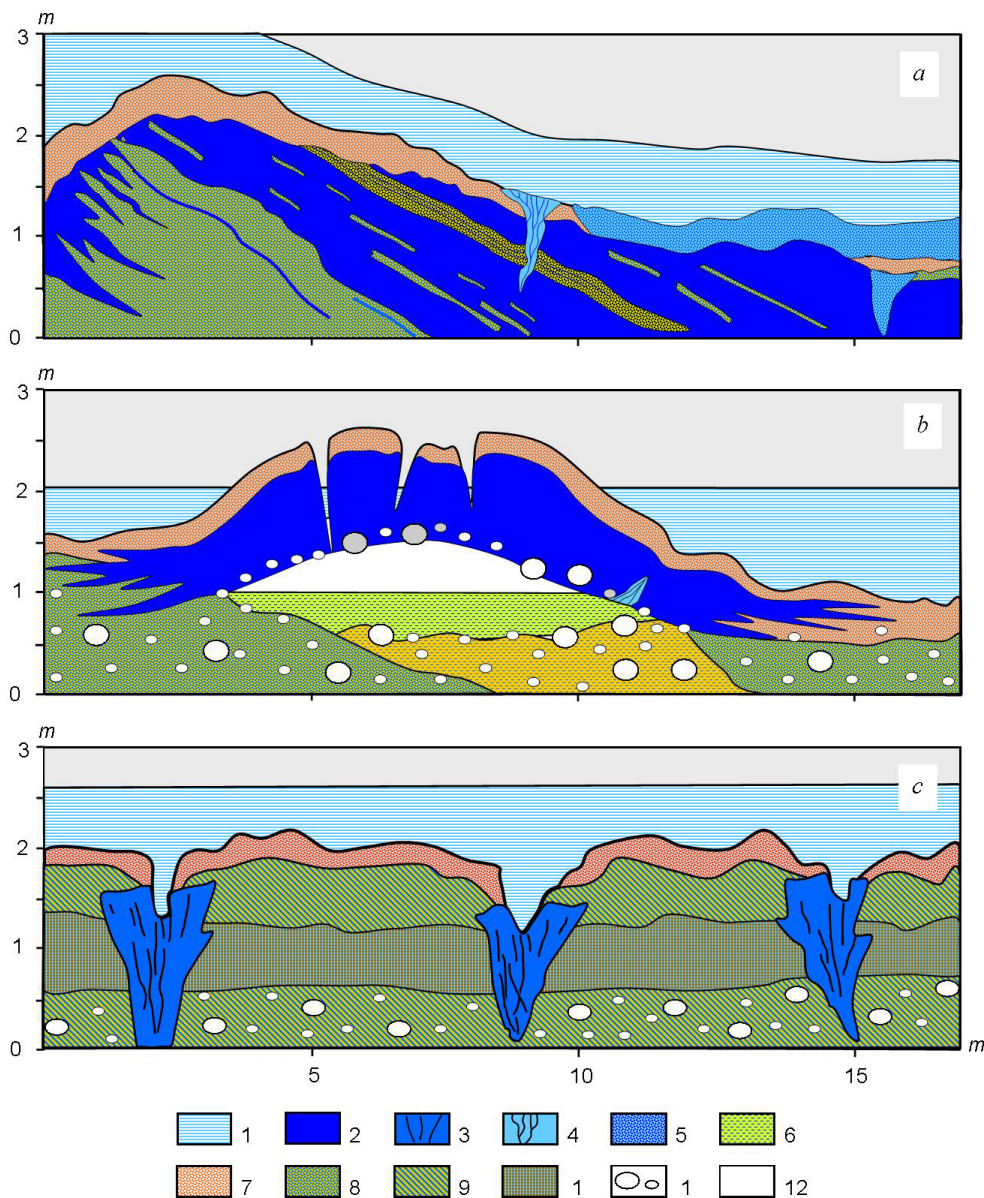


Fig. 3. Ice-ground complexes in the Charskie Peski aufeis polygon, the northern Transbaikalia.

a – Kholodny creek valley; *b* – Bolotny creek valley; *c* – right-side bank of the Middle Sakukan river. 1 – groundwater aufeis deposit. Ice types: 2 – injection ice, 3 – repeated-vein ice, 4 – fissure-vein ice, 5 – snow ice; 6 – water. Ground materials: 7 – seasonally thawing sand, 8 – perennially frozen sand, 9 – perennially frozen sandy loam, 10 – frozen peat, 11 – boulders and pebbles; 12 – air cavity in the ice mound.

Рис. 3. Ледогрунтовые комплексы на наледном полигоне Чарские Пески. Северное Забайкалье.

a – долина руч. Холодного; *b* – долина руч. Болотного; *c* – правый берег реки Средний Сакукан. 1 – наледь подземных вод. Лед: 2 – инъекционный, 3 – повторно-жильный, 4 – трещинно-жильный, 5 – снежный; 6 – вода. Грунты: 7 – песок сезоннопротаивающий, 8 – песок многолетнемерзлый, 9 – супесь многолетнемерзлая, 10 – торф мерзлый, 11 – валуны и галька; 12 – воздушная полость в теле бугра пучения.

particles are displaced in various directions, and cryogenic pressure forces the water flow into the neighbouring soil sections. Stresses associated with water crystallization are compensated by the pressure of aufeis ice and lateral water outflow and thus do not cause any significant deformation of the ground surface. The above-described mechanism of subsurface icing is typical of

open cryogenic systems. In our studies, we observed such profiles in river valleys which water levels are frost-dependent. It is revealed that the lower is the air temperature, the higher is the water level in the open part of the channel or in the ice hole, which gives evidence of water squeezing out during freezing of the host rocks.

It is often observed that closed water-bearing systems are formed in the aufeis sections of the river valleys, and their formation is accompanied by injection icing that leads to soil pulling apart and uplifting. The mechanism of water injection in contact areas between water-resistant beds is described in [Gasarov, 1966; Klimovsky, 1978, Sannikov, 1988] and other publications. It was discovered and proved by experiments in the Permafrost Institute SB RAS [Feldman, 1988; Feldman, Borozinets, 1983], as well as by results of theoretical studies by Ya.B. Gorelik and V.S. Kolumin in the Institute of the Earth's Cryosphere [Gorelik, Kolumin, 2002]. Results of out field studies show that the injection mechanism causing accumulation of huge mass of ground ice is most evident in conditions of aufeis formation, i.e. in a specific thermal regime with a high moisture content of the underlying rocks.

Injection ice layers start to form when the soil freezes to some depth in the neighbouring sections of the river valley. During this period, an over-permafrost talik (or unfrozen pocket) persists underneath the aufeis deposit due to high emission of latent heat. High pressures occur when its top gets frozen in periods between aufeis-formation cycles, and water is squeezed out laterally due to cryogenic impacts. The pressure drops down abruptly when the groundwater breaks out to the surface or gets injected as an independent lense between the thawing and frozen soil beds. In the latter case, the top of the talik is uplifted to a height that is sufficient to compensate the hydrostatic pressure. Further freezing of the injected water may be partial or complete. In case that the water lense is completely frozen, the pressure (which was increasing before) drops down abruptly after repeated water outflow in subvertical fractures and fault zones, which is accompanied by active bubbling and emission of dissolved air, followed by 'outburst' of actively growing ice crystals.

This process is accompanied by vertical deformations of the ground surface, which often remain unobservable under the aufeis. In case of complete crystallization of the injected water, the bottom of the frozen water body is covered by frozen-up fine soil (with a typical laminated cryogenic texture that has formed as described above), pebbles, boulders or coarse rocks (Fig. 3, b). By the next injections, this frozen soil is lifted up together with this ice cap and then jammed inside the ground ice bed.

In some cases, water is injected between the aufeis deposit and its bed, and plants frozen in ice are thus torn off. Generally, the injection ice volume increases after outflow cycles followed by crystallization of aufeis-generating water, as evidenced by numerous tongues at the periphery of ice domes (see Fig. 3, b). In parallel, healing of cracks and fractures with ice takes place as lode ice and repeated-ice wedges are formed.

Ice infill of such types is specific as it is supplied by either aufeis water (from above) or groundwater uplifted by cryogenic pressure (from below).

It may be noted in puzzlement at the first glance that rock layers, consistent in thickness and strike, and rock lenses are present in the injection-ice mass. Frozen rock xenolithes look like suspended in ice; they have clear contacts with the host ice mass and, in some cases, arranged in a kind of tiers and chains. Isolated clusters of pebbles and large boulders are often found inside the ice mass (Fig. 4). In records of such profiles, researchers usually state that foreign inclusions were formed by ingress of this material to the aufeis surface and its subsequent burial due to layer-by-layer water freezing. Such comments do not consider the absence of lamination in ice and a possible injection origin of the structure.

It is revealed that aufeis phenomena play a special role in frost shattering of soil and development of vein ice and recurrent-vein ice (see Fig. 3, c). Cryogenic fracturing of frozen rocks is known to occur at high temperature and humidity gradients – the lower is the temperature of the ground surface and the higher is its moisture/ice content, the smaller polygons are generated due to stresses. In the cryogenic fractures, ice is usually formed during the period of snow melting or spring flood. The development of fissure-vein ice is significantly impacted by aufeis processes. Firstly, in winter, due to discharge of aufeis-generating water, frost shattering of rocks in floodplains and terraces may not take place at all or may be substantially transformed. If aufeis processes start in autumn and continue without any interruption until spring, groundwater icing occurs in the vacuum-filtration mode, i.e. polygons are not formed. If icing takes place from the second half of winter, thermal stresses in soil lead to fracturing of the frozen ground, and polygons are weakly manifested.

Secondly, recurrent-vein ice is formed in the aufeis sections of the river valleys due to discharged groundwater, rather than melted snow. In such cases, formation of ice wedges is deferred by 2–3 months, i.e. to the middle of the cold season. Thirdly, as the aufeis mass covers the polygons, their development in the warm season is transformed; in particular, the depth of seasonal thawing is reduced, the intensity and composition of thermal erosion and thermokarst are altered, and rock heaving is obscured.

Aufeis phenomena play a special role in the head-on growth of recurrent-vein ice. There are two possible scenarios of icing. If aufeis water fills in a cavity above the ice vein in the incompletely frozen seasonally melting layer, crystallization of aufeis-generating water is accompanied by wedging of the host rock and formation of a series of conjugated ice schlieren that are thinning out with the increasing distance from the frost-shattered fracture. The ice mass is thus a natural

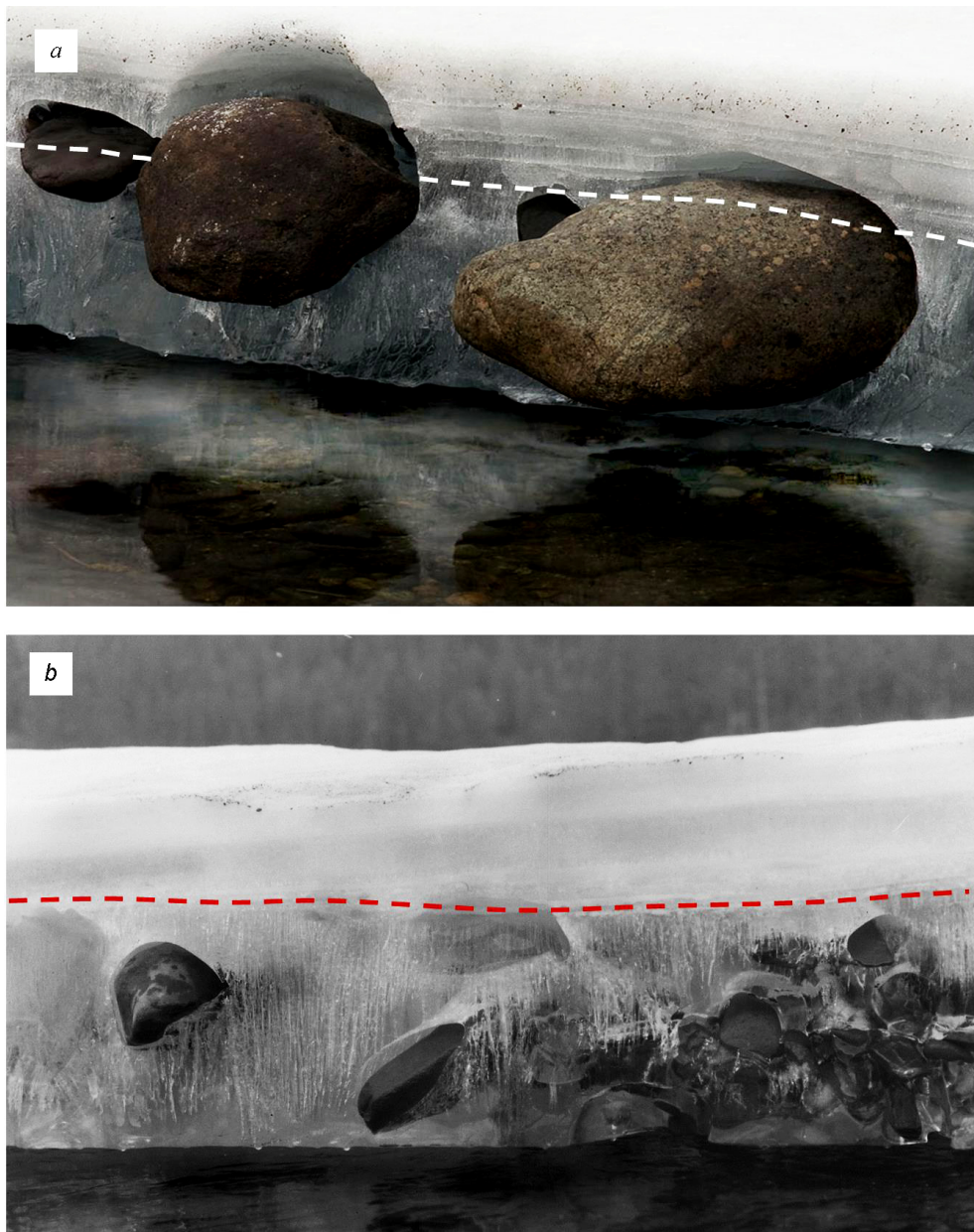


Fig. 4. Boulders and rock fragments in the vacuum-filtration ice layer.

a – on the aufeis glade in the Suntar river valley, Yakutia (photo by S. Karpukhin); *b* – on the aufeis glade in the Aunakit river valley, Patom plateau. The dashed line shows the lower boundary of the aufeis ice.

Рис. 4. Валуны и обломки горных пород в толще вакуум-фильтрационного льда.

a – на наледной поляне в долине реки Сунтар, Якутия (фото С. Карпухина); *b* – на наледной поляне в долине реки Аунакит, Патомское нагорье. Пунктиром показана нижняя граница наледного льда.

extension of the ice vein. It is typically characterized by a pronounced subhorizontal lamination that is complicated by subsequent frost shattering as ice occupies the cavity and gets fractured inside it.

If the cavity is located underneath the ice mass and filled in after the frozen seasonally thawing soil links with permafrost, water freezing takes place in a confined space. In this scenario, radially oriented crystals are formed, and gas bubbles are distributed concentri-

cally. In the central part of such ice mass, the mineral content is increased due to sequential freezing of dissolved salts.

In both scenarios, the build-up ice cap is often split by frost shattering and thus acquires a complicated texture. Under a corresponding regime of sedimentation, such processes seems to account for the major increase of the considered ice deposits. Sites with recurrent-vein ice of the similar origin are typically abundant at

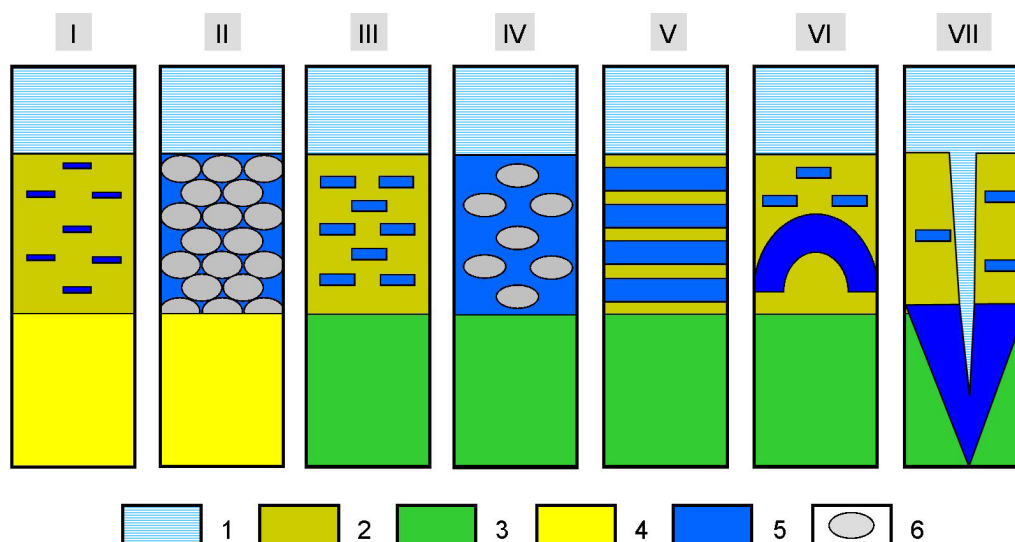


Fig. 5. Types of aufeis ice-ground complexes (IGC).

I – massive-segregation; *II* – cement-basal; *III* – layered-segregation; *IV* – basal-segregation; *V* – vacuum-filtration; *VI* – pressure-injection; *VII* – fissure-vein. 1 – aufeis deposit with intercalations of snow ice and snow; 2 – seasonally thawing layer of rocks; 3 – perennially frozen rocks; 4 – thawed and unfrozen ground materials; 5 – ground ice; 6 – boulders and pebbles.

Рис. 5. Типы наледных льдогрунтовых комплексов.

I – массивно-сегрегационный; *II* – цементно-базальный; *III* – слоисто-сегрегационный; *IV* – базально-сегрегационный; *V* – вакуум-фильтрационный; *VI* – напорно-инъекционный; *VII* – трещинно-жилковый. 1 – наледь с прослоями снежного льда и снега; 2 – сезонно протаивающий слой горных пород; 3 – многолетнемерзлые горные породы; 4 – талые и немерзлые грунты; 5 – подземный лед; 6 – валуны и галька.

the periphery of flat aufeis glades composed by fine sediments, as well as in river terraces formed below the floodplain regime level. The Middle Sakukan river valley in the Upper Chara basin can be viewed as an example of such environment. Its recurrent-vein ice mass (see Fig. 3, c) is classified as polygenetic. The bottom ice was formed epigenetically prior to aufeis depositing, while the top ice is of the syngenetic origin and accumulated during the long-term development of aufeis. It is most probable that 'purely' syngenetic ice veins may form in the lower parts of aufeis glades wherein accumulation of solid material usually prevails over its removal.

4. TYPES OF AUFEIS ICE-GROUND COMPLEXES

As described above, a complex two-tiered system containing paragenetically related frozen soil and surface ice is formed in aufeis areas of the permafrost zone. Its top is composed of aufeis ice, frozen sleet and snow, and its bottom contains ice-saturated rocks. The structure of the cryogenic system depends on two major processes, layer-by-layer water freezing on the ground surface and crystallization of groundwater in conditions of periodic variations of the heat flow density. By the ratio of components in the surface and sub-

surface tiers, we distinguish a series of genetically homogeneous structures termed 'aufeis ice-ground complexes' (IGC) that are significantly different from similar complexes located outside the aufeis glades. The IGC structure, joined development and locations determine geological engineering and landscape-geographical conditions that are of importance for development of such territories.

Since the upper tier does not show any diversity of its structure and consists of relatively homogeneous layers of aufeis (rarely, river ice and snow), it can be viewed as a single structural element of the system. Therefore, specific stratigraphic features of the profile are determined by the main types of subsurface icing (segregation, basal-cement, vacuum-filtration, pressure-injection, and fissure-vein). Together with surface ice accumulation, these processes generate patterns and cryogenic structures of the ice-ground complexes (Fig. 5). We distinguish seven major types of such complexes (see their descriptions below). IGC-I and IGC-II are typical of the open-system conditions when groundwater is crystallized without cryogenic head and without significant deformation of the host rocks. Other types result from freezing of closed water-bearing structures that are subject to high pressures during water transformation to ice. Under pressure, mineral soil particles are relocated, and the top layer of the ground sur-

face is uplifted and subject to considerable deformation. The IGC characteristics described below are based on the data collected during our field observations on the aufeis polygons.

IGC-I. Massive-segregation type. The top tier consists of two layers composed of aufeis ice and crystalline river ice mixed with frozen slush; its thickness ranges from 1.0 to 1.5 m. The bottom tier is formed in the middle or second half of winter and contains muddy, sand-and-gravel or pebble sediments with small, evenly spaced ice lenses or ice pockets; its thickness ranges from 0.2 to 0.8 m. The cryogenic texture of soil is mainly of massive lensoid type. The contact with the underlying non-frozen rocks is smooth. In spring, the water level is significantly below the bottom of the frozen layer. IGC-I is observed on floodplains and under the beds of freezing water flows in areas of over-permafrost and inter-permafrost taliks that get dry in winter. No visible movements of the ground or overlying ice layers are observed in such areas.

IGC-II. Cement-basal type. The upper tier consists of two or three layers composed of snow ice or crystalline river ice covered by river-water or groundwater aufeis; its thickness ranges from 1.0 to 2.0 m. The lower tier contains well-washed boulders and pebbles, and gaps between them are completely filled with ice; its thickness amounts to 1.0 m. The basal cryogenic texture forms in the second half of winter after freezing of the surface water flow in conditions of high water-cut of the channel alluvium. Such conditions are characteristic of river sections with 'diving' runoff (water appears and disappears through the channel length). In dry riverbed sediments, icing takes place in the middle or late winter due to ingress of aufeis water. In both cases, crystallization of water in cavities is accompanied by rock cementing/hardening with slight shifting of rock components relative to each another, but does not lead to uplifting of the top layer with frozen-up snow and ice.

IGC-III. Layered-segregation type. The upper tier (up to 2.5 m thick) consists of one or two layers composed of aufeis ice or aufeis plus snow ice. The lower tier is a seasonally thawing icy layer composed of fine rocks, such as sand, loamy soil, sandy clay or clay, underlain by permafrost. IGC-III is observed in peripheral areas of sodded aufeis glades in development stages I and IV. Three scenarios of freezing in the closed water-bearing system are revealed: (1) freezing of the layer starts before the beginning of aufeis formation, i.e. in November and December, and continues underneath the icing cover until its complete linkage with the permafrost base; (2) the soil freezes during layer-by-layer water freezing on the ground surface in between water discharge cycles; (3) the moist over-permafrost layer freezes after the decay of aufeis processes and stabilization of sub-zero temperatures throughout the profile. Layers of segregation ice (3 to 5 cm thick) are formed parallel to the

freezing front in the bottom part of the horizon in the first case, across the entire freezing bed in the second case, and under the aufeis in the contact layer in the third case. Cryogenic ground segregation is accompanied by uplifting of the ground surface together with the overlying aufeis ice by 10 to 30 cm, depending on the thickness of the seasonally thawing layer and its pre-winter moisture content.

IGC-IV. Basal-segregation type. The top single-layer tier (up to 3 m thick) consists of aufeis ice. In the bottom tier (0.5 to 1.0 m thick), boulders and large pebbles are suspended in transparent massive ice. Unfrozen water-bearing sediments are located below, overlaying the permafrost base or base rocks. When freezing, groundwater accumulates pressure and often gushes or penetrates into the contact zone between the ground surface and the aufeis deposit to form lenses and layers of clear blueish ice. Water transformation to ice is accompanied by ubiquitous relocation of boulders and pebbles relative to each other, and the frost-bound cap together with aufeis slabs is uplifted to a height of 0.5 to 1.2 m. In some locations, inside the sediment beds, there are horizontally consistent layers and lenses of injection ice (0.5 to 0.8 m thick) of the prismatic vertically oriented structure. IGC-IV formation lasts through the entire cold period of the year. It is abundant on beds of small rivers and streams that get dry by the beginning of winter. On mature aufeis glades, it can occupy dozens and hundreds of thousand square metres, while annual volumes of ground ice and magnitudes of ground movements due to hydrothermal factors may vary tremendously from year to year (Fig. 6). In summer, the lower tier of IGC-IV is often mistakenly viewed as an aufeis deposit that was 'dirtied' by the boulder-pebble material.

IGC-V. Vacuum-filtration type. The top single-layer tier (up to 2.5 m thick) consists of aufeis ice. The bottom tier (0.3 to 1.8 m thick) contains grass, sand and loamy soil mixed with small pebbles at some locations. Across the profile, there are layers of pure transparent ice (10 to 50 cm thick), going parallel to each other and separated by layers of jammed-in fine sediments with the lenticular cryogenic texture. At the periphery, ground ice layers are gradually tapering or split into branches looking like different-sized 'teeth' penetrating into the host rock. A gravity-feed water-bearing bed is located underneath the ground ice bed. No underlying permafrost has been revealed. In some outcrops, however, we observed fragments of ice-ground structures that are clearly of the vacuum-filtration genesis, yet might have been stored for more than one season. Transition of injection ice to permafrost might have resulted from re-deposition of sediments or storage of aufeis ice through the entire warm period of the year (during formation of the permanent snow patch). IGC-V is observed in outwash plain areas, that are devoid of vegetation, with dense networks of shallow multi-channel streams, as

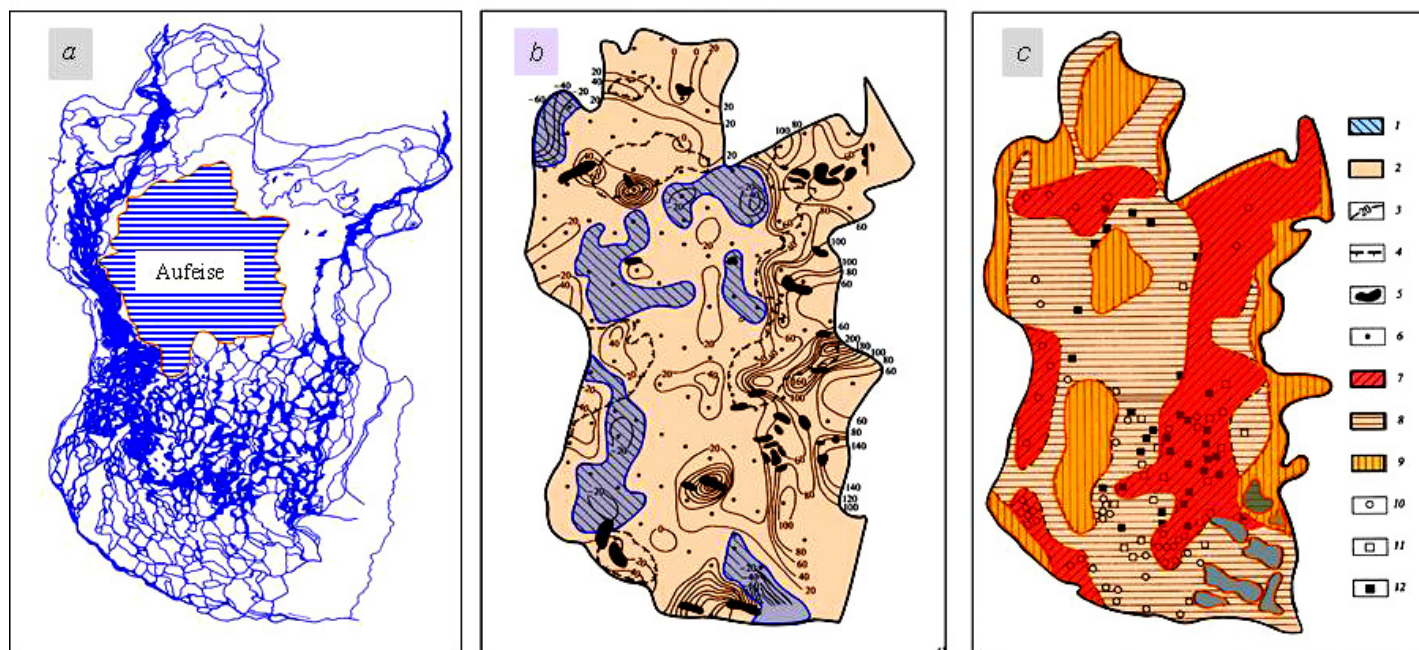


Fig. 6. The channel network on the aufeis glade and cryogenic movements of ground during formation of the gigantic Mururin aufeis deposit in the northern Transbaikalia.

a – channel network at the period of incomplete destruction of aufeis; *b* – situation according to observation data for the winter 1977–1978 [Kolotaev, 1980]; *c* – situation according to observation data for winter in 1978–1979 and summer 1980 [Deikin, 1985]. 1 – zone wherein the surface of the aufeis bed is subsided; 2 – zone wherein the rock surface is uplifted; 3 – isolines of higher elevation of the ground surface, m; 4 – zone of development of water-ice ridges; 5 – aufeis mound; 6 – measuring poles; 7 – zone of active water exchange and intensive uplifting of ground materials during formation of the injection-ice layer (0.73 m thick); 8 – zone of moderate water exchange and moderate uplifting of the ground surface during formation of the injection-ice layer (0.45 m thick in average); 9 – zone of weak injection icing or its absence; 10 and 11 – pits and profiles in areas of naturally outcropped injection-ice layers in 1979 (10) and in 1980 (11); 12 – pits and profiles in the ice-containing alluvium layer.

Рис. 6. Русловая сеть на наледной поляне и криогенное движение грунтов в процессе формирования гигантской Муруринской наледи на севере Забайкалья.

a – русловая сеть в период неполного разрушения наледи; *b* – ситуация по данным наблюдений [Kolotaev, 1980] в зиму 1977–1978 гг.; *c* – ситуация по данным наблюдений [Deikin, 1985] в зиму 1978–1979 гг. и летом 1980 г. 1 – зона понижения поверхности наледного ложа; 2 – зона повышения поверхности горных пород; 3 – изолинии повышения поверхности грунтов, м; 4 – зона развития водно-ледяных гряд; 5 – наледный бугор пучения; 6 – измерительные веши; 7 – зона активного водообмена и интенсивного поднятия грунтов при формировании инъекционных льдов средней мощностью 0.73 м; 8 – зона умеренного водообмена и умеренного поднятия поверхности земли при формировании и инъекционных льдов средней толщиной 0.45 м; 9 – зона слабого развития инъекционных льдов или их отсутствия; 10–12 – шурфы и разрезы, пройденные в 1979 г. (10), на участках естественного обнажения инъекционных льдов в 1980 г. (11) и в толще льдосодержащих аллювиальных отложений (12).

well as in some suffosion-erosional valleys near permanent groundwater sources (Fig. 6).

IGS-VI. Pressure-injection type. The top tier (0.5 to 1.5 m thick) consists of aufeis ice. The bottom tier (0.5–1.2 m thick) contains loamy soil, sandy loam, sand, grass, pebbles, large boulders or peat, i.e. rocks that differ in size of particles. In the profile, a plano-convex or biconvex lens of pure ice is always present; the lens contains torn-off trunks of shrubs, tree roots, grass, moss and pieces of rocks from the underlying layers. Ice domes as well as overlying ground are broken by gaping fractures; radially tilted trees are observed on slopes of heaving mounds, and there are air pockets and small lakes inside the mounds. No information is available on

configurations of the channels through which hydraulic-head groundwater is transported to the ground surface to form a ground ice lens and to cause uplifting of the ice-ground mass. Such channels may be represented by narrow talik fissures or oval 'tubes', judging by the fact that ISC-IV is observed in linear zones of tectonic faults, beds of small rivers and streams and local over-permafrost water discharge foci, all being clearly manifested in the terrain. In winter, the water discharge channels are blocked by ice and soil 'plugs'. Such plugs are periodically destroyed (sometimes with an outburst) under the pressure of ascending flows [Petrov, 1930; Podyakonov, 1903], and the ground surface bends down to acquire a parabolic profile. During freezing of closed

Table 1. Annual vertical ground movement amplitudes in aufeis sections of river valleys, according to observations on the Charskie Peski and Eden polygons (per 1 m profile), cm

Таблица 1. Амплитуда ежегодного вертикального движения грунтов на наледных участках речных долин по данным наблюдений на полигонах Чарские пески и Эден (в пересчете на 1 м разреза), см

| Development stages of aufeis sections of river valleys* | | Types of aufeis ice-ground complexes | | | | | | |
|---|-------------------------|--------------------------------------|--------|---------|--------|--------|---------|---------|
| | | IGC-I | IGC-II | IGC-III | IGC-IV | IGC-V | IGC-VI | IGC-VII |
| I | Periglacial development | 5–10 | 10–20 | 10–20 | | | | |
| II | Transgression | 10–20 | 20–30 | 20–30 | 40–50 | 50–100 | 100–500 | 20–40 |
| III | Stabilization | 10–20 | 20–30 | 30–40 | 30–40 | 40–70 | 50–300 | 10–30 |
| IV | Regression | 10–20 | 20–30 | 20–30 | 20–30 | 30–50 | 50–100 | 5–10 |
| V | Postglacial development | 5–10 | 10–20 | 10–20 | | | | |

Note. * – development stages are described below.

Примечание. * – описание стадий развития см. ниже.

cryogenic systems, pressures amount to dozens of thousand bar. In the Egegi river valley in East Sayan mountains, we recorded a case of a heaving mound located in front of a rocky bench composed of the flat-lying Proterozoic dolomite. In spring, the heaving mound was destroyed, and the rock slabs were literally broken out of the rock mass and set at an angle of about 40 degrees against their former position.

IGC-VII. Fissure-vein type. The upper tier (0.5–1.0 m thick) consisting of aufeis ice is underlain by fine icy sediments with the massive lenticular cryogenic texture and wedge-like inclusions of vein ice and/or recurrent-vein ice. In the period from mid-late December until the aufeis formation, the seasonally thawing layer of the bottom tier (0.5 to 0.8 m thick) is saturated with small lenses of randomly arranged segregated ice. In the same period, soil and permafrost are subject to frost shattering. In the second half of winter and in spring, snow melting provides for infill of fractures and fissures with ice. Depending on the composition and pre-winter soil moisture content, the ground surface can be uplifted to a height of 10 to 40 cm. IGC-VII is formed in conditions of low snow and low air temperatures at the periphery of the icing glades.

5. CRYOGENIC MOVEMENTS OF GROUND IN AUFEIS GLADES

Cryogenic movements of freezing rocks are well known [Rusanov, 1961] and described in many scientific and technical reports related mainly to issues of stability of buildings and facilities built on heaving soils. However, cryogenic movements of ground in aufeis glades have not been properly assessed yet. A few articles [Alekseyev, 1989; Kravchenko, 1983, 1985b] describe the dynamics of the ground surface under the influence of aufeis processes, as evidenced by instrumental monitoring data. In other publications [Gasa-

nov, 1966; Gorbunov, Ermolin, 1981; Klimovsky, 1978; Koreisha, 1969; Krendeleev, 1983; Petrov, 1930; Sannikov, 1988], the information is mainly descriptive. Nonetheless, the available data (Table 1) are sufficient to attempt at establishing regularities in annual morpho-structural transformations of aufeis sections of the river valleys.

The tabulated data suggest that mobility of the rocks underlying the aufeis deposit depends on types of the ice-ground complexes and development stages of the aufeis sections of the river valleys. The aufeis bed is uplifted due to formation of ground ice lenses and layers; it sinks down due to thawing of ice inclusions and thermal settlement of the mineral sediment mass. At the first and last stages of development of the aufeis sections, the ground surface deformation does not exceed values of the cryogenic movements recorded outside the zone wherein the aufeis deposit was formed. Moreover, deformation is reduced as the low floodplain and channel deposits are blocked from freezing by the aufeis-river ice cover. Neither soil heaving nor settlement can be visually detected in such areas, firstly, because the depth of seasonal freezing under freezing water streams seldom exceeds 0.2–0.5 m, and secondly, traces of winter movements of the subglacial alluvium are destroyed by spring-time ice drifting and erosion. At other stages of transformation of the aufeis valley, both positive and negative forms of the permafrost terrain are abundant, and the ground surface uplifting/sinking amplitude amounts to a maximum in the most active stage of transgression due to well-manifested processes of icing of the vacuum-filtration and pressure-injection types.

The scale and intensity of ground movements in mature aufeis glades are shown in Fig. 7. Our observations were conducted at the upper course of the Bolshoi Eden river at the boundary of the forest belt and the goltsy woodland (elevation 1800–1820 m). The aufeis

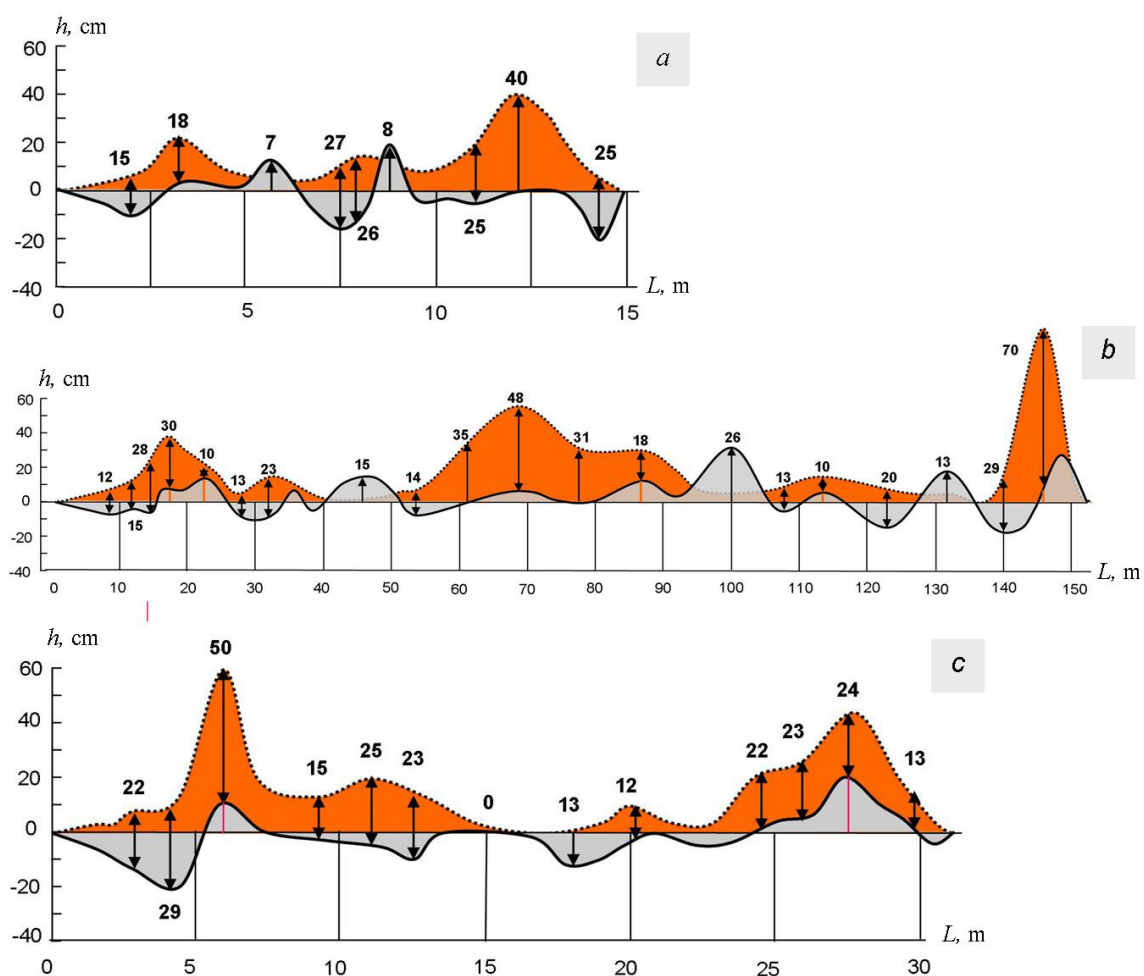


Fig. 7. Variations in the ground surface elevation of the aufeis glade in the Bolshoi Eden river valley in East Sayan, according to serial leveling data.

Heights above the reference points of observation (September 1986) with respect to the width of the aufeis section of the river valley, L : top curve – aufeis bed in May 1987, bottom curve – ground surface in September 1987 (after melting of the ice cluster). Arrows show directions of ground movements. Numbers correspond to absolute ground displacement values (cm) at the surface of the aufeis glade from May to September 1987. Colour codes: red – areas of ground heaving producing stratal ice and ice lenses of the vacuum-filtration and pressure types in winter in 1986–1987; grey – thermokarst and thermoerosion (below the zero line) and sediment redeposition and accumulation processes in conditions of injection-ice thawing in summer in 1987 (above the zero line). Positions of the profile: a – upper, b – middle, c – lower part of the aufeis glade.

Рис. 7. Изменение высоты земной поверхности наледной поляны в долине реки Большой Эден (Восточные Саяны) по данным серийных нивелировок.

Превышение h относительно базисных точек наблюдения (сентябрь 1986 г.) по ширине наледного участка долины L : верхняя кривая – ложе наледи в мае 1987 г., нижняя – поверхность земли в сентябре 1987 г. (после стаивания ледяного массива). Стрелками показано направление движения грунтов, цифрами абсолютное значение величины смещения (см) поверхности наледной поляны с мая по сентябрь 1987 г. Красный цвет идентифицирует процессы пучения грунтов с формированием пластовых и линзовидных льдов вакуум-фильтрационного и напорного происхождения в зиму 1986–1987 гг., серый цвет ниже нулевой линии – процессы термокарста и эрозии, выше нулевой линии – процессы переотложения и аккумуляции осадков в условиях вытаивания инъекционных льдов в летний период 1987 г. Положение профиля: a – верхняя, b – средняя, c – нижняя часть наледной поляны.

section (0.2 m² in total) is flat and gently sloping, composed of sand and gravel with inclusions of large (up to 2.5 m in diameter) boulders and rock fragments that had rolled down the steep slopes (almost 250 pieces). In winter, the aufeis glade is covered with ice (1.5 to 2.0 m thick) that melts completely only in mid-August.

Injection ice beds are located at depths from 0.3 to 0.5 m from the ground surface or directly underneath the aufeis deposit. The injection ice beds are consistent in strike, 0.5 to 1.2 m thick and occupy the area practically within the limits of the aufeis glades. In this area, the overlying soil is uplifted annually together with the

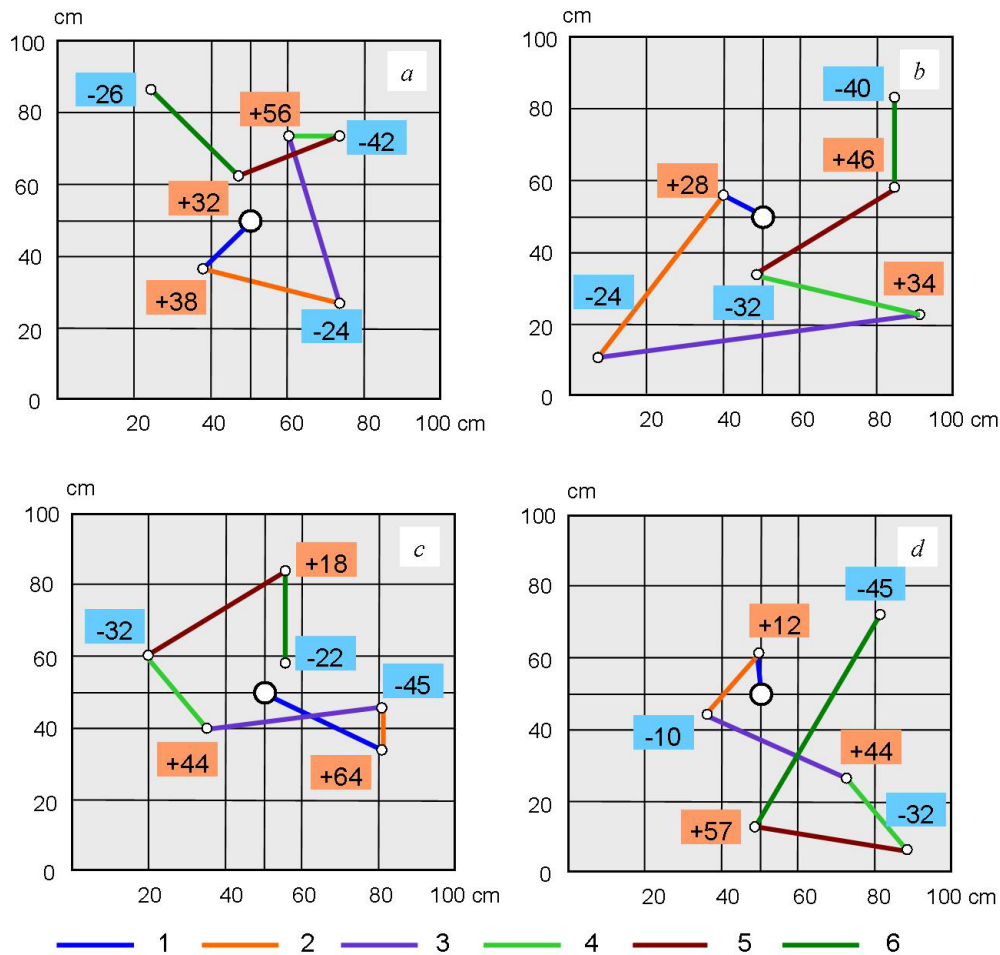


Fig. 8. Hydrothermal movements of large boulders in the aufeis glade in the upper reach of the Bolshoi Eden river in East Sayan according to serial leveling data for the period 1986–1989.

Horizontal (coloured lines) and vertical (numbers at reference points, cm) displacements of the reference marks: 1 – winter in 1986–1987; 2 – summer in 1987; 3 – winter in 1987–1988; 4 – summer in 1988; 5 – winter in 1988–1989; 6 – summer in 1989. Approximate weights of boulders: a – 0.5 t; b – 0.8 t; c – 1.2 t; d – 1.5 t.

Рис. 8. Гидротермическое движение крупных валунов на наледной поляне в верховьях реки Большой Эден в Восточных Саянах по данным серийных нивелировок 1986–1989 гг.

Смещение марки по горизонтали (цветные линии) и по вертикали (цифры у опорных точек, см): 1 – зима 1986–1987 гг.; 2 – лето 1987 г.; 3 – зима 1987–1988 гг.; 4 – лето 1988 г.; 5 – зима 1988–1989 гг.; 6 – лето 1989 г. Ориентировочный вес валунов: a – 0.5 т; b – 0.8 т; c – 1.2 т; d – 1.5 т.

aufeis deposit to a height of about 1.0 m. In spring, such locations are marked on the ground surface by fractured ice- or ice-ground mounds. It is noteworthy that some of the boulders (about 40 %), lying on the gravel base and scattered on the valley bottom, are frozen into the laminated aufeis mass, while the boulders located below the aufeis bed are enveloped by the near-contact or underground-water injection ice of the columnar structure. During the year, all the boulders, regardless of their positions in the profile and their weights, are displaced to distances of dozens centimetres in various directions both vertically and horizontally (Fig. 8). The movements are caused by cryogenic pressures of groundwater and solids during thermokarst and ther-

mal erosion processes. Any potential impact of the hydrodynamic pressure of surface water is excluded because the water flow is small and spread throughout the aufeis bed.

The dynamics of loose sediments in the aufeis valleys is specific – cryogenic movements take place in different directions in cold seasons, i.e. soil is uplifted together with ice in some locations, while in the other places it is subsided. This phenomenon was first discovered by hydrologists V.N. Kolotaev [Kolotaev, 1980] and V.N. Deikin [Deikin, 1985] at the Mururino aufeis deposit in the Upper Chara basin during the winter period of 1977–1978 (see Fig. 6). The mechanism of this process is not completely understood. It can be only

assumed that the ground surface subsides in the aufeis-formation zone in winter is due to redistribution of water reserves and groundwater head in the cryodynamic system as a result of its non-uniform freezing.

In the aufeis sections of the river valleys, local soil heaving deserves special attention. This process leads to formation of round-shaped or elongated mounds (hydrolaccoliths) which height ranges from 3 to 4 m (rarely 7 m), and the diameter is up to 150 m. In most cases, the mound height/width ratio is 1/10. The mounds can be annual or perennial, confined to areas of concentrated discharge of groundwater under pressure (around springs) or scattered at the periphery of mature aufeis glades in a random pattern (Fig. 9). Causes and mechanisms of their formation have not been properly studied yet. It is assumed that the mounds occur and grow due to cryogenic or hydraulic pressure of water-bearing systems during freezing; any details of this process are still unknown. As shown by profiles of the mounds, the top soil layer (0.5 to 0.8 m thick) is underlain by the ice dome (up to 1.5 m thick). Underneath the ice dome, there is a layer of water that is usually separated from the dome by an air bubble. A completely frozen water core of the mound is generally shaped as a plano-convex lens. Ground ice is transparent and latently laminated, with the hypidiomorphic-granular structure; it contains elongated cylindrical air bubbles that are oriented perpendicular to the freezing front.

While growing, the mounds periodically burst and let water and air gush out. The volume of water lenses may amount to dozens of cubic metres. An interesting case is a hydrolaccolith as big as a two-storey house (!) at the edge of the Charskie Peski mass. Geologists F.I. Anikeev and V.N. Samoylenko (Udokan Geological Expedition) drilled a small tunnel shaft at its base and let the water core discharge. Under the ice dome inside the hydrolaccolith, they found a large cavity, 7 m high and 28 m in diameter [Krendelev, 1983].

Generally, the ground-and-ice roof subsides after water discharges, and fractures are closed and sealed with frozen water. In winter, stress increasing/decreasing cycles repeat many times until the water-bearing system is completely frozen or until heat emission towards the day surface ceases. Formation of mounds starts in November and December and stops in spring during snow melt.

Destruction of mounds often leads to formation of roundish crater-like depressions framed by chaotically heaped ground banks with inclusions of fragments of ground, tree stems, shrubs and turf shred. The craters may transform to small lakes and thus become permanent ground water discharge sites. V.S. Preobrazhensky described an ice grotto located near the Charskie Peski mass, which replaced a partially destroyed hydrolaccolith, about 35 m in diameter and over 3.5 m high. At the

grotto bottom, there was a small lake (1.3+ m deep) and a streamlet flowing out of the lake along a fracture [Preobrazhensky, 1961].

Ablation of bedded ground ice may take place already during break-down of the aufeis deposit due to thermal erosion, and eventually thermokarst caverns (Fig. 10, *a*), furrows and ditches are formed in such locations. If the ground sinking areas are covered with vegetation, the vegetation is completely extinguished. In the postglacial development stage of the valley, it takes many years for the vegetation to restore. Uneven melt-out of ground ice often leads to formation of either single-level ice-ground terraces (0.5 to 0.8 m high) (Fig. 10, *b*) that are separated by shallow channels of migrating flows, or a series of flat-topped torso mountains underlain by injection-ice layers (Fig. 10, *c*). In summer, mushroom-shaped ice pillars may be found in the aufeis glades. A 'mushroom stalk' is made of melted-out ice, and a cap is either a piece of turfgrass with live plants or a large fragment of rock (Fig. 10, *d*). Besides, cones and chains can be formed, which interior is composed of aufeis- or underground injection ice.

While repeated-vein ice is melting out in the aufeis glades, deep ditches filled with water are first to form, surrounded by blocks of ground with the veins. In plan, such an area looks like a polygonal network with small lakes in nodes. Upon drainage of the ditches, permafrost soil rapidly degrades, and the aufeis bed is converted into a system of low butte mounds-silt pinacles that disappear soon due to thermal erosion activity of melt-aufeis-water flows.

Thermokarst processes are weakly manifested during melt-out of texture-forming ice. Thermokarst is mainly observed at the periphery of aufeis glades on sites where aufeis ice occurs only occasionally. Deformation of the surface of the aufeis bed are less significant on such sites. However, under certain conditions, there is potential for development of hazardous phenomena. In [Alekseyev, 1976], a case of the Tunka basin located in the south-western part of Pribaikalie is described. In May 1973, in the Tibelti river valley, aufeis melt water penetrated underneath seasonally frozen sand deposits. As a result, a large gully was formed in a few days. It was almost 250 m long, 10 to 15 m wide and 2 m deep (Fig. 10, *e*). The suffusion-erosion process was accompanied by typical subsidence fracturing and mass collapse of frozen blocks and overlaying aufeis-ice slabs.

6. AUFEIS IMPACT ON CHANNELLING

In the zone of continuous aufeis formation, pass-through water channels are influenced by specific glaciohydrological and cryo-geological phenomena, and seasonality of channelling is evident.

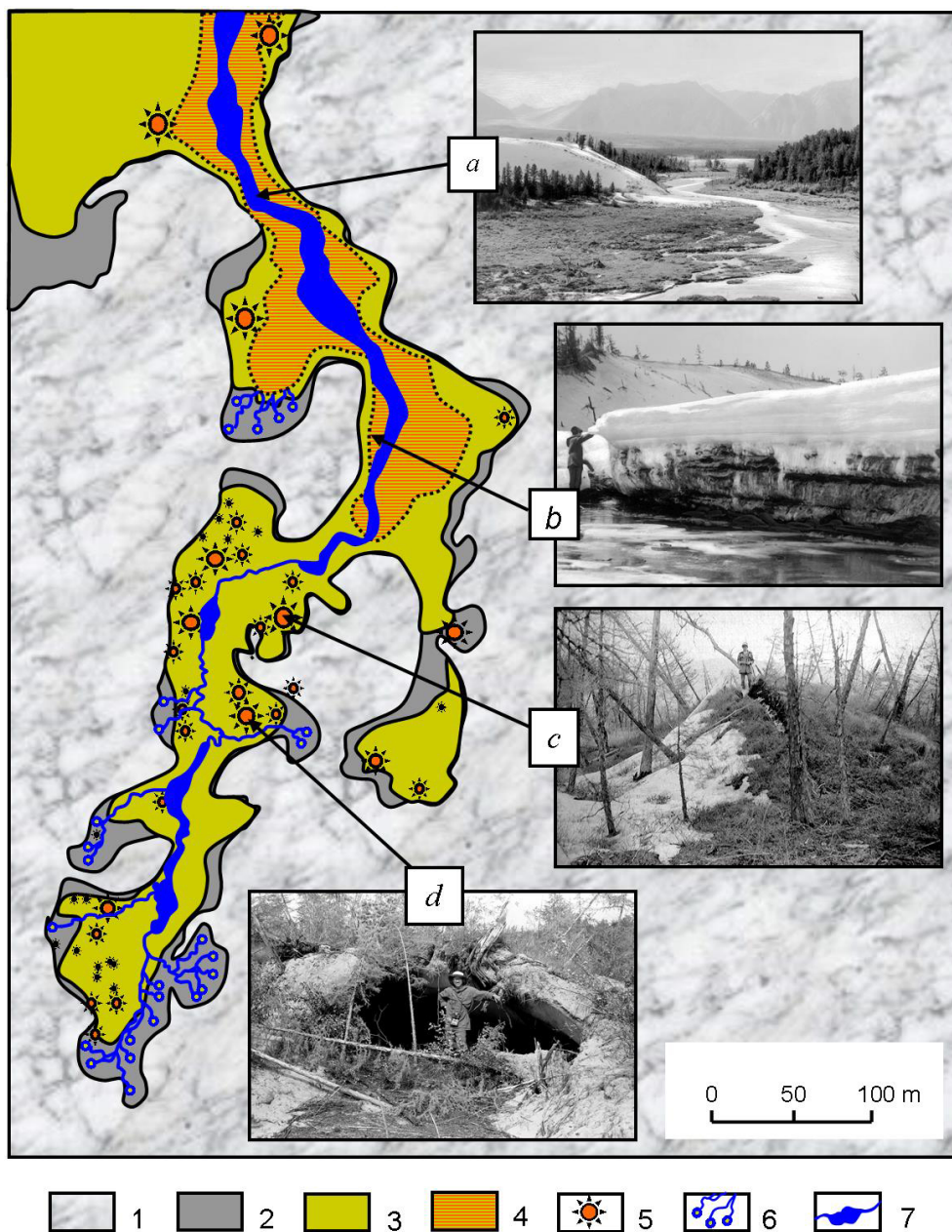


Fig. 9. Hydrothermal movements of ground materials in the aufeis valley of the Kholodny creek, Charskie Peski site in the northern Transbaikalia.

1 – cluster of deflated sandy deposits; 2 – aufeis-free section of the valley wherein the annual ground surface uplifting amount to 10 cm; 3 – section of the valley that is annually covered by the aufeis ice layer (1.0–2.5 m thick) and subject to hydrothermal vertical movements ranging from 0.1 to 0.3 m; 4 – section of the valley with vacuum-infiltration ice layers, wherein the amplitude of cryogenic movements of ground materials range from 0.8 to 1.2 m; 5 – icing mounds (0.5–3.5 m high) with pressure-injection ice lenses; 6 – permanent sources of subpermafrost groundwater; 7 – channel of the creek with thawed ground ice in the expanding sections. Photos: *a* – general view of the estuarine part of the aufeis valley after aufeis ablation, September 1978; *b* – vacuum-infiltration ground complex in early July 1978; *c* – icing mound with the ice core – pressure-injection ice-ground complex, June 1977; *d* – air cavity in the decaying hydrolaccolith, July 1978.

Рис. 9. Гидротермическое движение грунтов в наледной долине ручья Холодного. Урочище Чарские Пески на севере Забайкалья.

1 – массив развеваемых песчаных отложений; 2 – безналедный участок долины с величиной ежегодного поднятия земной поверхности до 10 см; 3 – участок долины, ежегодно покрываемый наледным льдом толщиной 1.0–2.5 м, с амплитудой гидротермических движений 0.1–0.3 м; 4 – участок долины с пластами вакуум-инфильтрационного льда с амплитудой криогенного движения грунтов 0.8–1.2 м; 5 – бугры пучения высотой 0.5–3.5 м с линзами напорно-инъекционного льда; 6 – постоянно действующие источники подмерзлотных подземных вод; 7 – русло ручья с вытаявшим подземным льдом на участках расширения. Фотографии: *a* – общий вид устьевой части наледной долины после стаивания наледи, сентябрь 1978 г.; *b* – вакуум-инфильтрационный грунтовый комплекс в начале июля 1978 г.; *c* – бугор пучения с ледяным ядром – напорно-инъекционный ледогрунтовый комплекс, июнь 1977 г.; *d* – воздушная полость в разрушающемся гидралакколите, июль 1978 г.

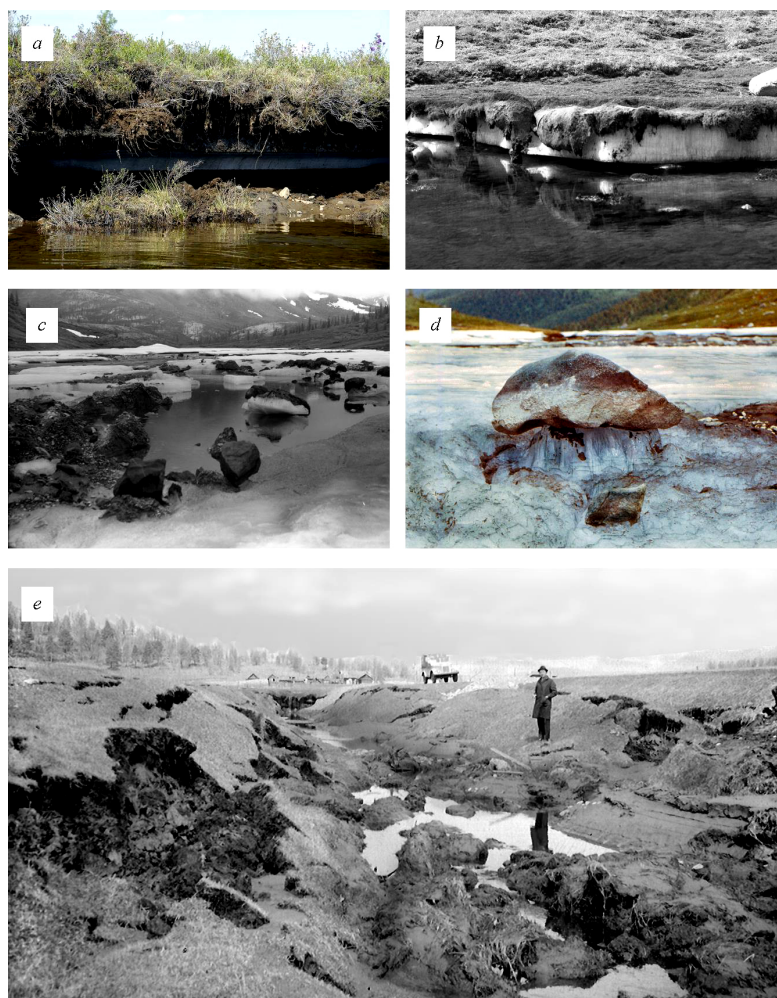


Fig. 10. Forms of cryogenic movements of ground materials in aufeis sections of river valleys.

a – thermokarst-induced subsidence of the roof of the injected ground-ice layer; *b* – thermoerosion terrace of the aufeis ice-ground complex; sod-cover pieces are squeezed in between the aufeis- and injection-ice layers; *c* – thermoerosion remnants in the place of the decaying vacuum-filtration ice mass; *d* – the boulder raised to a height of 1.2 m by injection icing; *e* – suffusion-erosion caving at the Irkutsk–Mondy motor road.

Рис. 10. Формы криогенного движения грунтов на наледных участках речных долин.

a – термокарстовая осадка кровли инъекционного подземного льда; *b* – термоэрозийная терраса наледного ледогрунтового комплекса; зимой куски дернины зажаты между слоями наледного и инъекционного льда; *c* – термоэрозийные останцы на месте разрушающегося массива вакуум-фильтрационного льда; *d* – валун, поднятый на высоту 1.2 м в результате инъекционно-го льдообразования; *e* – суффозионно-эрозийный провал у автомобильной дороги Иркутск–Монды.

In *winter*, water-carrying channels are influenced by three specific events: (1) obstruction of the water stream due to its freezing to complete cessation of the flow; (2) hydrodynamic impact of additional water inflow (subaqueous discharge of groundwater, water release from reservoirs etc.); and (3) static pressure of ice under external loads (snowfall, atmospheric pressure jump etc.). In the autumn-winter period (typically lasting for 2 or 3 months), nothing extraordinary happens – deformations develop under ice, and soils are redeposited according to schemes that are well-known and described in detail [Belokon', 1950]. In some sections of the river, as the runoff is depleting, river-water

ice is sagging or hanging over the water flow. In other sections, river-water ice is covered by a thin river-water aufeis deposit which boundaries are usually above the autumnal low water level by a few dozen centimetres.

In the winter-spring period (from December or January), channelling is completely finished, while a number of phenomena develop and later on play a dominant role throughout the course of transformation of the channel network. In this period, ice mounds are formed in the riverbeds between frozen river bars (Fig. 11), and stagnant water is periodically discharged at high pressure from the ice mounds. In small rivers

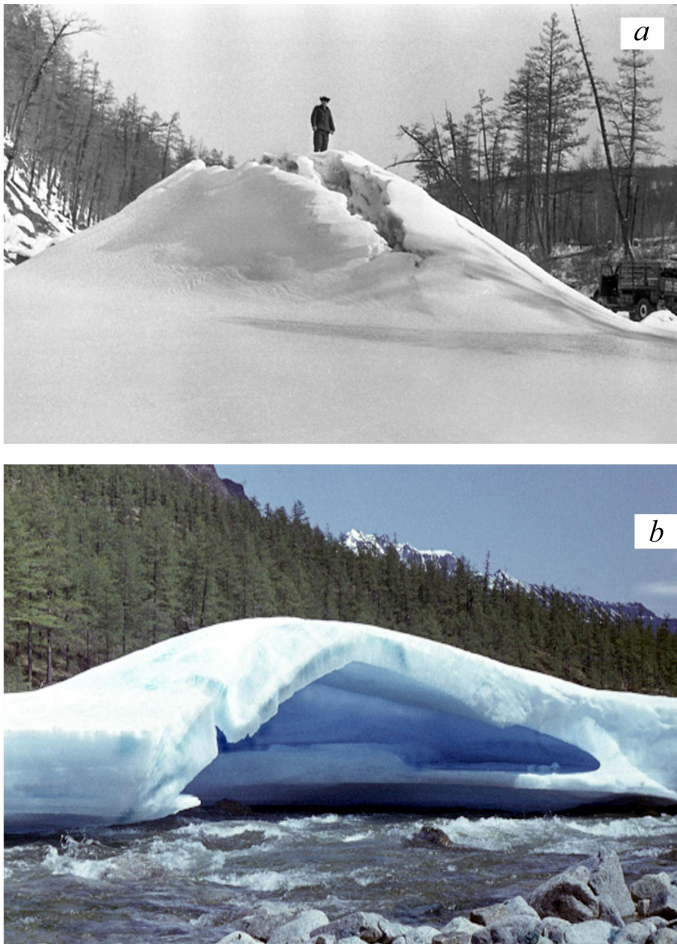


Fig. 11. Icing mounds in channels of icing rivers.

a – in winter (Oyumrak river in South Yakutia); *b* – in summer (Middle Sakukan river in the northern Transbaikalia) (photo by V.R. Alexeyev).

Рис. 11. Ледяные бугры пучения в руслах наледных рек.

a – зимой (река Оюмрак в Южной Якутии); *b* – летом (река Средний Сакукан в Северном Забайкалье) (фото В.Р. Алексеева).

beds, ice mounds are up to 3 m high, and radial fractures at their tops often follow each other for many kilometres. Once the water stream is completely frozen, the channel deposits are frozen up to the lower surface of the ice cover and uplifted together with ice during further freezing of the underflow, and a mound containing ground and ice is thus formed. Water, mud, large boulders and pebbles gush out of such a mound in case of its explosive failure. The Russian historical records describe a fatality case when a group of people and a caravan of horses were killed by explosive failure of the ice mound on the Zeya river in the Amur region. The only survivor was a little boy who had been knocked up by the air blast wave onto a nearby larch tree [Derpgolts, 1971]. Another example is explosive

failure of a ground-aufeis mound on the Onon river valley near the Amur-Yakutsk motor road in the spring of 1928. When the headwater cryogenic system exploded, large lumps of soil and ice were blasted out. Almost 19 m long, 5 m wide and 32 m thick lumps destroyed a motor-road bridge and, together with its debris, were carried away by gushing water streams to a distance of 120 meters down the river valley [Petrov, 1930].

In winter, the aufeis sections of the river valleys become an arena of intense ground movements through virtually their entire widths, not only within the limits of the freezing river beds. Under the aufeis deposits (including those located in forests), injection-ice layers and lenses (up to 1.0 m thick) are formed at depths from 0.3 to 0.8 m; they often include numerous boulders and pebbles. An area of their distribution can occupy from 10 to 80 % of mature aufeis glades. In the areas where stratal ice is formed, the overlying soil together with the aufeis ice can be uplifted to a height from 0.8 to 1.0 m, and, in case of a large local hydrodynamic pressure, by 4 to 5 m above its previous level. It is noteworthy that such vertical movements occur at some distance from the base of the mountain slopes and terraces, and by the spring time, the surface of the river valley's bottom acquires a pyramidal-convex shape complicated by hummocks and chains of hydrolocaliths. Thus, by the start of snow melting, an uplifted ice-ground plate (including icebound trees and shrubs) is formed in the zone of active aufeis formation in the river valley. Its thickness ranges from 1.5 to 3.5 m (up to 7–12 m in some locations). This ephemeral cryogenic structure extends across the entire width of the valley, blocks the way for flood waters (Fig. 12, *a*), and thus becomes an important factor predetermining further development of hydrological processes.

In *spring*, the river-water flow goes out of a narrow valley into a broad aufeis field, flattens and loses its speed, and its actual erosivity is vanishing. Gradually, however, water digs up several channels in ice, the channels quickly deepen, the flows cut through the ice mass and split it into several large ice slabs (Fig. 12, *b*) and begin to intensively erode the aufeis bed. The soil is actively redeposited in both the areas of open water flows and under the ice cover. At this time, subsurface erosion can significantly exceed soil drifting in the upstream sections of the river valley. Locations of ice channels tend to vary from year to year, and areas of erosion processes are thus shifted relative to each other. Therefore, the entire aufeis bed is subject to the mechanical impact of water flows. As a result, alluvial deposits are repeatedly mixed up, the soil-and-sod layer is destroyed, roots of trees and shrubs are washed out of the ground, the moss cover is torn off, the vegetation remain intact only in elevated parts of the terrain, i.e. on small islands and chains of hills with steeply-dipping, sloughing cliffs striking along the valley.

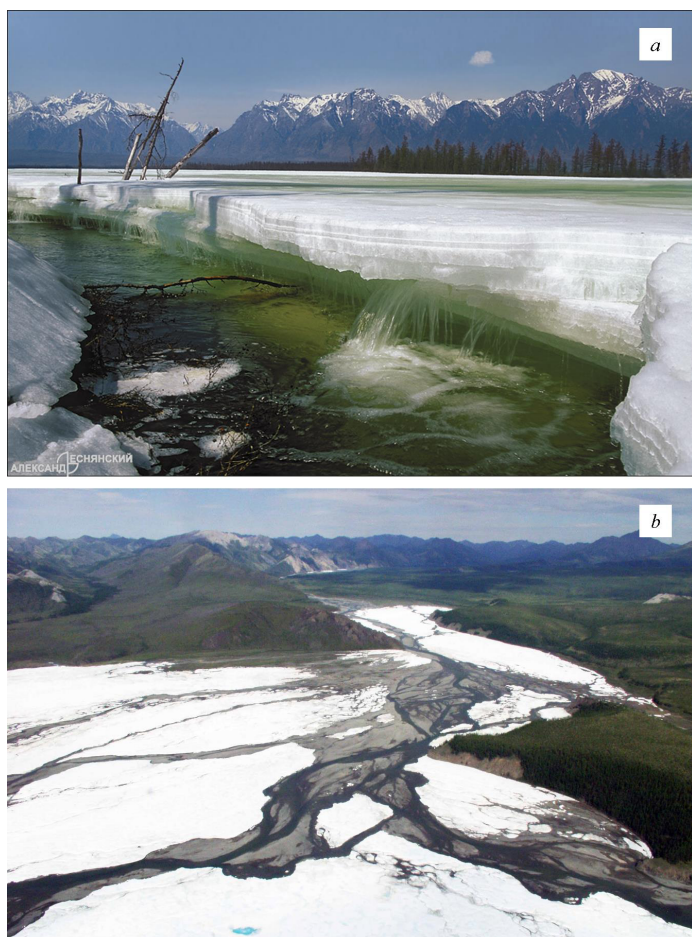


Fig. 12. Conditions of channeling in valleys of icing rivers.

a – during spring snow-melt period, a gigantic groundwater aufeis deposit in the Middle Sukakan river valley in the northern Transbaikalia (photo by A. Lesnyansky); *b* – in early summer, a gigantic aufeis deposit in the Bulkut river valley in the Verkhnekolymsky district of Yakutia (photo by A. Mekheda).

Рис. 12. Условия формирования русловой сети в долинах наледных рек.

a – в период весеннего снеготаяния; гигантская наледь подземных вод в долине реки Средний Сакукан на севере Забайкалья (фото А. Леснянского); *b* – в начале лета; гигантская наледь в долине реки Булкуп в Верхнеколымском районе Якутии (фото А. Мехеды).

During the snow-melt period, the channels are often blocked by ice masses, and river-water flows have to go through V-shaped gaps along the contact of aufeis deposits and beach scarps. Such gaps, looking like fractures, occur between ice and ground due to solar radiation absorption and gradually develop into deep drainage channels. Generally, during torrential flood in spring, the major portion of water is transported by such channels. Water streams rapidly erode the river-bank sediments, and suspended drift and debris are delivered to the bottom of the aufeis glades, deposited

into the ice tunnels and/or thrown onto the ice surface. Drift and debris may concentrate in large amounts on the ice surface and bury the ice bed. Quite often, water penetrates very quickly underneath the seasonally frozen ground layer and begins to wash away the underlying melt deposits, which causes catastrophically rapid retrogress of the river banks as the frozen beds collapse and get destroyed by thermal erosion (see Fig. 10, *e*).

In *summer*, dissected ice slabs and large ice masses shield the area from solar radiation and precipitation, hamper thawing of alluvial deposits, and control the direction of water flows. The ice slabs are displaced during rain floods, and ice drift may occur. The top and side surfaces of the ice masses are subject to ablation; the bottoms are destructed by abundant under-ice flows of water. During the melt period, large portions of the ice fields hang over their beds or lie on the ground-ice pillars and ledges of frozen rocks, and the ice cover has to bend, crack and collapse. Massive ice collapse creates a sound like a gunshot heard at a distance of many kilometres. Falling roofs of the ice tunnels and subsiding and rolling ice slabs compact the soil, press down the stems of plants, break up and flattened tree stems and shrubs. During rain floods, aufeis-ice slabs attached to the slopes are washed away and collapse together with the living soil cover that was frozen up to the sides and bottom of the ice slabs.

After retrogress of the aufeis-ice edge, ground ice melting begins and initiates formation of thermokarst caverns, furrows, ditches and/or series of single-level thermal erosion terraces (0.5–0.8 m high) separated by channels of migrating water streams. Melting of injection ice can create mushroom-shaped ice pillars – a 'mushroom stalk' is made of melted-out ice, and its 'cap' is a piece of turfgrass with live plants. In other cases, broken rock heaps, esker-like cones, mounds and chains are formed with interiors composed of non-laminated transparent ice. Typically, they subside by autumn, and the surface of the aufeis bed is levelled. Destruction of the mounds result in creation of quite specific thermokarst landforms. Melting of the mound ice cores or roofs leads to formation of roundish crater-like hollows framed by chaotically heaped ground with inclusions of fragments of soil, turf shred, stems of trees and shrubs (Fig. 13, *a*). Such craters may transform to small lakes and thus become permanent groundwater discharge sites. Springs flowing out of the lakes create and shape longitudinal furrows/channels.

In mountain river valleys, dissected masses of buried aufeis deposits can be observed (Fig. 13, *b*). Aufeis ice is buried due to ample deposition of suspended drift during the spring floods, mudslides, landslides and collapse of rocks from the adjacent slopes. When the buried aufeis deposit is destructed, flat hills (up to 1.5 m high) are formed, which change the direction



Fig. 13. Ground-ice outcrops on aufeis glades.

a – injection ice of a decayed mound in the north-western Yakutia (photo by Yu.A. Murzin); *b* – buried aufeis deposit in the Algama river valley in the southern Yakutia (photo by I. Karman).

Рис. 13. Обнажения подземных льдов на наледных полях.

a – инъекционный лед разрушенного бугра пучения на северо-востоке Якутии (фото Ю.А. Мурзина); *b* – погребенная наледь в долине реки Алгама в Южной Якутии (фото И. Карман).

of water flows. Dry channels filled with loose ground can be observed around the hills in autumn.

While repeated-vein ice is melting out in the aufeis glades, deep ditches filled with water are first to form, surrounded by blocks of ground with the veins. In plan, such sites look like a polygonal network. Gradually, small lakes are formed at the nodes of the network. If the ditches are drained, low butte mounds-silt pinacles are formed, which are separated by streamlets and mud flows.

During aufeis melting, erosion within the aufeis glades has to cease because the energy of branched or sprawled water flows is now insufficient for mass transfer of ground. However, the carrying capacity of

the main river above the aufeis deposit is not only maintained at the same level, but critically increases during rainfall floods. As a result, the major part of trailed and suspended drift is deposited onto the smoothed part of the valley bottom (Fig. 14). Below the aufeis glade, the river flow energy increases again, firstly, due to the additional influx of melt water (resulting from melting of the aufeis deposit and ground ice), and secondly, due to recombination of all the small branches into a single channel.

In *autumn*, the aufeis deposits remain only in areas covered with thick ice beds (over 5 to 7 m thick), shaded sites and regions where summer is very short and cold, such as in the Arctic and in the mountains above the limit of forest. In this period, aufeis remnants do not affect the development of erosion processes as the surface runoff is either small in the already formed channels or completely absent. With the onset of winter, such aufeis remnants become a part of 'fresh' masses and perform regulatory functions in the new regime. In other parts of the aufeis glades, the setting is stabilized in accordance with regimes of no-ice sections of the valleys, i.e. thawing of frozen soil is ceasing, the water level in the channel network is lowered, the aufeis glade is drained and acquire typical features of post-cryogenic areas (Fig. 15). Before the onset of winter, the total discharge of water flows on the aufeis glade is much smaller than the volume of flow in the river at the inlet due to the fact that a part of water infiltrates into the interior of thawed soil beds while sprawling across the entire width of the valley. If cryo-hydrogeological conditions are favourable, groundwater is accumulated again in the main channel at the outlet of the aufeis glade. In the absence of barrage (frozen rocks or base rock ledges), filtering of groundwater through the thick loose alluvium is continued, and groundwater comes up to the ground surface on sites considerably distant from the feed centres, often in front of a new aufeis glade.

Characteristics of the channel network dynamics during the warm period of the year are shown in Fig. 16.

7. DEVELOPMENT STAGES OF AUFEIS SECTIONS OF RIVER VALLEYS

In active icing zones, significant changes take place in micro- and mesorelief, composition and properties of soil, vegetation, water streams and other elements of the natural complex. The changes may be related to global warming/cooling cycles, regional environment variations or transformations of the water-and-heat balance of the ground surface due to impacts of human activities. Besides, the cryogenic system may transform in the course of its self-development in relatively stable



Fig. 14. The Malaya Lagorta river bed in Polar Ural after aufeis ablation (photo by A. Titov).

Рис. 14. Русло реки Малая Лагорта на Полярном Урале после стаивания наледи (фото А. Титова).

hydro-climatic conditions. In any case, transformations of the valley take place under a specific scenario reflecting the impact of the major factor, namely, long-term and centennial variability of icing (aufeis) parameters. Under the aufeis influence, the valley bottom is gradually extended and graded, the vegetation is either extinct or transformed depending on the ice thickness and life cycle, and the channel network evolves into a complex system of shallow meandering channels which orientations, shapes and configurations are variable through the evolution of the aufeis terrain.

Our analyses of the available data give grounds to distinguish five typical stages of aufeis development in the river valleys.

Stage I. Pre-glacial development. This development stage is typical of the majority of non-freezing rivers with constant runoff and decreasing water levels through the entire cold season. The double-layer ice cover of their cryosystem comprises (Fig. 17) the bottom horizon (h_3) consisting of crystalline ice (80 to 85% of the total thickness) and the top horizon (h_4) containing aufeis ice (15 to 20 %). The aufeis ice results from obstruction of the flow cross-section (h_2) during partial freezing of the flow, and also forms due to an overload of the ice by the settled snow. The outer limits of the ice do not propagate to the floodplain and go somewhat higher than the autumn low-water level. In winter, with depletion of the flow, the ice cover either subsides or bends. Under the ice cover, redeposition of the bottom sediments is slowed down and does not result in any critical changes in the riverbed. The channel deposits are not frozen. The riverbank slopes and the floodplain freeze to a depth of 0.5 to 1.0 m. In spring, ice drift and floods take place

in the 'normal' mode, without affecting the high floodplain. Ice jams are rare. The ice plough ability is moderate and most often completely obscured by summer rainfall floods and land floods.

Stage II. Transgression. This stage is typical of through-freezing rivers. In spring, the ice cover has three-layers (h_2 - h_5). By mid winter, the river channel at river bars is completely filled with crystalline ice, and the thickness amounts to h_3+h_2 . The middle layer (h_4) consists of frozen river water. The upper layer (h_5) is formed due to freezing of underflow groundwater after its discharge to the ice surface due to partial freezing of alluvium (horizon h_1). The groundwater aufeis deposit occupies the entire floodplain. It may go beyond the limits of the floodplain, but does not reach the valley wall and the distant bench of the above-floodplain terrace. Typically, this part of the ice cover (0.3 to 0.8 m thick) is destroyed by the start of spring floods and thus does not impose any significant impact on channelling. When the ice thickness exceeds 0.8-1.0 m, vegetation is transformed and extinguished later on (Fig. 18, a). The river runoff is maintained almost until the mid winter. By spring, the soil is frozen to depths from 1.0 to 1.5 m, so that the ice bed is firmly joined with the underlying rocks. In the floodplain areas, the ice bed's bottom is 'armoured' with tree stems, shrubs and herbaceous plants.

The most important factor for channelling is ice-ground barrage under the riverbed. In its presence, water lenses located between the river bars freeze and swell, and fracturing and explosive failure of ice mounds take place. On the floodplain of small rivers,

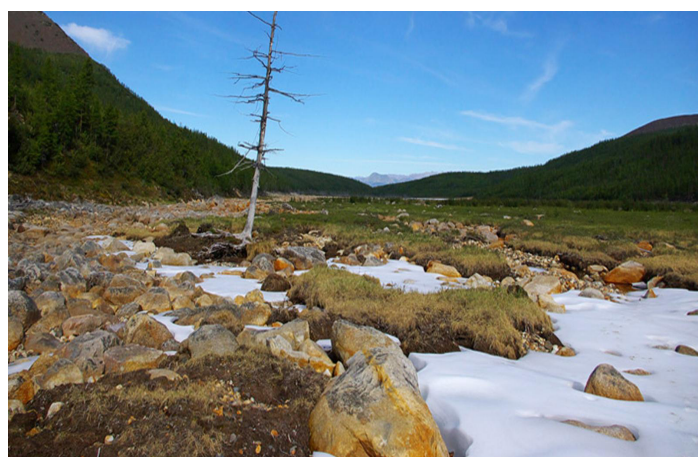


Fig. 15. The Aufeis glade in the Moma river valley in the north-eastern Yakutia in mid September (photo by Sandro).

Рис. 15. Наледная поляна в бассейне реки Мома на северо-востоке Якутии в середине сентября (фото Sandro).

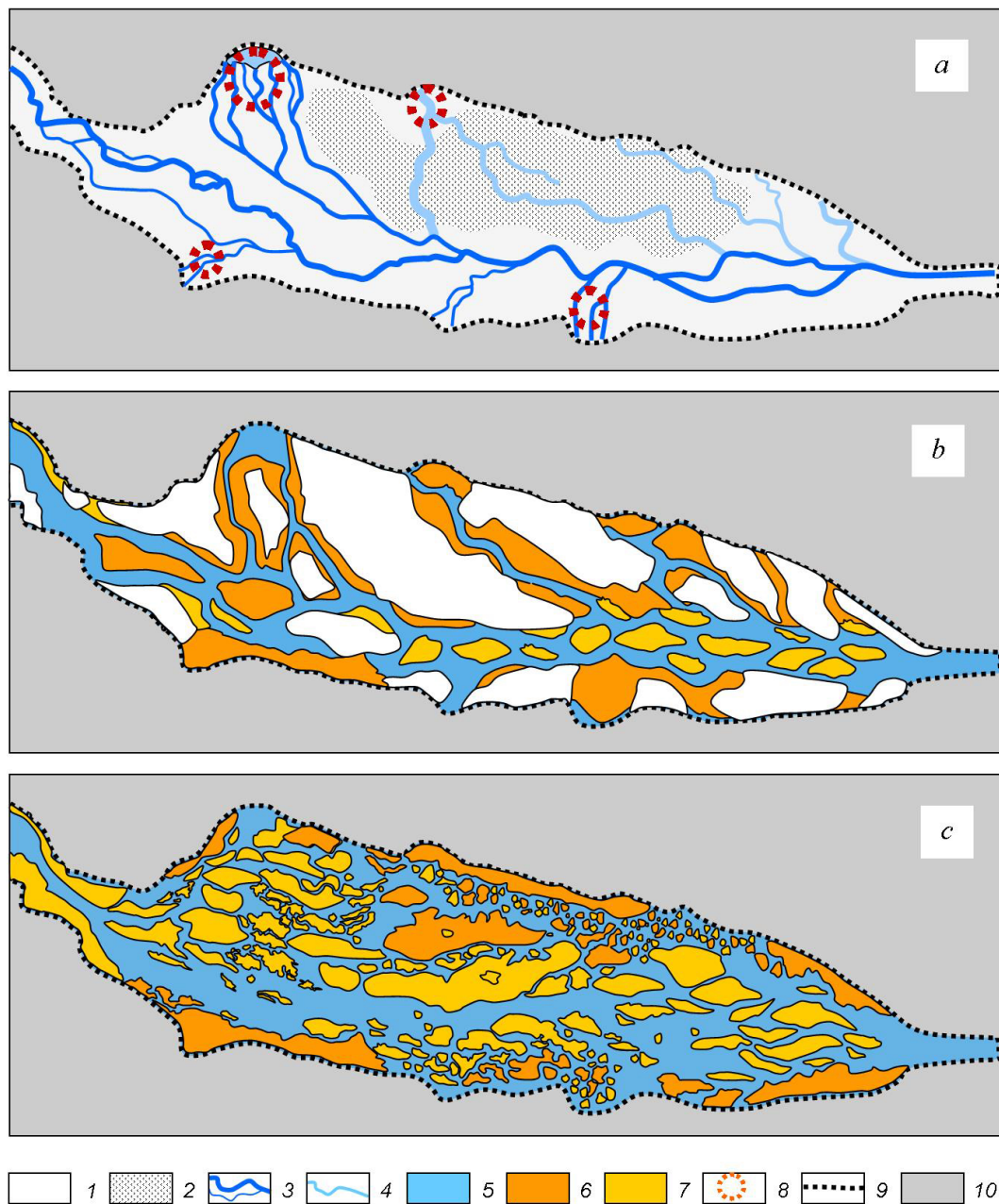


Fig. 16. Variations in the channel network configuration within the limits of the Bolshoi Eden aufeis deposit in East Sаяn according to ground-based survey data obtained in 1987. Absolute altitude 1800 m.

1 – subpermafrost groundwater aufeis; 2 – icing ‘bog’ on the surface of the ice cover; 3 – channel of the Bolshoi Eden river with ice banks in the snowmelt period; 4 – flows of melt water on the aufeis surface; 5 – river water flow in the period of intensive ablation of the aufeis and injected ground ice (20 June 1987) and after abundant summer snowfall (26 August 1987); 6 – gravel-sand deposits with inclusions of large boulders underlain by sheets of injected ground ice (flat outliers with scarp slopes, which heights range from 0.5 to 0.8 m); 7 – channel deposits without any visible signs of ground ice (ridges, beach plains, and mid-channel bars); 8 – icing mounds and fragments of ice domes; 9 – boundaries of the aufeis glade; 10 – slopes of the river valley which are composed of deluvial-colluvial sediments and covered with mountain-tundra vegetation.

Рис. 16. Изменение конфигурации русловой сети в границах Большой Эденской наледи в Восточных Саянах по данным наземных съемок 1987 г. Абсолютная высота 1800 м.

1 – наледь подмерзлотных подземных вод; 2 – наледное «болото» на поверхности ледяного покрова; 3 – русло реки Большой Эден в ледяных берегах в период снеготаяния; 4 – потоки талых вод на поверхности наледи; 5 – водный поток реки в период интенсивного разрушения наледи, инъекционных подземных льдов (20 июня 1987 г.) и после обильного летнего снегопада (26 августа 1987 г.); 6 – гравелисто-песчаные отложения с включениями крупных валунов, подстилаемые пластинами инъекционного подземного льда (плоские останцовые возвышенности с обрывистыми склонами высотой 0.5–0.8 м); 7 – русловые отложения без видимых признаков подземных льдов (гряды, косы, осередки); 8 – ледяные бугры пучения и фрагменты ледяных сводов; 9 – границы наледной поляны; 10 – склоны речной долины, сложенные делювиально-коллювиальными отложениями и покрытые горно-тундровой растительностью.

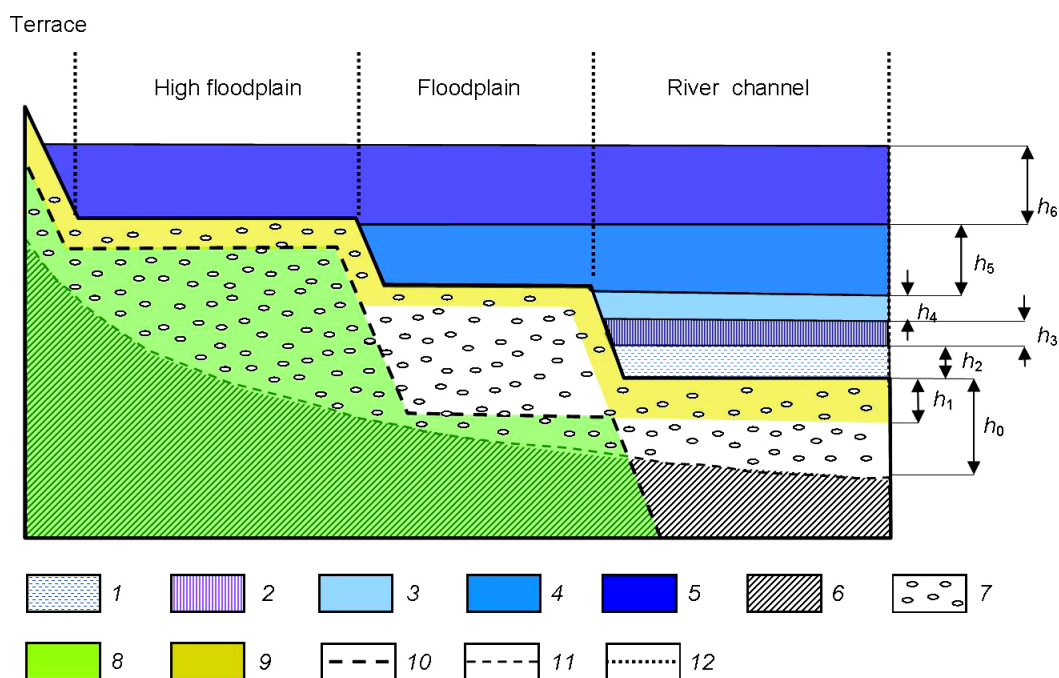


Fig. 17. Generalized scheme of cryogenic channeling conditions.

1 – water flow under the ice cover; 2 – crystalline river ice; 3 – river water aufeis and snow ice; 4 – aufeis deposits composed of suprapermafrost floodplain water and subchannel groundwater; 5 – aufeis deposits composed of intrapermafrost subchannel water and subpermafrost water; 6 – bedrocks; 7 – alluvium; 8 – perennially frozen rocks; 9 – layer of seasonal freezing and thawing ground materials. Boundaries: 10 – permafrost, 11 – rocks of different compositions, 12 – elements of the river valley with different ice-thermal regimes.

Рис. 17. Обобщенная схема условий криогенного преобразования русловой сети.

1 – подледный водный поток; 2 – кристаллический речной лед; 3 – наледь речных вод и снежный лед; 4 – наледь надмерзлотных пойменных и подрусловых подземных вод; 5 – наледь межмерзлотных подрусловых и подмерзлотных вод; 6 – коренные горные породы; 7 – аллювиальные отложения; 8 – многолетнемерзлые горные породы; 9 – слой сезонного промерзания и протаивания грунтов. Границы: 10 – вечной мерзлоты, 11 – горных пород различного состава, 12 – элементов речной долины с различным ледотермическим режимом.

icing is accompanied by formation of injection ice layers and ice-ground breccia. In spring, melted snow water have to pass the ice mounds and thus spread over the entire width of the valley's bottom. In valleys of small and medium-sized rivers, volumes of melted snow water are often insufficient to make the ice cover float up. Another hindering factor is the strong contact of the ice cover with the underlying frozen soil. As a result, ice drift does not take place on such rivers – ice is cut into fragments that gradually decay at their origin locations and protect the alluvium from erosion by the water flows. Flood waters are often concentrated at the contact of the ice bed with frozen riverbank sediments, penetrate beneath the sediments, easily wash out the thawing soil and cause fracturing and collapse of the frozen roof. Therefore, the riverbank slope is retrogressing, and a new channel is formed. A new channel can also be initiated along the ice channel-trenches following a system of random fractures and micro-depressions, including those across the valley. Thus, by the beginning of summer, the channel and

the floodplain are subject to annual changes that significantly affect further channelling.

Stage III. Stabilization. At this stage, the valley bottom is covered by aufeis ice from side to side. By spring, the aufeis thickness can reach 5 to 8 m. River crystalline ice is absent, i.e. in fact, a single-tier ice bed is formed (Fig. 18, b). Water freezing lasts through the whole cold period of the year. In the aufeis bed, layers and lenses are made of vacuum-filtration ground ice, which cause uplifting of the top rocks together with the aufeis deposit. Ice-ground chains and round-shaped mounds crack or explode, and water or mud flows gush out of the fractures. In 30 to 70 % of aufeis glades, underlying ground and ice are subject to heaving. The heaving zone's location shifts from year to year. In summer, ground layers are freed from ice and decomposed when ground ice is melting; small mineral fractions are transferred by numerous water flows to the bottom of the aufeis glade and further outside the aufeis zone. The rocks are thus not only annual 'shaken up', but also intensively washed. Finally, a specific 'aufeis' facies of alluvium is formed.

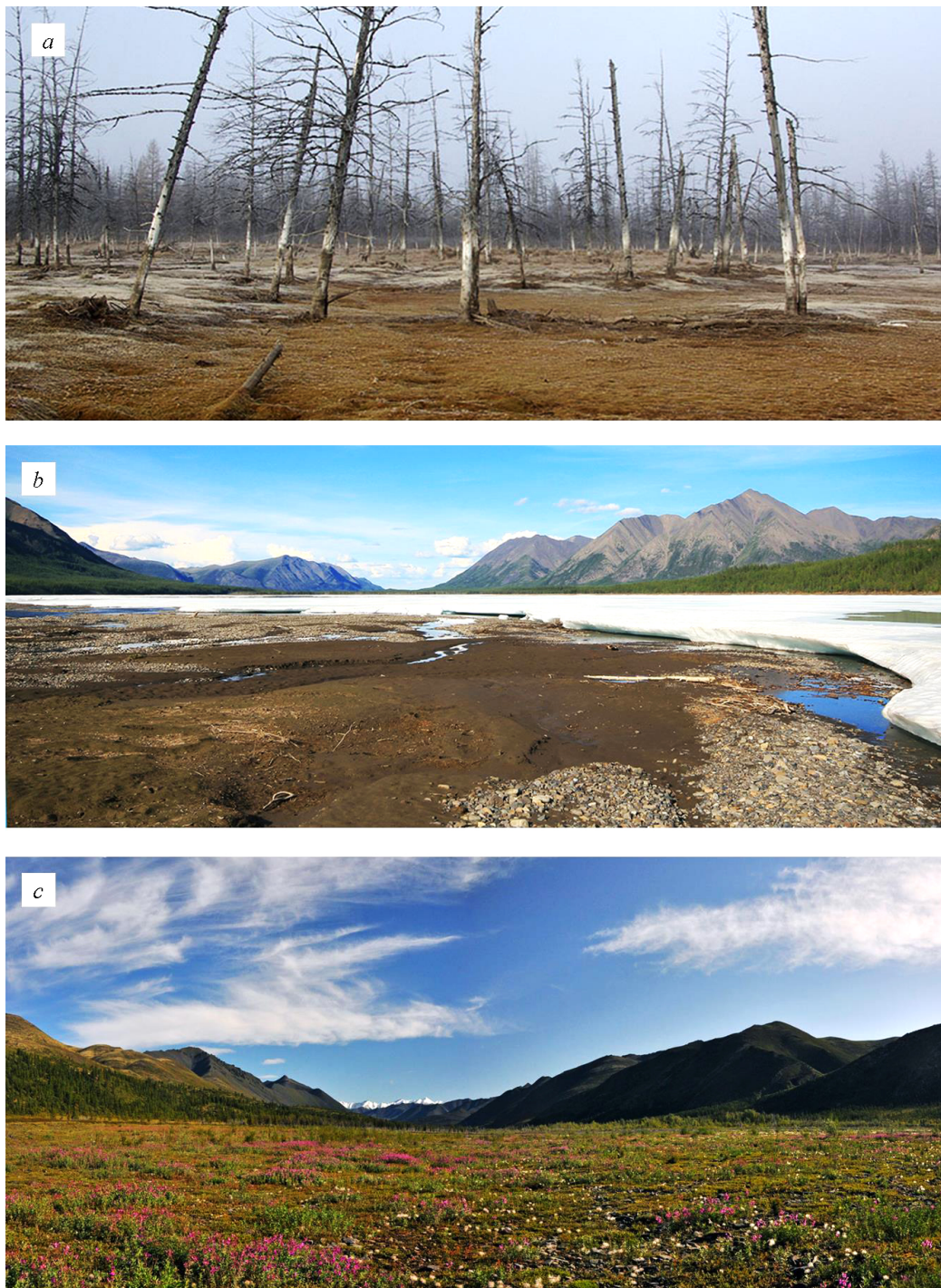


Fig. 18. Active development stages of aufeis sections of river valleys in Yakutia.

a – transgression: the soil-vegetation is destroyed, trees are extinguished, and the ice thickness can be determined from bleached stems of trees (the north-western Yakutia; photo by V. Solodukhin); *b* – stabilization: the vegetation cover is destroyed, and the underlying ground is redeposited and compacted (the Suntar-Khayata river channel divided into several broad shallow distributaries, and the Suntar-Khayata ridge in the north-eastern Yakutia; photo by M. Mestnikov); *c* – regression: the ice thickness is decreased, or the aufeis deposit has completely disappeared, the soil-vegetation cover is recovering (the Boryndzha river channel reassembled into one or several distributaries in the lower part of the valley, and the Momsky ridge in the north-eastern Yakutia; photo by Sandro).

Рис. 18. Активные стадии развития наледных участков речных долин в Якутии.

a – трансгрессивная: гибнут деревья, уничтожается растительный и почвенный покров; мощность льда фиксируется по отбеленным стволам деревьев; Северо-Западная Якутия (фото В. Солодухина); *b* – стабилизационная: растительный покров уничтожен, подстилающий грунт переотложен и уплотнен; русло реки Сунтар разбито на ряд мелких широких протоков; хребет Сунтар-Хаята на северо-востоке Якутии (фото М. Местникова); *c* – регрессивная: мощность льда уменьшилась или наледь полностью исчезла; восстанавливается почвенно-растительный покров; русло реки Борынджа собирается в один или несколько протоков в пониженной части долины; Момский хребет, Северо-Восточная Якутия (фото Sandro).

Transformations of the aufeis bed continue until cessation of underground icing and completion of subsequent erosion-thermokarst redeposition of sediments. Afterwards, denudation processes gradually cease. The stabilization stage can last for a very long time, until the icing mode is significantly changed. As a result, the riverbed can spread through the entire width of the aufeis glade, loses its shape, and the aufeis bed often looks like a stone pavement with compactly and tightly placed boulders of flatiron-like forms (flat sides up).

Stage IV. Regression. The reduction of the aufeis volume or complete cessation of icing is accompanied by localization of the transit water channel. It gradually deepens and becomes the main drainage artery of the aufeis glade. Branches are drained or converted into small ditch-shaped lakes with stagnant water. Micro-depressions and gaps between stones are filled with fine-grained soil resulting from cryogenic weathering of rocks or brought by melt water from the slopes and the upper parts of the valley. The fine-grained soil is compacted and colonized by pioneer plant species. Soil-forming processes are activated; mosses, meadow and shrub vegetation come up; soils are secured by root system of plants and become more resistant to erosion caused by aufeis melt water and rainwater (Fig. 18, c). The above processes are accompanied by long-term freezing of aufeis alluvium. The ground-filtration talik persists only under the main river flow bed. Sodded areas initially appear at the periphery of the aufeis glades wherein snow and ice are the first to melt. Later on, sodded zones occupy the entire width of the valley as the seasonal icing area is steadily decreasing. In case of aufeis migration, some sections of the sodded area may be outcropped again, i.e. fall back to the previous regime. In the final phase of regression of the valley, the river comes into one channel and acquires characteristics of the adjacent (upper and lower) flow sections. Generally, aufeis degradation, i.e. reduction of the mean annual aufeis volume, lasts for many dozens and even hundreds of years. This process depends primarily on the intensity and duration of changes in climate characteristics and corresponding transformations of cryo-hydrogeological structures that are feeding the aufeis deposit.

Stage V. Postglacial development. This stage starts after the valley bottom is completely and permanently freed from ice, boulders are covered by soil and vegetation that is typical of no-aufeis sections of the valley. At this time, the ice-thermal regime of the river and the main channel configuration are almost identical to the flow regime and the runoff channel morphology in the periglacial stage. However, the former icing area can be clearly detected by a number of characteristic features, such as the lack of low terraces, flat terrain with typical chains and mounds, specific structure

of loose sediments, age, morphology and physical properties of soils, distribution and floristic composition of vegetation etc.

Generally, the development stages of the aufeis sections of the river valleys are well detectable from aerial and satellite images of medium and large scales (Fig. 19). However, determining their boundaries and assessment of duration of the development stages and phases is challenging as the relevant experience is lacking, and structural and dynamic features of the aufeis terrains have not been properly studied yet. Our observation data show that even one aufeis section may contain a wide variety of components of the aufeis bed (Fig. 20), and the wider is the range of annual and long-term variability of aufeis characteristics, the more difficult is establishment of trends in development of the aufeis segments, and more challenging is determination of the phase status of the entire cryogenic system. Moreover, aufeis terrains are variable depending on geographic latitudes and altitudes, underlying rock compositions, morphological parameters of the valleys, water-discharge talik configurations, thicknesses of permafrost and seasonal frost-bound layers etc. Therefore, studying aspects of channelling in the permafrost zone is a fairly complex problem of nature studies. This problem can be solved only by combined analyses of cryo-hydrogeological, hydroclimatic and landscape data. In this laborious research process, it is important to analyse the structure of the hydrographic network.

8. AUFEIS STRUCTURE OF THE CHANNEL NETWORK

Due to a combined effect of the above-described processes, the valley bottom is gradually extended and levelled in the aufeis sections. The vegetation cover is either extinct or transformed depending on the aufeis thickness. The channel network evolves into a complex system of shallow meandering channels which orientations, shapes and configurations are variable through the evolution of the aufeis terrain. Hydrographic networks in the active icing zones can be studied from large-scale aerial and satellite images and ground-based observation data. Besides, remote sensing techniques are particularly effective in obtaining parameters of the hydrographic networks and detecting the aufeis terrain boundaries within specified time limits. By comparing series of images taken in different years, it is possible to assess the channelling dynamics in annual and long-term cycles.

Based on our analyses of satellite images of the aufeis valleys located in East Siberia and the north-eastern regions of Russia, five types of channel network patterns can be distinguished: fan-shaped, cone-shaped, treelike, reticular, and longitudinal-insular types.

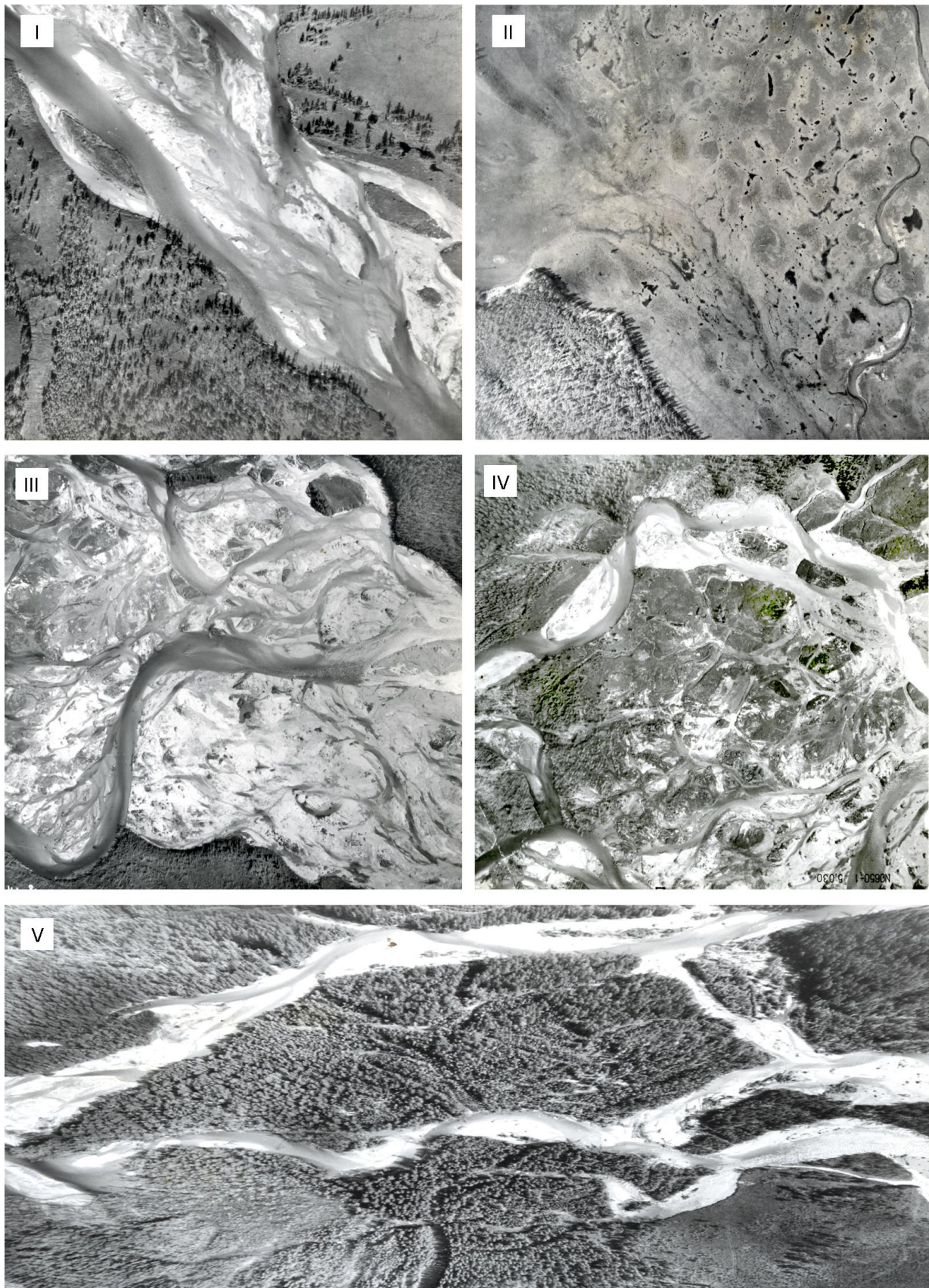


Fig. 19. Development stages of the aufeis section of the Middle Sakukan river valley. Chara basin. Stanovoe upland.

I – periglacial development, *II* – transgression, *III* – stabilization, *IV* – regression, *V* – postglacial development.

Рис. 19. Стадии развития наледного участка долины реки Средний Сакукан. Чарская котловина. Становое нагорье.

I – перигляциальная, *II* – трангрессивная, *III* – стабилизационная, *IV* – регрессионная, *V* – постгляциальная.

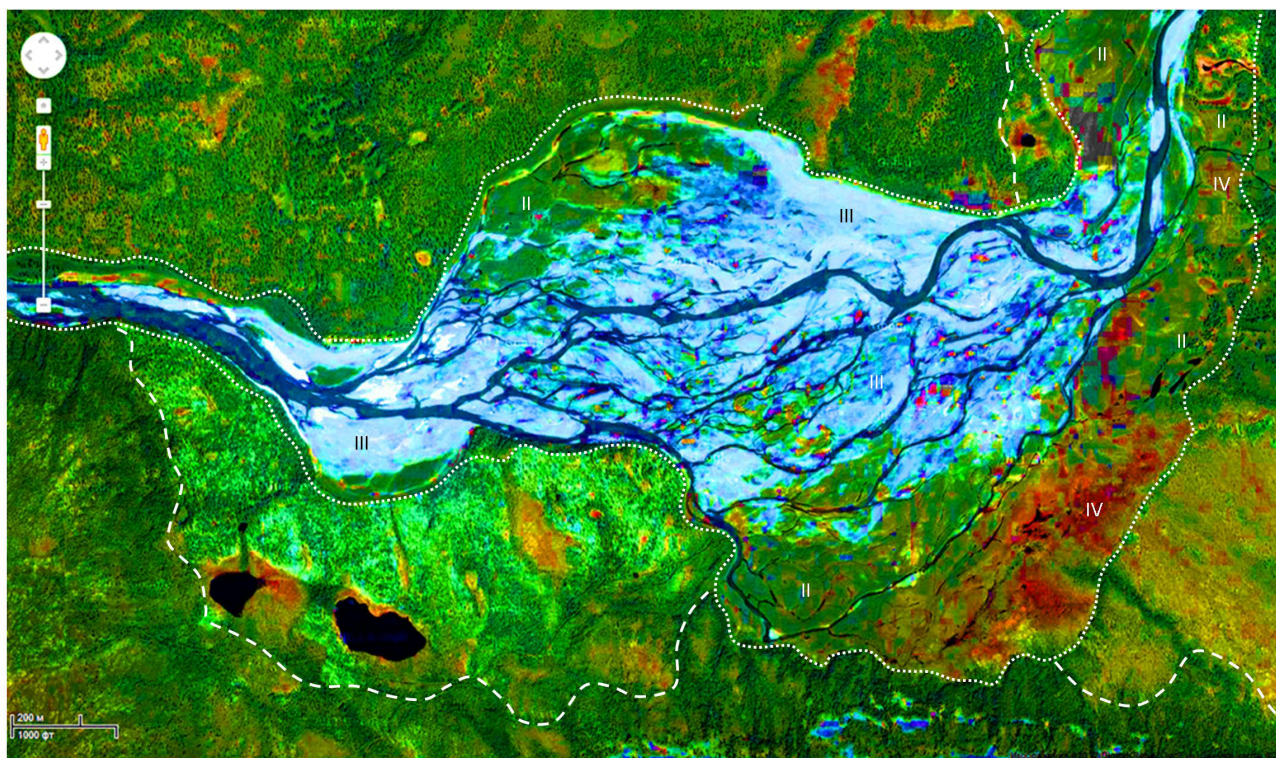


Fig. 20. A space image of the aufeis section of the Lower Ingamakit river valley (rank 3) in the northern Transbaikalia.

The dotted line contours the current aufeis glade with different stages of its development (Roman numerals). The dashed line outlines the relict icing zone.

Рис. 20. Космический снимок наледного участка долины реки Нижний Ингамакит третьего порядка. Северное Забайкалье.

Точечной линией показан контур современной наледной поляны с различными стадиями ее развития (римские цифры), пунктиром обозначена внешняя граница реликтовой зоны наледообразования.

The **fan-shaped pattern** is a system of disbanding and gradually disappearing channels, dry beds and ditches separated by outcropped primary surface zones with deformed or completely destroyed vegetation (Fig. 21, *a*). It forms in cases when aufeis-generating water can be discharged to the day surface as a concentrated flow, and it freely spreads over the slope to create a blade-shaped ice mass. This pattern can be observed (1) at outlets of side branches of small and medium-sized rivers, (2) at outlets of mountain streams going to flat terrain areas, (3) in front of frontal benches of retreating glaciers that are not wide (on outwash surfaces). The channel network is laid mainly in spring, during the passage of melt water flows that not only cut through the ice thickness in different directions, but also penetrate underneath the ice cover to intensely erode the bed. In most cases, the runoff channels are not connected with each other; they are straight and may be quite deep, with sloughing steep walls. Generally, the sediments are coarse.

The **cone-shaped pattern** of the channel network is typical of the lower parts of aufeis glades. This part of

the icing zone is the first to get free of ice. The runoff channels are formed in summer due to melt aufeis water, which spread in a wide front along the retreating ice mass (Fig. 21, *b*). With distance from the aufeis deposit, the water-intake ditches are split up. Downstream, they gradually gather into a single channel. The ditches are shallow, with low gently dipping slopes (0.2 to 0.3 m high) composed of fine material.

The **treelike pattern** of the channel network is typical of the upper parts of mature aufeis glades of any modification and location. Its shape resembles a branching tree trunk (Fig. 21, *c*). The runoff channels are formed in spring and early summer along fractures of tricky configurations in ice, which result from thermal erosion. The channels are rarely more than 0.5 m deep, with trapezoidal or roundish cross-sections. The channels are separated by outcropped or sodded elongated islands with flat surfaces. At the periphery of the aufeis glades, the water flow beds often join together for intake of the entire volume of river water and melted aufeis water. Loose sediments and the surface cover of the aufeis glade often contain wood scrap, dead grass,

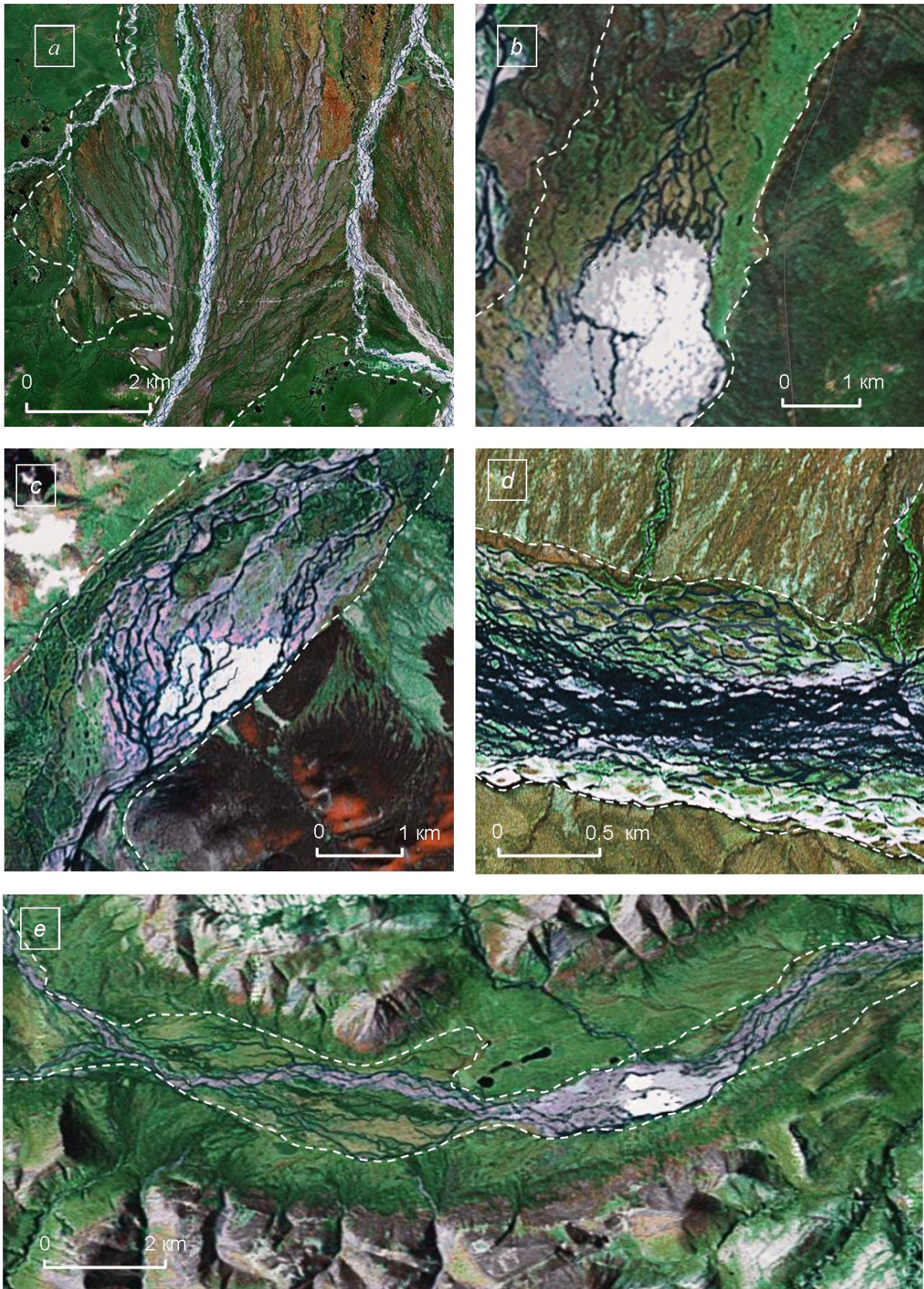


Fig. 21. Hydrographic network types in aufeis sections of river valleys in the north-eastern regions of Russia. *a* – fan-shaped, *b* – pyramidal, *c* – treelike, *d* – reticular, *e* – longitudinal-insular. The dashed line outlines the aufeis glades.

Рис. 21. Типы гидрографической сети на наледных участках долин северо-востока России.

a – веерная, *b* – пирамидальная, *c* – древовидная, *d* – сетчатая, *e* – продольно-островная. Пунктиром показаны внешние границы наледных полей.

humus-like residue and other foreign materials that are brought from the upper parts of the valley during the spring flood.

The **reticular pattern** is mainly typical of central parts of large aufeis glades (2.5 to 3.0+ m thick). Usually, it frames a wide shallow channel of the main stream (Fig. 21, *d*). The aufeis bed is flat, almost horizontal; runoff channels are bordered by numerous turf-covered islands composed of boulder-pebble deposits with gravel-and-sand infill. The steeply dipping channel walls are 0.5 to 0.8 m high, and often contain layers of thawing ground ice. The channel network is formed in mid summer during ice mass breakdown due to thermal erosion, as well as after ice melting associated with thermokarst phenomena (sinkholes, landslides and ground settlement). The reticular pattern of the runoff channels can be quickly transformed to function as a water-transfer system of boulder-and-gravel beds when the water flow is spread over the entire width of the aufeis glade and quickly changes its configuration depending on the volume of aufeis ice, the location and the actual precipitation volume, i.e. according to the transit river flow volume.

The **longitudinal-island pattern** of the river network is typical of aufeis sections of large lengths with well-developed longitudinal profiles of the valleys. In such areas, the flat bed has been repeatedly subject to cryogenic and fluvial processes; the alluvium is relatively uniform; the main channel is quite well defined; flat outlier chains go along the main channel, and every year they are covered by a thin aufeis deposit. Under the main channel, there is a cut-through water-release talik. In spring, it provides for thawing of the ice mass at its bottom and facilitates under-ice channeling for a concentrated transit runoff and the lower thermal-erosion activity of the melt water in the adjacent areas of the bed. Elongated islands and chains varying in shapes and lengths are typically stretching along the valley's sides for many kilometres (Fig. 21, *e*).

The channel network patterns in the aufeis sections of the river valleys are variable in both space and time, depending on icing conditions, volumes of freezing groundwater and surface water, destruction of ice and frozen rocks, transit flow volumes and other factors. Generally, the patterns of different types are conjugated without any clear boundaries between them. At any large aufeis glade, elements of all types of the patterns may be present. It is a challenging task to decipher their complex combinations in order to reveal the dynamics of the cryogenic system and to determine its development stages and phases, and special studies and observations are thus required. There are good reasons to believe that morphological indicators and properties of the aufeis terrains can be reliably defined. Based on such knowledge, it will be possible to clarify the history and the dynamic state of the cryogenic sys-

tem and to forecast possible ways of its transformation in the near future.

9. AUFEIS RATIO OF THE PERMAFROST ZONE AND INCREMENT OF THE CHANNEL NETWORK

A relative aufeis ratio, c shows the aufeis development scale in the studied region. It is calculated as a percentage ratio of the total area of ice masses, ΣF_a in the period of their maximum development to the total square area of the studied region, F : $c=100 \Sigma F_a/F$. The aufeis ratio can be calculated for each type of aufeis deposits (river, groundwater, ice, melted snow water) or for all the types. A commonly applied factor related to groundwater freezing is c_{uw} . Another aufeis coefficient is k_a , showing a ratio between the river length, L_r and its part occupied by the river-water or groundwater aufeis deposit, L_a : $k_a=L_r/L_a$ [Alekseyev, 2005]. This article provides information regarding groundwater aufeis deposits.

The formation of groundwater aufeis deposits depends on a complex set of environmental factors pre-determining conditions of water- and energy exchange at a given geographical point. Aufeis depositing is most active in regions of continuous and discontinuous permafrost and can be observed on practically all the river valleys and basins. At some locations, aufeis deposits occur on mountain slopes and in watershed areas. The largest groundwater aufeis deposits are located in the Arctic regions and in mountains in the regions of contrasting neotectonic movements in Yakutia, Chukotka, Khabarovsk region, Transbaikalia and Pribakalie, the Altai [Alekseyev, 1975, 1976; Alekseyev et al., 2012; Alekseyev, Gienko, 2002; Alekseyev et al., 2011; Shesternev, Verkhoturov, 2006; Shmatkov, Kozlov, 1994; Tolstikhin, 1974], as well as in Spitzbergen, mountain regions in Alaska, Middle Asia, and Tibet [Åkerman, 1982; Carey, 1973; French, 1976; Gorbunov, Ermolin, 1981; Olszewski, 1982; Revyakin, 1981].

An aufeis deposit may occupy dozens of square kilometres, and a specific water reserve in aufeis ice is almost identical to the water reserve in the snowpack. In the southern regions characterized by discontinuous and sporadic permafrost, the number of aufeis deposits per unit area increases, while their average size decreases (Fig. 22). In mountain valleys, the groundwater aufeis thickness may reach 10 to 12 m. In average, the ice thickness ranges from 1.0 to 2.5 m. The aufeis deposits are fed by a complex system of water-absorbing and water-releasing taliks. In glacial areas, the feed depends on the number and altitudes of periglacial lakes that function as natural regulators of the surface and groundwater runoff.

The groundwater aufeis deposits are usually marked by *aufeis glades*. In [Alekseyev, 2005], a set of

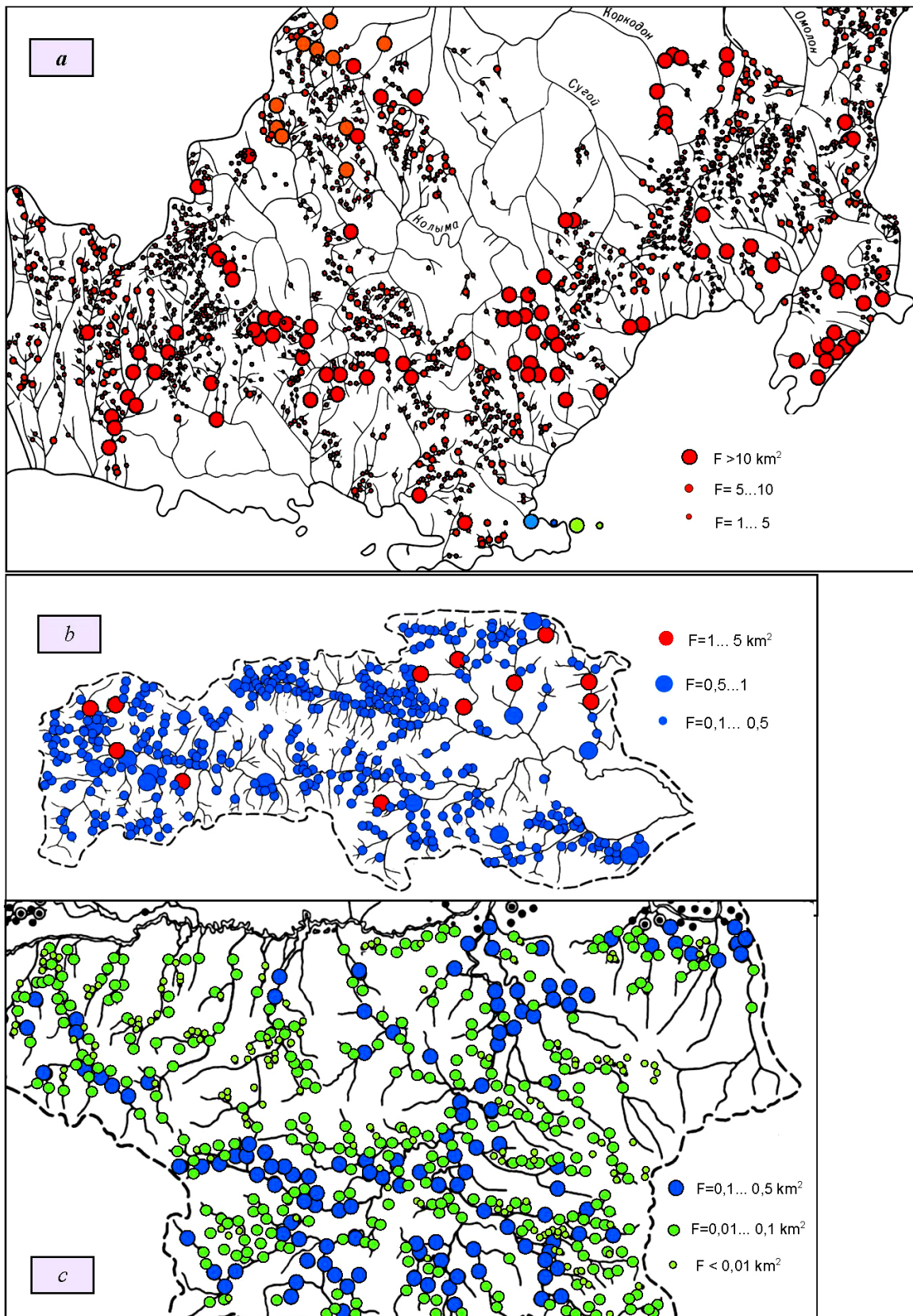


Fig. 22. Schematic maps showing distribution of groundwater augeis deposits in the territories of the Kolyma upland (a), the Muya river basin (Stanovoe upland, and Baikal-Amur Railroad zone) (b), and the southern part of the Irkut river basin (Khamar-Daban ridge, and Tunka valley) (c).

Рис. 22. Схемы распространения наледей подземных вод на территории Колымского нагорья (a), в бассейне реки Муя (Становое нагорье, зона БАМ) (b) и в южной части бассейна реки Иркут (хребет Хамар-Дабан и Тункинская долина) (c).

aufeis glade indicators is established, mean long-term characteristics of ice masses are estimated, and aufeis locations and dynamics are determined. The landscape-indication method was used to compile catalogues of the aufeis deposits observed in the Verkhoyansk-Kolyma mountain country, Chukotka, regions near the Okhotsk Sea, Putorana, South Yakutia, the Baikal-Amur Railroad zone, Transbaikalia and Pribaikalie, and the central part of East Sayan [Alekseyev, 1976; Alekseyev, Gienko, 2002; Alekseyev et al., 2011; Deikin, Abakumenko, 1986; Catalogue..., 1980, 1981, 1982; Shmatkov, Kozlov, 1994; Simakov, 1961; Tolstikhin, 1974; Topchiev, Gavrilov, 1981]. Based on the catalogued data, it became possible to determine quantitative indicators of aufeis of the permafrost zone and, based on the indicators, to assess the role of aufeis in development of the channel network.

The relative aufeis ratio in the permafrost zone varies widely. It is the lowest in flatlands and low-mountain regions ($c_{uw}=0.01...0.1$) and the highest ($c_{uw}=0.1...1.0$) in mountain-folded regions. The more contrasting is the terrain, the more active are neotectonic movements, the lower is the mean annual air temperature, and the higher is the annual percentage of the territory covered by aufeis ice. At the Putorana plateau, the region of the volcanic origin, the average relative aufeis ratio amounts to 0.37 % (maximum 0.87 %). At the Stanovoe upland with its sharply dissected terrain and thick discontinuous permafrost, the value of c_{uw} is increased to 0.69 %. In the north-eastern regions of Russia with the complex systems of frozen mountain ranges and plateaus, the value of c_{uw} amounts to 1.0 %. Thus, in the regions of more severe permafrost conditions, the aufeis deposits occupy larger areas and have larger lengths and widths, in average.

It is revealed that some characteristics of the aufeis deposits depend on ranks and lengths of water streams (Fig. 23). The ranks of water streams are roughly correspondent to the hydrologic classification of lengths of rivers. In average for the area, the higher is the rank of the river valley, and the larger are the average width and volume of groundwater aufeis deposits, while the aufeis-ice thickness is lower, and the aufeis ratio of the water streams is smaller. This trend is maintained as the river systems come to piedmont plains and lowlands. However, for rivers of ranks 5 and 6 and higher, the groundwater aufeis volume decreases sharply, and on the rivers longer than 500 km, no groundwater aufeis is formed, and it is replaced by river-water ice layers. In all natural zones, the majority of ice masses with maximum dimensions are located in the river valleys of ranks 3 and 4 (Fig. 23).

A similarity is established between the majority of cryo-geomorphological and hydrological processes on the aufeis sections of the river valleys located in different climatic zones and altitude belts [Alekseyev, 2005].

Practically at all stages of aufeis channeling, only relative sizes of the elements of the cryogenic system are changing, while their interface schemes remain the same. We rely on this important conclusion in estimations of the space-and-time regularities of aufeis control of erosion-accumulation processes taking pace in the permafrost zone. A channeling intensity indicator is given by the value of ρ calculated as a total incremental length of runoff channels, ΣL_a per unit length of an aufeis glade through its entire length, L_{ag} (km/km) or per unit square area of the aufeis section of the river valley, F_a (km/km²): $\rho_l = \Sigma L_a / L_{ag}$; $\rho_F = \Sigma L_a / F_a$. Parameter ρ characterises the channel network density within the limits of the aufeis glade without taking into account the length of the major water stream. Specific regional features of aufeis channeling can be also estimated with reference to the total incremental length of the river branches per one aufeis: $\rho_n = \Sigma L_t / n$, where ΣL_t is the total incremental length of the channel network in the given river basin, n is the total number of aufeis deposits of the similar size in the same territory.

In the study of the hydrographic structure of the aufeis sections of the river valleys, it is reasonable to consider the number of channels, m_a resulting from erosion and accumulation processes in the aufeis-formation zone (incremental values, σ_l and σ_F are determined as follows: $\sigma_l = \Sigma m_a / L_{ag}$; $\sigma_F = \Sigma m_a / F_a$), as well as the ratio of the total width of the water flows along the typical transverse profiles of the valley bottom, Σb_{ag} to the riverbed width above the aufeis, b_a and below the aufeis, b_b , to the width of the main water artery in the aufeis zone, b_r or to the width of the entire aufeis glade, L_{ag} . In a similar way, variations of depths of the erosion landforms can be estimated.

The scale of the channeling processes is estimated from $\rho_l = 2.5$ km/km. This value was obtained in the study of representative aufeis sections of the river valleys in the mountainous regions of the southern East Siberia (Table 2). It is an average value for the ice masses with the following parameters: $F_a=0.2...3.7$ km², $L_{ag}=1.4...4.7$ km, and $H_i=1.5...2.9$ m, which provide for the bed expansion to $b_l=100...350$ m. These values correspond to the prevailing range of aufeis characteristics in the territory of continuous and discontinuous permafrost. Here H_i is an average thickness of ice at the end of the icing period. Average values ρ_F and ρ_n are also calculated for some basins and some regions as a whole.

The below data refer to the mature aufeis glades that are mainly in development stages III and IV and result from functioning of permanently active large-flow groundwater sources. The mature aufeis glades are well recordable by aerospace surveys. The available data are collected in published aufeis catalogues [Alekseyev, Gienko, 2002; Catalogue..., 1980, 1981, 1982; Deikin, Abakumenko, 1986; Deikin, Markov, 1983]. The

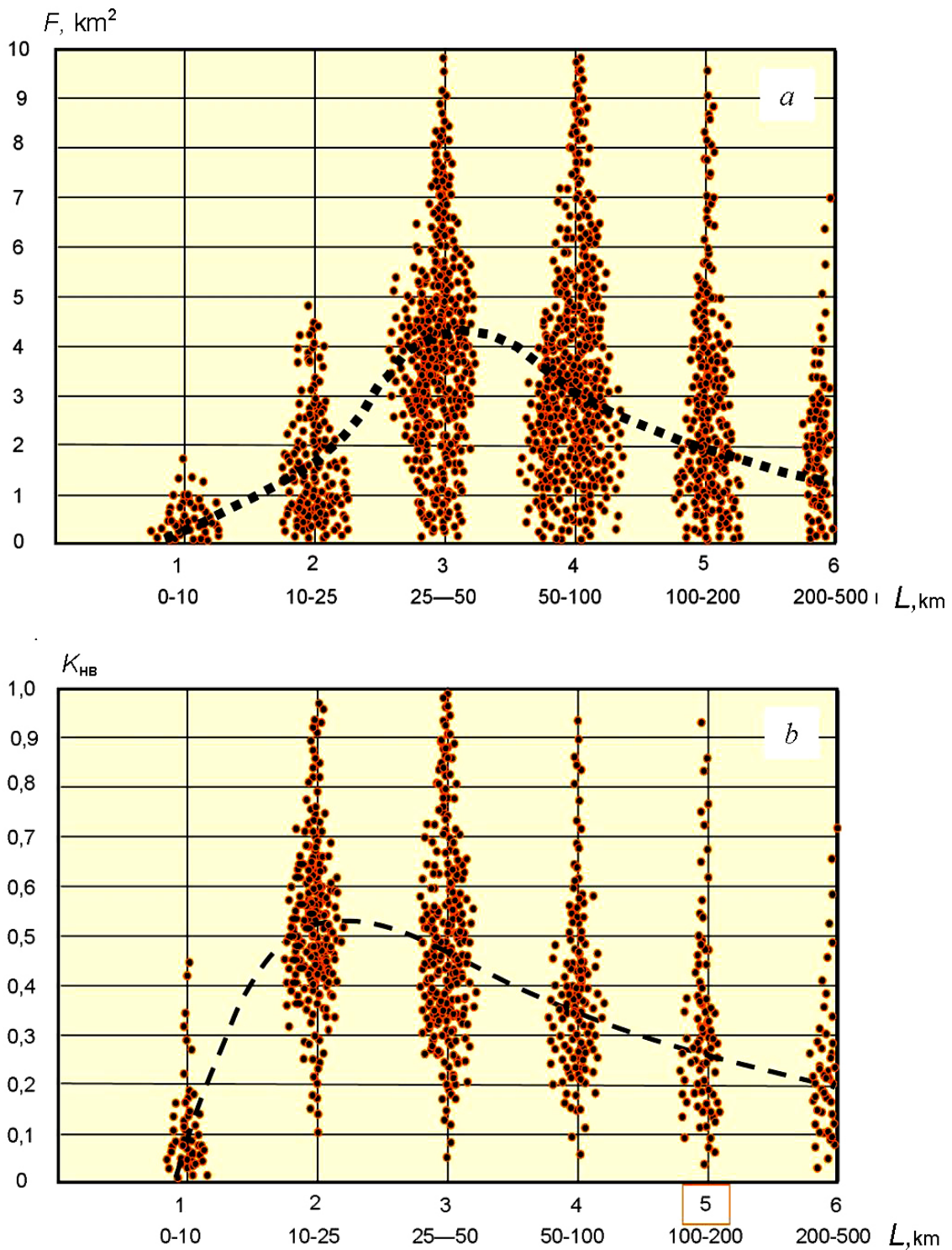


Fig. 23. Aufeis ratio variations depending on ranks and lengths of water streams.

a – variations in the square area of groundwater aufeis deposits with clearly defined aufeis glades (Putorana plateau); *b* – variations of the aufeis coefficient (%) of water streams fed by aufeis deposits composed by river water and groundwater in the river channels on the Stanovoe upland (Lower Ingamakit, Middle and Upper Sakukan, Apsat, and Chara rivers), Khamar-Daban (Khangarul, Tumusun, Zun-Murin, and Irkut rivers), and East Sayan (Bolshoi Eden, Ugega, and Uda rivers). Mean values are marked by dashed lines.

Рис. 23. Изменение некоторых характеристик наледности в зависимости от порядка и длины водотоков.

a – изменение площади наледей подземных вод с хорошо выраженными наледными полями (плато Путорана); *b* – изменение коэффициента наледности водотоков, обеспеченной наледями речных и подземных вод, сформировавшихся в руслах рек Станового нагорья (реки Нижний Ингамакит, Средний и Верхний Сакукан, Апсат, Чара), Хамар-Дабана (реки Хангарул, Тумусун, Зун-Мурин, Иркут) и Восточного Саяна (реки Большой Эден, Эгега, Уда). Пунктиром показаны средние значения характеристик.

Table 2. Comparison of channel networks in representative aufeis glades in East Siberia with regard to their square areas and development stages

Таблица 2. Сравнительная характеристика русловой сети репрезентативных наледных полей Восточной Сибири в зависимости от их площади и стадии развития

| Region | Aufeis glade and its development stage | F , km ² | H_i , m | L_{ag} , km | Channel parameters per 1 km river length | | | | | | Incremental length of channel network | | | |
|------------------|--|-----------------------|-----------|---------------|--|-------|----------|----------|-------|----------|---------------------------------------|------------------|-------------------------------|------|
| | | | | | width, m | | | depth, m | | | ΣL_a , km | ρ_l , km/km | ρ_F , km/km ² | |
| | | | | | b_a | b_b | b_{ag} | h_a | h_b | h_{ag} | | | | |
| Stanovoe upland | Lower Ingamakit | III | 3.7 | 2.0 | 4.7 | 25 | 50 | 300 | 1.3 | 1.0 | 0.7 | 11 | 2.3 | 3.0 |
| | Middle Sakukan | III | 2.5 | 1.8 | 3.6 | 45 | 65 | 250 | 1.2 | 0.9 | 0.5 | 8 | 2.2 | 3.2 |
| | Mururin | III | 2.2 | 2.0 | 2.4 | 40 | 55 | 350 | 1.2 | 1.0 | 0.3 | 7 | 2.9 | 3.2 |
| Aldanskoe upland | Leglier | II | 0.9 | 2.8 | 2.8 | 15 | 22 | 150 | 0.8 | 0.9 | 0.4 | 6 | 2.1 | 6.6 |
| | Samokit | III | 0.8 | 2.9 | 3.0 | 30 | 25 | 270 | 0.7 | 1.0 | 0.3 | 10 | 3.3 | 12.5 |
| East Sayan | Maly Eden | II | 0.3 | 1.5 | 1.5 | 8 | 15 | 120 | 0.8 | 0.5 | 0.3 | 3 | 2.0 | 10.0 |
| | Bolshoy Eden | II | 0.2 | 1.8 | 1.4 | 10 | 12 | 100 | 0.7 | 0.8 | 0.2 | 4 | 2.8 | 20.0 |
| Average | | | 1.5 | 2.1 | 2.8 | 25 | 35 | | 1.0 | 0.8 | 0.3 | 7.0 | 2.5 | 8.3 |

Note. Symbols: b_a , b_b , b_{ag} , h_a , h_b , h_{ag} – channel width (b) and water stream depth (h) above and below the aufeis and on the aufeis glade in autumn, average values. Other symbols are given in the text.

Примечание. Индексы: b_a , b_b , b_{ag} , h_a , h_b , h_{ag} – ширина русла b и глубина водного потока h выше, ниже наледи и на наледной поляне в осеннюю межень, средние. Остальные обозначения в тексте.

aufeis areas in development stage II usually do not have clear boundaries, do not form every year, and are not thick. Their role in channeling is insignificant, though numerous future runoff channels are often initiated within the icing zone.

The channeling effect of aufeis phenomena is well correlated with the main aufeis ratios in the river basins, morphostructural and cryo-hydrogeological conditions of the territory.

The incremental length of the channel network, ρ_n per one aufeis deposit is increased, in average, from 3.5 km in mountains in the southern regions of East Siberia (Table 3) to 11.4 km at the Putorana Plateau (Table 4) and 23 km in the Verkhoyansk-Kolyma mountain system and Chukotka (Table 5). The value of ρ_n is decreased to 2.2 km in the plains and intermountain depressions of the Baikal rift system where the average dimensions of the ice fields are smaller (Table 6).

In general, in the regions and the river basins, the total incremental length of the channel network, ΣL_t reaches gigantic values. For instance, in the section of the Baikal-Amur railroad zone from Ust Kut to Nyukzha (1256 km), 273 aufeis deposits occur near the railroad, and the total aufeis length is $\Sigma L_t=274$ km. The average square area of ice masses is $F_a=0.216$ km². The channel network length is increased by 685 km due to active icing processes. Therefore, the aufeis hazard is high in the territory along this railroad section (Table 6). In basins of the Chara (riverhead), Muya and Upper Angara rivers ($F=42000$ km²), the incremental length of the

runoff channels in the aufeis sections of the river valleys is $\Sigma L_t=3679$ km, i.e. about 80 metres per one square kilometre of this territory. In the river basins in the Putorana plateau ($F=433500$ km²), 2124 aufeis deposits are observed, the incremental length of the channel network exceeds 20.2 thousand km, i.e. in average, 11.4 km per one aufeis deposit or 40 m per square kilometre of this territory. In the north-eastern regions of Russia, the number of aufeis deposits is increased proportionally to the square area of the river basins, the average square area of the aufeis fields is dramatically increased, and the total length of watercourses in the aufeis glades is also increased correspondingly.

The average data for the studied regions (total area over 1.5 mln km²) are shown in Table 7. To the east of the Yenisei river, a clear trend is evident - the scale of aufeis control of channeling is increasing from the East Sayan ridges in the south-west to Chukotka, inclusively, in the north-east. It is known that in the same main direction, severity of climatic and permafrost conditions is increasing. In the southern regions of East Siberia and the Far East, wherein sporadic permafrost is dominant, the aufeis ratio is nearly twice lower than in the northern regions of the permafrost zone, although almost all the river beds are covered by heterogeneous formations through 60 to 70 % of their lengths – the bottom is composed of crystalline river ice, and the top is composed of aufeis ice. The ice cover of a similar vertical structure is observed on many mountain rivers of the North, mainly in the areas located between large

Table 3. Icing characteristics and incremental lengths of channel networks in aufeis sections of river basins in the Stanovoe upland
Таблица 3. Характеристика наледей и прирост русловой сети на наледных участках долин в бассейнах рек Станового нагорья

| River basin | Basin square area, thou km ² | | Aufeis ratio, % | | Icing characteristics | | | | Incremental length of channel network, km | | | | |
|----------------|---|--------------------------|-----------------|--------------|------------------------------|-------------|------------|--------------|---|------------|--------------|----------------|-------------------------|
| | total | per 1000 km ² | cumulative | average | Square area, km ² | | Length, km | | Width, km | | total | per one aufeis | per one km ² |
| | | | | | average | cumulative | average | cumulative | average | cumulative | | | |
| Chara | 220 | 23 | 100 | 1.040 | 425 | 1.93 | 47 | 0.215 | 1062 | 4.8 | 0.110 | | |
| Муца | 417 | 39 | 77 | 0.186 | 509 | 1.22 | 542 | 0.130 | 1272 | 3.1 | 0.120 | | |
| Upper Angara | 475 | 22 | 68 | 0.140 | 538 | 1.13 | 43 | 0.090 | 1345 | 2.8 | 0.042 | | |
| Total | 1112 | | 245 | | 1472 | | 632 | | 3679 | | | | |
| Average | | 28 | | 0.455 | | 1.43 | | 0.145 | | 3.5 | 0.090 | | |

Table 4. Icing characteristics and incremental lengths of channel networks in river basins on the Putorana plateau

Таблица 4. Характеристика наледей и прирост русловой сети в бассейнах рек плато Путорана

| River basin, region | Basin square area, thou km ² | | Relative aufeis ratio, % | | Icing characteristics | | | | Incremental length of channel network, km | | | | |
|----------------------------|---|-------------------------|--------------------------|--------------|------------------------------|------------|------------|--------------|---|-------------|--------------|----------------|-------------------------|
| | Total | per one km ² | Cumulative | Average | Square area, km ² | | Length, km | | Width, km | | Total | per one aufeis | per one km ² |
| | | | | | average | cumulative | average | cumulative | average | cumulative | | | |
| North-western | 114 | 7.7 | 107.4 | 0.942 | 511 | 4.5 | 28 | 0.246 | 1277 | 11.2 | 0.086 | | |
| Kheta | 206 | 6.3 | 192.9 | 0.631 | 734 | 3.6 | 48 | 0.233 | 1835 | 8.9 | 0.056 | | |
| Maimecha | 49 | 1.6 | 45.6 | 0.931 | 132 | 2.7 | 15 | 0.306 | 330 | 6.7 | 0.010 | | |
| Kotui | 4 | 0.2 | 9.5 | 2.375 | 17 | 4.3 | 2 | 0.500 | 42 | 10.6 | 0.001 | | |
| Dudinka, Fokina | 37 | 4.1 | 36.9 | 0.997 | 109 | 3.0 | 10 | 0.270 | 272 | 7.4 | 0.030 | | |
| Norilskay | 160 | 7.7 | 178.0 | 1.113 | 543 | 3.4 | 43 | 0.269 | 1357 | 8.5 | 0.065 | | |
| Khangaikskoe water reserve | 123 | 4.3 | 115.2 | 0.937 | 358 | 2.9 | 35 | 0.285 | 895 | 7.3 | 0.031 | | |
| Kureika | 22 | 0.5 | 129.1 | 5.868 | 606 | 27.5 | 46 | 2.091 | 1515 | 68.9 | 0.036 | | |
| Kotui (upper stream) | 260 | 8.9 | 253.8 | 0.976 | 1027 | 4.0 | 60 | 0.231 | 2567 | 9.9 | 0.088 | | |
| Chirindakh | 58 | 4.0 | 117.0 | 2.017 | 248 | 4.3 | 21 | 0.362 | 620 | 10.7 | 0.042 | | |
| Prienseisky | 4 | 0.3 | 0.4 | 0.100 | 5 | 1.3 | 1 | 0.250 | 13 | 3.1 | 0.001 | | |
| Northern | 48 | 2.3 | 24.0 | 0.500 | 103 | 2.1 | 11 | 0.229 | 257 | 5.4 | 0.012 | | |
| Erachimo | 27 | 2.3 | 12.1 | 0.448 | 56 | 2.1 | 5 | 0.185 | 140 | 5.2 | 0.012 | | |
| Nimde, Kochumdek | 26 | 1.9 | 7.1 | 0.273 | 53 | 2.0 | 3 | 0.115 | 132 | 5.1 | 0.009 | | |
| Tutonchana | 66 | 2.5 | 26.3 | 0.398 | 195 | 3.0 | 10 | 0.152 | 487 | 7.4 | 0.019 | | |
| Viv | 215 | 8.0 | 166.4 | 0.774 | 889 | 4.1 | 39 | 0.181 | 2222 | 10.3 | 0.083 | | |
| Tembenchi, Yambukan | 236 | 7.1 | 159.4 | 0.675 | 854 | 3.6 | 43 | 0.182 | 2135 | 9.0 | 0.064 | | |
| Kochechum, Embenchme | 265 | 6.7 | 160.4 | 0.605 | 1049 | 4.0 | 38 | 0.143 | 2622 | 9.9 | 0.067 | | |
| Total | 2124 | | 1741.5 | | 7489 | | 458 | | 20220 | | | | |
| Average | | 4.2 | | 0.820 | | 3.5 | | 0.216 | | 11.4 | 0.040 | | |

Table 5. Icing characteristics and incremental lengths of channel networks in aufeis sections of river basins in the north-eastern regions of Russia
Таблица 5. Характеристика наледей и прирост русловой сети на наледных участках долин в бассейнах рек северо-востока России

| Icing areas according to [Tolstikhin, 1974] | Region square area, thou km ² | Relative aufeis ratio, % | Icing characteristics | | Square area, km ² | | Transiton coefficient* | Incremental length of channel network | | |
|---|--|--------------------------|-----------------------|-------------------------|------------------------------|---------|------------------------|---------------------------------------|--------------------|-------------------------|
| | | | Quantity | per one km ² | cumulative | average | | cumulative, thou km | per one aufeis, km | per one km ² |
| | | | | | | | | | | |
| Verkhoyano-Kolymskaya | 279.1 | 1.2 | 1026 | 3.7 | 2068 | 2.0 | 2.4 | 28.1 | 27.4 | 0.100 |
| Polousnensko-Verkhne-Kolymskaya | 135.2 | 1.3 | 534 | 3.9 | 1657 | 3.1 | 3.8 | 23.1 | 43.3 | 0.170 |
| Prilkolymskaya | 24.0 | 1.2 | 155 | 6.5 | 310 | 2.0 | 2.4 | 4.2 | 27.4 | 0.175 |
| Yano-Kolymskaya | 78.3 | 1.2 | 604 | 7.7 | 810 | 1.3 | 1.6 | 11.0 | 18.2 | 0.140 |
| Omolonskaya | 53.5 | 1.0 | 350 | 6.5 | 564 | 1.6 | 1.9 | 7.6 | 21.6 | 0.142 |
| Anyuisko-Chukotskaya | 21.2 | 0.4 | 65 | 3.1 | 84 | 1.3 | 1.6 | 1.2 | 18.2 | 0.057 |
| Okhotsko-Chukotskaya | 115.5 | 0.9 | 836 | 7.2 | 977 | 1.2 | 1.5 | 14.3 | 17.1 | 0.124 |
| Eastern Northern | 89.8 | 1.2 | 661 | 7.4 | 1130 | 1.7 | 2.1 | 15.8 | 23.9 | 0.176 |
| Kamchatsko-Koryakskaya | 140.0 | 0.6 | 415 | 3.0 | 771 | 1.9 | 2.3 | 10.8 | 26.2 | 0.077 |
| Pendzhinsko-Anadyrskaya | 61.3 | 0.8 | 342 | 5.6 | 244 | 0.7 | 0.8 | 3.1 | 9.1 | 0.050 |
| Total | 14.5 | 0.8 | 74 | 5.1 | 100 | 1.4 | 1.8 | 1.5 | 20.5 | 0.103 |
| Average | 1012.4 | 1.0 | 5062 | 5.4 | 8715 | 1.7 | 2.0 | 110.0 | 23.0 | 0.120 |

Note. * – transitional coefficient, k_t is a ratio between the average square area of icing in the north-eastern regions of Russia to the average square area of icing in the Putorana plateau. It is introduced due to the lack of data on the extension of icing in calculations of the total incremental length of the channel network: $\Sigma L_0 = k_t (n \rho_F)$, where $\rho_F = 11.4$.

Примечание. Переходный коэффициент k_t представляет собой отношение средней площади наледей на северо-востоке России к средней площади наледей на плато Путорана. Введен в связи с отсутствием данных о протяженности ледяных массивов для определения суммарной величины прироста русловой сети: $\Sigma L_0 = k_t (n \rho_F)$, где $\rho_F = 11.4$.

Table 6. Icing characteristics and incremental lengths of channel networks in aufeis sections of river basins located along the Baikal-Amur Railroad route in its section from Lake Baikal to Nyukzha (KR 622–1678)

Таблица 6. Характеристики наледей и прирост русловой сети на наледных полях, расположенных вдоль трассы Байкало-Амурской железной магистрали на участке от Байкала до Ньюкжи (622–1678 км)

| River basin | Distance from Ust Kut, km | Icing characteristics | | | | | | Incremental length of channel network, km | | |
|----------------|---------------------------|-----------------------|------|------------------------------|---------|------------|---------|---|---------|-------|
| | | Quantity | | Square area, km ² | | Length, km | | Width, km | | |
| | | | | cumulative | average | cumulative | average | cumulative | average | total |
| Upper Angara | 422–633 | 26 | 1.9 | 0.075 | 14.0 | 0.539 | 3.0 | 0.117 | 35.0 | 1.3 |
| Muya | 650–770 | 50 | 5.8 | 0.116 | 48.6 | 0.971 | 6.3 | 0.126 | 121.5 | 2.4 |
| Vitim | 787–834 | 30 | 2.6 | 0.086 | 19.0 | 0.635 | 2.8 | 0.092 | 47.5 | 1.6 |
| Konda | 840–921 | 60 | 6.0 | 0.101 | 46.1 | 0.769 | 3.7 | 0.062 | 115.2 | 1.9 |
| Maloe Leprindo | 925–927 | 4 | 0.2 | 0.043 | 1.6 | 0.392 | 0.3 | 0.085 | 4.0 | 1.0 |
| Chara | 944–1203 | 60 | 26.3 | 0.438 | 97.0 | 1.616 | 14.0 | 0.233 | 242.5 | 4.0 |
| Khani | 1210–1300 | 17 | 9.4 | 0.550 | 32.0 | 1.886 | 8.4 | 0.496 | 80.0 | 4.7 |
| Olyokma | 1335–1395 | 11 | 4.8 | 0.432 | 11.0 | 1.570* | 0.7* | 0.098* | 27.5 | 2.5 |
| Nyukzha | 1405–1678 | 15 | 1.6 | 0.107 | 5.1 | 0.854* | 0.6* | 0.094* | 12.7 | 0.8 |
| Total | | 273 | 58.6 | | 274.4 | | 39.8 | | 685.9 | |
| Average | | | | 0.216 | | 1.026 | | 0.156 | | 2.2 |

Note. * – Olyokma: seven aufeis deposits; Nyukzha: six aufeis deposits.

Примечание. * – данные по Олекме – 7 наледей, по Ньюкже – 6 наледей.

Table 7. General icing characteristics and incremental lengths of channel networks in aufeis glades in East Siberia and the north-eastern regions of Russia

Таблица 7. Общая характеристика наледности и прирост русловой сети на наледных полях Восточной Сибири и северо-востока России

| Icing area | Region square area, thou km ² | Relative aufeis ratio, % | Icing characteristics | | | | Incremental length of channel network | | |
|---------------------------------|--|--------------------------|-----------------------|-------------------------|------------------------------|--------------|---------------------------------------|--------------------|-------------------------|
| | | | Quantity | | Square area, km ² | | cumulative, thou km | per one aufeis, km | per one km ² |
| | | | total | per one km ² | cumulative | average | | | |
| North-eastern regions of Russia | 1012.4 | 1.00 | 5062 | 5 | 8715 | 1.700 | 110.0 | 23.0 | 0.120 |
| Putorana plateau | 433.5 | 0.37 | 2124 | 5 | 1741 | 0.820 | 20.2 | 11.4 | 0.040 |
| Priokhotsky | 117.1 | 0.84 | 1249 | 11 | 985 | 0.789 | 13.6 | 10.9 | 0.116 |
| Stanovoe upland | 42.0 | 0.69 | 1112 | 28 | 245 | 0.455 | 3.7 | 3.5 | 0.90 |
| South-western Pribaikalie | 14.8 | 0.39 | 1403 | 95 | 120 | 0.085 | - | - | - |
| T o t a l | 1619.8 | | 10950 | | 11806 | | 147.5 | | |
| A v e r a g e | | 0.66 | | 29 | | 0.770 | | 12.2 | 0.091 |

Note. Symbol “-” means “No data”.

Примечание. Прочерк в графе – нет данных.

ice masses (taryns). The major part of this channel system undergoes development stages I or V, i.e. the ice cover occupies the entire floodplain across the 'normal' flow cross-section, yet does not go beyond it. As a result, the cryogenic impact on channelling is mainly limited to destruction of the slopes during spring floods and expansion of the river channel due to thermal erosion. Thus, any 'additional' branching of the cryogenic origin does not take place, but shapes and dimensions of the runoff channels are significantly changed – they become wide and flat. A characteristic feature of such rivers is a smoothed longitudinal profile of the bed with long shallow natural bars or stretches.

10. LONG-TERM VARIABILITY OF THE AUFEIS CHANNEL NETWORK STRUCTURE

Even in the harshest climate conditions, the frozen zone of the lithosphere is penetrated by water-consuming and water-releasing taliks, which locations and configurations remain permanent for many years. Radical restructuring of the water-exchange system takes place only as a result of profound climate changes through many hundreds and thousands of years. Therefore, the aufeis deposits formed in the zone of permanently active groundwater sources are also quasi-constant in time, and their volumes range around some average values depending on local variations of the main characteristics of climate, particularly temperature and precipitation. However, substantial spatial changes occur depending on self-development of the cryogenic system with account of some random factors. Runoff channels maintain their relatively stable

positions only in aufeis development stages I and V when the ice-ground complex does not go beyond the level of high floodplain. In other cases, i.e. in stages of transgression, stabilization and regression, the channels are offset from year to year due to specific features of aufeis ablation and formation of cryogenic landforms. Another important factor is shifting of the geometric centres of ice masses from side to side of the valley and up or down the river.

During the snowmelt period, the runoff channels are cut at different places by melt water flows that spread over the vast ice field, so the configuration of the channel network varies from year to year. Such annual variations are accompanied by transformations of the aufeis glade, which mainly depend on the erosion-accumulation activity of branched water flows. A part of the aufeis glade may be temporarily out of the aufeis-formation regime and, later on, it is covered by new aufeis-ice layers. As a result, the valley bottom is flatten and expanded, and its longitudinal profile is stepped. It is noteworthy that in some years, many aufeis deposits demonstrate a sharp increase of their square areas (by 20 to 30 %), spread into the neighbouring forests (i.e. beyond the well-defined aufeis glade) and thus leave traces resembling passage of high floods. Inexperienced specialists are puzzled and led to false conclusions concerning the river regime in the warm season. In some cases, the aufeis deposits are steadily formed in the near-river forests and on islands and generate erosional landforms that are similar in shape to old channels but differ in genesis. The largest documented aufeis deposit located on the Moma river in Yakutia is such an example (Fig. 24). In other cases, the ice fields may decay or drastically reduce in size.



Fig. 24. The gigantic Moma aufeis deposit (Ulakhan Taryn) in the north-eastern Yakutia.

a – photo taken from an aircraft (photo by Sandro, Yandex: Fotki...0_6020d_1324d2b0_orig); *b* – hydrographic network after ice melt (satellite image, Google). According to different estimates, the area of the Moma aufeis deposit ranges from 76 to 112 km², its maximum thickness amounts to 6 m, and the average thickness ranges from 3 to 4 m. In spring, the width of the ice field exceeds 2 km, and large forested areas and numerous islands are ‘flooded’.

Рис. 24. Большая Момская наледь (Улахан Тарын) на северо-востоке Якутии.

a – снимок с самолета (фото Сандро, Яндекс. Фотки...0_6020d_1324d2b0_orig); *b* – структура гидрографической сети после таяния льда. Снимок из космоса, Google. Площадь Момской наледи по разным оценкам составляет 76–112 км², максимальная мощность достигает 6 м, средняя колеблется в пределах 3–4 м. Весной ширина ледяного поля превышает 2 км, при этом «заливаются» значительные участки леса и многочисленные острова.

Such a case is the Kyra-Nekharanskaya aufeis deposit (almost 100 km²) that has recently broken up into several separate ice masses.

In mature aufeis glades, annual transformations of the channel network are not always noticeable, as the runoff channels have low and flat banks, and inter-stream areas are devoid of vegetation. In some cases,

the aufeis bed can develop into a shallow pool that is periodically dried, and only special methods and observations can help detecting numerous traces of water flow movements taking place during ablation of ice masses (Fig. 25). Aerial surveys and satellite imagery are particularly effective in revealing the long-term changeability of the channel network. Valuable

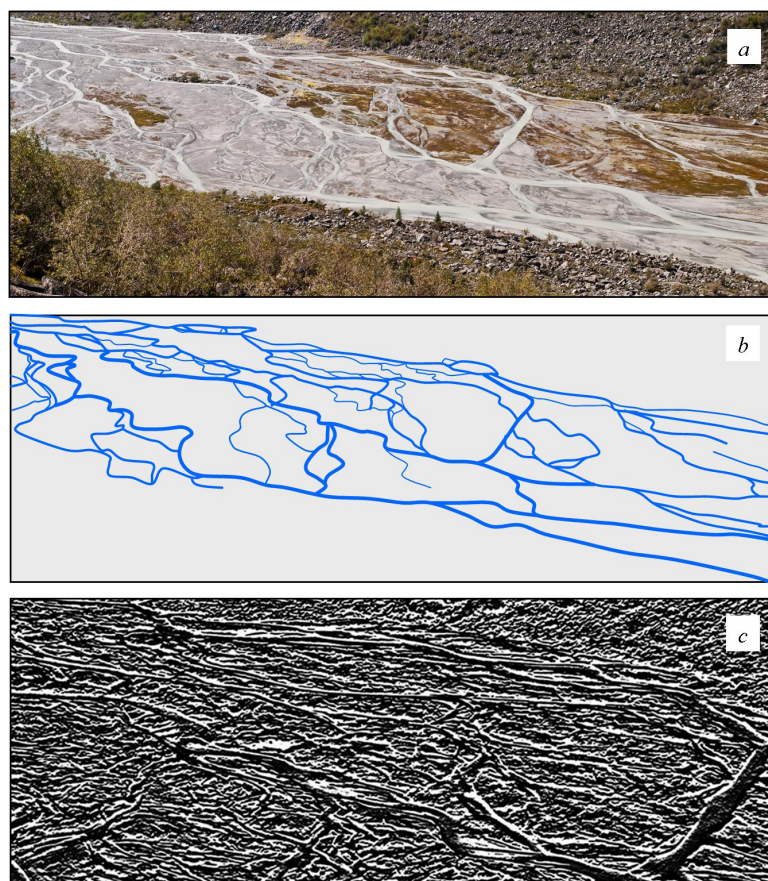


Fig. 25. The channel network on the aufeis glade in the Akkem river valley, Altai.

a – photo taken from a helicopter (NATA-SOLAR; Yandex: Fotki... 0_80592_66abc943_orig); *b* – configuration of the current river network as determined from the photo; *c* – surface of the aufeis glade with traces of erosion activity of water flows ('filtered-out' fragment of the photo of the middle part of the aufeis glade).

Рис. 25. Структура русловой сети на наледной поляне в долине реки Аккем, Алтай.

a – снимок с вертолета (NATA-SOLAR. Яндекс. Фотки... 0_80592_66abc943_orig); *b* – конфигурация современной речной сети, определенная по фотоснимку; *c* – поверхность наледной поляны со следами эрозионной деятельности водных потоков («отфильтрованный» фрагмент снимка центральной части наледной поляны).

information can also be obtained by comparing medium- and large-scale topographic maps constructed or updated in the past 60–70 years.

Our analysis of the available data shows that in the valleys of many rivers in the permafrost zone, aufeis multi-channeling does not occur locally and can be observed almost continuously for many dozens or even hundreds of kilometres (Fig. 26). This is caused by regional and local crustal faults, which zones are developed by river valleys of ranks 3 to 6. Tectonic faults of various generation ranks are associated with water-releasing taliks that feed large-flow groundwater sources and their corresponding giant aufeis deposits (taryns). Besides, it should be noted that square areas of the ancient aufeis glades are considerably larger than the areas of the current hydrographic network (Fig. 26, *a–f*). This fact gives an evidence of the activity and long-term variability of channeling in both the current

period and the distant past, including, probably, the Holocene (10–12 thousand years) and earlier periods. This aspect has not been studied at all, despite its high paleogeographical importance, in particular for exploration and evaluation of placer deposits of minerals.

11. ZONATION OF THE TERRITORY OF RUSSIA BY CRYOGENIC CHANNELING TYPES

Identification of large taxonomic categories from effects of ice and melt water to channeling should be based on the known axiomatic concepts that follow from the Grigoriev-Budyko periodic law of geographical zonality of natural processes [Grigoriev, 1966]. A channel is a linear type of landform which is formed by a water flow. Primarily, where there is no water, there is no channel (an example is the Moon surface). The

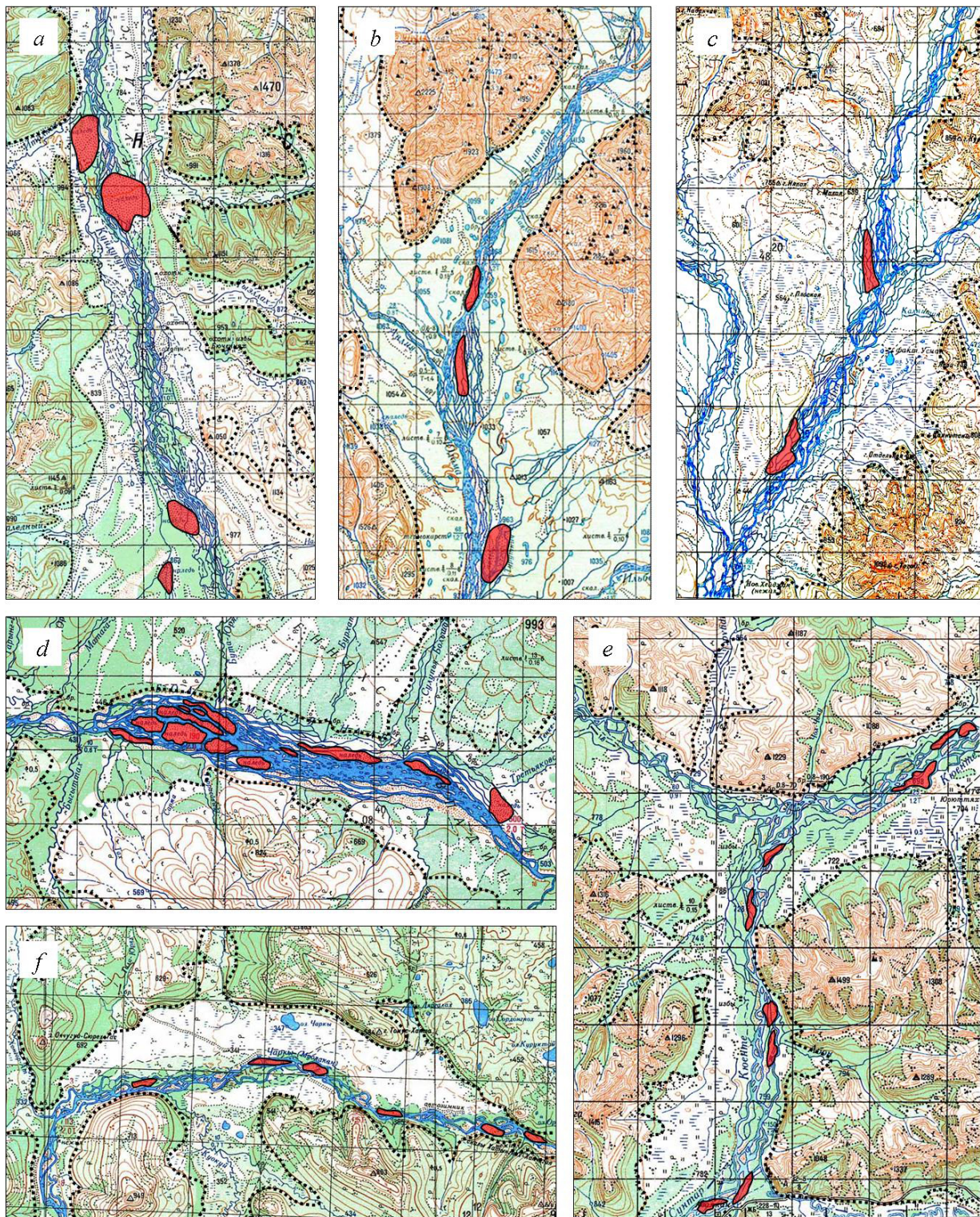


Fig. 26. Configurations of channel networks in areas of gigantic aufeis deposits (taryns) in the river valleys of the Verkhoyansk-Kolyma mountain system.

Fragments of topographic maps, scale 1:100000. Grid square 2×2 km. River valleys: *a* – Kuidusun, *b* – Yudoma, *c* – Inya, *d* – Moma, *e* – Suntar and Kyuente, *f* – Charky. The black dotted line outlines the ancient and contemporary aufeis glades. Remnants of the aufeis deposits as of the topographic survey data are shown in red.

Рис. 26. Конфигурация русловой сети на участках формирования гигантских наледей-тарынов в долинах рек Верхояно-Колымской горной страны.

Фрагменты топографических карт масштаба 1:100000. Квадрат сетки 2×2 км. Долины рек: *a* – Куйдусун, *b* – Юдома, *c* – Иня, *d* – Мома, *e* – Сунтар и Кюенте, *f* – Чаркы. Точечной линией черного цвета показаны внешние границы древних и современных наледных полей; красным цветом выделены остатки наледей на дату топографической съемки.

quantity of water involved in channeling is climate dependent. All climate zones of the Earth fall into one of three basic categories:

(1) zones with permanently positive temperatures of the near-ground air layer through the year; in such zones, channeling takes place under the laws of non-freezing rivers;

(2) zones with permanently negative temperatures at the boundary between the atmosphere and the lithosphere (permafrost conditions); in such zones, rivers are absent as all the water is accumulated as snow and ice (for example, in Antarctica and inner regions of Greenland);

(3) zones with alternating positive and negative temperatures at the ground surface; in such zones, rivers are covered by ice for many months, and the majority of the rivers freeze either partially or completely.

Zones in category 3 are parts of the transitional belt of the cryosphere, wherein the regime of water flows and corresponding erosional-accumulation events are dependent on the duration and severity of the cold period of the year, solid precipitation volumes, types of feed, presence of permafrost and seasonally frozen areas etc. Ratios of water, ice and frozen rocks, which determine specific features of channeling in the transitional belt of the cryosphere, are shown in Fig. 9. If the water layer in the runoff channel of thickness h_1 , does not get covered by ice through the year, channeling takes place under the laws of non-freezing rivers. In the permafrost zone, processes of this type take place rarely, mainly on sites of large permanent polynya formed by strong subaqueous groundwater sources, as well as at afterbays of river dams, and are always influenced by icing events that occur in the adjacent river sections. In all other cases, the presence of the ice cover and its temporal and spatial changeability provide for the stage-by-stage cryogenic development of the hydrographic network, which reflects principles of self-development of the geosystems within the limits of specific climate characteristics and uniform geological and geomorphological conditions. Obviously, seasonal, long-term and perennial changeability of the cryogenic systems of this types is manifested not only along the river of a certain rank, but also within natural and climatic zones and altitudinal belts, and this is reflected in characteristics of ice, the underlying bed and the hydrographic structure in general. These conclusions follow from an unsophisticated physical geographical analysis of the situation and are supported by the materials presented in the previous sections of this paper.

Based on the above, we propose a general classification of cryogenic channeling types. It refers to conditions of formation of the channel networks in practically all cold regions of the Earth (Table 8), primarily regions of the permafrost zone.

In our classification, the key indicator is represented by a ratio of thicknesses of genetically inhomogeneous glacial formations on rivers, specifically snow-ice thickness, h_{sn} , river- and groundwater aufeis thickness, h_a , and crystalline river ice thickness, h_{cr} . Five types of cryogenic channeling are distinguished according to the following conditions: (1) $h_{sn} > h_{cr} > h_a$; (2) $h_{snow} > h_{cr} < h_a$; (3) $h_{sn} < h_{cr} > h_a$; (4) $h_{sn} < h_{cr} < h_a$; and (5) $h_{sn} > 0 < h_a$.

Type 1. Snow ($h_{sn} > h_{cr} > h_a$). Snow-type channeling is typical of the regions characterised by short-term and seasonal freezing, short freeze-up periods (up to 4 months) and a relatively thin ice cover. Ice does not extend above the autumnal low-water level, sags while the subsurface feed is depleting, decays without ice drift, and does not put any significant impact on channeling. The floodplain sections of the valley are deformed and the sediments are redeposited during the spring-flood period due impacts of melted-snow water.

Type 2. Snow-ice ($h_{snow} > h_{cr} < h_a$). Snow-ice channeling is typical of the regions characterized by deep seasonal freezing of soils and rocks, sporadic and massive sporadic permafrost (up to 50 % of the area) on mountain slopes and in boggy river terraces (rarely on high floodplains). By spring, due to river-water aufeis depositing, the ice cover extends beyond the autumnal low-water level and reaches the inner boundary of the floodplain. During the snow-melt period, the ice slabs floats with melted snow water and contributes to redeposition of riverbed material and floodplain alluvium, but does not cause any significant changes in the structure of the river banks and the river bed.

Type 3. Ice-aufeis ($h_{sn} < h_{cr} > h_a$). Ice-aufeis channeling is typical of the regions with discontinuous permafrost (50 to 95 % of the area) and freezing river systems. In the first half of winter, the crystalline-ice cover is overlaid by river-water aufeis deposits and, in the second half of winter, by groundwater aufeis deposits. In the aufeis-formation period, the snow cover gets included in the ice bed and creates cloudy bubble-rich ice sublayers. The glacial complex, extending to the level of high floodplain, is complicated by aufeis- and ground-aufeis mounds. In spring, the river bed is significantly transformed during the ice-drift period – the bank slopes are deformed; alluvial deposits, that are frozen in and frozen up to the ice slabs' bottoms, are transferred; bars, chains and scattered structures containing sand, gravel boulders and pebbles are constructed on the beaches; subaqueous furrows and runoff channels are formed. During the ice-drift period, ice may be deposited outside the floodplain. It melts in place and thus does not put any impact on channeling.

Type 4. Aufeis ($h_{sn} < h_{cr} < h_a$). Aufeis channeling is typical of regions with continuous permafrost (more than 95 % of the area) and ubiquitous freezing of water flows. The thick aufeis deposit (composed mainly of

Table 8. Characteristics of cryogenic channeling types (for rivers of ranks 1 to 6)

Таблица 8. Типологическая характеристика условий криогенного руслообразования (для рек 1–6-го порядка)

| Characteristics | Types of cryogenic channeling | | | | | |
|--|-------------------------------|-------------------------|-------------------------|-----------------------------------|-----------------------------------|-----------------------------|
| | 1. Snow (S) | 2. Snow-ice (SI) | 3. Ice-aufeis (IA) | 4. Aufeis (A) | 5. Glacier (G) | |
| Map symbol | 1 | 2 | 3 | 4 | 5 | |
| Intensity of cryogenic channeling | Very low | Low | Medium | High | Very high | |
| Period of maximum manifestation, month | III | IV | V–VI | V–VII | VI–VIII | |
| River runoff under ice, month | Continuous XI–III | Continuous X–IV | Intermittent X–I | Intermittent X–XI | None | |
| Duration of freeze-up period, number of month | 1–4 | 4–6 | 6–7 | 7–8 | 8–10 | |
| Average ice thickness, m | snow, h_{sn} | 0.3 | 0.3 | 0.2 | 0.5 | |
| | crystalline, h_{cr} | 0.2 | 0.5 | 0.7 | 0.3 | |
| | aufeis, h_a | 0.1 | 0.2 | 0.5 | 1.5 | |
| | total | 0.6 | 1.0 | 1.5 | 2.0 | |
| | ratio | $h_{sn} > h_{cr} > h_a$ | $h_{sn} > h_{cr} < h_a$ | $h_{sn} < h_{cr} > h_a$ | $h_{sn} < h_{cr} < h_a$ | $h_{sn} > 0 < h_a$ |
| Presence of permafrost | seasonal ($h > 1$ m) | None | In floodplain | In floodplain and under river bed | Under river bed | None |
| | perennial | None | Sporadic | Discontinuous | Continuous | Continuous |
| Taliks | over-permafrost | None | None | In floodplain | Under river bed | Under river bed |
| | inter-permafrost | None | None | Under river bed | In floodplain and under river bed | Under river bed and glacier |
| Snow cover thickness, m | 0.5–0.8 | 0.3–1.0 | 0.2–0.8 | 0.5–1.0 | 1.0–1.5 | |
| River feed in the critical period of the year (zero precipitation) | Subsurface | Subsurface | Subsurface | Aufeis | Glacier | |

groundwater) occupies the channel, floodplain and low terraces and often spreads through the entire width of the river valley. Lenses and layers of injection ice form under the aufeis deposit, and the soil layers have to bulge and thus obstruct the way for melt and rain water. As a result, the water flows are forced to change their directions. The underlying bed and the beach scarps are intensely eroded. Due to melting of aufeis ice and injection ice, an additional network of streamlets is created, and thermokarst collapse is accompanied by the formation of small lakes or lengthy trenches that accumulate the melt water runoff. In the icing zone, the sediments are redeposited, and large fragments of rocks are displaced every year. As a result, the river bed is expanded and flattened, and the water flow is spread and divided into a series of shallow-water branches and loses its velocity and carrying capacity.

Type 5. Glacier ($h_{sn} > 0 < h_a$). Glacier-type channeling develops below tongues of mountain-valley glaciers and at the walls of ice caps in conditions of continuous recent or relict permafrost. In case of complete freezing of the icing bed, the channel network is formed only due to erosion-accumulation activity of thawing snow and glacial water. The runoff regime is characterised by evident daily water level variations due to atmospheric air temperature changes. The flow rates may reach catastrophic values; in such cases, glacial materials are

considerably redeposited and reworked, and river channels shaped in the previous year are significantly transformed. Generally, the bottoms of glacial valleys are flat and cut by numerous channel branches that are filled during daily increase of the water level and in case of rains. The impact of glacier floods can be traced for dozens and hundreds of kilometres down the valley; it is reflected in the morphological structure of near-glacier outwash plains.

At the edge of the warm glaciers containing the reserve of intra- and subglacial water that is discharged in winter, the snow-aufeis complex is formed. It modifies the activity of melt water, and in some cases leads to formation of typical aufeis glades with mounds and intra-soil injection-ice layers that are sometimes viewed as remnants of a degraded glacier.

Zonation by the cryogenic channelling types is shown in Fig. 27. Almost 2/3 of the territory of Siberia and the Far East, the northern part of the Ural and Priuralie and the Arctic islands are strongly influenced by cryogenic processes, which is evidenced by the structure and functioning of the hydrographic network, in particular its upper part (water streams of ranks 1 to 5). The aufeis deposits play a significant role in this large-scale natural phenomenon, which should be taken into account in infrastructure engineering projects aimed at development of the permafrost zone.

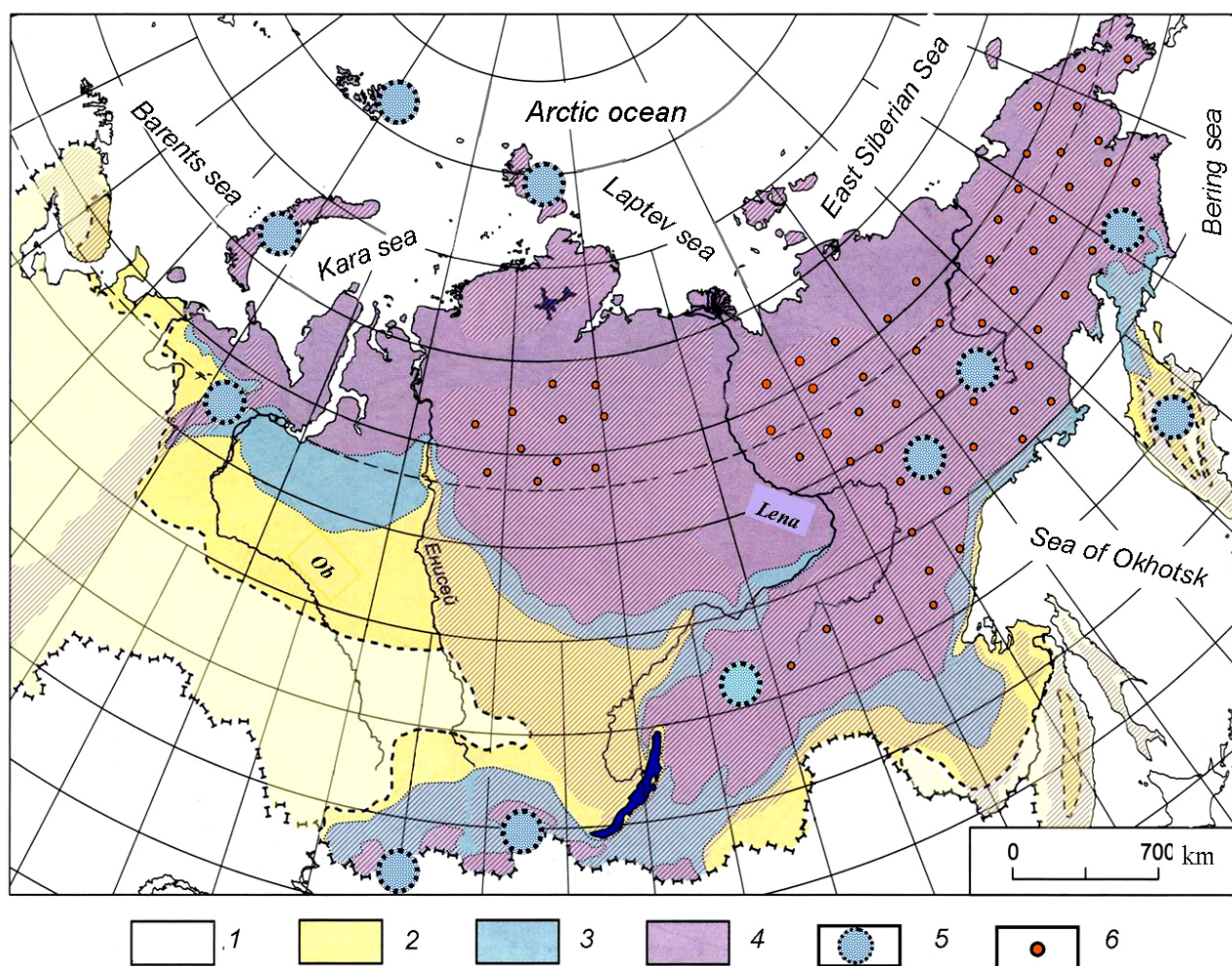


Fig. 27. Zonation of the territory of Russia by cryogenic channeling types.

Cryogenic channeling types: 1 – snow, 2 – snow-ice, 3 – aufeis-ice, 4 – aufeis, 5 – glacier (channeling conditions are described in table 8); 6 – areas of gigantic aufeis deposits (taryns). Mountains and plateaus are shaded.

Рис. 27. Районирование территории России по типам криогенных руслообразующих процессов.

Типы криогенных руслообразующих процессов: 1 – снежный, 2 – снежно-ледовый, 3 – наледно-ледовый, 4 – наледный, 5 – ледниковый (характеристика условий руслогенеза см. в таблице 8); 6 – районы распространения гигантских наледей-тарынов. Штриховкой показаны горы и плоскогорья.

12. DISCUSSION

According to the recent studies [Koroleva, 2011], the permafrost zone of Russia amounts to 10.7 mln km² (65 % of the territory), including 5.2 mln km² (49 %) of continuous permafrost, 2.4 mln km² (22 %) of discontinuous perennial permafrost, and 3.1 mln km² (29 %) of mass-sporadic and sporadic permafrost. Groundwater aufeis zones are large and well manifested by aufeis glades in the territory of 7.6+ mln km² (71 % of the permafrost zone). The relative aufeis ratio determined from parameters of 10000 ice fields amounts to 0.66 % in average (see Table 7), i.e. almost 56000 km². If an error of 20 %, that occurs because the aufeis fields are less numerous in the lowland plains, the total annual

square area of the groundwater aufeis deposits amounts to almost 45000 km². The number of ice masses, each occupying an area of 0.770 km² in average, may be significantly larger than 60000. Many or few? For comparison, we can refer to the square area (F_g) and the number (N_g) of glaciers in the continental Russia: $F_g=2551$ km², and $N_g=1727$ [Dolgushin, Osipova, 1989]. Thus, the total aufeis (congelation-ice) square area in the permafrost zone is higher by a factor of 18 than the 'classical' (sublimation, sedimentation-metamorphic) icing area. The number of large groundwater aufeis deposits, which square area is equivalent to the mountain-valley glaciers in the Asian regions of Russia, is significantly more than 60000, i.e. by a factor of 35 exceeds the number of glaciers. Estimations

based on the above-mentioned data show that the total increment of the hydrographic network amounts to 690000 km in the territories of continuous and discontinuous permafrost ($F=7.6$ mln km²).

The above values do not take into account aufeis deposits of the heterogeneous origin (fed by river water and groundwater) which, as a minimum, occupy 60 % lengths of the rivers of ranks 1 to 5 in the remaining regions wherein permafrost is developed. In Siberia and the Far East, the total length of rivers of ranks 1 to 5 (up to 500 km long) amounts to 6.641 mln km. Almost half of such rivers run in the territories of continuous and discontinuous permafrost. Rough estimates for Siberia and the Far East show that the total square area of the aufeis deposits occupying the entire river channels, but not exceeding the limits of the 'standard' floodplain, amounts to 68000 km², i.e. twice as large as all the groundwater aufeis deposits with 'fixed' beds (taryns).

The above-mentioned values are just the first approximation. Anyway, such data give evidence of the significant role of aufeis phenomena in channeling, as well as in the evolution of the structure and dynamics of the geosystems in the northern territories. Considering hydrological, geological and landscape development aspects, there are grounds to conclude that the role of aufeis deposits is many times more important in this respect than the role of glaciers. This conclusion is based not only on the above-mentioned information, but also on the comparison of the aufeis and glacier runoff volumes. The thaw-aufeis water volumes are just incomparable to the glacier water runoff. Most of the aufeis deposits are subject to complete ablation during the warm season each year, and their annual 'active layer' equals the aufeis-ice thickness. All the thaw-aufeis water goes into the river network and actively participates in channelling. As for the glaciers, only the top thin parts are 'in operation' and only in the ablation zone, which square area is generally significantly smaller than that of the accumulation zone.

Anyway, glaciers have always been given special attention in all the regions in the USSR and Russia. There is still a trend to report a 'geographical discovery' even when presenting a description of a small-sized glacier located somewhere in Pribaikalie or on the Koryak tableland. Aufeis deposits were less 'lucky' and became the subject of active studies only about 50–60 years ago; however, in the past two decades, the aufeis studies ceased. Why the current situation is inadequate? There is no need here to mention factors of 'perestroika' and the social and economic crisis; the negative consequences are evident. There is, however, a number of subjective factors – an adequate understanding of glacial phenomena and especially aufeis is lacking among many researchers, engineers and science managers, and the importance of such phenomena for de-

velopment of regions with cold climate is underestimated. The aufeis sections of the river valleys, being the 'hottest' spots of the permafrost zones, are unavoidable and cannot be eliminated. The only way is planning human activities with account of the aufeis phenomena, which requires the knowledge of laws and regularities of development, structure and properties of the cryogenic systems. Long-term monitoring, testing and experiments are needed to obtain such knowledge. Besides, a wide-scale inventory of relevant research subjects needs to be conducted. Neither Skolkovo nor Olympic Games projects can be sufficient for solving the scientific and applied problems of nature resources development in our country of abundant snow, ice and permafrost. It is critical to plan and implement independent nature research programmes targeted at problem solving in the specified fields of science and practice.

In late 1980, large-scale research data were consolidated in the USSR Glaciers Catalogues. The World Atlas of Snow and Ice Resources, presenting a unique summary of the current knowledge on snow and ice on the Earth, was published in 1997. Less ambitious, yet no less successful initiatives and publications by individual scientists and research teams should be also mentioned as valuable contributions to the knowledge on aufeis phenomena [Alekseyev, 2007; *Catalogue...*, 1980, 1981, 1982; *Shesternev, Verkhoturov, 2006; Sokolov, 1975; Tolstikhin, 1974*]. Unfortunately, the techniques and methods applied in these studies were imperfect, and the input information was motley. Now it is challenging to analyse and compare such data. Many aspects were skipped as the input data was lacking. Today, when data obtained by highly efficient GIS technologies and nearly simultaneous serial space imagery can be available, the pressing demand to revise and update the databases can be met. It becomes feasible to stock-take the icing and glaciation objects of the entire Earth or the territory of Russia, as a minimum, by establishment of monitoring sites for ground-truth observations to confirm satellite data. Studies of ice-ground complexes as a unique phenomena of icing on the Earth should be also included in a comprehensive research programme. With this approach, many issues of cryogenic morpholithogenesis, including those mentioned in this article, can be clarified.

The materials reviewed herein and data on other regions published in [Petrov, 1930; Podyakonov, 1903; Romanovsky, 1983, 1993; Sannikov, 1988; Strugov, 1955; Tsvid, Khomichuk, 1981] show that annual formation and ablation of aufeis and subsurface ice are accompanied by soil heaving, thermokarst and thermal erosion. Combined, these processes lead to a rapid (often unexpected) reconfiguration of the surface and subsurface runoff channels, abrupt uplifting and subsiding of the ground surface, decompaction and 'shaking-up' of sea-

sonally thawing and seasonally freezing rocks, thereby producing exceptionally unfavourable conditions for construction and operation of engineering structures. All the above-described phenomena need to be taken into account in applied research and engineering for development of natural resources in the northern regions.

It should be noted that aufeis hazard has not been duly considered yet in applied aspects, despite the availability of scientific and engineering publications on glaciology, hydrogeology and geocryology of the northern and north-eastern regions of Russia [Alekseev, 2005]. Researchers are mainly focused on studies of ice and water above ice. Processes under the ice caps and aufeis deposits remain unknown, and the lack of such knowledge hampers the search for solutions of applied problems. An indicative case is the Kerak aufeis deposit at the Transbaikalian (Far East) Railroad (KP 7352). For over 50 years, the railroad bed and icing on site were monitored [Rumyantsev, 1964, 1991]. Nearly every year, management decisions concerning assurance of safe railroad operations were taken on the basis of theoretical considerations, without any research of 'inherent' factors leading to hazardous engineering geological processes, and such decisions were actually useless. Only after core-drilling studies initiated by hydrogeologist P.N. Lugovoy and detailed observations on this site, a correct and reliable method was selected for protection of the railroad bed, and the aufeis hazard was thus eliminated.

Obviously, aufeis problems are well known to scientists and engineers, especially those involved in road construction projects [Chekotillo et al., 1960; Kazakov, 1976], yet aufeis studies are generally limited to road sides. Typically, front-end engineering surveys do not include long-term field observations that would facilitate clarification of the origin and dynamics of aufeis and cryogenic-geological phenomena – it is conventionally believed that aufeis hazard can be eliminated by standard protection actions. It is, however, evident that regularities of formation of ice-ground complexes and their development depend on a complex combination of many natural factors, including the topography and geological setting of the territory, permafrost and hydrogeological conditions, geographic latitudes and elevations of areas subject to icing etc. In order to solve applied problems, it is required to employ specialized approaches on a case-by-case basis as specific indicators of the above-mentioned relationships have not been established yet. Besides, total and unit sizes of aufeis deposits should be taken into account. Based on results of his studies of the northern Amur region, B.N. Deykin made the following conclusion: within the limits of the well-defined aufeis glades, the square area and the volume of stratal ice amount to 41.5 % and 15 % of the unit dimensions of an average aufeis de-

posit, respectively [Deikin, 1985]. In our preliminary calculations based on the established indicators, similar values (55 % and 20 %) are obtained. What is the extent of distribution of injection ice and mounds in the areas wherein giant aufeis deposits (taryns) occupy dozens of square kilometres? Does formation of the ice-ground complexes differ in the northern and southern areas of the permafrost zone? These questions remain unanswered. The studies that started 30–35 years ago at the Baikal-Amur Railroad, in Yakutia and the north-eastern regions of Russia were suspended and have not been resumed yet. The information collected for road construction projects in the southern regions of the permafrost zone is evidently insufficient for assessment of the extent and specific development features of hazardous aufeis phenomena in areas of harsh climate conditions. That is why the express methods applied for engineering design of industrial linear facilities, such as the East Siberia - Pacific Ocean pipeline (ESPO), fail to fully provide for reliable assurance of stability and environmental safety of the industrial systems.

The problem will be surely aggravated in construction of linear facilities of large lengths, such as a transcontinental railroad to Alaska – by-passing or crossing the 'hot spots' without any environmental risk will be the major challenge. In view of the above, special studies are required to catalogue the data on aufeis glades and to study the aufeis dynamics, conditions and development with account of interactions of the ice masses with the underlying rocks and the environment. Upgrading the methods for identification and assessment of aufeis hazards is of high practical importance, and new techniques should be developed with application of remote sensing and ground-truth observations to confirm satellite data.

In order to solve engineering problems related to aufeis sections of the river valleys, it is proposed to establish sites for pilot testing and monitoring. Studies on such sites can facilitate the identification of specific features in the behaviour of natural and man-made systems, such as pipelines, embankments, bridges, underground and surface utilities and other facilities operating in complicated conditions, as well as contribute to establishing principles and methods of design, construction and operation of engineering structures in territories subject to aufeis hazards. It will be possible to test theoretical models and technological schemes aimed at development of the territories wherein hundreds of thousand square kilometres are ice-covered each year.

In our opinion, it is also important to study the aufeis alluvium, specifically its structure, locations and development. This well-washed and sorted material is affordable and can be widely used in construction of various facilities. The aufeis glades can be considered

as a kind of traps for placer gold due to the annual 'shake-up' of loose sediments, decay of the energy of water flows and morphological characteristics of the channel network in the aufeis glades. The aufeis glades are abundant in the 'golden belt' stretching from the Sayan mountains to the Kolyma upland in the north-eastern regions in Asia, as well as in Alaska. It stands for reason that Yu.A. Bilibin, the pioneer and expert in geology of gold placers, gave much attention to studies of aufeis phenomena when prospecting for 'gold-bearing sands' [Bilibin, 1963]. Specialized mining and tunnelling works are needed to study this aspect. Hopefully, this problem will attract the attention of specialists who can conduct proper scientific and applied studies.

Based on our analyses of the current state of knowledge on the aufeis sections of the river valleys, some topical problems can be stated for the future studies. In our opinion, objectives for the near future shall be as follows:

(1) Conduct detailed studies of cause-and-effect relationships and regularities in seasonal and long-term development of geodynamic and glaciohydrological phenomena in the zone of active icing; such studies shall be based on long-term observations on special aufeis polygons;

(2) Develop a technique for field surveys and mapping of aufeis hazard sites in the regions wherein giant aufeis deposits (taryns) are abundant; reveal and evaluate indicative properties of the aufeis deposits and aufeis glades;

(3) Study how industrial facilities, such as pipelines, utilities, roads, railroads, bridges, dams, towers of overhead power and communication lines etc., interact with aufeis deposits and aufeis ice-ground complexes of the main types;

(4) Determine principles of engineering development of the aufeis sections of the river valleys in zones differing in climate and geocryological conditions; propose and develop standard technological schemes for design, construction and operation of engineering structures on sites of active icing;

(5) Study deposits on the aufeis glades as sources of building materials and accumulators of some useful minerals.

The above-mentioned problems can be solved only by joint efforts of specialists from interested institutes and authorities, who can establish a multi-discipline team for implementation of a comprehensive project titled "*Development of concepts and methods for assessment, mitigation and elimination of aufeis hazard in the permafrost zone of Russia*". It is reasonable to conduct activities aimed at preparation and implementation of the project with resources of the Siberian Branch of RAS, particularly with involvement of specialists from Melnikov Permafrost Institute (Yakutsk),

Institute of the Earth's Crust (Irkutsk), Earth Cryosphere Institute (Tyumen), and Sochava Institute of Geography (Irkutsk).

13. CONCLUSION

1. The groundwater aufeis deposits, which are abundant in the territory of Siberia and the Far East, are many times more substantial than the 'classical' (sedimentary-metamorphic) form of icing, considering their number, dimensions and the current morholithogenetical importance. The more contrasting is the terrain, the more active are neotectonic movements, the lower is the mean annual air temperature, and the higher is the annual percentage of the territory covered by aufeis ice. The aufeis ratio of the permafrost zone, which is determined from parameters of over 10000 ice fields, amounts to 0.66 % (50000 km²). In mountains and tablelands, the total area of aufeis deposits amounts to 40000 km², and the number of ice clusters (0.77 km² in average) exceeds 60000. On the rivers as long as 500 km, the size of aufeis depends on ranks of the streams. In all the natural zones, the majority of gigantic aufeis spots produced by groundwater are located in river valleys of ranks 3 or 4. The area of aufeis deposits of mixed feed, i.e. produced by river water and groundwater, which occupy the entire river channel, yet do not go beyond an ordinary floodplain, amounts to 68000 km², i.e. by a factor of 1.7 larger than the area of all the aufeis deposits (taryns).

2. Due to local groundwater seeping and freezing in layers that accumulate over each other and create large ice clusters on the ground surface, specific conditions of energy- and mass transfer are created in the atmosphere – soil – lithosphere system. In winter, the vertical temperature distribution curve is significantly disrupted due to heat emission from the aufeis layer of water during its freezing, and a thermocline is thus formed. Deformation of the temperature curve is gradually decreasing in size downward the profile and decays at the interface of frozen and thawed rocks. Values and numbers of temperature deviations from a 'normal' value depend on heat reserves of aufeis water and the number of water seeps/discharges at a given location. Upon occurrence of a thermocline, the mode of water freezing and the mechanism of ice saturation of the underlying layers is changed, and double-layered ice-ground complexes (IGC) are formed. IGCs are drastically different from cryogenic deposits in the adjacent segments of the river valley. By specific genetic characteristics and ratios of components in the surface and underground layers, seven types of aufeis IGCs are distinguished as follows: massive-segregation, cement-basal, layered-segregation, basalt-segregation, vacuum-filtration, pressure-injection, and fissure-vein. IGC struc-

tures and properties are variable depending on icing conditions and processes.

3. Annual processes of surface and subsurface icing and ice ablation are accompanied by highly hazardous geodynamic phenomena, such as winter flooding, water freezing, soil heaving, thermokarst and thermal erosion. Combined, these processes lead to a rapid (often unexpected) reconfiguration of the surface and subsurface runoff channels, abrupt uplifting and subsiding of the ground surface, decompaction and 'shaking-up' of seasonally thawing and seasonally freezing rocks, thereby producing exceptionally unfavourable conditions for construction and operation of engineering structures.

Impacts of aufeis deposits and genetically associated cryogenic-geological processes are most actively manifested in the formation and development of the channel network. Five types of cryogenic channelling are distinguished with regard to ratios of thicknesses of crystalline (h_{cr}), aufeis (h_a) and snow (h_{sn}) ice layers, conditions and specific impacts of icing: (1) snow ($h_{sn} > h_{cr} > h_a$), (2) snow-ice ($h_{sn} > h_{cr} < h_a$), (3) aufeis-ice ($h_{sn} < h_{cr} > h_a$), (4) aufeis ($h_{sn} < h_{cr} < h_a$), and (5) glacier ($h_{sn} > 0 < h_a$). The cause-and-consequence relationships concerning the above-mentioned types of channelling are controlled by infill of the runoff channels with ice and the ice thickness, as well as by the degree of discontinuity of permafrost and depths of seasonal freezing and thawing of soil.

4. The impact of aufeis ice on channeling and the underlying rocks is most vivid in the regions with discontinuous and continuous permafrost. The average thickness of the ice cover on rivers ranges from 1.0 to 2.5 m, and its major part (90–95 %) is formed due to discharge and subsequent freezing of river- and groundwater. It is revealed that the intensity of cryogenic channeling depends on aufeis deposits above the autumnal low-water level. If the runoff channel is filled with ice up to the level of high floodplain, channeling of the *ice-aufeis type* takes place, and the river bed is deformed mainly due to thermal erosion and exaration during the spring ice-drift period. The beach scarps, river bars, islands and midstream sandbanks are cut off; chains, bars and scattered structures containing sand, gravel boulders and pebbles are constructed at the river sides; subaqueous furrows and other cryogenic terrain structures are formed; the riverbed is expanded and box-shaped. If ice extends above the level of high floodplain, all the indicators of channeling of the *aufeis type* are observed. This type of channeling is manifested by aufeis glades, i.e. expanded and flattened sections of the river valley, devoid of wood vegetation, with flat terrain and the network of shallow-water branches. The aufeis glades are arranged as a 'string', one after another, on the main water-artery bed and indicate locations of permanent groundwater

sources with large flow rates.

5. It is revealed that the aufeis sections of the river valleys develop by a typical sequence of events due to self-development of the geosystems and transformations under the influence of climate changes and cryo-hydrogeological conditions. In the regions with continuous and discontinuous permafrost, five stages of cryogenic channelling are distinguished: I – pre-glacial development, II – transgression, III – stabilization, IV – regression, and V – post-glacial development. Each stage is characterised by a specific glaciohydrological regime of runoff channels and their specific shapes, sizes and spatial patterns. In the mature aufeis glades, there are sites undergoing various development stages, which gives evidence that aufeis channelling is variable in a wide range in both space and time. The channel network is subject to the maximum transformation in aufeis development stages III and IV, when the transit flow channel is split into several shallow-water branches, producing a complicated plan pattern of the terrain.

With respect to sizes of aufeis glades, river flow capacities and geological, geomorphological, cryo-hydrogeological conditions, the aufeis patterns of the channel network are classified into five types as follows: fan-shaped, cone-shaped, treelike, reticular, and longitudinal-insular. Trends in further development of the river valleys with aufeis deposits can be determined from the structure and the status of their channel networks, and such knowledge is valuable for industrial and economic development of the regions.

6. The cumulative morpholithogenetical effect of aufeis phenomena is expressed by an increment in the channel network as compared to parameters of the river segments located upstream and downstream of the aufeis glade. This indicator is quite well correlated with the main characteristics of the aufeis deposits in the river basins, morphostructural and cryo-hydro-meteorological conditions of the territory under study. In the mountain regions, multiple branches of small and medium-sized rivers, which are formed due to aufeis processes, can be traced for dozens and hundreds of kilometres almost without any gaps; such branches are highly variable in both time and space. The increment in the channel network, ρ_n per one groundwater aufeis deposit is increased, in average, from 3.5 km in mountains in the southern regions of East Siberia to 23 km in the Verkhoyansk-Kolyma mountain system and Chukotka. The value of ρ_n is decreased to 2.2 km in the plains and intermountain depressions of the Baikal rift system where the ice fields are smaller in size. The average increment in the channel network per one groundwater aufeis deposit amounts to 12.2 km, and the total increment in continuous and discontinuous permafrost areas ($F=7.6$ mln km²) is estimated at 690000 km.

7. A combination of impacts of aufeis and icing processes on underlying rocks and the channel network is a specific form of cryogenic morpholithogenesis that is typical of regions with inclement climate and harsh environment. Annual formation and ablation of aufeis deposits provide for development of specific geodynamic processes and phenomena, such as destruction and transformation of vegetation, formation of laminated and lenticular ground ice layers, activation of cryogenic weathering of rocks, soil heaving, formation of ice- and ice-ground barriers, mechanical compaction and cryogenic relocation of alluvial deposits, thermokarst subsidence and caving, thermal erosion and exaration, redistribution of water resources, and melted aufeis runoff. The above-mentioned processes create specific

conditions, in which the riverbeds and river valley bottoms are subject to major changes, leading to variations in their status in the seasonal, perennial and secular cycles of development. The aufeis morpholithogenesis predetermines not only the geometric structure and dynamics of the system of rivers of ranks 1 to 5, but also the composition, structure and properties of alluvial deposits in the vast regions of the permafrost zone. In order to reveal regularities in the formation and development of the aufeis sections of the river valleys, it is required to conduct long-term studies with application of simultaneous aerospace imagery and ground-truth observations to confirm satellite data on the polygons for monitoring and observation of the aufeis phenomena.

14. REFERENCES

- Åkerman J., 1982. Studies on naleidi (icings) in West Spitsbergen. In: Proceedings of the Fourth Canadian Permafrost Conference. National Research Council of Canada, Ottawa, p. 189–202.
- Alekseyev V.R., 1968. Morpholithogenesis of aufeis segments of river valleys. In: Issues of Morpholithogenesis of River Valleys. Publishing House of Transbaikalian Branch, the USSR Geographical Society, Chita, p. 32–36 (in Russian) [Алексеев В.Р. Морфолитогенез наледных участков речных долин // Вопросы морфолитогенеза в речных долинах. Чита: Изд-во Забайкальского филиала Географического общества СССР, 1968. С. 32–36].
- Alekseyev V.R., 1973. Aufeis as a factor of river valley morpholithogenesis. In: Regional geomorphology in Siberia. Irkutsk, p. 89–134 (in Russian) [Алексеев В.Р. Наледи как фактор долинного морфолитогенеза // Региональная геоморфология Сибири. Иркутск, 1973. С. 89–134].
- Alekseyev V.R., 1975. Aufeis of the Lena–Amur Interstream Area. In: Siberian geographical collection, No. 10. Nauka, Novosibirsk, p. 46–127 (in Russian) [Алексеев В.Р. Наледи Лено-Амурского междуречья // Сибирский географический сборник. № 10. Новосибирск: Наука, 1975. С. 46–127].
- Alekseyev V.R., 1976. Aufeis of the Sayan–Baikal upland. *Notes of the Transbaikalian branch of the Geographical Society of the USSR* 101, 22–87 (in Russian) [Алексеев В.Р. Наледи Саяно-Байкальского нагорья // Записки Забайкальского филиала Географического общества СССР. 1976. Вып. 101. С. 22–87].
- Alekseyev V.R., 1989. Paragenesis of aufeis and subsurface ice. *Materials of Glaciology Studies* 65, 81–86 (in Russian) [Алексеев В.Р. Парагенез наледей и подземных льдов // Материалы гляциологических исследований. 1989. Вып. 65. С. 81–86].
- Alekseyev V.R., 1997. Specific morphodynamic features of aufeis sections of river valleys. In: Hydrology and geomorphology of river systems. Proceedings and abstracts of the scientific conference. Irkutsk, p. 207–208 (in Russian) [Алексеев В.Р. Морфодинамические особенности наледных участков речных долин // Гидрология и геоморфология речных систем. Материалы и тезисы научной конференции. Иркутск, 1997. С. 207–208].
- Alekseyev V.R., 2005. Landscape Indication of Aufeis Phenomena. Siberian Branch of Nauka Publishing House, Novosibirsk, 364 p. (in Russian) [Алексеев В.Р. Ландшафтная индикация наледных явлений. Новосибирск: Наука. Сиб. отд., 2005. 364 с.].
- Alekseyev V.R., 2007. Aufeis Studies. Glossary. Siberian Branch of Nauka Publishing House, Novosibirsk, 434 p. (in Russian) [Алексеев В.Р. Наледеведение. Словарь-справочник. Новосибирск: Наука. Сиб. отд., 2007. 434 с.].
- Alekseyev V.R., 2013. Impact of aufeis on development of the channel network (aufeis channelling). *Lyd i Sneg (Ice and Snow)* (4) 95–106 (in Russian) [Алексеев В.Р. Влияние наледей на развитие русловой сети (наледный руслогенез) // Лед и снег. 2013. № 4. С. 95–106].
- Alekseyev V.R., Boyarintsev E.L., Dovbysh V.N., 2012. Long-term dynamics of dimensions of the Amangynda aufeis in conditions of climate changes. In: Current problems of stochastic hydrology and runoff regulation. Proceedings of the All-Russia scientific conference devoted to the memory of A.V. Rozhdestvensky, outstanding hydrology researcher, 10–12 April 2012. Moscow, p. 298–305 (in Russian) [Алексеев В.Р., Бояринцев Е.Л., Добыш В.Н. Многолетняя динамика размеров Амангындинской наледи в условиях изменений климата // Современные проблемы стохастической гидрологии и регулирования стока: Труды Всероссийской научной конференции, посвященной памяти выдающегося ученого-гидролога А.В. Рождественского. Москва, 10–12 апреля 2012 г. М., 2012. С. 298–305].
- Alekseyev V.R., Furman M.Sh., 1976. Aufeis and Runoff. Nauka, Novosibirsk, 118 p. (in Russian) [Алексеев В.Р., Фурман М.Ш. Наледи и сток. Новосибирск: Наука, 1976. 118 с.].

- Alekseyev V.R., Gienko A.Ya., 2002. Aufeis of the Putorana Plato. Publishing House of the Institute of Geography, SB RAS, Irkutsk, 101 p (in Russian) [Алексеев В.Р., Гиенко А.Я. Наледи плато Путорана. Иркутск: ИГ СО РАН, 2002. 101 с.].
- Alekseyev V.R., Gorin V.V., Kotov S.V., 2011. Taryn aufeis in the Northern Chukotka. *Lyd i Sneg (Ice and Snow)* (4) 85–93 (in Russian) [Алексеев В.Р., Горин В.В., Котов С.В. Наледи-тарыны Северной Чукотки // *Лед и снег*. 2011. № 4. С. 85–93].
- Alekseyev V.R., Kirichenko A.V., 1997. Estimation of aufeis at the Kodar and Udokan ridges by the landscape indication method. *Materials of Glaciology Studies* 82, 58–63 (in Russian) [Алексеев В.Р., Кириченко А.В. Оценка наледности хребтов Кодар и Удокан методом ландшафтной индикации // *Материалы гляциологических исследований*. 1997. Вып. 82. С. 58–63].
- Alekseyev V.R., Kovalchuk O.A., 2004. Aufeis and river-bed ice reserves in mountains in Siberia. In: Rational use and protection of water resources in changing environment. Publishing House of Yerevan State University, Yerevan, vol. 2, p. 38–42. (in Russian) [Алексеев В.Р., Ковальчук О.А. Наледи и русловые запасы льда в горах Сибири // *Рациональное использование и охрана водных ресурсов в изменяющейся окружающей среде*. Ереван: Изд-во Ереванского гос. ун-та, 2004. Т. 2. С. 38–42].
- Baranowski S., 1982. Naled ice in front of some Spitsbergen glaciers. *Journal of Glaciology* 28 (98), 211–214.
- Belokon' P.N., 1950. Engineering Hydraulic Flow Controls under Ice Cover. Gosenergoizdat, Moscow–Leningrad, 160 p. (in Russian) [Белоконь П.Н. Инженерная гидравлика потока под ледяным покровом. М.–Л.: Госэнергоиздат, 1950. 160 с.].
- Berkin N.S., 1964. About aufeis in mountain areas in Pribaikalie. In: Materials on permafrost in Siberia and the Far East. Irkutsk–Moscow, p. 86–92 (in Russian) [Беркин Н.С. О наледях в горной области Прибайкалья // *Материалы по мерзлотоведению Сибири и Дальнего Востока*. Иркутск–Москва, 1964. С. 86–92].
- Bilibin Yu.A., 1963. Foundations of Placer Geology. Publishing House of the USSR Acad. Sci., Moscow, 463 p. (in Russian) [Билибин Ю.А. Основы геологии россыпей. М.: Изд-во АН СССР, 1963. 463 с.].
- Boitsov A.V., 1979. About specific features of development of perennial permafrost and groundwater-produced aufeis in the Iengra river basin at the route of the Baikal–Amur Railroad. In: Regional and geocryological studies in Siberia. Permafrost Institute SB RAS, Yakutsk, p. 98–107 (in Russian) [Бойцов А.В. Об особенностях развития многолетнемерзлых пород и наледей подземных вод в бассейне р. Иенгры (трасса БАМ) // *Региональные и геокриологические исследования в Сибири*. Якутск: ИМЗ СО РАН, 1979. С. 98–107].
- Carey K.L., 1973. Icings Developed from Surface Water and Ground Water. Corps of Engineers. U. S. Army, Cold Regions Research and Engineering Laboratory, Hanover, New Hampshire, 67 p.
- Catalogue of Aufeis in the Baikal–Amur Railroad Zone, 1980. Issue 1. Aufeis in the Upper Part of the Chara River Basin. Gidrometeoizdat, Leningrad, 63 p. (in Russian) [Каталог наледей зоны БАМ. Вып. 1. Наледи верхней части бассейна р. Чары. Л.: Гидрометеоиздат, 1980. 63 с.].
- Catalogue of Aufeis in the Baikal–Amur Railroad Zone, 1981. Issue 2. Aufeis in the Muya River Basin. Gidrometeoizdat, Leningrad, 84 p. (in Russian) [Каталог наледей зоны БАМ. Вып. 2. Наледи бассейна р. Муи. Л.: Гидрометеоиздат, 1981. 84 с.].
- Catalogue of Aufeis in the Baikal–Amur Railroad Zone, 1982. Issue 3. Aufeis in the Upper Angara River Basin. Gidrometeoizdat, Leningrad. 96 p. (in Russian) [Каталог наледей зоны БАМ. Вып. 3. Наледи бассейна р. Верхней Ангары. Л.: Гидрометеоиздат, 1982. 96 с.].
- Chekotillo A.M., Tsvid A.A., Makarov V.N., 1960. Aufeis in the USSR Territory and Aufeis Mitigation Actions. Amur Publishing House, Blagoveshchensk, 207 p. (in Russian) [Чекотилло А.М., Цвид А.А., Макаров В.Н. Наледи на территории СССР и борьба с ними. Благовещенск: Амурское кн. изд-во, 1960. 207 с.].
- Chernyavskaya K.A., 1973. Specific features of aufeis distribution in the central part of the Olyakma–Vitim mountainous region. In: The 2nd International Permafrost Conference. Reports. Issue 5. Underground water of cryolithosphere. Book Publishing House, Yakutsk, p. 74–81 (in Russian) [Чернявская К.А. Особенности распространения наледей в центральной части Олекмо-Витимской горной страны // *Вторая международная конференция по мерзлотоведению. Доклады и сообщения*. Вып. 5. Подземные воды криолитосферы. Якутск: Кн. изд-во, 1973. С. 74–81].
- Clark I., Lauriol B., 1997. Aufeis of the Firth River basin, northern Yukon, Canada: Insights into permafrost hydrogeology and karst. *Arctic and Alpine Research* 29 (2), 240–252. <http://www.jstor.org/stable/1552053>.
- Deikin B.N., 1985. Research methods and estimations of characteristics of injection ice in icing river valleys. In: *Glaciological Studies in Siberia*. Institute of Geography SB RAS, Irkutsk, p. 146–158 (in Russian) [Дейкин Б.Н. Методика исследования и расчет характеристик инъекционных льдов на наледных участках речных долин // *Гляциологические исследования в Сибири*. Иркутск: Институт географии СО РАН, 1985. С. 146–158].
- Deikin B.N., Abakumenko A.E., 1986. Development of underground water icing in the central part of the Baikal–Amur Railroad zone (according to aerial and space images). In: Remote studies of natural resources of Siberia. Nauka, Novosibirsk, p. 86–94 (in Russian) [Дейкин Б.Н., Абакуменко А.Е. Распространение наледей подземных вод в центральной части зоны БАМА (по материалам аэрокосмического фотографирования) // *Дистанционные исследования природных ресурсов Сибири*. Новосибирск: Наука, 1986. С. 86–94].
- Deikin B.N., Markov M.L., 1983. Development of icing in the Kuanda river basin (according to aerial visual surveys) In: *Proceedings of the State Hydrological Institute*. Issue 290. Issues of Hydrology of the Baikal–Amur Railroad Zone.

- Gidrometeoizdat, Leningrad, p. 68–83 (in Russian) [Дейкин Б.Н., Марков М.Л. Распространение наледей в бассейне р. Куанды (по результатам аэровизуальных обследований) // Труды ГГИ. Вып. 290. Вопросы гидрологии зоны БАМ. Л.: Гидрометеоиздат, 1983. С. 68–83].
- Deikin B.N., Markov M.L., 1985. Estimation of water reserves in icing cover of rivers and aufeis for assessment of underground water resources in the central regions of the Baikal–Amur Railroad zone. In: Glaciological studies in Siberia. Irkutsk, p. 92–101 (in Russian) [Дейкин Б.Н., Марков М.Л. Расчет запасов воды в ледяном покрове рек и наледях для оценки ресурсов подземных вод в центральных районах зоны БАМ // Гляциологические исследования в Сибири. Иркутск, 1985. С. 92–101].
- Derpgolts V.F., 1971. Water in the Universe. Nedra, Leningrad, 224 p. (in Russian) [Дерпгольц В.Ф. Вода во Вселенной. Л.: Недра, 1971. 224 с.].
- Dolgushin L.D., Osipova G.B., 1989. Glaciers. Mysl, Moscow, 447 p. (in Russian) [Долгушин Л.Д., Осипова Г.Б. Ледники. М.: Мысль, 1989. 447 с.].
- Feldman G.M., 1988. Moisture Movements in Thawing and Freezing Soils. Nauka, Novosibirsk, 258 p. (in Russian) [Фельдман Г.М. Передвижение влаги в талых и промерзающих грунтах. Новосибирск: Наука, 1988. 258 с.].
- Feldman G.M., Borozinets V.E., 1983. Possible mechanism of formation of large ice inclusions in dispersed soil. In: Regional geocryological studies in East Asia. Permafrost Institute SB RAS, Yakutsk, p. 19–28 (in Russian) [Фельдман Г.М., Борозинец В.Е. Возможный механизм образования крупных ледяных включений в дисперсных грунтах // Региональные геокриологические исследования в Восточной Азии. Якутск: ИМЗ СО РАН, 1983. С. 19–28].
- Fotiev S.M., 1964. About the role of aufeis in formation of morphology of aufeis fields in river valleys. In: Geocryological conditions of West Siberia, Yakutia and Chukotka. Nauka, Moscow, p. 111–114 (in Russian) [Фотиев С.М. К вопросу о роли наледей в формировании морфологии наледных участков речных долин // Геокриологические условия Западной Сибири, Якутии и Чукотки. М.: Наука, 1964. С. 111–114].
- French H.M., 1976. The Periglacial Environment. Lingman, London and New York, 309 p.
- Froehlich W., Slupik J., 1982. River icings and fluvial activity in extreme continental climate: Khangai Mountains, Mongolia. In: Proceedings of the Fourth Canadian Permafrost Conference. National Research Council of Canada, Ottawa, p. 203–211.
- Gasanov Sh.Sh., 1966. Injection ice (structure, mechanism of formation, and regularities of patterns). In: Proceedings of the 8th All–Russia Joint Meeting on Geocryology. Permafrost Studies. Issue 2. General, Theoretical and Historical Geocryology. Permafrost Institute SB RAS, Yakutsk, p. 139–153 (in Russian) [Гасанов Ш.Ш. Инъекционные льды (строение, механизм образования и закономерности распространения) // Материалы VIII Всесоюзного межведомственного совещания по геокриологии (мерзлотоведению). Вып. 2. Общая, теоретическая и историческая геокриология. Якутск: ИМЗ СО РАН, 1966. С. 139–153].
- Gorbunov A.P., Ermolin E.D., 1981. Relief-forming role of icing in Tien Shan and Pamir. In: Icing in Siberia and the Far East. Nauka, Novosibirsk, p. 160–166 (in Russian) [Горбунов А.П., Ермолин Е.Д. Рельефообразующая роль наледей Тянь-Шаня и Памира // Наледи Сибири и Дальнего Востока. Новосибирск: Наука, 1981. С. 160–166].
- Gorelik Ya.B., Kolunin V.S., 2002. Physical Modelling of Cryogenic Processes in Lithosphere. GEO Branch, Publishing House of SB RAS, Novosibirsk, 317 p. (in Russian) [Горелик Я.Б., Колунин В.С. Физика моделирования криогенных процессов в литосфере. Новосибирск: Изд-во СО РАН, Филиал «Гео», 2002. 317 с.].
- Grigoriev A.A., 1966. Regularities of Structure and Development of Geophysical Medium. Selected Theoretical Works. Publishing House of the USSR Acad. Sci., Moscow, 300 p. (in Russian) [Григорьев А.А. Закономерности строения и развития географической среды. Избранные теоретические работы. М.: Изд-во АН СССР, 1966. 300 с.].
- Harden D., Barnes P., Reimnitz E., 1977. Distribution and character of icings in northeastern Alaska. *Arctic* 30 (1), 28–40. <http://dx.doi.org/10.14430/arctic2681>.
- Heldmann J.L., Pollard W.H., McKay C.P., Andersen D.T., Toon O.B., 2005. Annual development cycle and associated perennial spring activity on Axel Heiberg Island, Canadian High Arctic. *Arctic, Antarctic, and Alpine Research* 37 (1), 127–135. [http://dx.doi.org/10.1657/1523-0430\(2005\)037\[0127:ADCOAI\]2.0.CO;2](http://dx.doi.org/10.1657/1523-0430(2005)037[0127:ADCOAI]2.0.CO;2).
- Hu X., Pollard W., 1997. The hydrologic analysis and modeling of river icing growth, North Fork Pass, Yukon Territory, Canada. *Permafrost and Periglacial Processes* 8 (3), 279–294. [http://dx.doi.org/10.1002/\(SICI\)1099-1530\(199709\)8:3<279::AID-PPP260>3.0.CO;2-7](http://dx.doi.org/10.1002/(SICI)1099-1530(199709)8:3<279::AID-PPP260>3.0.CO;2-7).
- Kazakov A.P., 1976. Studies of icing on motor roads in Siberia. *Notes of the Transbaikalian branch of the Geographical Society of the USSR* 101, 124–151 (in Russian) [Казиков А.П. Исследование наледей на автомобильных дорогах Сибири // Записки Забайкальского филиала Географического общества СССР. 1976. Вып. 101. С. 124–151].
- Klimovskiy I.V., 1978. Aufeis and injection ice in the Buordakh river valley (Ulakhan–Chistai ridge). In: Geocryological and hydrogeological studies in Yakutia. Permafrost Institute SB RAS, Yakutsk, p. 118–125 (in Russian) [Климовский И.В. Наледи и инъекционные льды долины р. Буордах (хр. Улахан–Чистай) // Геокриологические и гидрогеологические исследования в Якутии. Якутск: ИМЗ СО РАН, 1978. С. 118–125].
- Koloskov K.N., Koreisha M.M., 1975. Aufeis at the northern slope of the Momsy ridge. In: PNIIS Proceedings. Issue 36. Geocryological studies during engineering surveys. Stroizdat, Moscow, p. 124–134 (in Russian) [Колосков К.Н.,

- Корейша М.М.* Наледи северного склона Момского хребта // Труды ПНИИИС. Вып. 36. Геокриологические исследования при инженерных изысканиях. М.: Стройиздат, 1975. С. 124–134].
- Kolosov D.M.*, 1938. About aufeis phenomena as the geomorphological process. In: Problems of physical geography, vol. VI, Publishing House of the USSR Acad. Sci., Moscow, p. 125–134 (in Russian) [*Колосов Д.М.* О наледных явлениях как геоморфологическом процессе // Проблемы физической географии. М.: Изд-во АН СССР, 1938. Т. VI. С. 125–134].
- Kolotaev V.N.*, 1980. Formation of large underground water aufeis (case of the Mururinskaya aufeis). In: Issues of land hydrogeology. Reports at the conference of young researchers and specialists. Gidrometeoizdat, Leningrad, p. 37–45 (in Russian) [*Колотаев В.Н.* Процесс формирования крупных наледей подземных вод (на примере Муруринской наледи) // Вопросы гидрологии суши: Доклады конференции молодых ученых и специалистов. Л.: Гидрометеоздат, 1980. С. 37–45].
- Koreisha M.M.*, 1969. Formation of injection ice in channel deposits in aufeis areas in river valleys at the Suntar-Khayata ridge. In: Proceedings of the scientific research conference, April 1969. PNIIS, Moscow, p. 121–123 (in Russian) [*Корейша М.М.* Формирование инъекционного льда в русловых отложениях наледных участков долин рек хр. Сунтар-Хаята // Материалы научно-технической конференции, Апрель 1969. М.: ПНИИИС, 1969. С. 121–123].
- Koroleva N.A.*, 2011. Cryolitic Ecological Mapping of the Cryolitic Zone in Russia. Synopsis of the thesis for Candidate of Geology and Mineralogy degree. Geographic Faculty, Moscow State University, Moscow, 24 p. (in Russian) [*Королева Н.А.* Мерзлотно-экологическое картографирование криолитозоны России: Автореф. дис. ... канд. геогр. наук. М.: МГУ, геогр. ф-т, 2011. 24 с.].
- Kravchenko V.V.*, 1983. Hydrothermal movement of soil under aufeis. In: Glaciology of East Siberia. Irkutsk, p. 53–64 (in Russian) [*Кравченко В.В.* Гидротермические движения грунтов под наледными массивами // Гляциология Восточной Сибири. Иркутск, 1983. С. 53–64].
- Kravchenko V.V.*, 1985a. Regularities of formation and distribution of aufeis at rivers in the southern regions of East Siberia. In: Glaciological Studies in Siberia. Institute of Geography SB RAS, Irkutsk, p. 19–38 (in Russian) [*Кравченко В.В.* Закономерности формирования и распространение наледей на реках юга Восточной Сибири // Гляциологические исследования в Сибири. Иркутск: ИГ СО РАН, 1985. С. 19–38].
- Kravchenko V.V.*, 1985b. Studies of hydrothermal movement of soil under aufeis at freezing rivers. In: Geocryological forecast for construction. Moscow, p. 86–88 (in Russian) [*Кравченко В.В.* Изучение гидротермических движений грунтов под наледями на замерзающих реках // Геокриологический прогноз при строительстве освоении местности. М., 1985. С. 86–88].
- Krendelev F.P.*, 1983. Varchans and aufeis moulds in the Chara basin. *Priroda* (2), 58–66. (in Russian) [*Кренделев Ф.П.* Барханы и ледяные бугры Чарской котловины // *Природа*. 1983. № 2. С. 58–66].
- Lebedev V.M.*, 1969. Monitoring of aufeis in the Anmangynda river basin. In: Magadan GMO collection of works. Kolytma UGMS, Magadan, Issue 2, p. 122–137 (in Russian) [*Лебедев В.М.* Стационарные наблюдения за наледью в бассейне реки Анмангында // Сборник работ Магаданской ГМО. Магадан: Колымское УГМС, 1969. Вып. 2. С. 122–137].
- Oberman N.G.*, 1985. Aufeis component of underground water discharge in the Transpolar, Polar and Subpolar Ural. In: Cryohydrogeological studies. Permafrost Institute SB RAS, Yakutsk, p. 15–23 (in Russian) [*Оберман Н.Г.* Наледная составляющая подземного стока на Заполярном, Полярном и Приполярном Урале // Криогидрогеологические исследования. Якутск: ИМЗ СО АН СССР, 1985. С. 15–23].
- Oberman N.G.*, 1989. Some features of the relationship between underground water and river water in the aufeis belt of Ural. In: Permafrost hydrogeological studies in the zone of free water exchange. Nauka, Moscow, p. 64–73 (in Russian) [*Оберман Н.Г.* Некоторые черты взаимосвязи подземных и речных вод наледного пояса Урала // Мерзлотно-гидрогеологические исследования зоны свободного водообмена. М.: Наука, 1989. С. 64–73].
- Olszewski A.*, 1982. Icings and geomorphological significance exemplified from Oscar II Land and Prins Karls Forland. *Acta Universitatis Nicolai Copernici. Geographia XVI. Nauki Matematyczno-Przyrodnicze. Zeszyt 51*, p. 91–122.
- Petrov V.G.*, 1930. Aufeis at the Amur-Yakutia Highway. The USSR Acad. Sci. Publishing House and Motor Road Research Institute of the USSR NKPS, 177 p. (in Russian) [*Петров В.Г.* Наледи на Амуро-Якутской магистрали. Л.: Изд-во АН СССР и научно-исследовательского автодорожного института НКПС СССР, 1930. 177 с.].
- Piguzova V.M., Shepelev V.V.*, 1972. Regime of aufeis-generating sources of Central Yakutia. In: Geocryological and hydrogeological studies in Siberia. Permafrost Institute SB RAS, Yakutsk, p. 177–186 (in Russian) [*Пигузова В.М., Шепелев В.В.* Режим наледобразующих источников Центральной Якутии // Геокриологические и гидрогеологические исследования Сибири. Якутск: ИМЗ СО АН СССР, 1972. С. 177–186].
- Piguzova V.M., Shepelev V.V.*, 1975. Aufeis Study Method. Permafrost Institute SB RAS, Yakutsk, 62 p. (in Russian) [*Пигузова В.М., Шепелев В.В.* Методика изучения наледей. Якутск: ИМЗ СО АН СССР, 1975. 62 с.].
- Podyakovon S.A.*, 1903. Aufeis in East Siberia and its causes. *Izvestiya Russkogo Geograficheskogo Obshchestva (Proceedings of the Russian Geographical Society)* XXXIX, 305–337 (in Russian) [*Подъяконов С.А.* Наледи Восточной Сибири и причины их возникновения // *Известия Русского географического общества*. 1903. Т. XXXIX. С. 305–337].

- Pollard W.H, Franch H.M. 1983. Seasonal frost mound occurrence North Fork Pass, Ogilvie Mountains, Northern Yukon, Canada. In: Permafrost. Proceedings of the Fourth International Conference on Permafrost, July 17–22, 1983, Fairbanks, Alaska. National Academy Press, Washington, DC, p. 1000–1004.
- Preobrazhensky V.S., 1961. Barchans and hydroloccaliths in the Chara basin. *Priroda* (5), 93–95 (in Russian) [Преображенский В.С. Барханы и гидролакколиты Чарской котловины // Природа. 1961. № 5. С. 93–95].
- Priesnitz K., Schunke E., 2002. The fluvial morphodynamics of two small permafrost drainage basins, northwestern Canada. *Permafrost and Periglacial Processes* 13 (3), 207–217. <http://dx.doi.org/10.1002/ppp.424>.
- Prokacheva B.G., Snishchenko D.V., Usachev V.F., 1982. Remote Methods in Hydrogeological Studies of the Baikal–Amur Railroad Zone. Guidebook. Gidrometeoizdat, Leningrad, 224 p. (in Russian) [Прокачева Б.Г., Снущенко Д.В., Усачев В.Ф. Дистанционные методы гидрологического изучения зоны БАМа. Справочно-методическое пособие. Л.: Гидрометеоиздат, 1982. 224 с.].
- Revyakin V.S., 1981. Natural Ice in the Altai-Sayan Mountain Region. Gidrometeoizdat, Leningrad, 288 p. (in Russian) [Ревякин В.С. Природные льды Алтае-Саянской горной области. Л.: Гидрометеоиздат, 1981. 288 с.].
- Romanovsky N.N., 1972. About the impact of aufeis on formation of the landscape in pra-valleys in Poland under periglacial conditions of the Pleistocene icing. *Izvestiya AN SSSR. Seriya geograficheskaya* (4), 54–60 (in Russian) [Романовский Н.Н. О влиянии наледей на формирование рельефа прадолин Польши в перигляциальных условиях плейстоценового оледенения // Известия АН СССР. Серия географическая. 1972. № 4. С. 54–60].
- Romanovsky N.N., 1973. About geological activity of aufeis. In: Permafrost studies. Publishing House of the Moscow University, Moscow, Issue XIII, p. 66–89 (in Russian) [Романовский Н.Н. О геологической деятельности наледей // Мерзлотные исследования. М.: Изд-во Моск. ун-та, 1973. Вып. XIII. С. 66–89].
- Romanovsky N.N., 1974. Nalodzie jako zjawisko peryglacialne. *Czas. Geogr.* 45 (4), 473–484.
- Romanovsky N.N., 1983. Underground Water in Permafrost Zones. Publishing House of the Moscow University, Moscow, 231 p. (in Russian) [Романовский Н.Н. Подземные воды криолитозоны. М.: Изд-во Моск. ун-та, 1983. 231 с.].
- Romanovsky N.N., 1993. Fundamentals of Lithosphere Cryogenesis. Publishing House of the Moscow University, Moscow, 336 p. (in Russian) [Романовский Н.Н. Основы криогенеза литосферы. М.: Изд-во Моск. ун-та, 1993. 336 с.].
- Romanovsky N.N., 1997. Icing formation and topography in the valleys of the east Siberian mountains. In: Abstracts of the 4th International Conference on Geomorphology, Bologna, 28 Aug. – 3 Sept., vol. 1. Bologna, p. 332.
- Romanovsky N.N., Afanasenko V.E., Koreisha M.M., 1973. Dynamics and geological activity of gigantic aufeis in the Selenyakh tectonic basin. *Bulletin of the Moscow State University. Geology* (6), 52–74 (in Russian) [Романовский Н.Н., Афанасенко В.Е., Корейша М.М. Динамика и геологическая деятельность гигантских наледей Селеняхской тектонической впадины // Вестник Московского государственного университета. Геология. 1973. № 6. С. 52–74].
- Romanovsky N.N., Afanasenko V.E., Koreisha M.M., 1978. Long-term dynamics of underground water aufeis. In: Proceedings of the 3rd International Conference on Permafrost, Edmont, 1978. vol. 1. Ottawa, p. 212–218 (in Russian) [Романовский Н.Н., Афанасенко В.Е., Корейша М.М. Многолетняя динамика наледей подземных вод // Proceedings of the 3rd International Conference on Permafrost, Edmont, 1978. Ottawa, 1978. V. 1. P. 212–218].
- Rumyantsev E.A., 1964. Physical climatic conditions and dynamics of formation of the Kerak aufeis at the Transbaikalian railroad. In: Works of Khabarovsk Institute of Railroad Transport Engineers. Issue XVIII. Khabarovsk Publishing House, Khabarovsk, p. 93–120 (in Russian) [Румянцев Е.А. Физико-климатические условия и динамика образования Керакской наледи на Забайкальской железной дороге // Труды ХаБИИЖТа. Хабаровск: Хабаровское кн. изд-во, 1964. Вып. XVIII. С. 93–120].
- Rumyantsev E.A., 1991. Mechanism of aufeis development. In: Aufeis problems. Nauka, Novosibirsk, p. 55–66 (in Russian) [Румянцев Е.А. Механизм развития наледного процесса // Проблемы наледоведения. Новосибирск: Наука, 1991. С. 55–66].
- Rusanov B.S., 1961. Geothermal Movements of the Earth's Surface. Publishing House of the USSR Acad. Sci., Moscow, 226 p. (in Russian) [Русанов Б.С. Гидротермические движения земной поверхности. М.: Изд-во АН СССР, 1961. 226 с.].
- Sannikov S.A., 1988. Studies of injected ice in aufeis glades (Transbaikalie). In: Methods and techniques of geocryological studies. Nauka, Novosibirsk, p. 134–145 (in Russian) [Санников С.А. Изучение инъекционных льдов наледных полей (на примере Забайкалья) // Методика и техника геокриологических исследований. Новосибирск, 1988. С. 134–145].
- Shesternev D.M., Verkhoturrov A.G., 2006. Aufeis in Transbaikalia. Institute of Natural Resources, Ecology and Cryology, SB RAS, Chita, 213 p. (in Russian) [Шестернев Д.М., Верхотуров А.Г. Наледи Забайкалья. Чита: ИПРЭК СО РАН, 2006. 213 с.].
- Shmatkov V.A., Kozlov A.A., 1994. Aufeis in the Northern Priokhotie. *Geografiya i Prirodnye Resursy (Geography and Natural Resources)* (1), 189–192 (in Russian) [Шматков В.А., Козлов А.А. Наледи Северного Приохотья // География и природные ресурсы. 1994. № 1. С. 189–192].

- Shvetsov P.F., Sedov V.P., 1941. Gigantic Aufeis and Underground Water in the Tas-Khayakhtakh ridge. Publishing House of the USSR Acad. Sci., Moscow-Leningrad, 81 p. (in Russian) [Швецов П.Ф., Седов В.П. Гигантские наледы и подземные воды хребта Тас-Хаяхта. М.-Л.: Изд-во АН СССР, 1941. 81 с.].
- Simakov A.S., 1959. About some specific features of taryn development in the north-eastern regions of the USSR and a possible permafrost structure. In: General permafrost studies. Publishing House of the USSR Acad. Sci., Moscow, p. 210-214 (in Russian) [Симаков А.С. О некоторых особенностях развития тарынов на северо-востоке СССР и вероятном строении криолитозоны // Материалы по общему мерзлотоведению. М.: Изд-во АН СССР, 1959. С. 210-214].
- Simakov A.S., 1961. Aufeis in the north-eastern regions of the USSR. In: The 3rd Conference on Underground Water and Engineering Geology of Siberia and the Far East. Abstracts. Issue 2. Engineering Geology and Permafrost Studies. Irkutsk, p. 117-118 (in Russian) [Симаков А.С. Наледеи северо-востока СССР // Третье совещание по подземным водам и инженерной геологии Сибири и Дальнего Востока. Тезисы докладов. Вып. 2. Инженерная геология и мерзлотоведение. Иркутск, 1961. С. 117-118].
- Sloan Ch.E., Zenone C., Mayo L.R., 1976. Icings along the Trans-Alaska Pipeline Route. USGS Professional Paper 979. United States Government Printing Office, Washington, 31 p.
- Sokolov B.L., 1975. Aufeis and River Runoff. Gidrometeoizdat, Leningrad, 190 p. (in Russian) [Соколов Б.Л. Наледеи и речной сток. Л.: Гидрометеоиздат, 1975. 190 с.].
- Strugov A.S., 1955. Explosion of hydrolaccolith (Chita region). *Priroda* (6), 117 (in Russian) [Стругов А.С. Взрыв гидролакколита (Читинская область) // Природа. 1955. № 6. С. 117].
- Tolstikhin O.N., 1974. Aufeis and Underground Water in the North-Eastern Regions of the USSR. Nauka, Novosibirsk, 164 p. (in Russian) [Толстихин О.Н. Наледеи и подземные воды северо-востока СССР. Новосибирск: Наука, 1974. 164 с.].
- Topchiev A.G., 1979. Satellite methods of studies of valley and aufeis in the Chulman area. In: Issues of Geography. Collection III. Geomorphology and Construction. Mysl, Moscow, p. 169-175 (in Russian) [Топчиев А.Г. Космические методы изучения долин и наледей Чульманского района // Вопросы географии. Сб. III. Геоморфология и строительство. М.: Мысль, 1979. С. 169-175].
- Topchiev A.G., Gavrilov A.V., 1981. Satellite methods of studies and mapping of aufeis (South Yakutia). In: Aufeis in Siberia and the Far East. Nauka, Novosibirsk, p. 64-71 (in Russian) [Топчиев А.Г., Гаврилов А.В. Космические методы изучения и картирования наледей (на примере Южной Якутии) // Наледеи Сибири и Дальнего Востока. Новосибирск: Наука, 1981. С. 64-71].
- Tsvid A.A., 1957. Aufeis in Primorie and Anti-Aufeis Actions. Magadan. 86 p. (in Russian) [Цвид А.А. Наледеи в Приморском крае и борьба с ними. Магадан, 1957. 86 с.].
- Tsvid A.A., Khomichuk A.N., 1981. Aufeis in the south-eastern Sikhote Alin. In: Aufeis in Siberia and the Far East. Nauka, Novosibirsk, p. 86-91 (in Russian) [Цвид А.А., Хомичук А.Н. Наледеи на юге-востоке горной страны Сихотэ-Алинь // Наледеи Сибири и Дальнего Востока. Новосибирск: Наука, 1981. С. 86-91].
- Veillette J., Thomas R., 1979. Icings and seepage in frozen glaciofluvial deposits, District of Keewatin, NWT. *Canadian Geotechnical Journal* 16 (4), 789-798. <http://dx.doi.org/10.1139/t79-084>.
- Yoshikawa K., Hinzman L.D., Kane D.L., 2007. Spring and aufeis (icing) hydrology in Brooks Range, Alaska. *Journal of Geophysical Research: Biogeosciences* 112 (G4), G04S43. <http://dx.doi.org/10.1029/2006JG000294>.



Alekseyev, Vladimir R., Doctor of Geography, Professor, Chief Researcher
P.I. Melnikov Permafrost Institute, Siberian Branch of RAS
36 Merzlotnaya street, Yakutsk 677010, Russia
V.B. Sochava Institute of Geography, Siberian Branch of RAS
1 Ulan-Batorskaya street, Irkutsk 664033, Russia
Tel.: (3952)427767; ✉ e-mail: Snow@Irk.ru

Алексеев Владимир Романович, докт. геогр. наук, профессор, г.н.с.
Институт мерзлотоведения им. П.И. Мельникова СО РАН
677010, Якутск, ул. Мерзлотная, 36, Россия
Институт географии им. В.Б. Сочавы СО РАН
664033, Иркутск, ул. Улан-Баторская, 1, Россия
Тел.: (3952)427767; ✉ e-mail: Snow@Irk.ru



THE SEISMICITY MIGRATION STUDY BASED ON SPACE-TIME DIAGRAMMS

E. A. Levina, V. V. Ruzhich

Institute of the Earth's Crust, Siberian Branch of RAS, Irkutsk, Russia

Abstract: Seismicity migration is studied by a new method based on space-time diagrams and a combination of cluster and regression analyses. Data from the global and Baikal regional earthquake catalogues are analysed with the application of the specially designed geographic information system (GIS) in order to establish parameters and mechanisms of seismicity migration in space and time. We study the migration of seismic events in the following geostructural systems: the Baikal rift zone (BRZ), the area between BRZ and the Indo-Eurasian interplate collision zone, the area between BRZ and the West-Pacific seismic foci Benoiff zone, and two segments of the Middle Atlantic ridge.

As evidenced by the obtained results, studying regimes of seismic migration provides for analyses of space-time distribution of seismic energy in the fault-block structure of the lithosphere and facilitates more detailed studies of the origin of deformation waves and mechanisms of the seismotectonic regime of the Earth. Forward (from the equator) and backward (towards the equator) migration of seismic events are established in all the regions under study. It is assumed that this phenomenon may result from regular changes of the polar compression of the Earth due to variations of its rotation regime. Besides, it is revealed that energy clusters of migration are regularly generated, and the regularity may be related to the 11-year cycle of the solar activity which impacts the seismic regime. We discuss the need to study the interference of wave deformations in the lithosphere which are initiated by several external energy sources. It is proposed to consider the regimes of planetary seismicity migration as a reflection of redistribution of endogenic (primarily heat) energy of the Earth during the destruction of its lithospheric shell under the impacts of cosmogenic factors via triggering mechanisms. With reference to our positive experiences of applying the proposed concept to BRZ, we consider possibilities of using the seismicity migration data for prediction of earthquakes in the planetary and regional scales.

Key words: seismicity migration, space-time diagrams, cosmogenic factors, deformation waves, interference of wave deformations, prediction of earthquakes.

Recommended by V.A. Sankov

For citation: Levina E.A., Ruzhich V.V. 2015. The seismicity migration study based on space-time diagrams. *Geodynamics & Tectonophysics* 6 (2), 225–240. doi:10.5800/GT-2015-6-2-0178.

ИЗУЧЕНИЕ МИГРАЦИЙ СЕЙСМИЧЕСКОЙ АКТИВНОСТИ С ПОМОЩЬЮ ПОСТРОЕНИЯ ПРОСТРАНСТВЕННО-ВРЕМЕННЫХ ДИАГРАММ

Е. А. Левина, В. В. Ружич

Институт земной коры СО РАН, Иркутск, Россия

Аннотация: Изучение процессов сейсмомиграции проводилось новым методом построения пространственно-временных диаграмм и посредством сочетания кластерного и регрессионного анализа. С помощью разработанной геоинформационной системы (ГИС) и с использованием всемирного и байкальского регионального каталогов землетрясений решались задачи по выяснению параметров и механизмов пространственно-временной миграции сейсмической активности. Сейсмомиграционные явления изучались в следующих гео-

структурных системах: в пределах Байкальской рифтовой зоны (БРЗ), между БРЗ и областью Индо-Евразийской межплитной коллизии, между БРЗ и Западно-Тихоокеанской сейсмофокальной зоной Бенъофа, а также в двух сегментах Срединно-Атлантического хребта.

На основе анализа полученных результатов показано, что изучение режимов сейсмомиграций позволяет анализировать пространственно-временное перераспределение сейсмической энергии в разломно-блоковой структуре литосферы и, соответственно, более углубленно изучать деформационно-волновую природу и механизмы формирования сеймотектонического режима Земли. Установлено проявление прямых (от экватора) и обратных (к экватору) сейсмомиграций для всех рассмотренных районов. Предполагается, что такое явление может быть объяснено периодическим изменением полярного сжатия Земли за счет вариаций ее ротационного режима. Выявлена также периодичность в режиме генерации энергетических кластеров миграции, что может быть связано с влиянием на сейсмический режим 11-летнего цикла солнечной активности. Обсуждается необходимость изучения интерференции волновых деформаций в литосфере, возбужденных несколькими внешними энергетическими источниками. С этих позиций режимы планетарной сейсмомиграции предлагается рассматривать как отражение перераспределения эндогенной, преимущественно тепловой, энергии нашей планеты в ходе деструкции ее литосферной оболочки под воздействием космогенных факторов через триггерные механизмы. На основе положительного опыта для БРЗ обсуждаются возможности применения полученных сведений о сейсмомиграции для прогноза землетрясений в планетарном и региональном масштабе.

Ключевые слова: сейсмомиграция, пространственно-временные диаграммы, космогенные факторы, деформационные волны, интерференция волновых деформаций, прогноз землетрясений.

1. INTRODUCTION

Earthquake migration, that was first recognized in the middle of the 20th century, has been revealed in all the seismic belts of the Earth [Mogi, 1968; Ruzhich et al., 1989; Ruzhich, Levina, 2012; Vikulin et al., 2000; Chery et al., 2001; Bykov, 2005; Liu et al., 2010; Levina, Ruzhich, 2010; Levina, 2011; Vikulin et al., 2012; Sherman, 2013, 2014; Novopashina, 2013; Novopashnina, San'kov, 2015; Dolgaya, Vikulin, 2015]. The term of 'earthquake migration', however, has not been unanimously accepted due to the fact that earthquake foci and epicentres do not actually migrate but occur in the inter-block medium and are manifested in implicit patterns and trends in space and time. In some publications, parameters of seismic migration were estimated from data on rare separate epicentres of strong earthquakes, while the analysed data ranges were small and not representative statistically. Some studies were focused on sequences of the occurrence of earthquake epicentres along fault zones of various scales, including interplate ones, and considered trends in the distribution of earthquake epicentres in the lithosphere blocks in space and time. In our opinion, among the synonyms, the term of 'seismicity migration' seems preferable for describing space-time patterns and statistically significant trends in the distribution of seismic events that occur between the hierarchically regular blocks of the lithosphere.

The phenomenon of 'seismicity migration' is typically characterized by two parameters, direction and velocity. In our previous publications [Levina, Ruzhich, 2010; Levina, 2011; Ruzhich, Levina, 2012], it was shown that estimations of the velocity of earthquake

foci migration can differ significantly depending on grouping of seismic events by their energy levels. Moreover, due to the lack of a uniform approach to studies of seismic migration, an adequate comparison of published regional data and estimations is impossible, and geodynamic conditions causing the seismicity migration phenomena during the destruction of the lithosphere cannot be reliably clarified.

Since 2009, we have been developing our method that refers to total amounts of seismic energy released by earthquakes, instead of data on separate earthquake epicentres of various energy levels. A total amount of released seismic energy is calculated for a selected area in appropriate space and time windows [Levina, Ruzhich, 2010; Levina, 2011; Ruzhich, Levina, 2012]. Our approach is sufficiently formalized and can be applied to studies and analyses of seismicity of the entire Earth or separate regions, pending the availability of earthquake catalogues containing records of coordinates, time and energy of each seismic event.

2. DESCRIPTION OF THE METHOD

In order to study seismicity migration within the Baikal rift zone (BRZ) and the Baikal-Himalayan region, we use data from the BRZ Earthquake Catalogue published by the Baikal Branch of the Geophysical Centre, Siberian Branch of RAS (Irkutsk, Russia). The catalogue contains records from 1963 to 2014. We also use data on earthquakes ($M \geq 3.5$) from the world catalogue published by the Northern California Earthquake Data Center (USA) [Northern California Earthquake..., 2015].

In order to study the seismic process, we analyse

coordinates, time and energy levels of seismic events and actually deal with the following equation containing three variables:

$$E = f(\varphi, \lambda, t),$$

where E is seismic energy, φ is latitude, λ is longitude, and t is time. It is a complicated task to visualise and study the function of the three variables as its diagram needs to be a 4D curve; therefore, we apply the dimension reduction method [Popov, 2013] as described below. For the region under study, a belt-shaped area is selected with specified coordinates of datum points and a specified width. The band is split into rectangular segments which sides are perpendicular to the central line. The length of such a segment is equal to that of the specified spatial window (Fig. 1). For each segment, we estimate total amounts of the seismic energy released within specified time windows. The space-time matrix is established, and the above-mentioned function is transformed as follows:

$$E = f(r, t),$$

where r is distance from the datum point at the central line of the selected band. This exercise provides for presenting the two spatial coordinates, φ and λ by one value, r . It becomes possible to make a function containing two variables and construct its 3D surface. For further analyses, a cross-section of the studied surface by plane $K=Ks$ and its projection to the space-time plane are constructed (Fig. 2). Values of Ks are selected with regard to specific features of the seismic regime of the region under study and aims of the study. In further data processing, differences in energy classes of individual cells are not taken into account, while each cell is considered as a point on the space-time plane. As a result, the function is transformed as follows:

$$T = f(r),$$

where T is time, and r is distance from the estimation start point.

To clarify a method for analyses of the obtained diagrams, we compile a test catalogue of 12 restraint events. Maps and diagrams constructed on the basis of the test catalogue are given in Fig. 3. Two tests use data on the same events but in different sequences. In the first test (left top map), restraint events 'migrate', i.e. propagate in time in the following sequence: from SW to NE (red dots), then backward, to SW (green dots), and again to NE (purple dots). The corresponding diagram is shown next to the map. In the second test (right bottom map), the events migrate from NE to SW (purple dots) and then backward, to NE (green

dots) and again to SW (red dots). The corresponding diagram is shown next to the map. The diagrams show that the migration of the events in time along the specified line correspond to diagonal chains of dots in the diagrams. It is noted that if the events migrate away from the datum point, the chains are inclined to the right, and if the events migrate toward the datum point, the chains are inclined to the left. The inclination to the left, which is often recorded in the latter case, means the backward seismicity migration. This phenomenon is demonstrated in BRZ (Fig. 2). Generally, researchers pay little or no attention to the backward seismicity migration.

For further studies of the obtained diagrams, we combine methods of cluster and regression analyses. The cluster analysis deals with sets (n) of objects, and each of such objects is characterized by measurements (k). Clustering is the task of grouping a set of objects in such a way that objects in the same group (called a 'cluster') are more similar (in some sense or another) to each other than to those in other groups (clusters) [Zagoruiko, 1999]. In the past 10–15 years, thanks to the development of IT technologies, cluster analysis was widely used to address the need to process larger and larger data sets.

Typically, input data are presented as clustering algorithms. We use a modification of the non-hierarchical clustering method that is often called 'k-mean values method' [StatSoft..., 2015]. In our study, clusters are identified by grouping elements of the diagram around diagonal chains of the elements which are visually identified, and then specific elements are added into one cluster or another with respect to their proximity to the initial chain. The proximity is defined as a Euclidean distance from the given point to the straight line constructed across the initial chain and calculated from the equation. Values of distances, which determine whether the point is a member of a specified cluster, are fixed for each diagram with regard to the study aims and actual ranges of values. The difference between this method and the conventional k-mean method is that as the centre of the cluster is considered to be the line, instead of the point. By applying the algorithm, three clusters are identified in the diagram (Fig. 4). A linear regression is constructed for the set of points in the given cluster: $Y=aX+b$, where X is distance (km), Y is time (year), and a and b are coefficients.

3. RESULTS

The regression analysis results for BRZ are shown in Table 1.

The first column of the table gives a list of clusters (from the earliest one) identified in the diagram. The second and third columns show coefficients of the

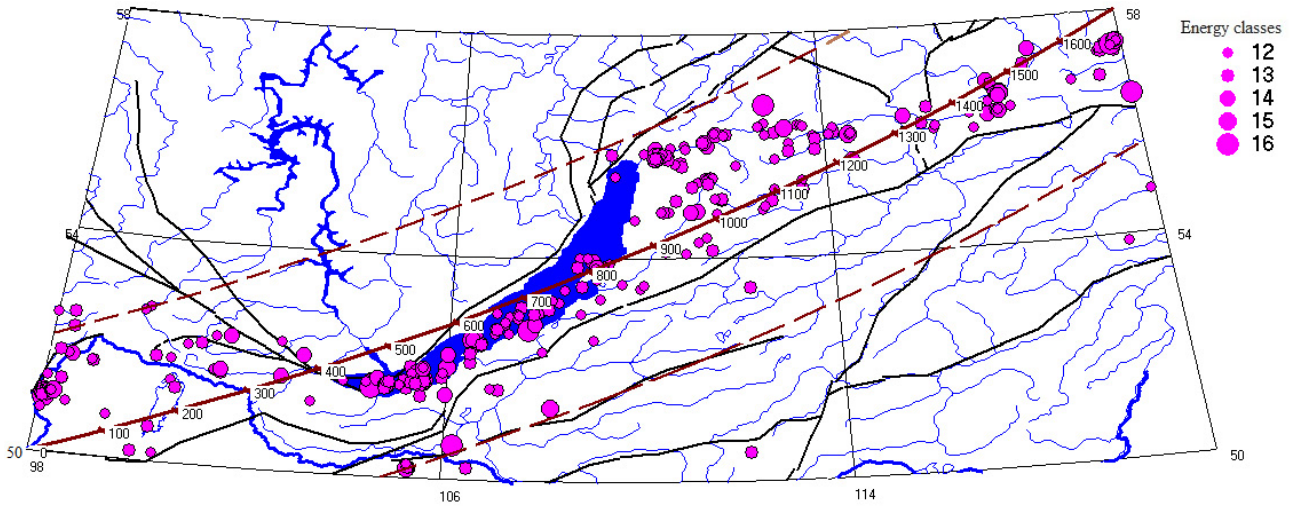


Fig. 1. In the map, the solid graduated line shows the central line of the zone under study; distances are shown in kilometres from the datum point; dotted lines show boundaries of the studied epicentral field. To consolidate the earthquake data for the period from 1963 to 2005 ($K=12-17$), the BRZ territory was divided into rows of rectangles, and the total energy amount released by the earthquakes was calculated.

Рис. 1. На карте сплошной линией показана центральная ось рассматриваемой зоны с нанесенными на нее делениями и указанием расстояния в километрах при удалении от начальной точки, пунктиром отмечены границы изучаемого эпицентрального поля. Данные о землетрясениях в БРЗ за период 1963–2005 гг. ($K=12-17$) собирались путем разделения территории на ряды прямоугольников и подсчета выделившейся суммарной энергии землетрясений.

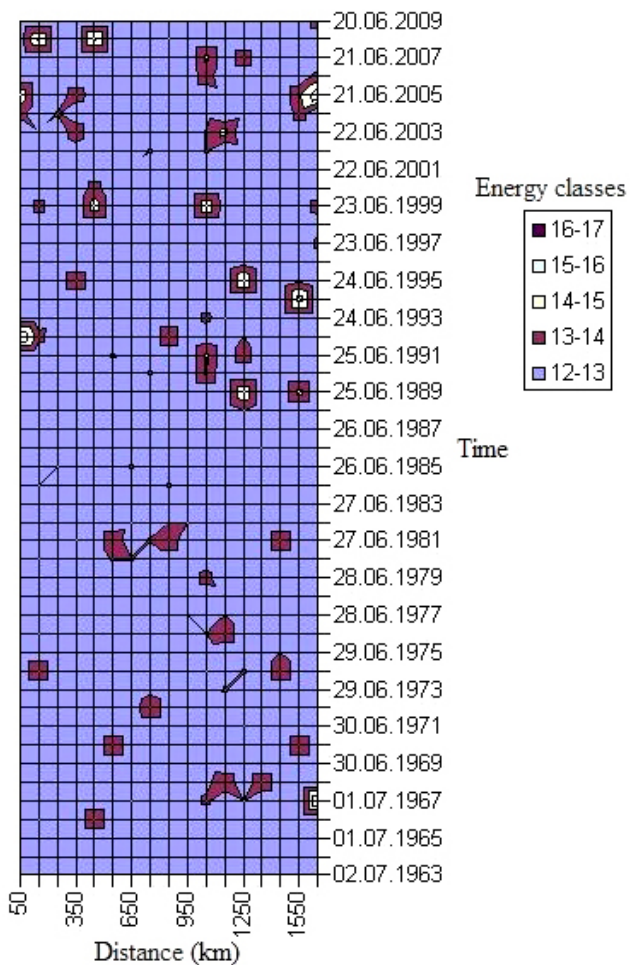


Fig. 2. Space-time diagram for seismic events ($K>8$) in the entire BRZ. The general blue background of the diagram is a cutting plane ($K=12$); other colours show maximums of seismic energy in excess of this value.

Рис. 2. Пространственно-временная диаграмма событий с $K>8$ для всей БРЗ. Общий синий фон диаграммы – это секущая плоскость ($K=12$), другими цветами показаны максимумы сейсмической энергии, превышающие это значение.

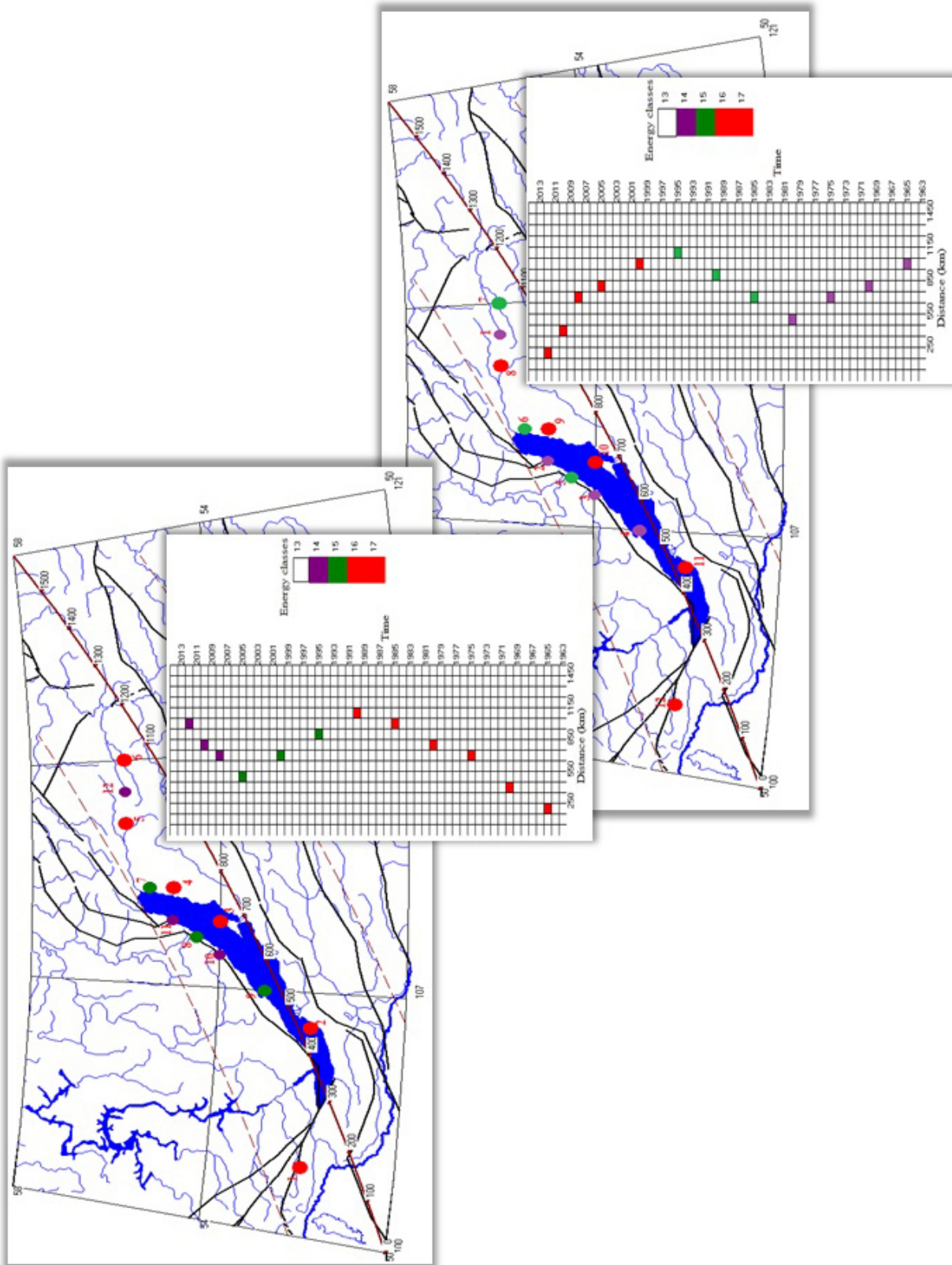


Fig. 3. Maps and diagrams constructed on the basis of the test catalogue. Restraint events are numbered according to their time sequence.

Рис. 3. Карты и диаграммы, построенные по тестовому каталогу. Нумерация условных событий соответствует их упорядоченности во времени.

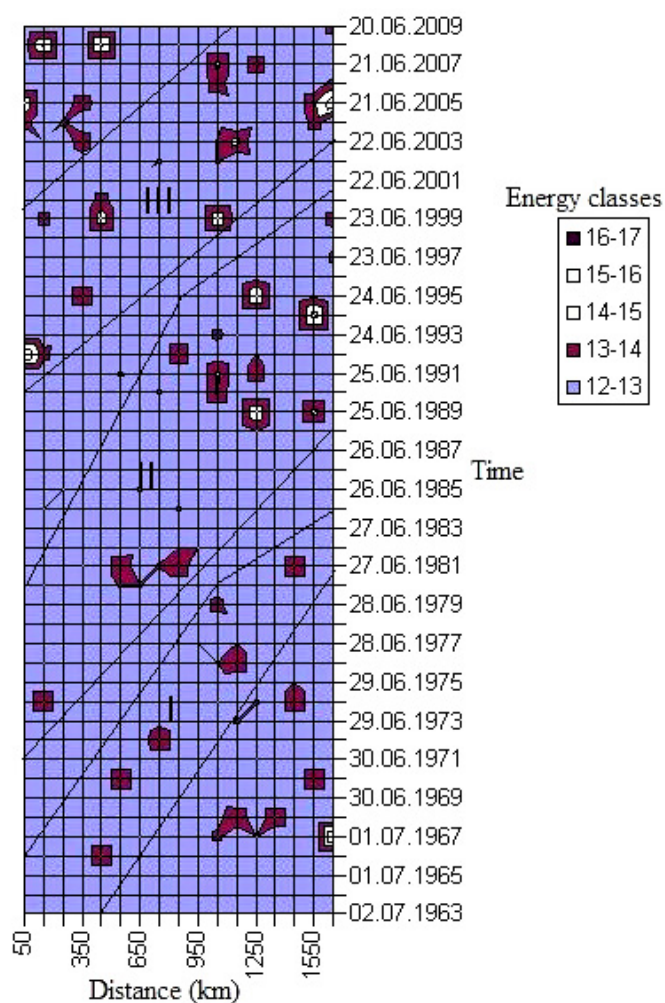


Fig. 4. Space-time clustering of events ($K \geq 8$). Clusters are revealed by grouping elements of the diagram in areas stretching from SW to NE, which reoccur regularly with time.

Рис. 4. Выделение пространственно-временных кластеров для событий с $K \geq 8$. Критерием для выделения кластеров служила группировка элементов диаграммы в областях, простирающихся с юго-запада на северо-восток и повторяющихся с некоторой временной периодичностью.

regression equation. The fourth and fifth columns show the correlation coefficient and its errors. The sixth column shows migration velocities for the given cluster according to the following equation:

$$V = \frac{1}{a},$$

where V is velocity, and a is coefficient of the regression equation.

The seventh, eighth and ninth columns show start time, finish time and duration of each cluster, which

are calculated from the regression equation. The space-time diagram and assumed migration lines are shown in Fig. 5.

The above-described calculation method is also applied to studying seismicity migration in other territories. The map showing boundaries of the regions under study is given in Fig. 6. Studied regions: 1. BRZ; (2) Himalayas – BRZ; (3) Japan – BRZ; (4) Northern Atlantic Ocean; (5) Southern Atlantic Ocean.

Seismicity migration in the Pamir-Baikal segment, including the territory from the Himalayan collision area to BRZ, is studied for the period from 1963 to

Table 1. Parameters of three clusters identified for BRZ

Таблица 1. Параметры трех выделенных кластеров для БРЗ

| Cluster | a | b | r | sr | V | Started in (year) | Finished in (year) | Duration (years) |
|------------|--------|---------|------|-------|--------|-------------------|--------------------|------------------|
| 1 | 2 | 3 | 4 | 5 | 6 | 7 | 8 | 9 |
| 1 - bottom | 0.0141 | 1961.27 | 0.95 | 0.041 | 70.92 | 1961 | 1985 | 24 |
| 2 - medium | 0.0121 | 1976.15 | 0.77 | 0.11 | 82.64 | 1976 | 1996 | 30 |
| 3 - top | 0.0086 | 1993.87 | 0.85 | 0.09 | 116.28 | 1994 | 2008 | 14 |

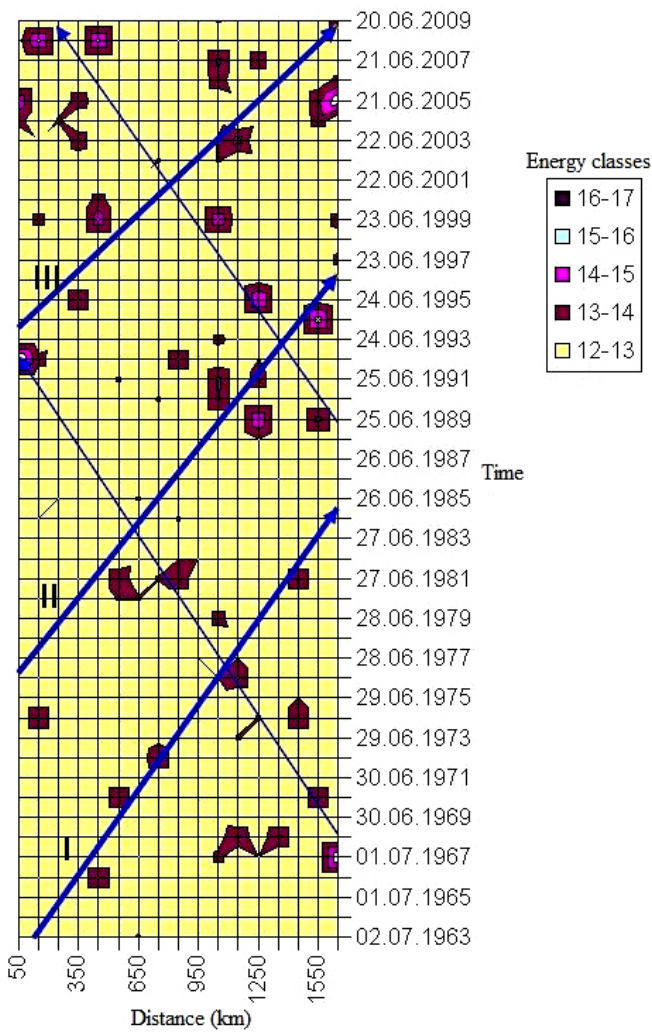


Fig. 5. Space-time diagram showing assumed lines of migration from SW to NE (solid lines) and backward (thin lines).

Рис. 5. Пространственно-временная диаграмма с нанесенными на нее предполагаемыми линиями миграции в направлении с юго-запада на северо-восток (толстые линии) и в обратном направлении (тонкие линии).

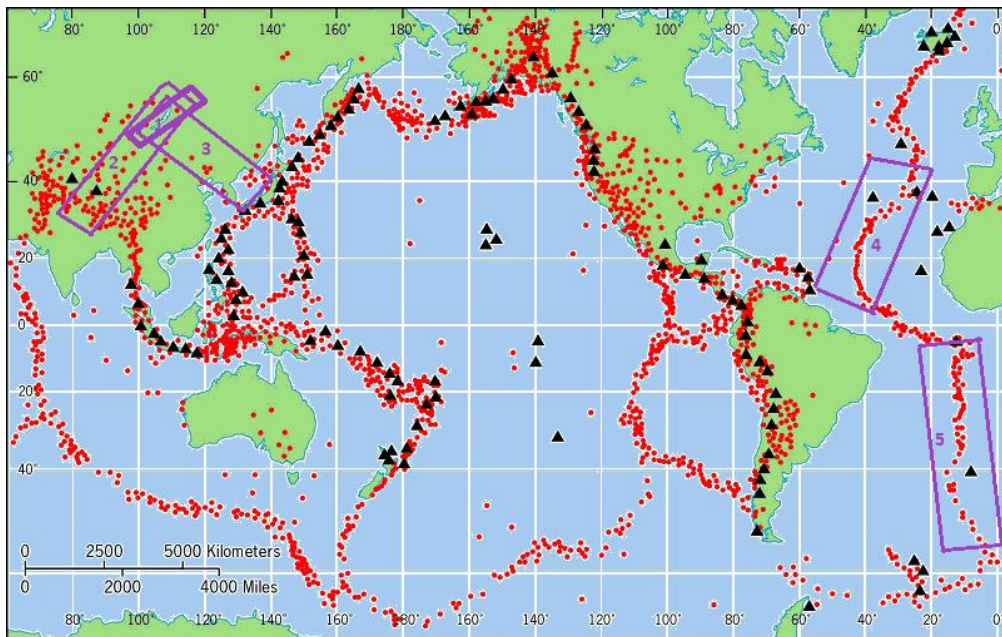


Fig. 6. Map showing boundaries of studied regions of seismicity migration. Red dots show earthquake epicentres; black triangles show volcanoes.

Рис. 6. Карта с нанесенными на нее границами рассмотренных районов миграции сейсмической активности. Красными точками отмечены эпицентры землетрясений, черными треугольниками – вулканы.

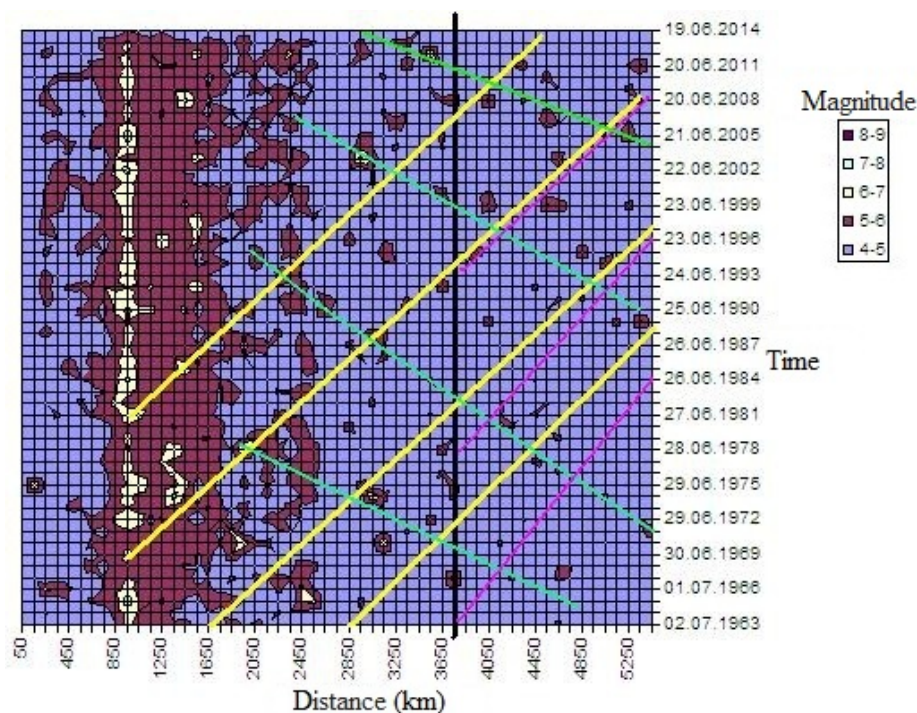


Fig. 7. Diagram of seismic activity propagation from the collision region to NE, towards BRZ in the period from 1963 to 2014 ($M \geq 4.5$). Thick yellow lines show assumed lines of migration from SW to NE; thin green lines show backward migration. In the diagram, the BRZ area is located to the right of the black vertical line. Migration lines for BRZ from diagram 8 are shown in pink.

Рис. 7. Диаграмма распространения сейсмической активности от коллизионной области на северо-восток, в сторону БРЗ, за период 1963–2014 гг. ($M \geq 4.5$). Предполагаемые линии миграции в направлении с юго-запада на северо-восток показаны толстыми желтыми линиями, в обратном направлении – тонкими зелеными линиями. Справа от вертикальной черной линии на диаграмме располагается область БРЗ. Линии миграции для нее с диаграммы 8 показаны розовым цветом.

2014 (events $M \geq 4$). The dynamics of the seismic events within the specified area in space and time is shown in the diagram (Fig. 7).

According to the diagram, the seismic regime of the Pamir-Tien Shan segment (P average direct = 11 years) is quasi-cyclic, and earthquake foci tend to migrate as deformation fronts from SW to NE with velocities of about 90 km/year. It is also noted that the migration is intermittently progressive and thus reflects the impulse regime of the propagation of the deformation fronts.

Based on our studies of the regularities in seismicity migration within the specified area, it can be concluded that the observed occurrence of seismicity migration waves can be explained by the quasi-periodic propagation of the deformation fronts in the crust from SW to NE, i.e. from the side of the Indo-Eurasian collision area [Levina, 2011; Ruzhich, Levina, 2012]. In this respect, the rotation model of the block geomegium, which is proposed by A.V. Vikulin and A.G. Ivanchin [Vikulin, Ivanchin, 2015], is of interest. In terms of geomechanics, it assumes that rotation movements of the Earth

are related with the occurrence of wave deformation and the generation of earthquakes.

In the transgression stage, movement of the deformation wave fronts to NE and actions of triggering mechanisms are accompanied by the activation of potential earthquake sources varying in ranks; such sources are located on sites characterized by the extremely high dynamic instability. Therefore, the seismicity migration mechanism of the initiation of seismic activity and directional trends of migration processes within BRZ (being a linear zone of the developing megafault) are a reflection of the kinematics of the recent deformation and destruction of the lithosphere under the influence of the external energy sources. This point of view of the authors does not contradict with concepts developed by other researchers [Vikulin, 2003; Sherman, 2013, 2014].

Another region under study is the territory from the Japan islands to BRZ. The space-time diagram is given in Fig. 8. The belt-shaped area selected for studying the seismicity migration in this region is oriented from SE to NW. Since the proposed method can be applied to

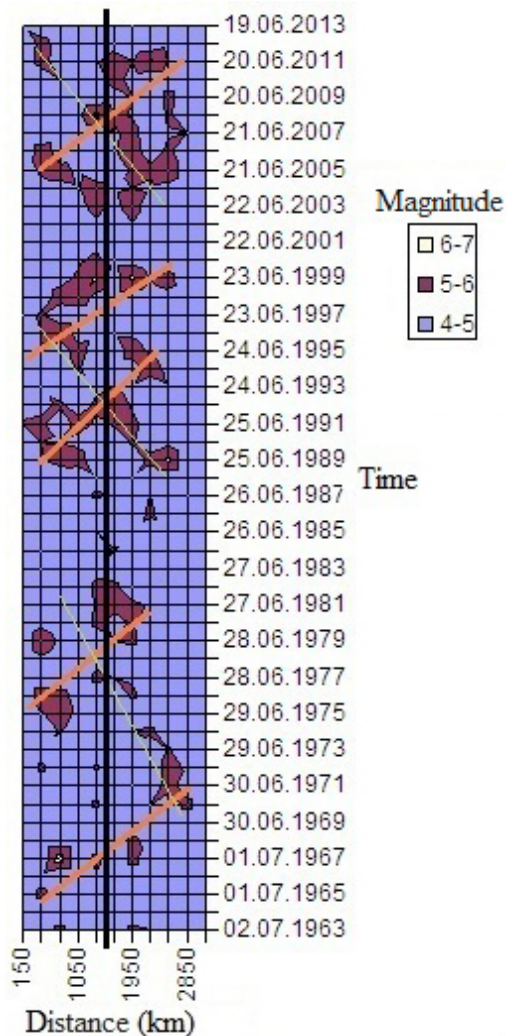


Fig. 8. Diagram of seismic activity propagation from the Benioff zone to NE, towards BRZ in the period from 1963 to 2013 ($M \geq 4.5$). Thick orange lines show assumed lines of migration from SE to NW; thin green lines show backward migration. In the diagram, the BRZ area is located to the right of the black vertical line.

Рис. 8. Диаграмма распространения сейсмической активности от зоны Бенъофа на северо-запад в сторону БРЗ за период 1963–2013 гг. ($M \geq 4.5$). Предполагаемые линии миграции в направлении с юго-востока на северо-запад показаны толстыми оранжевыми линиями, в обратном направлении – тонкими зелеными линиями. Справа от вертикальной черной линии на диаграмме располагается область БРЗ.

areas of various orientations, an obvious question is how to compare directional trends of earthquake foci migration in different regions. In this study, migration from the equator (in the northern hemisphere) is termed as 'forward', and migration to the equator is called 'backward'.

Windows of 300 km (space) and one year (time) are used to construct the diagram (Fig. 8). Five clusters

of forward migration are identified. An average forward velocity amounts to 365 km/year, and an average forward interval between the tracks is 11 years. For backward tracks, an average backward velocity amounts to 233 km/year, and an average backward interval between the tracks is 16 years. Special attention should be given to results obtained in the study of seismicity migration in the southern and northern segments of the Atlantic mid-oceanic ridge (being an interplate boundary zone). Two space-time diagrams shown in Fig. 9 are constructed with windows of 300 km (space) and one year (time). For forward tracks in the Northern Atlantic Ocean, an average forward velocity amounts to 335 km/year, and an average forward interval between the tracks is 8 years. For backward tracks, an average backward velocity amounts to 225 km/year, and an average backward interval between the tracks is 9 years. For the Southern Atlantic Ocean, an average forward velocity amounts to 411 km/year, and an average forward interval between the tracks is 10 years; an average backward velocity amounts to 437 km/year, and an average backward interval between the tracks is 10 years. It is noteworthy that the starting points of the seismicity migration tracks from the equator towards the poles are close in time in both parts of the Atlantic Ocean.

Table 2 contains parameters of seismicity migration for all the regions of the world in our study.

4. DISCUSSION OF RESULTS

The data obtained by the proposed method are briefly reviewed and interpreted below. In Fig. 10, there are two diagrams for BRZ with the time difference of four years. In the right diagram, the horizontal pink line separates a part of the diagram with the end of the earlier left diagram. It can be observed that some of the dots, that are not included in any clusters in the left diagram, are included in the new developing cluster in the right (newer) diagram. The top yellow line at the right shows an assumed migration line in it. Comparing these two diagrams illustrates seismic prediction capacities of the proposed method that is similar to the method described in [Sherman, 2013]. According to the figure, in 2014 and 2015, the most clearly manifested maximums of seismic activity migrated to the NE flank of BRZ.

It is reasonable therefore to assume that earthquake migration along the fault zones and inside the geoblocks is currently related to the propagation of deformation waves of various amplitudes and frequencies which are capable of initiating the activation of seismicity in the lithosphere [Bykov, 2005; Vikulin et al., 2000; Levina, Ruzhich, 2010; Sherman, 2014]. It can be thus concluded that the directional trends of the

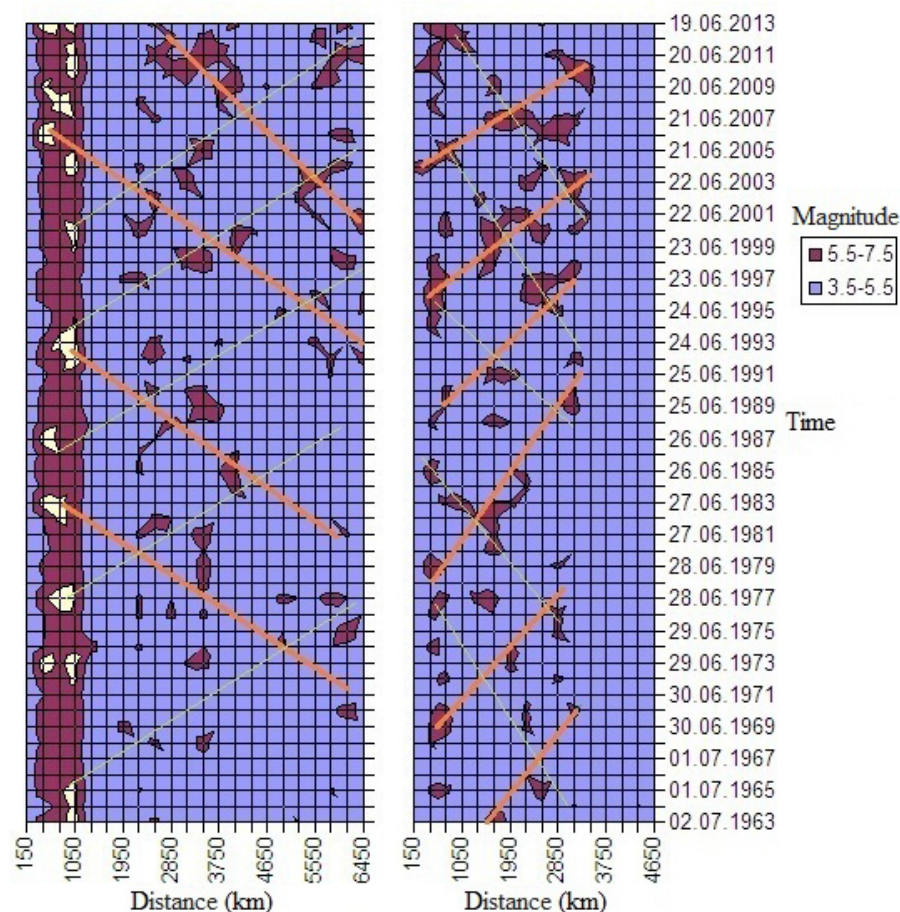


Fig. 9. Diagram of seismic activity propagation in the Southern (left) and Northern (right) Atlantic Ocean in the period from 1963 to 2013 ($M \geq 5$).

Thick orange lines show assumed lines of 'forward' migration (from the equator); thin green lines show 'backward' migration (to the equator).

Рис. 9. Диаграмма распространения сейсмической активности в южной (слева) и северной (справа) части Атлантического океана за период 1963–2013 гг. ($M \geq 5$).

Предполагаемые линии миграции в «прямом» направлении (от экватора) показаны жирными оранжевыми линиями, в «обратном» направлении (к экватору) – тонкими зелеными линиями.

migration of seismic sources can help reveal the character of deformations in the form of deformation waves or disturbance fronts.

One of the sources of wave deformation of the crust is the rotational regime of the Earth. A potential relationship between the global seismicity of the Earth and irregularities in its rotation has been a subject of intensive studies [Vikulin *et al.*, 2000; Sidorenkov, 2004; Tyapkin, 2012]. It is known that the Earth is in an elliptical orbit around the Sun. The distance between the Earth and the Sun is changing due to the ellipticity of the orbit. According to the Kepler's second law of planetary motion, the speed of the Earth increases at peri-

helion (early January) and decreases at aphelion (early July), and the speed difference amounts to almost 1 km/sec [Odessky, 1972]. Since the total momentum of the system's motion quantity remains constant, an increase of the orbital speed of the Earth should cause a decrease of its rotation velocity, and vice versa. It is now established that the angular velocity of the Earth rotation decreases centennially due to tidal friction. In the 20th century, the day's length increased by 0.0016 sec [Odessky, 1972]. Besides, it is revealed that the angular velocity of the Earth rotation is subject to regular annual changes (minimum in April, and maximum in August) and irregular sharp fluctuations.

Table 2. Parameters of seismicity migration for regions of the world

Таблица 2. Параметры миграции сейсмической активности для различных районов мира

| Region | Number of events | V average forward (km/year) | P average direct (year) | V average backward (km/year) | P average backward (year) |
|--------------------------------|------------------|-----------------------------|-------------------------|------------------------------|---------------------------|
| BRZ | 31305 | 90 | 14 | 62 | 16 |
| Himalayas - BRZ | 14960 | 90 | 11 | 160 | 16.5 |
| Japan - BRZ | 3107 | 365 | 11 | 233 | 16 |
| Northern Atlantic Ocean | 1901 | 335 | 8 | 225 | 9 |
| Southern Atlantic Ocean | 5339 | 411 | 10 | 437 | 9.5 |

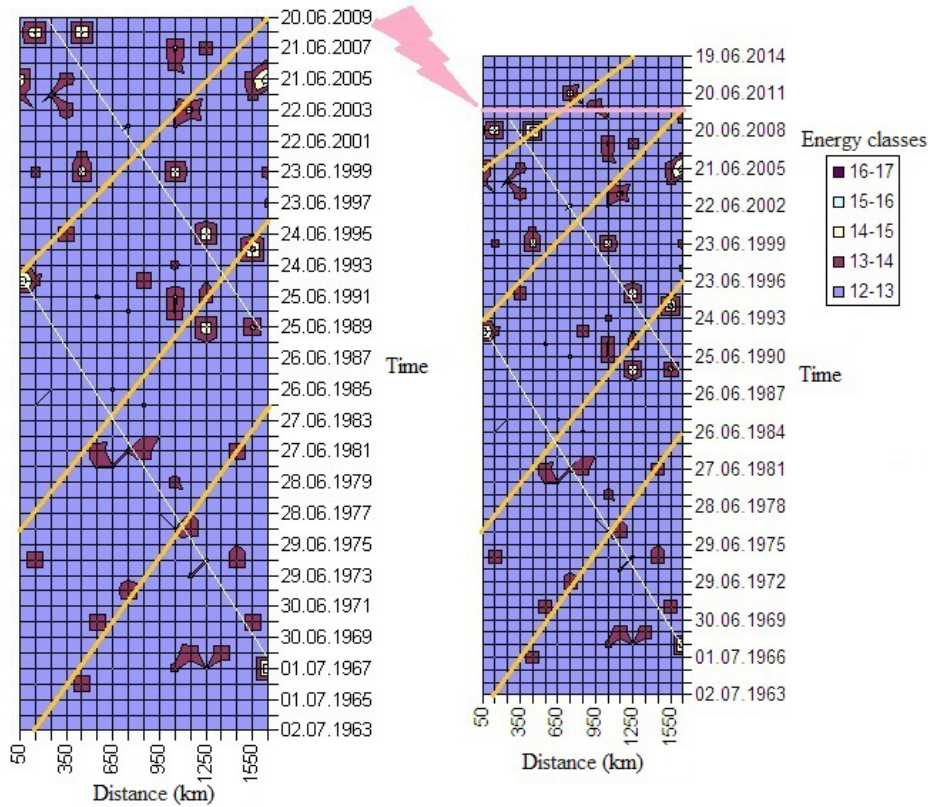


Fig. 10. The diagrams differ by four (4) years. The top yellow line at the right shows an assumed migration line in the developing cluster.

Рис. 10. Правая диаграмма построена через четыре года после левой. Верхняя желтая линия справа показывает предполагаемую линию миграции в новом формирующемся кластере.

Being in the state of hydrostatic equilibrium, the Earth reacts to a change of its angular velocity by a change of its polar compression (Fig. 11):

$$\alpha = \frac{a - c}{a},$$

where α is equatorial radius, and c is polar radius of the Earth.

The Earth rotation axis is not fixed in space. Since the rotation axis is precessing due to the gravity of the Sun and Moon, the celestial pole moves in a loop around the ecliptic pole in a cycle of approximately 26000 years. Gravity forces are changeable as the Sun and Moon continuously change location relative to each other and relative to the Earth, and thus the Earth's axis is subject to nutation. The largest component of Earth's nutation has a period of 18.6 years, the same as that of the precession of the Moon's orbital nodes. The movements of the Earth axis in space are schematically shown in Fig 12. Moreover, the Earth wobbles around the rotation axis, and the current pole (while moving from west to east) follows a spiral-shaped centroid curve within a 30×30 m square area on the surface of the Earth. Concerning the pole

movements, the centennial trend is revealed, and two periodic wobbles – the free (Chandler) which has a period of 14 months, and a forced wobble with a period of one year – and non-periodic wobbles are recognized.

In 1970s, some of the researchers concluded that stresses that occur in the Earth crust due to the rotation are sufficiently large to disturb the integrity of the crustal layer [Stovas, 1963; Tsaregradsky, 1963; Vikulin et al., 2000; Bykov, 2005]. Besides, it was revealed that the gravity interrelations in the Sun–Earth–Moon system are periodically changing [Vorobiev, 1971; Dovbnich, 2007; Maximov et al., 1967; Revuzhenko, 2013].

According to [Utkin et al., 2012], variations of the Earth rotation regime are always preceding an increase of the general seismicity of the Earth: the change of the sign of the Earth movement acceleration is a general (for all the earthquakes on the planet) short-term precursor of a tectonic earthquake, and all the earthquakes with $M > 6$ were mandatory preceded by a sudden change of the Earth rotation acceleration. In analyses of Table 2 and the space-time diagrams (Fig. 5, and 7 to 10), it is noted that the migration lines are located in an encheleone pattern and reoccur with time. The regular

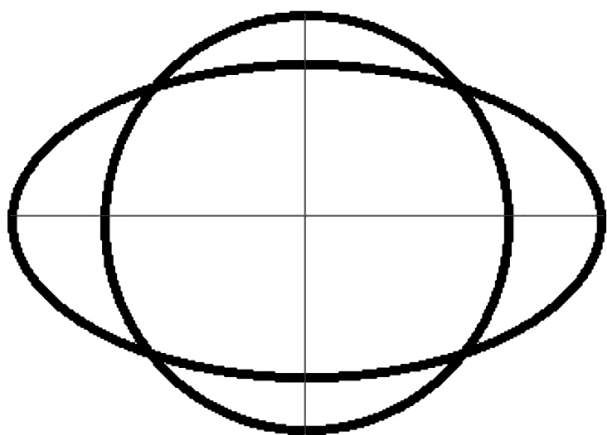


Fig. 11. Variations of the polar compression of the Earth.

Рис. 11. Схема, иллюстрирующая изменение полярного сжатия Земли.

occurrence of earthquakes in BRZ is noted by many researchers, and an 11-year cycle is related to the cycle of the solar activity [Lyubushin et al., 1998]. There are grounds to suggest that the seismicity migration along BRZ and the regular occurrence of earthquakes in BRZ may manifest the same regularities. If so, the identified cycle of the reoccurrence of the migration clusters (≈ 11 years) is another confirmation of the fact that seismicity is influenced by the solar activity cycles [Sobolev et al., 1998; Shestopalov, Kharin, 2004].

In Fig. 13, the curve shows earthquake quantities in BRZ in the period from 1963 to 2013 versus changes of the Wolf (relative sunspot) number [Levi et al., 2012] in the same period; the values are averaged in the one-year cycles. A relationship between two rows of digits can be given by the following equation: $y=0.28 \cdot x^{195.41}$, with correlation coefficient $R=0.47 \pm 0.11$.

An interpretation of the curves can provide an additional support for the conclusion that the seismotectonic regime of the Earth is influenced by the solar activity. In this respect, noteworthy is another concept of a potential mechanism of the relationship between the Earth seismicity and the solar activity. According to [Orlov et al., 2007], the mechanical recoil momentum, that is received by the Sun in case of a strong emission during the flare, can change the gravity field and thus cause corresponding deformation disturbances in the crust of the Earth. This conclusion is based on long-term oscillation records by laser deformation meters and an assumption that the planetary orbits are stable.

In our studies of the earthquake migration in BRZ, it is noted that maximums of seismic activation can relocate in space under a complicated pattern [Levina, Ruzhich, 2010; Levina, 2011]. This assumption is well illustrated by a case of seismicity migration in the peri-

od from December 2012 to January-March 2015. In this period, the Irkutsk Seismic Station registered a strong earthquake ($M=7-8$) at the boundary between BRZ and the Republic of Tyva and indicators of the seismicity migration from the boundary towards the NE flank of BRZ. Near Severomuisk, starting from 03 January 2015, an energy cluster continued its development. This spatially dense swarm of earthquakes is represented by a series of seismic events, including earthquakes with $K \leq 13.2$ ($M=7-8$) and numerous (160+) weak and measurable shocks. In [Ruzhich, 1997], it is discussed that such a high swarm-type seismic activity occurs typically at the intersections of faults generating seismicity and may last for many months and even years.

In view of the above-mentioned periodicity, that is characteristic of the seismic regime of BRZ, the observed seismicity migration regime can be considered as a manifestation of the whole range of deformation waves with various amplitude, frequency and velocity values. Important information on parameters of deformation waves was published in [Sherman, 2013, 2014].

Taking into account a wide variety of energy sources capable of generating the wave oscillations in the lithosphere of the Earth, it becomes obvious that their interference needs to be studied, and the challenge of

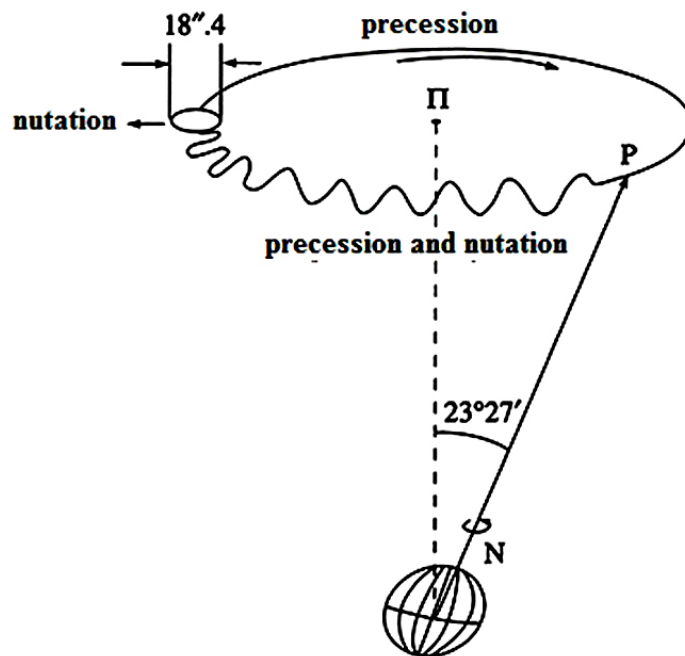


Fig. 12. The Earth's axis movement in space as viewed by an extraterrestrial observer. The scheme was published in [Sidorenkov, 2004].

Рис. 12. Схема движения оси Земли в пространстве для внеземного наблюдателя (схема из статьи [Sidorenkov, 2004]).

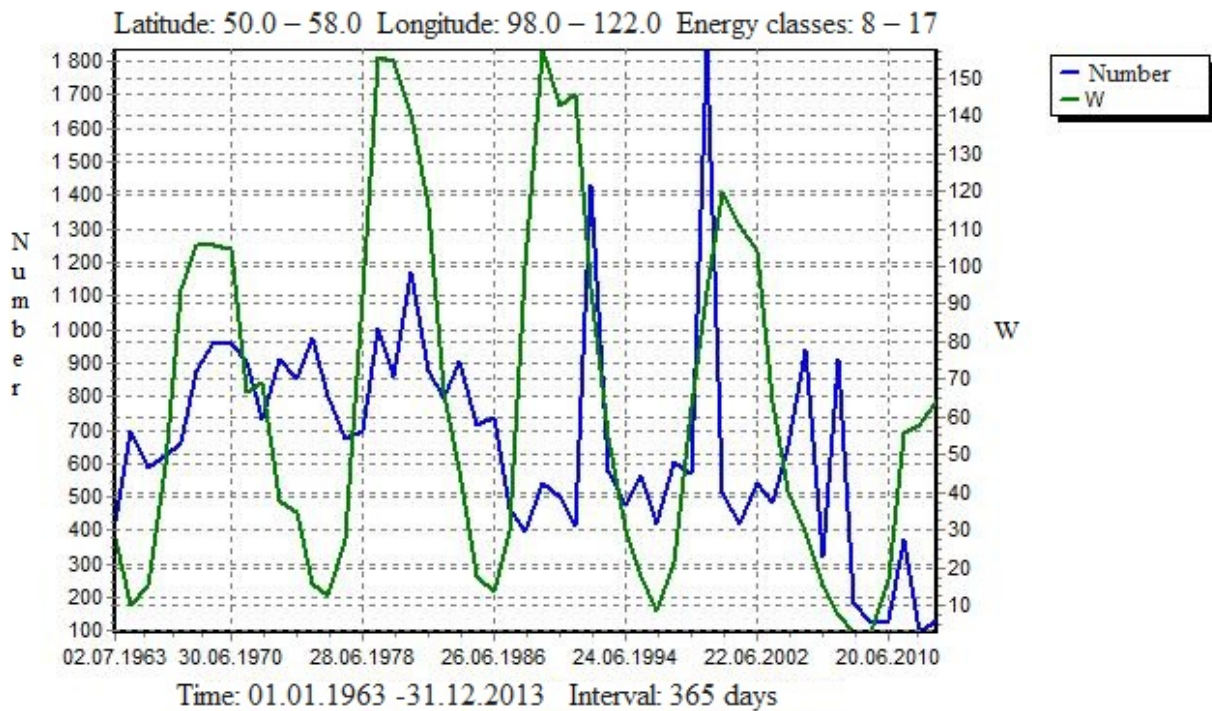


Fig. 13. Comparison of number-of-earthquake curves for BRZ and variations of Wolf numbers (both values are averaged in one-year intervals) for the period from 1963 to 2013.

Рис. 13. Сравнение графиков количества землетрясений в БРЗ и изменения чисел Вольфа (обе величины усреднены по интервалу времени в 1 год) за период 1963–2013 гг.

determining the wave parameters and their origin becomes even more complicated due to wave superposition and interaction.

5. CONCLUSION

Many researchers are interested in studies of the seismicity migration and search for possibilities to estimate and analyse its parameters in space and time with account of contact interactions in the interblock lithospheric medium at different scale levels. Our method applied to studies of seismicity migration can be viewed as an instrument for identification of causes and mechanisms of directional propagation of the seismic energy generated by recent destruction of the

lithosphere of the Earth. The knowledge of seismicity migration parameters can help in distinguishing fast-response extraterrestrial energy sources that facilitate the propagation of various deformation waves in the lithosphere of the Earth. Despite the fact that the latter do not have a significant energy, their impact is sufficient for triggering the seismic activity in tectonic zones of faults in the lithosphere, which are characterised by high stresses.

As shown by the results of our study of the seismicity migration in BRZ developing as a megafault in the Eurasian plate, the phenomenon of seismicity migration can be considered as an additional factor that can be referred to in attempts of middle-term prediction of earthquakes, as discussed in [Ponomareva *et al.*, 2014].

6. ЛИТЕРАТУРА / REFERENCES

- Bykov V.G., 2005. Deformation waves of the Earth: concept, observations and models. *Geologiya i Geofizika (Russian Geology and Geophysics)* 46 (11), 1176–1190.
- Chery J., Merkel S., Bouissou S., 2001. A physical basis for time clustering of large earthquakes. *Bulletin of the Seismological Society of America* 91 (6), 1685–1693. <http://dx.doi.org/10.1785/0120000298>.
- Dolgaya A.A., Vikulin A.A., 2015. Study of space-time regularities of seismicity in the Baikal rift zone. In: *Tectonics and geodynamics of the continental and oceanic lithosphere: general and regional aspects*. Proceedings of the XLVII

- Tectonic Meeting, vol. 1. GEOS, Moscow, p. 130–133 (in Russian) [Долгая А.А., Викулин А.А. Исследование пространственно-временных закономерностей сейсмичности Байкальской рифтовой зоны // Тектоника и геодинамика континентальной и океанической литосферы: общие и региональные аспекты: Материалы XLVII Тектонического совещания. М.: ГЕОС, 2015. Т. 1. С. 130–133].
- Dovbnich M.M., 2007. The influence of variations of Earth's rotational mode and lunar-solar tides on a stressed state of the tectonosphere. *Reports of the National Academy of Sciences of Ukraine (Dopovidі Natsionalnoi Akademii Nauk Ukrainy)* (11), 105–112 (in Ukrainian) [Довбнич М.М. Влияние вариаций ротационного режима Земли и лунно-солнечных приливов на напряженное состояние тектоносферы // Доповіді Національної академії наук України. 2007. № 11. С. 105–112].
- Levi K.G., Zadonina N.V., Yazev S.A., Voronin V.I., Naurzbaev M.M., Khantemirov R.M., 2012. Heliogeodynamics: Natural Aspects of Global Solar Minimums. In 3 volumes. Vol. 1, Book 1. Publishing House of the Irkutsk State University, Irkutsk, 511 p. (in Russian) [Левин К.Г., Задонина Н.В., Язев С.А., Воронин В.И., Наурызбаев М.М., Хантемиров Р.М. Гелиогеодинамика: Природные аспекты глобальных солнечных минимумов. В 3 т. Т. 1, кн. 1. Иркутск: Изд-во ИГУ, 2012. 511 с.].
- Levina E.A., 2011. Geoinformation System for Prediction of Earthquakes and Rock Shocks: Development and Application for the Baikal Rift Zone and the Norilsk Field. Synopsis of the Thesis, PhD in Geology and Mineralogy. Irkutsk, 19 p. (in Russian) [Левина Е.А. Геоинформационная система для прогноза землетрясений и горных ударов: разработка и примеры применения в Байкальской рифтовой зоне и Норильском месторождении: Автореф. дис. ... канд. геол.-мин. наук. Иркутск, 2011. 19 с.].
- Levina E.A., Ruzhich V.V., 2010. Earthquake migration of various scales as manifestation of the initiated energy flow in case of wave deformations of the lithosphere of the Earth. In: Triggering mechanisms in geosystems: proceedings of the All-Russia Workshop-Meeting. GEOS, Moscow, p. 71–78 (in Russian) [Левина Е.А., Ружич В.В. Разномасштабная миграция землетрясений как проявление инициированного энергопотока при волновых деформациях литосферы Земли // Триггерные эффекты в геосистемах: Материалы Всероссийского семинара-совещания. М.: ГЕОС, 2010. С. 71–78].
- Liu M., Stein S., Wang H., 2010. A 2000-year record of migrating earthquakes in North China: Implications for earthquake hazards in continental interiors. *Geophysical Research Abstracts* 12, EGU2010-6785.
- Lyubushin A.A., Pisarenko V.F., Ruzhich V.V., Buddo V.Yu., 1998. Identification of periodicity in seismic regime. *Vulkanologiya i Seismologiya* (1), 62–76 (in Russian) [Любушин А.А., Писаренко В.Ф., Ружич В.В., Буддо В.Ю. Выделение периодичностей в сейсмическом режиме // Вулканология и сейсмология. 1998. № 1. С. 62–76].
- Maximov I.V., Vorobiev V.N., Gindin B.V., 1967. On quasi-periodic long-term variations of tide-generating force of the Moon and the Sun. *Geomagnetism i Aeronomiya* 7 (2), 323 (in Russian) [Максимов И.В., Воробьев В.Н., Гиндин Б.В. О квазипериодическом характере долгопериодических изменений приливообразующей силы Луны и Солнца // Геомагнетизм и аэрномия. 1967. Т. 7. № 2. С. 323].
- Mogi K., 1968. Migration of seismic activity. *Bulletin of Earthquake Research Institute* 46, 53–74.
- Northern California Earthquake Data Center, On-line Catalogue, 2015. Available from: <http://www.ncedc.org> (last accessed May 13, 2015).
- Novopashina A.V., 2013. The method for identification of seismicity migration in Pribaikalie by GIS. *Geoinformatika* (1), 33–36 (in Russian) [Новопашина А.В. Методика выявления миграций сейсмической активности Прибайкалья средствами ГИС // Геоинформатика. 2013. № 1. С. 33–36].
- Novopashnina A.V., San'kov V.A., 2015. Migration of seismic activity in strike-slip zones: A case study of the boundary between the North American and Pacific plates. *Russian Journal of Pacific Geology* 9 (2), 141–153. <http://dx.doi.org/10.1134/S1819714015020050>.
- Odessky I.A., 1972. Wave Movements of the Earth's Crust. Nedra, Leningrad, 206 p. (in Russian) [Одесский И.А. Волновые движения земной коры. Л.: Недра, 1972. 206 с.].
- Orlov V.A., Panov S.V., Parushkin M.D., Fomin Yu.N., 2007. On relationship between seismicity of the Earth and solar activity from results of precision deformographic observations. In: Geodynamics and the State of Stresses of the the Earth Interior. Proceedings of the conference with participation of foreign researchers, 02–05 October 2007. Novosibirsk, p. 77–83 (in Russian) [Орлов В.А., Панов С.В., Парушкин М.Д., Фомин Ю.Н. О связи сейсмичности Земли с солнечной активностью по результатам прецизионных деформографических наблюдений // Геодинамика и напряженное состояние недр Земли: Труды конференции с участием иностранных ученых, 2–5 октября 2007 г. Новосибирск, 2007. С. 77–83].
- Ponomareva E.I., Ruzhich V.V., Levina E.A., 2014. On-line middle-term forecast of earthquakes in Pribaikalie and its possibilities. *Izvestia, Irkutsk State University. Earth Sciences Series* 8, 67–78 (in Russian) [Пономарёва Е.И., Ружич В.В., Левина Е.А. Оперативный среднесрочный прогноз землетрясений в Прибайкалье и его возможности // Известия Иркутского государственного университета. Серия «Науки о Земле». 2014. Т. 8. С. 67–78].
- Popov V.L., 2013. Mechanics of Contact Interaction and Friction Physics. From Nanotribology to Dynamics of Earthquakes. Fizmatlit, Moscow, 350 p. (in Russian) [Попов В.Л. Механика контактного взаимодействия и физика трения. От нанотрибологии до динамики землетрясений. Москва: Физматлит, 2013. 350 с.].
- Revuzhenko A.F., 2013. Tidal Waves and Directional Transfer of the Earth's Masses. Nauka, Novosibirsk, 204 p. (in Russian) [Ревуженко А.Ф. Приливные волны и направленный перенос масс Земли. Новосибирск: Наука, 2013. 204 с.].

- Ruzhich V.V., 1997. Seismotectonic Destruction of the Earth's Crust in the Baikal Rift Zone. Publishing House of SB RAS, Novosibirsk, 144 p. (in Russian) [Ружич В.В. Сейсмотектоническая деструкция в земной коре Байкальской рифтовой зоны. Новосибирск: Изд-во СО РАН, 1997. 144 с.].
- Ruzhich V.V., Khromovskikh V.S., Peryazev V.A., 1989. Analysis of global space-time migration of strong earthquake foci from geotectonic positions. In: Engineering geodynamics and geological medium. Nauka, Novosibirsk, p. 72–80 (in Russian) [Ружич В.В., Хромовских В.С., Перязев В.А. Анализ глобальной пространственно-временной миграции очагов сильных землетрясений с геотектонических позиций // Инженерная геодинамика и геологическая среда. Новосибирск: Наука, 1989. С. 72–80].
- Ruzhich V.V., Levina E.A., 2012. Seismomigrational processes as the reflection of internal dynamics in zones of intraplate and interplate faults. In: Recent geodynamics of Central Asia and hazardous natural processes: results of quantitative studies. Proceedings of the All-Russia Meeting and Youth School on Recent Geodynamics (23–29 September 2012, Irkutsk). In 2 volumes. Vol. 2. Institute of the Earth's Crust, SB RAS, Irkutsk, p. 71–74 (in Russian) [Ружич В.В., Левина Е.А. Сейсмомиграционные процессы как отражение внутренней динамики в зонах внутриплитных и межплитных разломов // Современная геодинамика Центральной Азии и опасные природные процессы: результаты исследований на количественной основе: Материалы Всероссийского совещания и молодежной школы по современной геодинамике (г. Иркутск, 23–29 сентября 2012 г.). В 2-х т. Иркутск: ИЗК СО РАН, 2012. Т. 2. С. 71–74].
- Sherman S.I., 2013. Deformation waves as a trigger mechanism of seismic activity in seismic zones of the continental lithosphere. In: Triggering effects in geosystems. Proceedings of the All-Russia Workshop-Meeting. Institute of Geosphere Dynamics (IGD) RAS, Moscow, p. 46–53 (in Russian) [Шерман С.И. Деформационные волны как триггерный механизм активизации разломов в сейсмических зонах континентальной литосферы // Триггерные эффекты в геосистемах: Материалы II всероссийского семинара-совещания. М.: ИДГ РАН, 2013. С. 46–53].
- Sherman S.I., 2014. Seismic Process and the Forecast of Earthquakes: Tectonophysical Conception. Academic Publishing House "Geo", Novosibirsk, 359 p. (in Russian) [Шерман С.И. Сейсмический процесс и прогноз землетрясений: тектонофизическая концепция. Новосибирск: Академическое издательство «Гео», 2014. 359 с.].
- Shestopalov I.P., Kharin E.P., 2004. On relationship between the Earth seismicity and solar and geomagnetic activity. In: Solar-Earth Relationships and Electromagnetic Precursors of Earthquakes. IKIR FEB RAS, Petropavlovsk-Kamchatsky, p. 64–76 (in Russian) [Шестопалов И.П., Харин Е.П. О связи сейсмичности Земли с солнечной и геомагнитной активностью // Солнечно-земные связи и электромагнитные предвестники землетрясений. Петропавловск-Камчатский: ИКИР ДВО РАН, 2004. С. 64–76].
- Sidorenkov N.S., 2004. Instability of the Earth rotation. *Vestnik, Russian Academy of Sciences* 74 (8), 701–715 (in Russian) [Сидоренков Н.С. Нестабильность вращения Земли // Вестник Российской академии наук. 2004. Т. 74. № 8. С. 701–715].
- Sobolev G.A., Shestopalov I.P., Kharin E.P., 1998. Implications of solar flares for the seismic activity of the Earth. *Izvestiya, Physics of the Solid Earth* 34 (7), 603–607.
- StatSoft, *On-line Statistics Guidebook*, 2015. Available from: <http://www.statsoft.ru/home/textbook/modules/stcluan.html> (last accessed May13, 2015).
- Stovas M.V., 1963. On the loaded state of the crustal layer in the zone between 30 and 40°. In: Problems of Planetary Geology. Gosgeoltekhizdat, Moscow, p. 275–284 (in Russian) [Стовас М.В. О нагруженном состоянии корового слоя в зоне между 30 и 40° // Проблемы планетарной геологии. М.: Госгеолтехиздат, 1963. С. 275–284].
- Tsaregradsky V.A., 1963. On the issue of deformation of the Earth's crust. In: Problems of planetary geology. Gosgeoltekhizdat, Moscow, p. 149–221 (in Russian) [Цареградский В.А. К вопросу о деформациях земной коры // Проблемы планетарной геологии. М.: Госгеолтехиздат, 1963. С. 149–221].
- Tyapkin K.F., 2012. Variations of the position of the rotation axis in the Earth body: cause, mechanism and use for explanation of global tectonic processes in the Earth's crust. *Geophysical Journal* 34 (6), 91–100 (in Russian) [Тяпкин К.Ф. Изменение положения оси вращения в теле Земли: причина, механизм и использование для объяснения глобальных тектонических процессов в земной коре // Геофизический журнал. 2012. Т. 34. № 6. С. 91–100].
- Utkin V.I., Yurkov A.K., Tsurko I.A., 2012. Variations of irregularity of earth rotation as triggering factor of seismicity. *Geologiya i Geofizika Yuga Rossii* (1), 3–13 (in Russian) [Уткин В.И., Юрков А.К., Цурко И.А. Вариации неравномерного вращения Земли как триггирующий фактор сейсмичности планеты // Геология и геофизика юга России. 2012. № 1. С. 3–13].
- Vikulin A.V., 2003. Physics of Wave Seismic Process. KOMSP GS RAS, KSTU, Petropavlovsk-Kamchatsky, 152 p. (in Russian) [Викулин А.В. Физика волнового сейсмического процесса. Петропавловск-Камчатский: КОМСП ГС РАН, КГПУ, 2003. 152 с.].
- Vikulin A.V., Akmanova D.R., Vikulina S.A., Dolgaya A.A., 2012. Migration of seismic and volcanic activity as display of wave geodynamic process. *Geodynamics & Tectonophysics* 3 (1), 1–18. <http://dx.doi.org/10.5800/GT-2012-3-1-0058>.
- Vikulin A.V., Bykov V.G., Luneva M.N., 2000. Nonlinear deformation waves in a rotational model of a seismic process. *Computational Technologies* 5 (1), 31–39 (in Russian) [Викулин А.В., Быков В.Г., Лунева М.Н. Нелинейные волны деформации в ротационной модели сейсмического процесса // Вычислительные технологии. 2000. Т. 5. № 1. С. 31–39].

Vikulin A.V., Ivanchin A.G., 2015. Rotational movements of geomedium – an alternative to plate tectonics. In: Tectonics and geodynamics of continental and oceanic lithosphere: general and regional aspects. Proceedings of the XLVII Tectonic Meeting. Vol. 1. GEOS, Moscow, p. 62–67 (in Russian) [Викулин А.В., Иванчин А.Г. Вращательные движения геосреды – альтернатива тектонике плит // Тектоника и геодинамика континентальной и океанической литосферы: общие и региональные аспекты: Материалы XLVII Тектонического совещания. М.: GEOS, 2015. Т. 1. С. 62–67].

Vorobiev V.N., 1971. Some consequences of analysis of total potential of long-term part of tide-generation force. *Geomagnetism i Aeronomiya* 11 (1), 189 (in Russian) [Воробьев В.Н. Некоторые следствия анализа суммарного потенциала долгопериодической части приливообразующей силы // Геомагнетизм и аэрномия. 1971. Т. 11. № 1. С. 189].

Zagoruiko N.G., 1999. Applied Methods of Data and Knowledge Analysis. Publishing House of Institute of Mathematics, SB RAS, Novosibirsk, 270 p. (in Russian) [Загоруйко Н.Г. Прикладные методы анализа данных и знаний. Новосибирск: Изд-во Ин-та математики СО РАН, 1999. 270 с.].



Levina, Elena A., Candidate of Geology and Mineralogy
Institute of the Earth's Crust SB RAS
128 Lermontov street, Irkutsk 664033, Russia
✉ e-mail: levina@crust.irk.ru

Левина Елена Алексеевна, канд. геол.-мин. наук, н.с.
Институт земной коры СО РАН
664033, Иркутск, ул. Лермонтова, 128, Россия
✉ e-mail: levina@crust.irk.ru



Ruzhich, Valery V., Doctor of Geology and Mineralogy, Chief Researcher
Institute of the Earth's Crust SB RAS
128 Lermontov street, Irkutsk 664033, Russia
Tel. +7(3952)422776; e-mail: ruzhigh@crust.irk.ru

Ружич Валерий Васильевич, докт. геол.-мин. наук, г.н.с.
Институт земной коры СО РАН
664033, Иркутск, ул. Лермонтова, 128, Россия
Тел. (3952)422776; e-mail: ruzhigh@crust.irk.ru



LOCAL DEFORMATION AND RHEOLOGICAL PARAMETERS BY MEASUREMENTS IN TALAYA STATION GALLERY (BAIKAL REGION)

V. Yu. Timofeev¹, O. K. Masalsky², D. G. Ardyukov¹, A. V. Timofeev¹

¹ Trofimuk Institute of Petroleum Geology and Geophysics, Siberian Branch of RAS, Novosibirsk, Russia

² Baikal Branch of Geophysical Survey, Siberian Branch of RAS, Irkutsk, Russia

Abstract: Tilt measurements have been taken in the underground gallery at Talaya Seismological Station for almost three decades, from March 1985 till 2014. Based on such data, deformation curves were constructed and analysed in the frame of elastic and viscous-elastic models of the geological medium. From estimated annual deformation rates, it became possible to reveal deformation cycles ranging from 3 to 18 years with amplitudes up to 5 arc-seconds ($2 \cdot 10^{-5}$). For the bedrock in the Talaya stream valley, the elastic modulus was estimated at 20 GPa. In frame of the Kelvin visco-elastic model, the apparent viscosity of the medium was estimated at 10^{19} Pa·sec by deformation delay curve for 1989–2014 epoch. Observed vertical rates were used to estimate the size of the studied area (from 0.1 km to 6.0 km). The values estimated in our experimental investigation are used in a wide range of geophysical studies: modelling tectonic, co-seismic and post-seismic processes.

Key words: tidal quartz tiltmeter, viscoelastic model of deformation, apparent rheological parameters, Baikal region.

Recommended by V.A. Sankov

For citation: Timofeev V.Yu., Masalsky O.K., Ardyukov D.G., Timofeev A.V. 2015. Local deformation and rheological parameters by measurements in Talaya station gallery (Baikal region). *Geodynamics & Tectonophysics* 6 (2), 241–253. doi:10.5800/GT-2015-6-2-0179.

ЛОКАЛЬНОЕ ДЕФОРМИРОВАНИЕ И РЕОЛОГИЧЕСКИЕ ПАРАМЕТРЫ ПО ИЗМЕРЕНИЯМ В ШТОЛЬНЕ (СЕЙСМОСТАНЦИЯ ТАЛАЯ, БАЙКАЛЬСКИЙ РЕГИОН)

В. Ю. Тимофеев¹, О. К. Масальский², Д. Г. Ардюков¹, А. В. Тимофеев¹

¹ Институт нефтегазовой геологии и геофизики им. А.А. Трофимука СО РАН, Новосибирск, Россия

² Байкальский филиал Геофизической службы СО РАН, Иркутск, Россия

Аннотация: Наблюдения наклонов в штольне сейсмостанции Талая ведутся уже около трех десятилетий (с марта 1985 года по настоящее время). В работе представлены результаты измерений. Полученные графики хода деформаций анализируются с использованием упругих и упруговязких моделей геологической среды. Определены годовые скорости деформирования, выявлен его циклический характер с периодами от 3 до 18

лет и амплитудами до 5 секунд дуги ($2 \cdot 10^{-5}$). Различными методами определен упругий модуль коренных пород, слагающих долину р. Талой, его величина составила 20 ГПа. С использованием кривой затухания деформации за период 1989–2014 гг., в рамках вязкоупругой модели Кельвина получено значение эффективной вязкости среды 10^{19} Па·с. С привлечением данных о скоростях вертикальных движений проведена оценка области, представительной для полученных параметров (от 0.1 до 6.0 км). Экспериментально определенные параметры могут быть использованы при моделировании тектонических, косейсмических и постсейсмических процессов.

Ключевые слова: приливные кварцевые наклонометры, вязкоупругие модели деформирования, эффективные реологические параметры, Байкальский регион.

1. INTRODUCTION

In studies of recent movements, which are an integral part of geophysical monitoring of the Earth's crust, recent deformation of the crust and mantle is described by elastic, plastic, viscoelastic models and combinations of such models. Obtaining field experimental results is essential for development of theoretical models of recent shear and deformation fields. Variations of such fields are determined for periods from a few days to decades. In such studies, measurements by extensometers and the horizontal pendulums installed in special underground gallery is one of the common methods. Upon analyses of strain variations in time, a model showing deformation and rheology is selected, and it becomes possible to reveal factors and forces that influence the process of deformation. Interpreting of the obtained data can be challenging due to the fact that strain measurements are taken at the surface of the Earth and may be distorted by local impacts. Besides, there is an uncertainty of a total value of accumulated strain. Actually, accumulated strain can be estimated only at the qualitative level from neotectonic reconstructions, knowledge of the stage of seismic activation, and structural models of the region. Observed periods of deformation are indications of current regional activity; for instance, in the Baikal rift, i.e. in the intracontinental area, representative earthquakes occur in periods of 3 to 150 years. Determination of rheological parameters of the geological medium and estimation of deformation or strain rates are major objectives of our studies. We study processes on the data basis collected by long-term observations using tidal quartz tiltmeters that were installed in the underground gallery at Talaya Seismological Station (TSS, 51.68°N, 103.65°E) in March 1985 and ensure non-stop data recording. TSS situated near the northern boundary separated of the south-western part of the Baikal rift zone and the Siberian platform. The Main Sayan fault, being the boundary between the Siberian platform and the mobile area [Levi et al., 1997; Solonenko, 1993], is located a few kilometres to the north. In this region, lateral inhomogeneities of the

crust and upper mantle cause deviatoric stresses of 35–40 MPa, according to calculations published in [Kaban, Yunga, 2000], and such stress values are close to maximum stresses estimated for the Baikal Rift. Left-lateral shift motion takes place at the Main Sayan fault. According to the available geological data and tectonic models of south-western part of the Baikal rift zone, horizontal displacement rates are from 0.8 to 2.0 mm per year, and displacements are mainly directed to the east [San'kov et al., 1999, 2000; Calais et al., 2002; Lukhnev et al., 2010; Timofeev et al., 2012, 2013].

2. QUARTZ TILTMETERS, CALIBRATION METHODS, AND STRAIN RECORD

The first measurements of tidal and technogenic tilting were obtained in 1960s when a tiltmeter designed by A.E. Ostrovsky was used; the tiltmeter mechanism included steel springs [Ostrovsky, 1978]. A pilot quartz tiltmeter NK-1 (Zöllner suspension type) was designed in 1973, manufactured and tested in 1974; it provided for photoelectric recording, and a new calibration method was proposed for calibration of the tiltmeter [Bulanzhe et al., 1975]. Stations in Siberia used pilot NK-1 units and sets of tools manufactured at the pilot plant of the Siberian Branch and in the Institute of Geology and Geophysics SB. In the TSS gallery, quartz horizontal pendulums have been in use since March 1985 [Gridnev et al., 1990]. Analogue records of measurements were collected from 1985 to 1998. Digital records are available since 1998. The tiltmeter is calibrated in laboratory conditions under the impact of elastic force of a quartz spring, and regular calibration checks are conducted on the permanent measurement inside the TSS tunnel. In the laboratory conditions, the calibration error amounts to 0.1 %. In situ conditions, when operator approaches the tiltmeter installed in the underground gallery (Fig. 1), an error may increase to a few percent. Maintaining stable recording of metrological parameters in time is challenging as measurements are impacted by the following factors: the electric

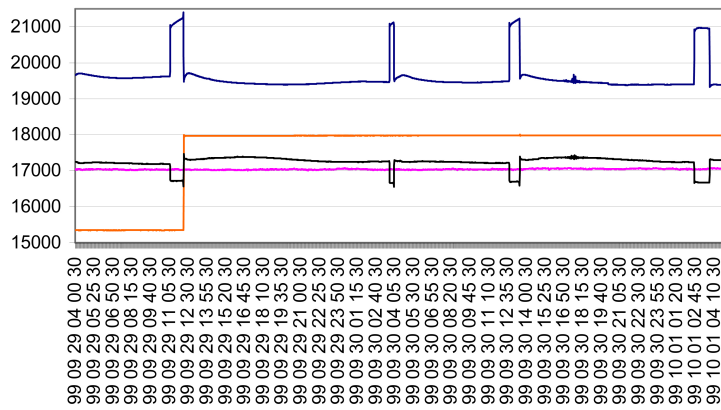


Fig. 1. Calibration pulses at the background of tidal variations of slope (underground gallery, Talaya seismic station). Minute interval of record.

Рис. 1. Калибровочные сдвиги на фоне приливных вариаций наклона (штольня сейсмостанции «Талая»).

power network of the seismic station is unstable, elements of the photo-electric sensor need to be periodically replaced, voltage may vary, it may be needed to disconnect the tiltmeter when seismological and geophysical equipment is in service operation. Such factors cause gaps in records and disturb stabilization of temperatures inside the TSS tunnel (+1°±1°C).

At Talaya Seismological Station, the tiltmeters were calibrated with the use of a quartz-spring micrometer or an electromagnetic calibration device [Gridnev, Timofeev, 1990]. For example, calibration for the period

from 29 September 1999 to 01 October 1999 was done by shifting with a quartz spring, as shown in Figure 1. Figure 2 shows examples of tiltmeter calibration and attenuation of natural oscillations of the pendulum after shifting. The tiltmeter base ranges from 300 to 100 millimetres. Measurements are conducted on a pedestal (0.7 m × 1.4 m) mounted on the bedrock.

The horizontal pendulums were installed in two azimuths, N-S and E-W. Examples of digital records of tilting for every component are shown in Figures 3 and 4. Tidal tilt amplitudes amounted to 0.03 arc-seconds.

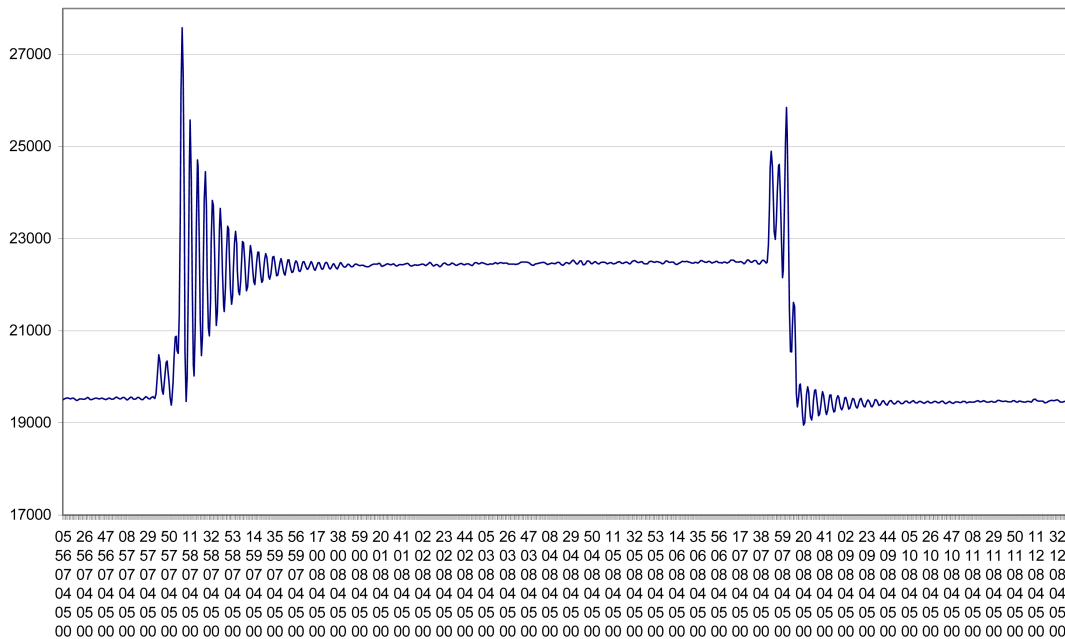


Fig. 2. Calibration pulses and inclinometer pendulum attenuation. A typical own period ranged from 8 to 18 seconds. Plotted time from 05 sec-56 m-07 h to 32 sec-12 m-08 h, 04 May 2000.

Рис. 2. Калибровочный сдвиг и затухание маятника наклономера. Обычно собственный период составлял от 8 до 16 секунд. Время на графике с 05 с-56 мин-07 ч по 32 с-12 мин-08 ч 4 мая 2000 г.

Tilt records in analogue and digital formats were analysed at the IPGG SB RAS, and the Royal Observatory of Belgium [Timofeev et al., 2000, 2008]. Then tidal parameters, i.e. amplitude and phase-lag factors, were compared with models of tidal deformations of the Earth. A good correlation was revealed with the DDW99 tidal model (static part) and SCW80 tidal ocean model (dynamic part) [Schwidorski, 1983; Dehant et al., 1999; Ducarme et al., 2008]. Deviations from the global tidal tilt model amounted to 7 % for amplitudes (E-W) and +9° for phases (N-S), which can be explained by the effect of the geological structure of the Main Sayan fault. This fault is located 3 km to the north of Talaya Station and strikes sub-latitude the region where the station is located.

3. SHORT-PERIOD VARIATIONS AND EFFECTIVE ELASTIC MODULI

Based on measurements of short-period variations associated with atmospheric pressure drops, we calculated effective elastic moduli of rocks in situ [Gridnev, Timofeev, 1989a, 1989b]. Variations were recorded in periods from a few minutes to hours in case of rapid air pressure variation. A simple Young modulus (E) ratio was used for interpretation:

$$E = \Delta P / \Delta \epsilon, \tag{1}$$

where ΔP is an atmospheric pressure drop; $\Delta \epsilon$ is a corresponding variation of vertical strain.

The first data were received using a vertical quartz extensometer, quartz tiltmeters and a quartz microbarograph [Gridnev, 1975]. Calculations based on records by the vertical strain meter yielded an effective elastic modulus of the rocks which is quite low, $E=4.7 \cdot 10^9$ Pa. In this case, significant impacts of cavity effects should be noted as such effects are maximum when the tool is installed (in a vertical or horizontal position) across the tunnel. According to calculations reported in [Harrison, 1976; Blair, 1977], horizontal strain is variable:

$$e_{xx} = (3e_{xx} + 0.5e_{yy}), \tag{2}$$

where e_{xx} and e_{yy} are horizontal strain values for the homogeneous medium.

A similar reduction of the modulus value is due to the strain value as follows:

$$e_{zz} \cong 3e_{zz}. \tag{3}$$

The effect of the triple increase of the tidal amplitude of vertical strain was also revealed in Osakayama (Japan), an old tunnel where vertical strain meters

were installed [Ozawa, 1967, 1974; Melchior, 1982]. The effect disappears when a vertical strain meter is installed in the tunnel in a specially drilled hole.

In case of short-period pressure variations (half a minute, less than 1 hour), it is possible to determine the effective modulus from records by tidal tiltmeters. In such cases, the following ratio is used:

$$E_{ef} = (2\Delta P_i \ln r_i) / (\pi \Delta \psi_i), \tag{4}$$

where: ΔP_i ΔP_i is a load; r_i is a distance between tilt and load measurement points (in case of rapid variations, frontage orthogonally to isolines) normalized to the tiltmeter base; $\Delta \psi_i$ is a tilt balance in the azimuth, orthogonal to the atmospheric front, i-th individual determination.

Our experiments show that the accuracy in this case is low because of difficulties in determining the position of the atmospheric front and challenges related to local mapping of pressure isolines in case of rapid variations (errors from 50 to 100 %). The effective modulus calculated from the tilt measurements is much closer to that estimated from petrophysical data, $E=1.5 \cdot 10^{10}$ Pa.

Based on petrophysical studies of core samples (Archean marble from Well 1608 located 100 m from the tunnel entrance in the TSS territory) (Fig. 5), the following values were estimated: density $\rho=2.87 \cdot 10^3$ kg/m³; seismic velocity $V_p = \sqrt{(\lambda + 2\mu)/\rho} = \sqrt{(K + 4/3 \mu)/\rho} = 4.16$ km/sec, velocity $V_s = \sqrt{\mu/\rho} = 2.62$ km/sec; and ratio $V_s/V_p = 0.63$. Core studies were conducted at IPGG SB RAS.

The obtained values are as follows: for Poisson ratio, $\nu=0.17$; for bulk modulus, $K=2.34 \cdot 10^{10}$ Pa; for shear modulus, $\mu = G = E/[2(1 + \nu)] = 1.97 \cdot 10^{10}$ Pa. From ratio $K = E/[3(1 - 2\nu)]$, Young modulus is $E=4.63 \cdot 10^{10}$ Pa, and Lamé parameter is

$$\lambda = \frac{2\nu G}{1 - 2\nu} = \frac{E_\nu}{(1 + \nu)(1 - 2\nu)} = 1.01 \cdot 10^{10} \text{ Pa.}$$

The most effective reference to short-period strain variations was demonstrated in the study of co-seismic deformations near earthquake locations. When an earthquake ($M=5.5-5.7$, 51.71°N, 102.70°E) took place on 29 June 1995, it was for the first time when a tilt change was recorded at a distance of 67 km to the west of the station. The anomalous tilt amounted to 0.25 microradian (extension, $+2.5 \cdot 10^{-7}$) at azimuth 124°N, which correlates with the solution of the earthquake mechanism [Melnikova, Radziminovich, 1998]. The most striking example is the Kultuk earthquake of 27 August 2008 ($M=6.5$, 51.61°N, 104.07°E) which occurred at a distance of 25 km from the station [Melnikova et al., 2009], when extension of $+1 \cdot 10^{-6}$ was

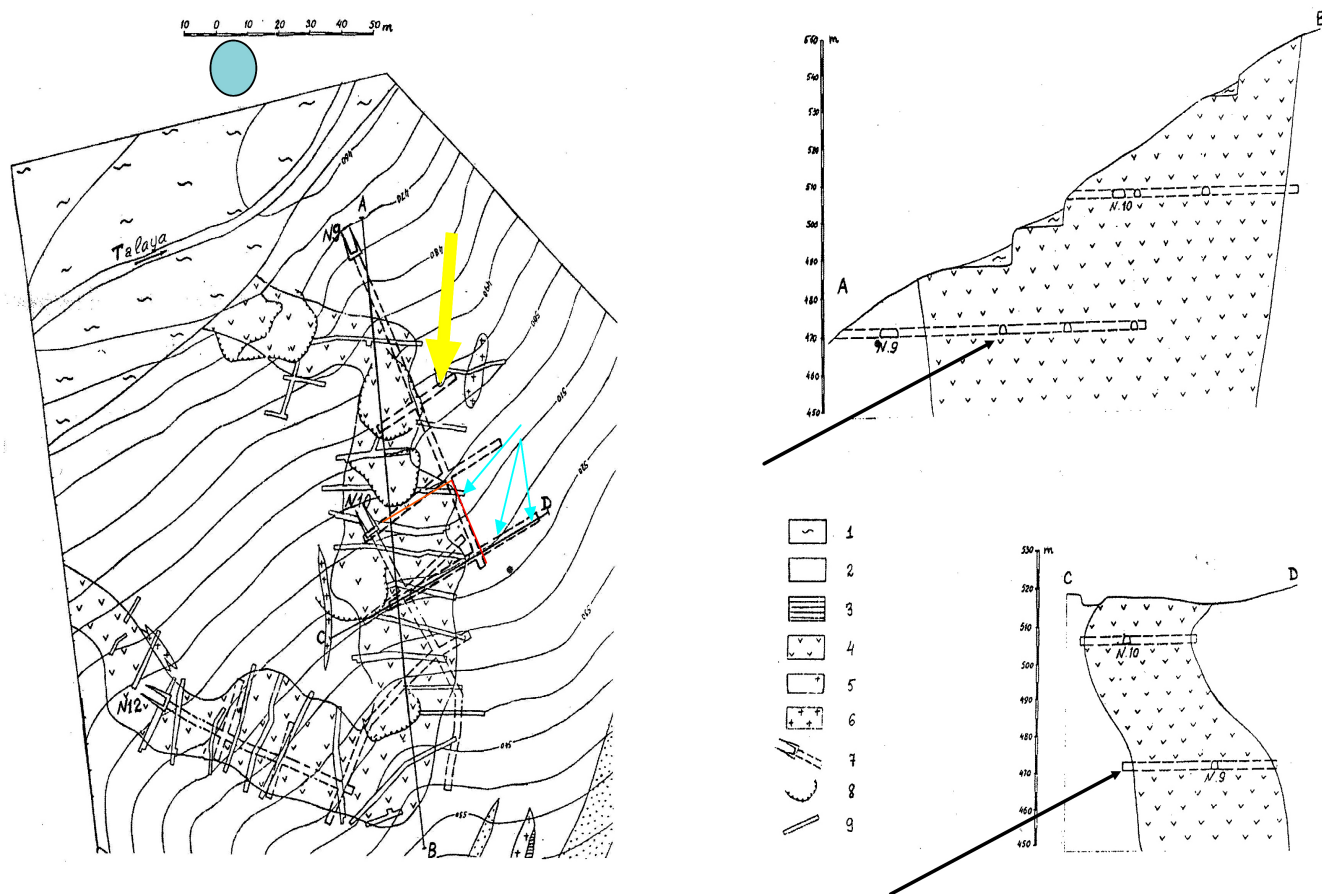


Fig. 5. Geological map and mining plan, underground gallery No. 9, Talaya seismic station. Scheme and cross section of the tunnels, Talaya seismic station.

The circle shows the location of Well 120; tilt meters were installed in the gangway, 50 m from the entrance; rod- and laser deformation meters were installed in distant gangways. 1 – alluvial deposits; 2 – marble; 3 – amphibole-piroxene crystalline schist; 4 – crystalline schist and skapolite-amphibole-diopside gneiss; 5 – garnet-biotite gneiss; 6 – garnet-pegmatite; 7 – shaft tunnels; 8 – quarries; 9 – trenches.

Рис. 5. Геологическая карта и совмещенный план горных выработок, штольня № 9 сейсмостанции «Талая». Схема и разрезы штольни сейсмостанции «Талая».

Кружком обозначена 120-метровая скважина, наклонометры установлены в штреке, в 50 метрах от входа, деформографы штанговые и лазерные, расположены в дальних штреках. 1 – аллювиальные отложения; 2 – мраморы; 3 – кристаллосланцы амфибол-пироксеновые; 4 – кристаллосланцы и гнейсы скаполит-амфибол-диопсидовые; 5 – гнейсы гранат-биотитовые; 6 – гранит-пегматиты; 7 – штольни; 8 – карьеры, 9 – канавы.

registered [Boiko et al., 2012]. This result is in good agreement with the model making by seismological data of the Baikal Branch GS SB RAS, Irkutsk.

4. LONG-TERM TILT VARIATIONS AND LOCAL RHEOLOGY

We consider long-term tilt variations by individual components of the tilt vector (N-S and E-W, Fig. 6 and 7). Dates of strong regional earthquakes are marked by changes in directions and rates of tilting at the curve. Arrows show dates of strong regional earthquakes as follows: 13 May 1989 (M=5.9, 50.2°N, 105.5°E), 27 December 1991 (M=6.5–7.0, 50.98°N, 98.08°E), 29 June

1995 (M=5.5–5.7, 51.71°N, 102.70°E), 25 February 1999 (M = 5.7–6.0, 51.63°N, 104.89°E), and 27 August 2008 (M=6.3, 51.61°N, 104.07°E).

Tilting runs manifest strain recurrence from 3 to 18 years (Fig. 6, 7, 8, and 9). In the vector diagram, this is reflected in the time period from 1985 to 2003 (Fig. 8). The average annual strain rate in some periods is variable from 0.05 second of arc to 2 second of arc per year (10^{-8} – 10^{-6}), and such values are consistent with data obtained by space geodesy techniques in this region [San'kov et al., 1999; Likhnev et al., 2010, Timofeev et al., 1994, 1999, 2012].

Tilting as local deformation of the geological medium can be caused by stress variations due to seismic

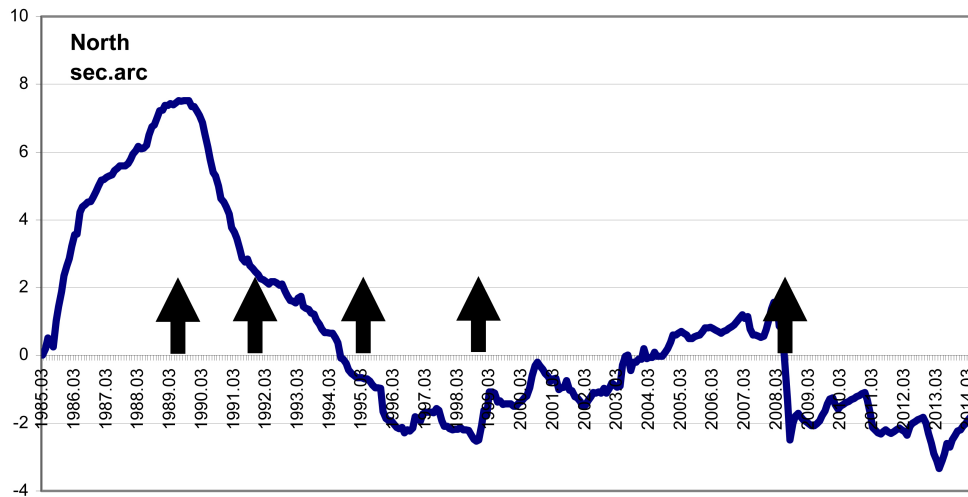


Fig. 6. Tilt variations at N-S azimuth (1 arc-second = $4.8 \cdot 10^{-6}$). Observations from March 1985 to April 2014. Arrows show time of strong regional earthquakes.

Рис. 6. Вариации наклона в азимуте север-юг в секундах дуги (1 секунда дуги = $4.8 \cdot 10^{-6}$). Период наблюдений с марта 1985 г. по апрель 2014 г. Стрелками показаны моменты сильных региональных землетрясений.

activity in the region. In the vector diagram (Fig. 9), all the registered events are shown: $M \geq 3$ at a distance of 50 km (L), $M \geq 4.5$ at $50 \text{ km} < L < 100 \text{ km}$, and $M \geq 5$ at $100 \text{ km} < L < 200 \text{ km}$. At the start period the tilt curve shows that northward motion when a strong earthquake occurred to the south of the station on 13 May 1989 ($M=5.9$, 50.2°N , 105.5°E). It was followed by strong aftershocks that occurred within a few months. In the area where in 13 May 1989 earthquake took

place, several strong events were recorded in the past: $M=5.6$ on 10 May 1929, $M=6.5$ on 06 February 1957, and $M=5.1$ on 01 March 1987.

After the earthquake, the stress state changed. The measurements had lasted for ten years before the next group of strong earthquakes ($M > 5$) was registered to the west and east of the station. The first strong event occurred on 29 June 1995 ($M=5.5$), and the second on 25 February 1999 ($M=5.8$). For 50 km zone around the

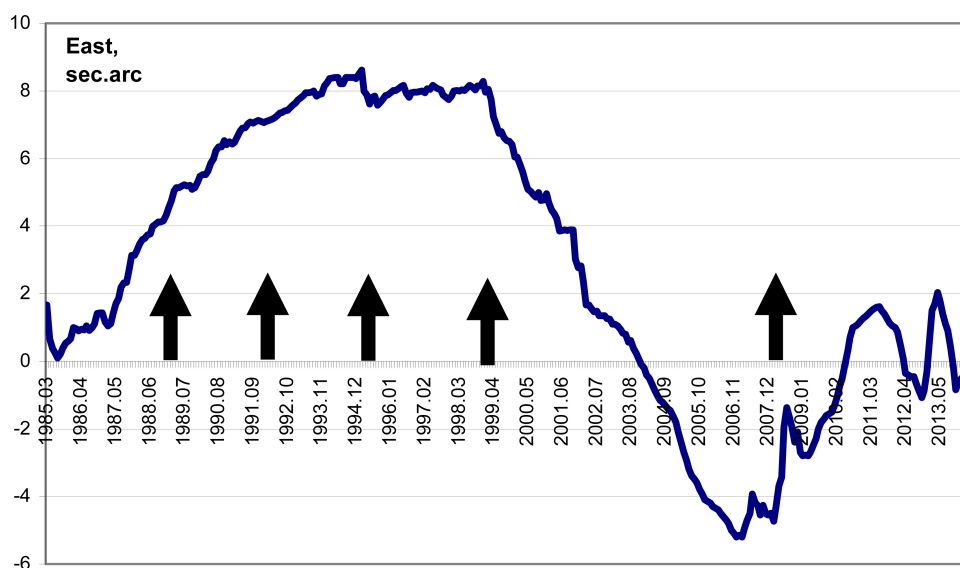


Fig. 7. Tilt variations at E-W azimuth (arc-second) from March 1985 to April 2014.

Рис. 7. Вариации наклона в азимуте восток-запад в секундах дуги (03.1985 г. – 04.2014 г.).

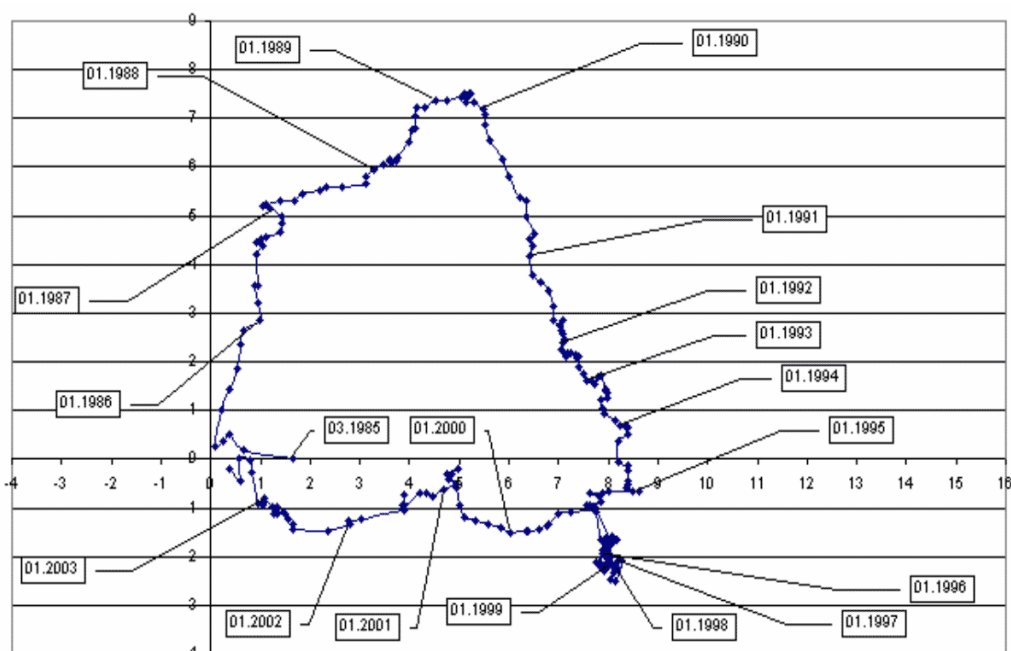


Fig. 8. Vector diagram of tilt run (arc-second) from 1985 to 2003 as per monthly data. January dates are shown for each year.

Рис. 8. Векторная диаграмма хода наклона в секундах дуги за период 1985–2003 гг., построенная по ежемесячным данным, показаны январские даты каждого года.

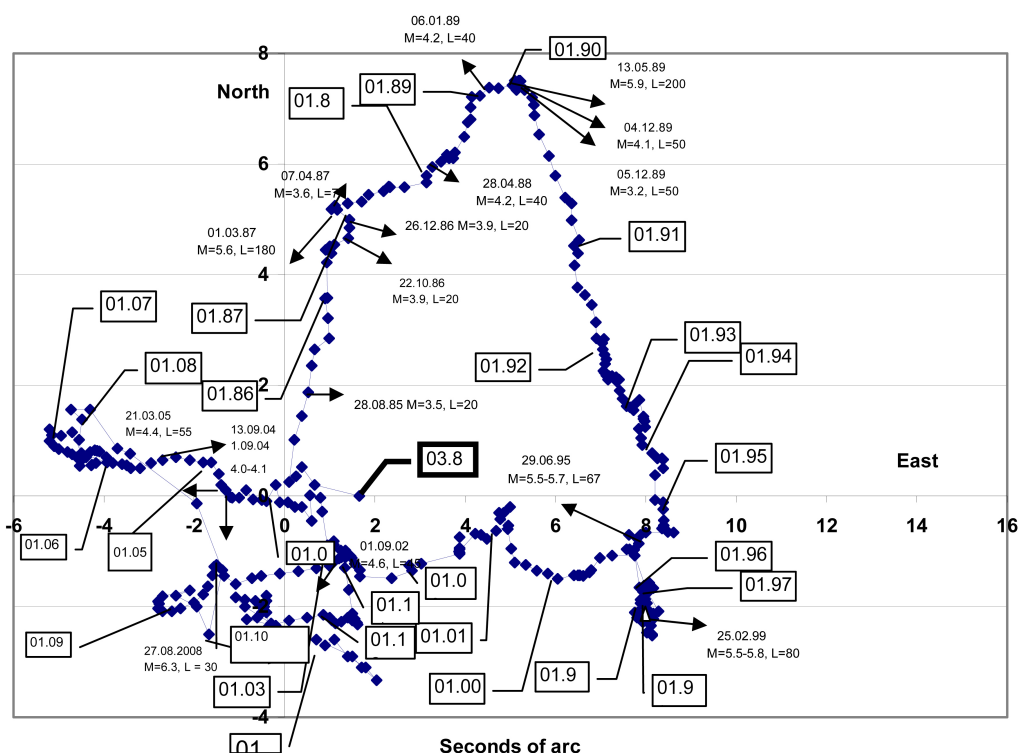


Fig. 9. Vector diagram of tilt run (arc-second) as per monthly data. January dates are shown in the box. Arrows show time of neighbouring earthquakes (magnitude and distance, km).

Рис. 9. Векторная диаграмма хода наклона в секундах дуги. График построен по ежемесячным данным. Время (январь каждого года) показано в рамке. Стрелками отмечены моменты близких землетрясений (магнитуда и расстояние в километрах).

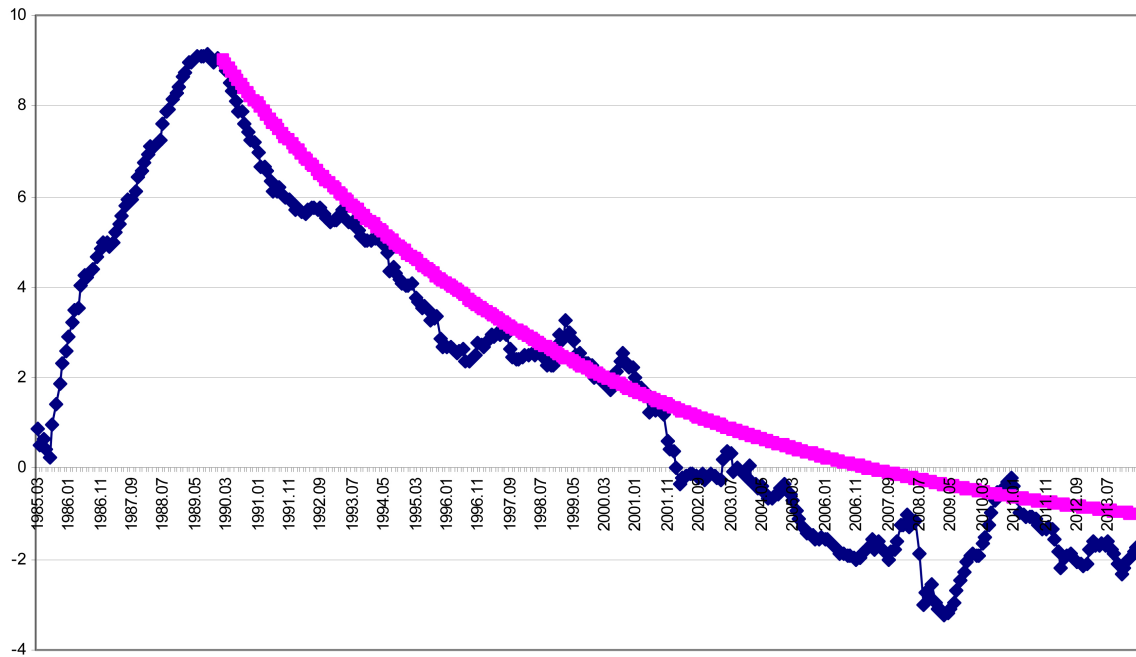


Fig. 10. Tilt variations at -33°NE azimuth (arc-second). Observations from March 1985 to April 2014. Theoretical calculations of shear deformation release (arc-second) are plotted: $\Psi(t)=[11 \cdot e^{-(t/T)} - 2]$.

Рис. 10. Вариации наклона в азимуте -33°N в секундах дуги. Период наблюдений с марта 1985 года по апрель 2014 года. Приведен теоретический график разгрузки сдвиговой деформации в секундах дуги: $\Psi(t)=[11 \cdot e^{-(t/T)} - 2]$.

station, it is possible to distinguish two periods: the first period until 1990 (weak earthquakes, $M=3.5 \div 4.0$; one or two events per year), and the second period from 1990 to 1994 (no earthquakes) (Fig. 9).

Continuous tilt underground sites measurements allow us to estimate both elastic and viscous parameters of the geological medium. Structural rock mass elements are known to have rheological properties, i.e. they can be deformed with time under constant loading or release stresses in case of constant deformation. In simulations, equations of state generally include elastic and viscous elements. The number of such elements and their combinations (serial, parallel) are determined by the available experimental data. Definitely, the basic model envisages elastic deformation (Hooke body). As shown above, the elastic response is clearly manifested in case of rapid pressure changes and nearby strong earthquakes (co-seismic effect). Data on long-term variations of strain provide for estimation of effective viscous parameters, and the simplest viscoelastic models consisting of two elements are analysed as follows:

$$\text{Maxwell body } \dot{\varepsilon} = \sigma/\mu + \sigma/\eta, \varepsilon' = \sigma'/\mu + \sigma/\eta \quad (5)$$

and

$$\text{Kelvin body } \sigma = \eta \cdot \dot{\varepsilon} + \mu \cdot \varepsilon, \sigma = \eta \cdot \varepsilon' + \mu \cdot \varepsilon, \quad (6)$$

where σ and ε are tangential stresses and strain; μ is shear modulus; η is viscosity; ε' is differentiation of strain in time, t . The deviatoric form of (5) and (6) is due to the fact that viscous deformation does not change the volume.

Based on the experimental results concerning shear deformation progress / tilting and the simple concepts of stress changes from 1985 to 1989 $\sigma \neq 0$ and later on $\sigma = 0$, we use the Kelvin model and consider the strain attenuation curve at azimuth -33°N in the main gangway of the shaft tunnels; this direction is orthogonal to the Talaya stream valley, where in a zone of fracturing is revealed [Timofeev et al., 2012], and to the Main Sayan fault located a few kilometres to the north of the station (Fig. 10). There is an approximate correlation between the notion of the zero component at azimuth -33°N and principal strain orientations in the given period according to strain data obtained by rod- and laser measurement systems.

The rheological equation for a solid Kelvin body is obtained from a simple algebraic combination of equations for a solid Hooke and a Newtonian fluid. For strain, it can be written as follows:

$$e(t) = e_0 \cdot \exp(-t/T) [e_0 + 0.5\eta \int P_0 \cdot \exp(t/T) dt], \quad (7)$$

where e is deformation at time t ; e_0 is initial deformation; P_0 is instant stress; η is viscosity; t is time;



Рис. 11. Gangway located 50 m from the entrance to the shaft tunnel.

Quartz tidal slope meters installed on the pedestal (April 2014). In the zone of intrusion, the shaft tunnel walls are composed of crystalline schist and skapolite-amphibole-diopside gneiss. See zoomed-in photos of points marked by arrows in Fig. 12 and 13.

Рис. 11. Штрек в 50 метрах от входа в штольню.

Кварцевые приливные наклонометры на постаменте (апрель 2014 года). Породы, слагающие стены штольни в зоне интрузии – кристаллосланцы и гнейсы скаполит-амфибол-диопсидовые. Увеличенное изображение точек, указанных стрелками, показано на рис. 12 и 13.

$T = \eta/\mu$ is time constant or lag time for rigid-viscous movement; μ is shear module.

In case of permanent stress (1985–1989), $P_0 = \text{const}$, and equation (6) is as follows:

$$e = \frac{P_0}{2\mu_s} + \left(e_0 - \frac{P_0}{2\mu_s} \right) \cdot \exp\left(\frac{t}{T}\right). \quad (8)$$

After 1989, $P_0 = 0$:

$$e = e_0 \cdot \exp(-t/T). \quad (9)$$

A value of viscosity, η_s is determined from the strain attenuation curve and equation (9) as follows:

$$\psi(t) = [11 \cdot e^{(-t/T)} - 2], \quad (10)$$

where $\psi(t)$ is deformation (tilt of the ground surface at azimuth -33°N).

Figure 10 shows attenuation in case of recalculations of variations for azimuth -33°N in the N-S and E-W directions, and the curve based on experimental data covering 30 years of observations at Talaya Seismological Station. In our analysis of these data, time

constant, T is 10 years. For $\mu_s = 20\text{GPa}$, the effective viscosity of the crustal material, η_s amounts to $6.3 \cdot 10^{18}$ Pa·sec.

Based on the available measurement data, it is possible to estimate an additional local stress of the crust from the maximum tilt value:

$$\sigma_{zx} = \mu_s \cdot e. \quad (11)$$

For $e = 5 \times 4.8 \cdot 10^{-6}$ and $\mu_s = 20\text{GPa}$, the variable portion of the tectonic crustal stress, σ_{zx} amounts to 5 bar (0.5 MPa).

Estimating the size of the area being representative for tilt observations is complicated due to the following factors: in the area of Talaya Seismic Station, the terrain is strongly dissected; a zone of fracturing strikes along the Talaya stream valley; the Main Sayan fault zone is located 3 km to the north of the station. Based on the recorded tilt variations (from 0.1 to 3 arc-seconds per year) and velocities of vertical movements (according to space geodesy techniques, 1–3 mm per year) [Timofeev et al., 2013], the size of the zone can be estimated from the following ratio of the annual tilt rate:

$$\Delta\psi = \Delta h/l, \quad (12)$$

where l is size of deformation area; Δh is velocity of vertical movements.

For different rate, the estimated size of the deformation zone varies from 100 m to 6 km.



Fig. 12. Crystalline schist and gneiss in the shaft tunnel wall.

Рис. 12. Породы, слагающие стену штольни, – кристаллосланцы и гнейсы.



Fig. 13. Large mica inclusions in the shaft tunnel wall.

Рис. 13. Породы, слагающие стены штольни, – крупные включения слюды.

5. CONCLUSION

Determining the rheological parameters of rocks *in situ* is discussed. In the shaft tunnel of Talaya Seismological Station, it is possible to measure deformations from 0.1 nanostrain level (1 nanostrain = 10^{-9}). How-

ever, cavity and thermal effects can distort the obtained parameters. Such effects should be taken into account during developing observation in well or in tunnel. The petrophysical studies of the core samples yielded elastic parameters of the bedrocks in the Talaya stream valley (Archean marble) as follows: $\mu=G=2 \cdot 10^{10}$ Pa for the shear modulus, and $\nu=0.17$ for the Poisson ratio. The tilt measurement database covering 30 year period provided for strainattenuation analyses. Using the viscoelastic Kelvin model and the experimental curve, we estimated the apparent viscosity of rocks in the shaft tunnel: $\eta s \approx 10^{19}$ Pa·sec.

In our experiments, the obtained parameters are representative for the area ranging from 0.1 km to 6.0 km, i.e. may be valid to the underground gallery, the Talaya stream valley and the Main Sayan fault zone. In the shaft tunnel, viscoelastic behaviour of the rocks may be outcome of their composition and fine structure (see Fig. 5, 11, 12 and 13). In the Talaya stream valley and the Main Sayan fault zone, viscoelastic behaviour may be caused by the impact of the linear fracturing zone (striking along the valley and along the fault strike) which is characterized by high water-cut. The reported rheological parameters of the geological medium can be useful for modelling of tectonic, co-seismic and post-seismic effects.

The study was supported by Integration Project No. 76 in the Siberian Branch of RAS, RAS Presidium Project No. 4.1, and RAS Project No. ONZ 6-2.

6. REFERENCES

- Blair D., 1977. Topographic, geologic and cavity effects on the harmonic content of tidal strain. *Geophysical Journal International* 48 (3), 393–405. <http://dx.doi.org/10.1111/j.1365-246X.1977.tb03679.x>.
- Boiko E.V., Timofeev V.Yu., Ardyukov D.G., 2012. Rotation and Deformation of Tectonic Plates. Rotation of the Amur Plate and Deformation of the Baikal Rift According to Space Geodesy Data. LAMBERT Academic Publishing, 176 p. (in Russian) [Бойко Е.В., Тимофеев В.Ю., Ардюков Д.Г. Вращение и деформация тектонических плит. Вращение Амурской плиты и деформации Байкальского рифта по данным космической геодезии. LAMBERT Academic Publishing, 2012. 176 с.].
- Bulanzhe Yu.D., Gridnev D.G., Davydov V.I., Tenenbaum S.G., Vlasov B.V., 1975. Quartz inclinometer NK-1. In: Tidal deformation of the Earth. Nauka, Moscow, p. 149–157 (in Russian) [Буландже Ю.Д., Гриднев Д.Г., Давыдов В.И., Тененбаум С.Г., Власов Б.В. Кварцевый наклонмер НК-1 // Приливные деформации Земли. М.: Наука, 1975. С. 149–157].
- Calais E., Vergnolle M., Deverchere J., San'kov V., Likhnev A., Amariargal S., 2002. Are post-seismic effects of the M=8.4 Bolnay earthquake (23 July 1905) still influencing GPS velocities in the Mongolia-Baikal area? *Geophysical Journal International* 149 (1), 157–168. <http://dx.doi.org/10.1046/j.1365-246X.2002.01624.x>.
- Dehant V., Defraigne P., Wahr J.M., 1999. Tides for a convective Earth. *Journal of Geophysical Research* 104 (B1), 1035–1058. <http://dx.doi.org/10.1029/1998JB900051>.
- Ducarme B., Timofeev V.Yu., Everaerts M., Gornov P.Y., Parovishnii V.A., Van Ruymbeke M., 2008. A Trans-Siberian Tidal Gravity Profile (TSP) for the validation of the ocean tides loading corrections. *Journal of Geodynamics* 45 (2–3), 73–82. <http://dx.doi.org/10.1016/j.jog.2007.07.001>.
- Gridnev D.G., 1975. Quartz air density meter. In: Tidal deformation of the Earth. Nauka, Moscow, p. 130–140 (in Russian) [Гриднев Д.Г. Кварцевый измеритель плотности воздуха // Приливные деформации Земли. М.: Наука, 1975. С. 130–140].
- Gridnev D.G., Timofeev V.Yu., 1989a. The method for determination of rock elasticity modulus. Certificate of Authorship I 1668663. Application I 4685418. 28 April 1989. Registered in the USSR Registry of Inventions on 08 April 1989

- (in Russian) [Гриднев Д.Г., Тимофеев В.Ю. Способ определения модуля упругости горных пород: Авторское свидетельство И 1668663, заявка И 4685418 Приор. из. 28 апр. 1989. Зарег. в Гос. Р. изобр. СССР 8 апреля 1989 г.].
- Gridnev D.G., Timofeev V.Yu., 1989b. The method for determination of rock elasticity modulus. Author Certificate of Authorship I 1557318. Application I 4403402. 04 April 1988. Registered in the USSR Registry of Inventions on 15 December 1989 (in Russian) [Гриднев Д.Г., Тимофеев В.Ю. Способ определения модуля упругости горных пород: Авторское свидетельство И 1557318, заявка И 4403402 Приор. из. 4 апр. 1988. Зарег. в Гос. Р. изобр. СССР 15 декабря 1989 г.].
- Gridnev D.G., Timofeev V.Yu., 1990. Magnetically Controlled Quartz Inclinator. VINITI Deposit, 07.06.90.-I.3214-B-90. Moscow, 10 p. (in Russian) [Гриднев Д.Г., Тимофеев В.Ю. Кварцевый наклономер с магнитным управлением. Депон. ВИНТИ, 07.06.90. – И.3214-В-90. М., 1990. 10 с.].
- Gridnev D.G., Timofeev V.Yu., Sarycheva Yu.K., Anisimova L.V., Masal'sky O.K., Glevsky G.N., Panin S.F., 1990. Ground slopes in Talaya, Southern Baikal. *Geologiya i Geofizika (Russian Geology and Geophysics)* (5), 95–104 (in Russian) [Гриднев Д.Г., Тимофеев В.Ю., Сарычева Ю.К., Анисимова Л.В., Масальский О.К., Глевский Г.Н., Панин С.Ф. Наклоны земной поверхности на юге Байкала (Талая) // Геология и геофизика. 1990. № 5. С. 95–104].
- Harrison J.C., 1976. Cavity and topographic effects in tilt and strain measurement. *Journal of Geophysical Research* 81 (2), 319–328. <http://dx.doi.org/10.1029/JB081i002p00319>.
- Kaban M.K., Yunga S.L., 2000. Influence of density inhomogeneities on the stressed state and seismicity of the lithosphere in the Baikal rift zone. *Doklady Earth Sciences* 371 (3), 542–546.
- Levi K.G., Miroshnichenko A.I., San'kov V.A., Babushkin S.M., Larkin G.V., Badardinov A.A., Wong H.K., Colman S., Delvaux D., 1997. Active faults of the Baikal depression. *Bulletin des Centres de Recherches Exploration-Production Elf-Aquitaine* 21 (2), 399–434.
- Lukhnev A.V., San'kov V.A., Miroshnichenko A.I., Ashurkov S.V., Calais E., 2010. GPS rotation and strain rates in the Baikal–Mongolia region. *Russian Geology and Geophysics* 51 (7), 785–793. <http://dx.doi.org/10.1016/j.rgg.2010.06.006>.
- Melchior P., 1982. The Tides of the Planet Earth. 2-nd Edition. Pergamon Press, 641 p.
- Mel'nikova V.I., Gilyova N.A., Masal'skii O.K., Radziminovich Y.B., Radziminovich N.A., 2009. On generation conditions of strong earthquakes in Southern Baikal. *Doklady Earth Sciences* 429 (2), 1483–1487. <http://dx.doi.org/10.1134/S1028334X09090153>.
- Melnikova V.I., Radziminovich N.A., 1998. Mechanisms of action of earthquake foci in the Baikal region over the period 1991–1996. *Geologiya i Geofizika (Russian Geology and Geophysics)* 39 (11), 1598–1607.
- Ostrovsky A.E., 1978. Ground Deformation Revealed by Observation of Slopes. Nauka, Moscow, 184 p. (in Russian) [Островский А.Е. Деформации земной поверхности по наблюдениям наклонов. М.: Наука, 1978. 184 с.].
- Ozawa I., 1967. Observations of the tidal strains at Osakayama observatory. Part II. *Reports of Disaster Prevention Research Institute, Kyoto University* 10a, 63–75.
- Ozawa I., 1974. Pattern of tidal deformation on the Earth. *Contributions of the Geophysical Institute, Kyoto University* 14, 29–38.
- San'kov V., Deverchere J., Gaudemer Y., Houdry F., Filippov A., 2000. Geometry and rate of faulting in the North Baikal Rift, Siberia. *Tectonics* 19 (4), 707–722. <http://dx.doi.org/10.1029/2000TC900012>.
- San'kov V.A., Levi K.G., Calais E., Déverchère J., Lesne O., Lukhnev A.V., Miroshnichenko A.I., Buddo V.Yu., Zalutskii V.T., Bashkuev Yu.B., 1999. Present-day and Holocene horizontal movements on the Baikal geodynamic test ground *Geologiya i Geofizika (Russian Geology and Geophysics)* 40 (3), 422–430.
- Schwidewski E.W., 1983. Atlas of Ocean Tidal Charts and Maps. *Marine Geodesy* 6 (3–4), 219–265. <http://dx.doi.org/10.1080/15210608309379461>.
- Solonenko A.V., 1993. Symmetry of crustal stress fields in the Baikal rift. *Doklady AN* 328 (6), 674–677 (in Russian) [Солоненко А.В. Симметрия поля напряжений земной коры Байкальского рифта // Доклады АН. 1993. Т. 328. № 6. 674–677].
- Timofeev V.Y., Anisimova L.V., Ducarme B., Sarycheva Y.K., Gridnev D.G., Masal'skii O.K., 1999. Effective viscosity of the crust estimated from tilt measurements in the zone of the Main Sayan Fault. *Geologiya i Geofizika (Russian Geology and Geophysics)* 40 (10), 1475–1482.
- Timofeev V.Y., Ardyukov D.G., Boyko E.V., Griбанова E.I., Semibalamut V.M., Timofeev A.V., Yaroshevich A.V., 2012. Strain and displacement rates during a large earthquake in the South Baikal region. *Russian Geology and Geophysics* 53 (8), 798–816. <http://dx.doi.org/10.1016/j.rgg.2012.06.007>.
- Timofeev V.Y., Ducarme B., Saritcheva Y.K., Vandercoilden L., 2000. Tidal analysis of quartz-tiltmeter observations 1988–1998 at the Talaya Observatory (Baikal rift). *Marees Terrestres. Bulletin D'Informations* 133, 10447–10458.
- Timofeev V.Y., Ducarme B., Van Ruymbeke M., Gornov P.Y., Everaerts M., Griбанова E.I., Parovyshnii V.A., Semibalamut V.M., Woppelmann G., Ardyukov D.G., 2008. Transcontinental tidal transect: European Atlantic coast – Southern

Siberia – Russian Pacific coast. *Izvestiya, Physics of the Solid Earth* 44 (5), 388–400. <http://dx.doi.org/10.1134/S1069351308050042>.

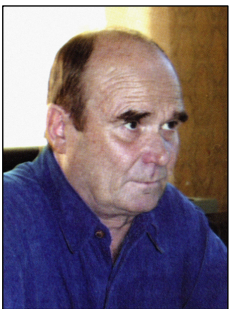
Timofeev V.Yu., Kalish E.N., Stus' Yu.F., Ardyukov D.G., Arnautov G.P., Smirnov M.G., Timofeev A.V., Nosov D.A., Sizikov I.S., Boiko E.V., Griбанова E.I., 2013. Gravity variations and recent geodynamics of the south–western part of the Baikal region. *Geodynamics & Tectonophysics* 4 (2), 119–134 (in Russian) [Тимофеев В.Ю., Калиш Е.Н., Стусь Ю.Ф., Ардюков Д.Г., Арнаутков Г.П., Смирнов М.Г., Тимофеев А.В., Носов Д.А., Сизиков И.С., Бойко Е.В., Грибанова Е.И. Вариации силы тяжести и современная геодинамика юго-западной части Байкальского региона // *Геодинамика и тектонофизика*. 2013. Т. 4. № 2. С. 119–134]. <http://dx.doi.org/10.5800/GT-2013-4-2-0094>.

Timofeev V.Yu., Sarycheva Yu.K., Panin S.F., Anisimova L.V., Gridnev D.G., Masalsky O.K., 1994. Studies of ground slopes and deformation in the Baikal rift zone. *Geologiya i Geofizika (Russian Geology and Geophysics)* 35 (3), 119–129 (in Russian) [Тимофеев В.Ю., Сарычева Ю.К., Панин С.Ф., Анисимова Л.В., Гриднев Д.Г., Масальский О.К. Исследование наклонов и деформаций земной поверхности в БРЗ // *Геология и геофизика*. 1994. Т. 35. № 3. С. 119–129].



Timofeev, Vladimir Yu., Doctor of Physics and Mathematics, Head of Laboratory A.A. Trofimuk Institute of Petroleum Geology and Geophysics, Siberian Branch of RAS
3 Akademika Koptuyuga Prosp., Novosibirsk 630090, Russia
Tel.: (383)3356442; ✉ e-mail: timofeevvy@ipgg.nsc.ru

Тимофеев Владимир Юрьевич, докт. физ.-мат. наук, заведующий лабораторией Институт нефтегазовой геологии и геофизики им. А.А. Трофимука СО РАН
630090, Новосибирск, пр. Академика Коптюга, 3, Россия
Тел.: (383)3356442, ✉ e-mail: timofeevvy@ipgg.nsc.ru



Masal'sky, Oleg K., Director
Baikal Branch of Geophysical Survey, Siberian Branch of RAS
128 Lermontov street, Irkutsk 664033, Russia
Tel.: 8(3952)428782

Масальский Олег Константинович, директор Байкальский филиал Геофизической службы СО РАН
664033, Иркутск, ул. Лермонтова, 128, Россия
Тел.: 8(3952)428782



Ardyukov, Dmitriy G., Senior Researcher
A.A. Trofimuk Institute of Petroleum Geology and Geophysics, Siberian Branch of RAS
3 Akademika Koptuyuga Prosp., Novosibirsk 630090, Russia
Tel.: (383)3356442; e-mail: ardjukovdg@ipgg.nsc.ru

Ардюков Дмитрий Геннадьевич, с.н.с. Институт нефтегазовой геологии и геофизики им. А.А. Трофимука СО РАН
630090, Новосибирск, пр. Академика Коптюга, 3, Россия
Тел.: (383)3356442, e-mail: ardjukovdg@ipgg.nsc.ru



Timofeev, Anton V., Engineer
A.A. Trofimuk Institute of Petroleum Geology and Geophysics, Siberian Branch of RAS
3 Akademika Koptuyuga Prosp., Novosibirsk 630090, Russia
Tel.: (383)3356442; e-mail: timofeevav@ipgg.nsc.ru

Тимофеев Антон Владимирович, инженер Институт нефтегазовой геологии и геофизики им. А.А. Трофимука СО РАН
630090, Новосибирск, пр. Академика Коптюга, 3, Россия
Тел.: (383)3356442; e-mail: timofeevav@ipgg.nsc.ru



COMPOSITIONAL AND THERMAL DIFFERENCES BETWEEN LITHOSPHERIC AND ASTHENOSPHERIC MANTLE AND THEIR INFLUENCE ON CONTINENTAL DELAMINATION

A. I. Kiselev, A. V. Ivanov, B. S. Danilov

Institute of the Earth's Crust, Siberian Branch of RAS, Irkutsk, Russia

Abstract: The lower part of lithosphere in collisional orogens may delaminate due to density inversion between the asthenosphere and the cold thickened lithospheric mantle. Generally, standard delamination models have neglected density changes within the crust and the lithospheric mantle, which occur due to phase transitions and compositional variations upon changes of P-T parameters. Our attention is focused on effects of phase and density changes that may be very important and even dominant when compared with the effect of a simple change of the thermal mantle structure. The paper presents the results of numerical modeling for eclogitization of basalts of the lower crust as well as phase composition changes and density of underlying peridotite resulted from tectonic thickening of the lithosphere and its foundering into the asthenosphere. As the thickness of the lower crust increases, the mafic granulite (basalt) passes into eclogite, and density inversion occurs at the accepted crust-mantle boundary ($P=20$ kbar) because the newly formed eclogite is heavier than the underlying peridotite by 6 % (abyssal peridotite, according to [Boyd, 1989]). The density difference is a potential energy for delamination of the eclogitic portion of the crust. According to the model, $P=70$ kbar and $T=1300$ °C correspond to conditions at the lower boundary of the lithosphere. Assuming the temperature adiabatic distribution within the asthenosphere, its value at the given parameters ranges from 1350 °C to 1400 °C. Density inversion at dry conditions occurs with the identical lithospheric and asthenospheric compositions at the expense of the temperature difference at 100 °C with the density difference of only 0.0022 %. Differences of two other asthenospheric compositions (primitive mantle, and lherzolite KH) as compared to the lithosphere (abyssal peridotite) are not compensated for by a higher temperature. The asthenospheric density is higher than that of the lithospheric base. Density inversion occurs if one assumes the presence of the asthenospheric material in the composition similar to that of the primitive mantle or lherzolite KH in amounts no less than 1.40 and 0.83 wt. %, respectively, of the conventionally neutral fluid. This amount of the fluid seems to be overestimated and thus does not fully correlate with the current estimates of the fluid content in the mantle. Therefore, the most appropriate material for delamination of the thickened lithosphere is only the fluid-bearing asthenosphere which composition corresponds to that of the depleted mantle of middle-ocean ridges (DMM) being the reservoir existing from the Precambrian. In our model, abyssal peridotite is most similar to DMM as compared with other more fertile compositions of the lithosphere. Heat advection due to uplift of fluid-bearing plumes that occurred much time after collisional events may initiate repeated delamination of gravitationally instable parts of the orogenic and cratonic lithosphere.

Key words: delamination, lithosphere, asthenosphere, collisional orogen, craton, eclogites.

Recommended by S.I. Sherman

For citation: Kiselev A.I., Ivanov A.V., Danilov B.S. 2015. Compositional and thermal differences between lithospheric and asthenospheric mantle and their influence on continental delamination. *Geodynamics & Tectonophysics* 6 (2), 255–265. doi:10.5800/GT-2015-6-2-0180.

Вещественные и термальные различия между литосферной и астеносферной мантией и их влияние на континентальную деляминацию

А. И. Киселев, А. В. Иванов, Б. С. Данилов

Институт земной коры СО РАН, Иркутск, Россия

Аннотация: В коллизионных орогенах нижняя часть литосферы может отслаиваться (деляминировать) из-за возникшей инверсии плотностей между астеносферой и более холодной утолщенной литосферной мантией. Обычно в моделях деляминации не рассматриваются плотностные изменения в коре и литосферной мантии, обусловленные фазовыми переходами и вариациями минерального состава при изменении Р-Т условий. Мы акцентируем внимание на том, что эти эффекты могут быть очень важными, возможно преобладающими, по отношению к эффекту простого изменения термальной структуры мантии. В статье изложены результаты численного моделирования с помощью программного комплекса «Селектор» эклогитизации базальтов нижней коры, а также изменения фазового состава и плотности нижележащего перидотита, обусловленных тектоническим утолщением литосферы и ее погружением в астеносферу. Для нижней коры с увеличением глубинности основные гранулиты (базальты) переходят в эклогиты. При этом на принятой границе – корамантия (Р=20 кбар) отмечается инверсия плотностей, так как новообразованный эклогит на 6 % тяжелее нижележащего перидотита (абиссального перидотита по Ф. Бойду). Разница в плотностях является потенциальной энергией деляминации эклогитовой части коры. По условиям моделирования нижней границе литосферы соответствуют Р=70 кбар и Т=1300 °С. Принимая адиабатическое распределение температуры в астеносфере, ее значение при данных параметрах оценивается в пределах 1350–1400 °С. Инверсия плотности в сухих условиях достигается только при изохимичности составов литосферы и астеносферы за счет перепада температур в 100 °С. Однако разница в плотностях при этом составляет всего 0.0022 %. Вещественные различия двух других модельных составов астеносферы (примитивная мантия, лерцолит КН) по отношению к литосфере (абиссальному перидотиту) не компенсируются более высокой температурой. Плотность астеносферы получается более высокой, чем плотность низов литосферы. Инверсия плотностей достигается, если допустить присутствие в составе астеносферы, аналогичном примитивной мантии, или лерцолиту КН, соответственно, не менее 1.40 и 0.83 мас. % условно нейтрального флюида. Такое количество флюида явно завышено и совершенно не согласуется с современными оценками содержания флюидов в мантии. Следовательно, только флюидосодержащая астеносфера, отвечающая составу деплетированной мантии срединно-океанических хребтов (ДММ) – резервуару, существующему с докембрия, – является наиболее подходящей средой для деляминации утолщенной литосферы. В настоящей модели абиссальный перидотит ближе всего соответствует ДММ по отношению к другим более фертильным составам астеносферы. Адвекция тепла, связанная с подъемом флюидосодержащих плюмов, далеко отстоящих по времени от коллизионных событий, также может вызывать гравитационную нестабильность орогенной и кратонной литосферы и ее деляминацию.

Ключевые слова: деляминация, литосфера, астеносфера, коллизионный ороген, кратон, эклогиты.

1. INTRODUCTION

Mechanical exfoliation and removal of lower parts of the mantle lithosphere are typically termed as delamination, no matter which mechanism they result from. The term 'delamination' was introduced by *P. Bird* [1979] who used it to describe how the lithospheric mantle is peeled off from the overlying crust due to uplifting and emplacement of the asthenospheric material between them. In [Houseman et al., 1981], another mechanism was proposed for gravitational (convective) instability of the base of the tectonically thickened lithosphere accompanied by complete or partial separation of its mantle part and its foundering into the as-

thenosphere. Another commonly used term is 'mantle unrooting' [Marotta et al., 1998].

Fairly recently, delamination has been referred to as an alternative explanation for rapid regional uplift and extension, accompanied by lithospheric thinning and increased magmatic production within mobile belts [Peccherillo, Lustrino, 2005]. Delamination involves an abrupt separation and rapid foundering of the lower tectonically thickened lithosphere into the asthenospheric mantle due to density inversion at the post-collisional stage. A potential energy that drives this process is released as the hot low-density asthenospheric mantle replaces the separated part of the cold dense lithosphere and interacts with its remaining

thinned part. Thermal and mechanical effects of the asthenosphere on lithosphere thinned by delamination is considered as a main cause of post-collisional magmatism, including batholith formation within mobile belts which undergone strong tectonic thickening during the collision. The purpose of the present discussion is to study by means of numerical modeling the effect of compositional differences between the lithosphere and the asthenosphere as well as the phase transition for possibilities of mechanical destruction of the lower lithosphere after its tectonic thickening. Some consequences of delamination in terms of structure and composition are discussed.

2. PHYSICAL AND CHEMICAL BASIS FOR DELAMINATION FOR THE LOWER CONTINENTAL LITHOSPHERE

The lithosphere is usually considered as the strong mobile surface layer resistant to the high tangent (up to 1 kbar) tension, despite the less strong underlying asthenosphere. It should be emphasized that the definition of the lithosphere relies on rheological characteristics, but does not take into account the composition that changes laterally from continents to oceans especially at the crustal level. In the context of rheology, the lithosphere is a bilayer. The upper mechanical boundary layer (MBL) possess properties of an elastic rigid body exposed to fragile destruction [Anderson, 1994]. A thermal boundary layer (TBL) is situated below the isotherm of 650 ± 100 °C; within its limits, the lithosphere behaves as a viscous (fragile-elastic) fluid capable to flow but transferring deep-seated heat by conduction from depths where the temperature is close to the temperature of solidus of mantle rocks. The lifetime of TBL depends on its growth rate and viscosity. Its own weight is a cause of its instability. If TBL occurs at a plume side or it thickens in orogenic belts, it became instable. The lower part of TBL cannot resist high stresses and remains bounded with the mechanical boundary layer during a long period of time. The continental lithosphere is destroyed by partial or complete separation of TBL due to its convective instability resulting from quick thickening, and such destruction is defined as 'thermal thinning' [Houseman et al., 1981] analogous to 'delamination'.

According to evaluations of the surface heat flow and the available seismological and thermodynamic data, the oceanic lithosphere thickness ranges from 75 to 100 km, and the continental lithosphere thickness amounts to 200+ km.

Stabilization of the lithosphere is determined not only by simple cooling of the mantle substance but its chemical stratification. A newly formed oceanic crust is hot and thin in zones of spreading. Changes of the lithosphere thickness are controlled by dynamics of its heat

balance. As the lithosphere moves away from constructive boundaries, its thickness increases due to slow conductive cooling. The lithostatic equilibrium between the lithosphere and the asthenosphere is governed by partial melting of the ascending asthenospheric matter at the boundary between plates and differential moving of melting and solid phases. Upon removal of the basaltic liquid from the asthenospheric peridotitic substrate, its density decreases due to the loss of the iron part, while the solidus temperature increases. However, basaltic liquid extraction cools the asthenospheric mantle; the process which partially compensate the decrease of density [Jordan, 1978].

In general cases, when thermal and compositional parameters determining the mantle lithosphere are combined, the lithosphere density is lower than that of the underlying asthenosphere. However, during compression, the lithosphere becomes denser, thicker and more instable due to its quasithermal 'transition' into the asthenosphere. Under such conditions, the lithosphere may delaminate itself, i.e. it can exfoliate in its lower part but only after a critical amount of reduction determined by the difference between densities of the asthenospheric and lithospheric mantle at specific P-T parameters. A theoretical possibility of the lithosphere excessive density relative to the asthenosphere may be realized in collisional orogens where compressive thickening of the lithosphere is followed by extension. Delamination is crucial in this case.

Together with thickening of the lithosphere, the phase transition of basalt into denser modification-eclogite [Ringwood, Green, 1969] makes a significant contribution to inversion of densities between the lithosphere and the asthenosphere. The low-pressure pyroxene-plagioclase-olivine paragenesis of minerals passes into a high-pressure eclogite composed of pyrope garnet and omphacite. The density of eclogite is similar to or may exceed the density of underlying mantle. Eclogitization may occur both in the lower crust and the lithospheric mantle. If basaltic melts pass into eclogites in the mantle, each 10 % of eclogite will increase its density by 1 % [Kay, Kay, 1993]. The contribution of the lower crust in delamination depends on its density, which determines the direction of movement of the lower crust material. In continental regions with the crust thinner than 45 km, the density of the lower crust of any composition must be lower than that of the mantle. In this case, the crust material can flow (especially in the presence of melt) laterally or towards the surface. Conversely, in the regions where compression results in thickening of the crust to 50 km and more (up to 70 km in Tibet), the density of rocks of basaltic composition in the lower crust is increased to higher values at the transition into eclogites and the trend to foundering. According to [Sobolev, Babeyko, 1989], the crust thickness can reach maximum values

at phase transitions because the rocks of basaltic composition are classified (by their density and seismic velocities) as 'crust' if they are gabbroid in terms of mineralogy, but as 'mantle' if eclogitic. Thus, only the lithospheric mantle is assumed as gaining the negative buoyancy, and the lowest part of the thickened crust (if it is of basaltic composition) also contributes to the negative buoyancy. In regions with the thick crust, when the lithospheric mantle delaminates, the lower part of the crust delaminates also. Thermal thinning without advection of heat as an alternative to delamination is unrealistic since conductive mass transport and radioactive heating are very slow [Yuen, Fleitout, 1985]. Heating and softening of a large volume of the lithospheric mantle for its transition into the asthenosphere are impossible during short-time intervals corresponding to the observed tectonic transformations in the orogenic zones.

3. NUMERICAL MODELING OF PHASE AND DENSITY CHANGES IN THE CONTINENTAL LITHOSPHERE DURING ITS TECTONIC THICKENING

Generally, standard delamination models have neglected density changes within the crust and the lithospheric mantle which occur due to phase transitions and compositional variations during tectonic thickening. Our attention is focused on effects of phase and density changes that may be very important and even dominant when compared to effect of a simple change of the thermal mantle structure. This section reports results of numerical modeling of the basaltic lower crust eclogitization as well as changes of phase composition and density of the underlying peridotite, which result from tectonic thickening of the lithosphere and its foundering into the asthenosphere.

Our concept of the delamination model is illustrated in Figure 1 that shows geotherm positions and lithosphere sections before and after lithospheric thickening followed by delamination. Data on accepted model compositions of the lower crust, lithospheric mantle and asthenosphere are given in Table 1. Chemically, the lower crust is presented by quartz tholeiite and alkaline olivine basalt used in the experiments to study the phase transition of basalt into eclogite [Ringwood, Green, 1969]. The composition of abyssal peridotite characterizing of the post-Archean lithosphere [Boyd, 1989] is used in the model as the analogue of the lithospheric mantle. A quantitative determination of the bulk composition of the asthenosphere is indistinct. Thus, the primitive mantle (A1) after [McDonough, 1990] and abyssal peridotite (A3) are accepted as two-side constraints of its composition. Moderately depleted spinel lherzolite from Kilbourne Hole (Mexico) is accepted as the model composition of the asthenosphere (A2), which is intermediate between compositions

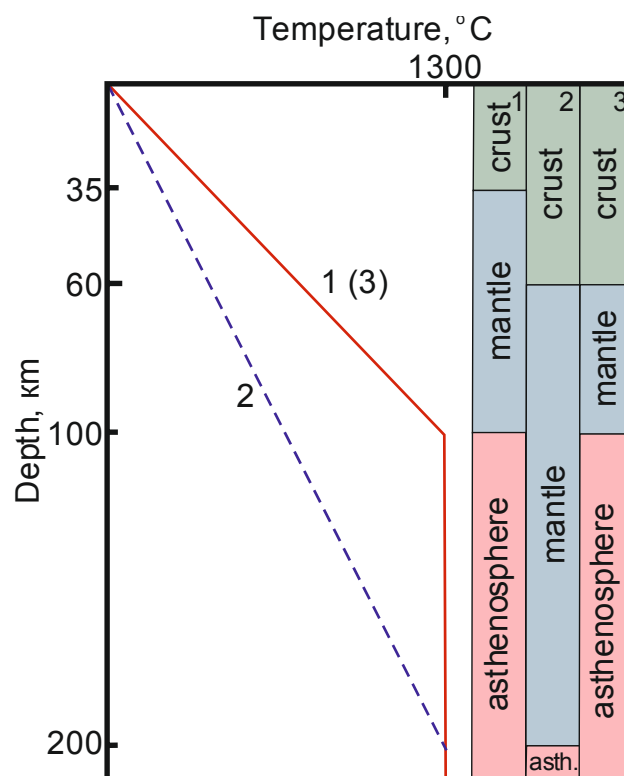


Fig. 1. Lithospheric sections and geotherm positions before and after tectonic thickening followed by delamination. From [England, Houseman, 1989], with minor additions.

Рис. 1. Традиционное отображение литосферных разрезов и положений геотерм до и после тектонического утолщения с последующей деляминацией (по [England, Houseman, 1989], с минимальными дополнениями).

sphere (A2), which is intermediate between compositions of the primitive mantle and abyssal peridotite [Basaltic volcanism..., 1981]. It should be noted that the primitive mantle is the most dense and fertile among possible bulk model compositions of the asthenosphere that is depleted, to a certain degree, in the basaltic component and, most likely, consistent with the asthenosphere of early stages of the mantle evolution in the Early Precambrian.

Besides, there is geological evidence concerning the asthenosphere composition. Some peridotitic orogenic massifs (Lanzo in Italy, Lerz in France and others) are considered as examples of local contacts and the lithosphere-asthenosphere boundary [Menzies et al., 1991]. Within these massifs, unmetasomatized porphyroclastic plagioclase and spinel peridotites, that are compositionally similar to DMM (depleted mantle of the mid-ocean ridges), are assigned to the asthenospheric substance. It is believed that DMM, which fragments are alpinotype ophiolites and abyssal peridotites, represent a global reservoir existing from the Precambrian,

Table 1. Model compositions of the lower crust (1, 2), the lithospheric mantle (3), and the asthenosphere (3, 4, 5)

Таблица 1. Модельный состав нижней коры (1, 2), литосферной мантии (3) и астеносферы (3, 4, 5)

| Oxides | Quartz tholeiite poor in alkaline | Alkaline olivine basalt | Abyssal peridotite A3 | Spinel lherzolite A2 | Primitive mantle A1 |
|--------------------------------|--------------------------------------|----------------------------|--------------------------|-------------------------|------------------------|
| | 1 | 2 | 3 | 4 | 5 |
| SiO ₂ | 49.88 | 45.39 | 43.60 | 44.80 | 44.80 |
| TiO ₂ | 2.14 | 2.52 | 0.02 | 0.12 | 0.21 |
| Al ₂ O ₃ | 13.89 | 14.69 | 1.18 | 3.34 | 4.45 |
| Fe ₂ O ₃ | 2.84 | 1.87 | 0.00 | 0.00 | 0.00 |
| FeO | 9.65 | 12.42 | 8.22 | 8.72 | 8.40 |
| MgO | 8.48 | 10.37 | 45.20 | 39.24 | 37.20 |
| CaO | 10.82 | 9.14 | 1.13 | 3.14 | 3.60 |
| Na ₂ O | 1.84 | 2.62 | 0.02 | 0.27 | 0.34 |
| K ₂ O | 0.08 | 0.78 | 0.00 | 0.03 | 0.03 |
| P ₂ O ₅ | 0.22 | 0.02 | 0.00 | 0.01 | 0.02 |
| MnO | 0.16 | 0.18 | 0.14 | 0.00 | 0.14 |
| Cr ₂ O ₃ | 00.00 | 0.00 | 0.22 | 0.46 | 0.43 |
| NiO | 0.00 | 0.00 | 0.00 | 0.26 | 0.27 |
| Сумма | 100.00 | 100.00 | 99.73 | 100.07 | 99.89 |

Note. 1–2 – data from [Ringwood, Green, 1969], 3 – [Boyd, 1989], 4 – [Basaltic volcanism..., 1981], 5 – [McDonough, 1990].

Примечание. 1–2 – [Ringwood, Green, 1969], 3 – [Boyd, 1989], 4 – [Basaltic volcanism..., 1981], 5 – [McDonough, 1990].

of which the asthenosphere forms a part [Menzies, 1989].

The Selector software complex [Karpov et al., 1997] was used for calculations of equilibrated mineral assemblages from the accepted bulk compositions (Table 1) and P-T parameters corresponding to the geotherm characteristic for the tectonically thickened lithosphere (Fig. 2). One of the starting conditions for modeling is that thickening proceeds under isothermal conditions at the constant temperature of the lowermost lithosphere (1300 °C) followed only by the decrease of the temperature gradient in the lithospheric column. In this model, the temperature of the asthenosphere at a depth of 200 km is 1400 °C, according to the adiabatic gradient about 0.5 °C/km. Thus, the lithospheric section, including the lower crust and the lithospheric mantle, and the upper asthenosphere represent three thermodynamically closed systems building on each other with the given bulk composition and relevant P-T parameters. Our model aimed at determination of equilibrated mineral assemblages and their densities within the range of pressure and temperature values according to the accepted geotherm (Fig. 2) and the list of probable mineral phases (separately for every system), and, finally, elucidation of probable density inversion in zones of transition from the crust to the lithospheric mantle and from the latter to the asthenosphere.

According to the modeling conditions, the chemical compositions/systems representing the lower crust, the lithospheric mantle and the asthenosphere do not contain any fluid phase and can be described by ten

independent components (Al, Ca, Fe, Mg, Mn, K, Na, Si, Ti, and O). A 'neutral' fluid (C-O-H-N) was added to the asthenosphere composition at the final stages of modeling in order to estimate its effect on the density. Intercoordinated data of thermodynamic properties of minerals [Holland, Powell, 1998] were used in the systems for choosing probable dependent components / mineral phases. The chosen phases / minerals are represented by solid solutions in their ideal miscibility and separate components. Below is the list of such solutions (solid solution names are given in italics): Ol (olivine) – *forsterite + fayalite + tephroite*; Opx (orthopyroxene) – *enstatite + ferrosilite*; Cpx (clinopyroxene) – *diopside + hedenbergite + Ca-tschermakite + Mg-tschermakite + acmite + leucite*; Gr (garnet) – *almandine + andradite + grossular + pyrope + spessartine*; Sp (spinel) – *hercynite + Mg-spinel*; Pl (plagioclase) – *albite + anortite*; Mt (magnetite) – *magnetite + magnesioferrite + ulvospinel*; Ilm (ilmenite) – *ilmenite + geikielite + pyrophanite*; And (andalusite); Ky (kyanite); Sil (sillimanite); Cor (corundum); Q (quartz); Crb (cristobalite); Td (tridimite); Co (coesite); St (stishovite); Hm (hematite); Fe (metallic iron); Per (periclae); Ru (rutile).

Volumes of solid solutions components were calculated by the method described in [Holland, Powell, 1998]. The total components volume is equal to the phase volume; therefore, the weight/volume value is the pure rock density. Changes of density with pressure and temperature are related both to phase transitions (spinel-garnet or quartz-coesite type) and redistribution of elements between phases with changes of P-T parameters. Equilibrated assemblages of mineral pha-

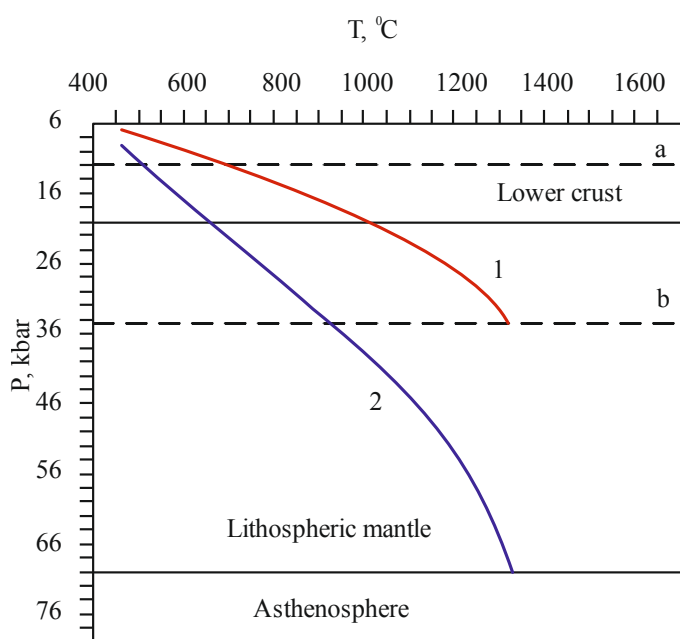


Fig. 2. Geotherms before (1) and after (2) tectonic thickening of the lithosphere.

1 – continental geotherm (50 mWm^{-2}), from [Pollack, Chapman, 1977]. 2 – calculated geotherm provided that the temperature was constant at the lithospheric base ($1300 \text{ }^\circ\text{C}$) before and after thickening. Dotted lines show initial positions of the lower crust base (a) and the lithospheric mantle base (b).

Рис. 2. Геотермы до (1) и после (2) тектонического утолщения литосферы.

1 – континентальная геотерма (50 мВт/м^2), по данным [Pollack, Чарпан, 1977]. 2 – рассчитанная геотерма при условии фиксированной температуры ($1300 \text{ }^\circ\text{C}$) в основании литосферы до и после утолщения. Пунктирными линиями показаны начальные положения основания нижней коры (а) и литосферной мантии (b).

ses, their quantitative composition and density values (Fig. 3) are determined from calculations of equilibrium in the multisystem composed of three systems in the range of $T=400\text{--}1300$ and $1400 \text{ }^\circ\text{C}$ and $P=6\text{--}20$, $20\text{--}70$, $70\text{--}75$ kbar. As the thickness of the lower crust increases, the eclogitic paragenesis replaces the granulitic one, and the density increases considerably. A difference between contents of the major elements in the model composition of the lower crust (Table 1) does not significantly impact the density variability of the newly formed eclogites.

Sharp density inversion occurs at the lower crust-mantle boundary ($P=20$ kbar), where abyssal peridotite is about 6 % lighter than eclogites. A similar situation occurs in the Kwinling-Dubi orogenic belt where the density of unaltered eclogites of the lower crust amounts to $3.47 \pm 0.04 \text{ g/sm}^3$, i.e. 0.2 g/sm^3 higher than that of peridotitic xenoliths representing the upper mantle of the Eastern China [Gao et al., 1999]. A diffe-

rence in the density values mentioned above drives delamination of eclogites and is very important for the evolution of the continental crust and the crust-mantle interaction.

According to the model, the lower lithospheric boundary corresponds to conditions of $P=70$ kbar and $T=1300 \text{ }^\circ\text{C}$. The asthenospheric temperature is $100 \text{ }^\circ\text{C}$ higher. This temperature change is conventionally related to ‘instantaneous’ foundering of the lowermost thickened lithosphere into the hot asthenosphere ($T=1400 \text{ }^\circ\text{C}$). The given assumption follows from the relation of the time interval of tectonic, metamorphic and magmatic events in the collisional orogen evolution and the time interval (that is longer) of thermal relaxation of the thickened lithosphere during conductive heat transfer from depth. The calculated asthenospheric density at the boundary zone is higher than that of the lithosphere (Fig. 3, B). This is related to the fact that compositional differences between the model compositions for the lithosphere (A3 – abyssal peridotite) and the asthenosphere (A1 – primitive mantle, A2 – KH lherzolite) are too significant to be compensated by the accepted temperature differences ($100 \text{ }^\circ\text{C}$) between them. These differences are expressed in different quantities of olivine, garnet, clino- and orthopyroxene contained in the lithospheric mantle and the asthenosphere (Fig. 3, A). Under dry conditions, density inversion due to the temperature difference between the lithosphere and the asthenosphere occurs only if their compositions are similar to each other and comprises 0.0022 wt. %. In this case, density inversion between the asthenosphere represented by A1 and A2 compositions and the lithosphere occurs only if they contain no less than 1.4 and 0.83 wt. % of the conventionally neutral fluid, respectively (Fig. 4). These values exceed the estimated fluid content in the primitive mantle (0.83 wt. %, from [Zotov, 1989]). In case when the 30-km eclogitic crust is added to the 170-km peridotitic mantle, density inversion occurs because the lithospheric mantle becomes denser by about 1 %.

The available estimates of the fluid content for the entire mantle are uncertain and range between relatively low values from 0.04 % [Dreibus et al., 1997] to 0.1 % for H_2O [Ringwood, 1966] and 0.83 % for the complex fluid in the primitive mantle [Zotov, 1989]. This suggests that only the fluid (melt)-bearing as the asthenosphere compatible with the DMM composition is the most appropriate medium for delamination of the tectonically thickened lithosphere. In the proposed model, abyssal peridotite is most closely corresponding to the DMM reservoir. More fertile asthenospheric compositions (lherzolite KH, primitive mantle) can support delamination of the overlying lithosphere only at higher fluid content.

The numerical modeling results suggest, in general, a probability of gravitational instability both at the

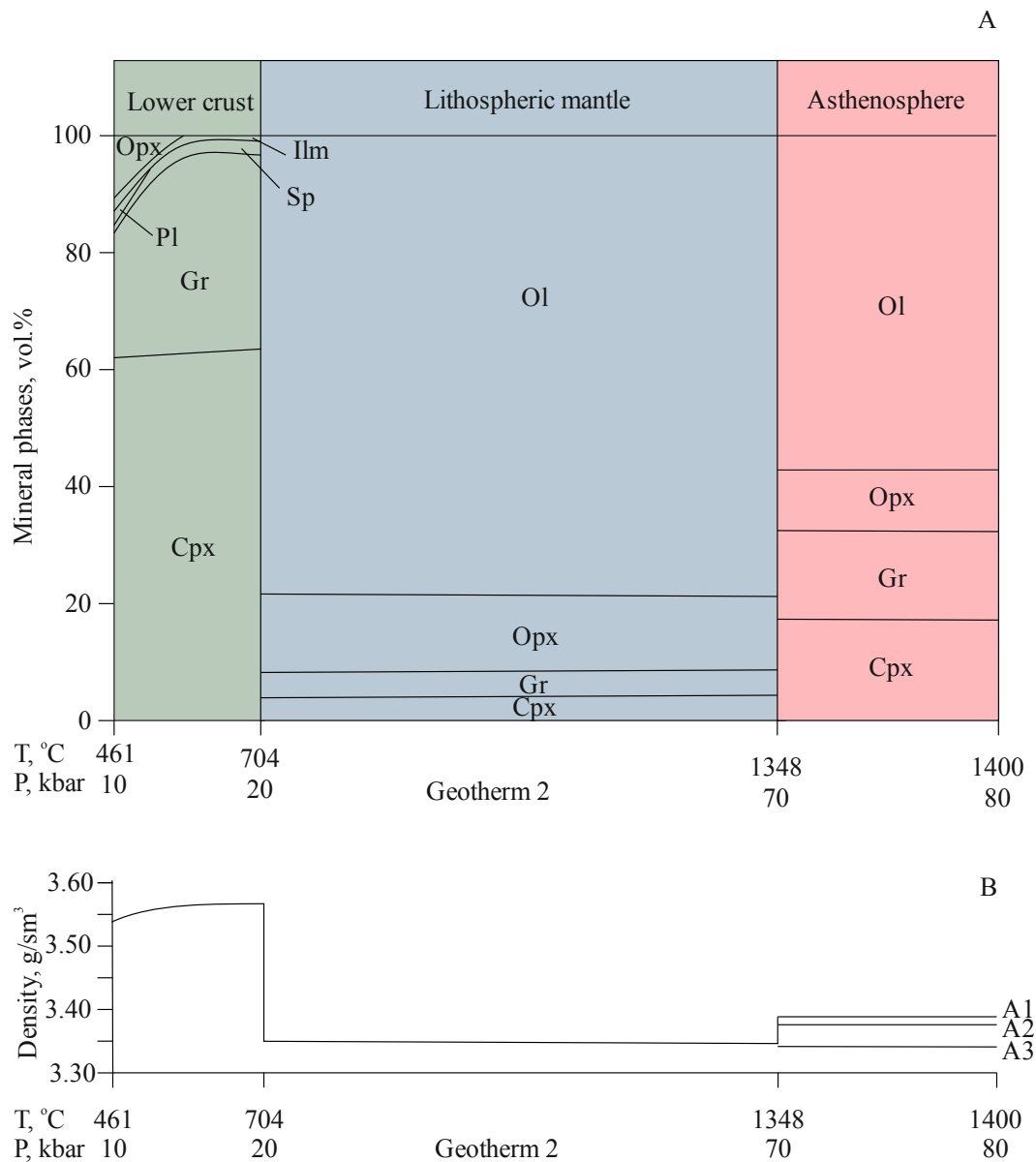


Fig. 3. *A* – results of calculations of equilibrium mineral assemblages for the lower crust, the lithospheric mantle (A3) and the asthenosphere (A1) after tectonic thickening in accordance with geotherm 2. *B* – calculated density and its variations at the boundaries (lower crust – lithospheric mantle – asthenosphere) under dry conditions with different model compositions of the asthenosphere (Table 1, A1, A2, A3).

Рис. 3. *A* – результаты расчетов равновесных минеральных ассоциаций для нижней коры, литосферной мантии (A3) и астеносферы (A1) после тектонического утолщения в соответствии с геотермой 2. *B* – рассчитанные плотности коры, литосферной мантии и астеносферы в сухих условиях с различным модельным составом астеносферы (Табл. 1, A1, A2, A3).

lower crust–mantle boundary under dry conditions resulted from eclogitization of the mafic lower crust and the lithosphere–asthenosphere boundary. At the lithospheric–asthenospheric level, delamination under dry condition is possible only if their compositions are almost the same. In other cases, it is necessary to assume the presence of a certain amount of the fluid-phase or melt in the asthenosphere, which decreases not only its density, but its viscosity as well.

4. TECTONIC CONDITIONS FOR DELAMINATION MAGMATISM

Favorable conditions for delamination occurred within collisional orogens that appeared at regular intervals. Delamination was preceded by lateral shortening and thickening of the crust and the lithosphere. The tectonic increase of the lithospheric thickness after the main stage of deformation was followed by submergence of the lithospheric basement, foundering of

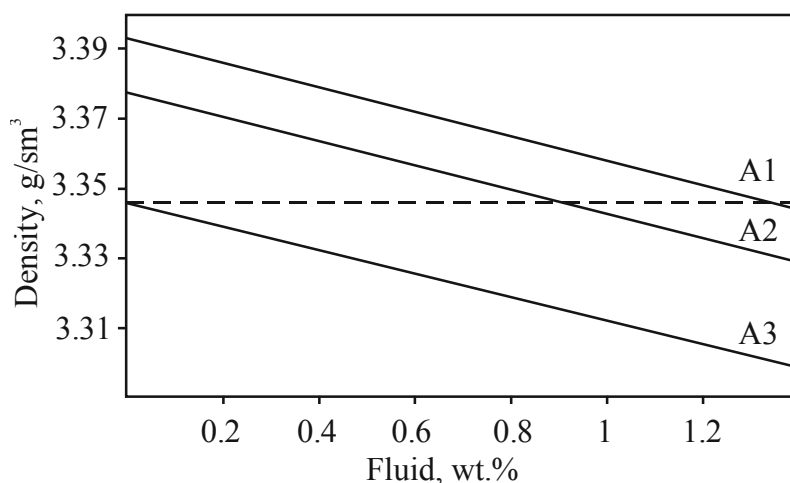


Fig. 4. Density of the model asthenospheric compositions versus their fluid contents (C-O-H-N) at the lithospheric basement ($T=1400\text{ }^{\circ}\text{C}$, $P_{\text{total}}=70\text{ kbar}$). A1 – abyssal peridotite, A2 – spinel-lherzolite KH, A3 – primitive mantle.

Рис. 4. Зависимости плотности модельного астеносферного состава от концентрации флюида (C-O-H-N) в основании литосферы ($T=1600\text{ }^{\circ}\text{C}$, $P_{\text{сумм}}=70\text{ кбар}$).

geotherms, and the decrease of the geothermal gradient relative as compared to the initial state. About 130 Ma [Houseman *et al.*, 1981] are required in case of conductive heating for the return of the isotherms to their original positions after the double thickening of the lithosphere at starting lithospheric thickness of 100 km. In reality, however, the double thickening of the lithosphere in zones of continental convergence may occur during 30–50 Ma, which is consistent with the temporal relationship between deformation, metamorphism and magmatism in the intercontinental mobile folded belts. It follows that conductive heating of the thickened lithosphere cannot provide thermal conditions for regional metamorphism and granitic magmatism during 30–50 Ma.

A significant decrease of the lithospheric thickness resulting from delamination furnishes conditions for quick heating of the remaining part of the lithospheric mantle and the lower crust as regards to the thickened lithosphere, which, in its turn, provides for regional metamorphism and melting of the crust. The hot asthenospheric substance is not only a source of heating; it also produces basaltic melts which propagate to the crustal levels heating the crust. Delamination provides conditions for postorogenic extension and uplifting on sites of its manifestation. In collisional orogens, the thickening of the crust prior to delamination (thus increase of pressure of crustal rocks) was followed by metamorphism of the crustal rocks with eclogitic facies in the lowermost crust. Delamination invoked the increase of heat flow, magmatism and postorogenic extension, formation of gently pitching structures of extension with pure shear at deep levels of the crust and

simple displacement with detachment at levels of the upper crust. Postdelamination collapse due to exfoliation of the lithospheric root is characterized by extension in the form of transtension and isothermal uplift of the territory. Vertical shortening of the crust thickness during this stage is exemplified by development of subhorizontal gneiss structures with plates of granites intruded in the zone of shearing below of the upper crust extending detachment. Formation of the large volume of granites is synchronous with rapid lithospheric thinning involving weakness of the crust and its extension. Within metamorphic rocks of amphibolite facies, the subhorizontal structures of extension comprise numerous lens-shaped boudins, i.e. remains of the eclogitic facies formations with structures of early subvertical compression indicating the presence of the eclogitic basement of the crust at the stage of its thickening [Dewey, 1995].

Evidence of delamination under the areas that recently underwent tectonic thickening are rapid uplifting and changes in tension field, tangible changes in crustal and mantle magmatism, which reflect changes in thermal and compositional structures of the lithosphere. Criteria that indicate delamination tectonics and magmatism in the Cenozoic are discovered, for example, in the southern Puna Plateau in Central Andes [Kay, Kay, 1993] and the northern Tibetan plateau [Beghoul *et al.*, 1993].

P. Bird [1979] introduced the term ‘delamination’ to describe the mechanism explaining the formation of the Colorado plateau. The Puna Plateau in Argentina is the most significant example of delamination in the recent past. The presence of a seismic ‘window’, i.e. the

lack of earthquakes under this plateau, geochemical peculiarities of mafic lavas within its boundaries (OIB-type) are due to delamination of the continental lithosphere part. The delaminated block comprising the crustal and mantle parts of the lithosphere was involved in the circulating asthenospheric system below the submerging slab. Examples of structural and compositional evidences of delamination in other young orogens are also numerous [Girbacea, Frisch, 1998].

It is likely that delamination was more common process during supercontinental accretion. It could be an important element in the mechanism of generation of the sialic crust in the Archean [Rudnik, 1995] as well as shortening of the thick cratonic lithosphere in periods of upwelling of the low-dense hot mantle material to the cratonic basement [O'Reilly et al., 1998; Gao et al., 2009]. Together with subduction, delamination is an important factor contributing to lithospheric recycling [Anderson, 2005]. Recognition of delamination-related magmas may be a unique way to recognize past delamination events, because the magmas when compared with other signatures are the most indelible indicators.

5. CONCLUSION

The available geological and geophysical data suggest that in collisional orogens, the lithosphere becomes gravitationally unstable and can be delaminated both by removal of the thickened eclogitic portion of the lower crust and by removal of the mantle lithospheric root, in general, resulting from generated density inversion upon tectonic thickening. Generally, the standard delamination models neglect density changes within the crust and the lithospheric mantle which take place due to phase and composition changes while P-T parameters change. These effects may be very important and they are probably dominant when compared with the effect of a simple change of the thermal structure of the mantle.

Conditions of changes of the lithospheric density

structure are determined from modeling of eclogitization of the lower crust basalts as well as changes of the phase composition and the density of underlying peridotite caused by tectonic thickening of the lithosphere and its foundering into the asthenosphere. While thickness of the lower crust is increasing, the mafic granulites (basalts) pass into eclogites. In this case, density inversion occurs at the crust-mantle boundary (P=20 kbar) because eclogite is by 6 % heavier than underlying peridotite. The difference in the densities is a driving force for delamination of the eclogitic portion of the crust.

Density inversion at the lithosphere-asthenosphere boundary is accomplished only at equilibrium of their chemical compositions due to the temperature difference of 100 °C, and it is no more than 0.0022 %. The compositional difference of two other bulk compositions of the asthenosphere (primitive mantle and lherzolite KH) as compared to the lithosphere is not compensated by its higher temperature. The density of asthenosphere is higher than that of the lowermost lithosphere. Density inversion occurs in case of presence of the conventionally neutral multicomponent (C-O-H-N) fluid in amounts of 1.40 wt. % and 0.83 wt. %, respectively, in the primitive mantle and the lherzolite KH simulating fertile asthenosphere. Consequently, the fluid-bearing asthenosphere corresponding to the composition of the depleted mantle of middle-ocean ridges (DMM) is most suitable for delamination of the lithosphere.

Advection of heat by plumes occurring after collisional events can initiate gravitational instability and delamination of the lowermost lithosphere due to the decrease of the asthenospheric density resulting from the temperature increase and the fluid phase in its composition. This is probably reflected in the tomographic sections of the 'anomalous mantle' of contemporary areas of tectonothermal activity in the form of lateral alterations of relatively high-velocity (cold lithospheric?) and low-velocity (hot asthenospheric) portions of the mantle substance.

6. REFERENCES

- Anderson D.L., 1994. The sublithospheric mantle as the source of continental flood basalts; the case against the continental lithosphere and plume head reservoirs. *Earth and Planetary Science Letters* 123 (1), 269–280. [http://dx.doi.org/10.1016/0012-821X\(94\)90273-9](http://dx.doi.org/10.1016/0012-821X(94)90273-9).
- Anderson D.L., 2005. Large igneous provinces, delamination, and fertile mantle. *Elements* 1 (5), 271–275. <http://dx.doi.org/10.2113/gselements.1.5.271>.
- Basaltic Volcanism Study Project, 1981. Basaltic Volcanism on the Terrestrial Planets. Pergamon Press, Inc., New York, 1286 p.
- Beghoul N., Barazangi M., Isacks B.L., 1993. Lithospheric structure of Tibet and western North America: Mechanisms of uplift and a comparative study. *Journal of Geophysical Research* 98 (B2), 1997–2016. <http://dx.doi.org/10.1029/92JB02274>.
- Bird P., 1979. Continental delamination and the Colorado Plateau. *Journal of Geophysical Research* 84 (B13), 7561–7571. <http://dx.doi.org/10.1029/JB084iB13p07561>.

- Boyd F.R., 1989. Compositional distinction between oceanic and cratonic lithosphere. *Earth and Planetary Science Letters* 96 (1), 15–26. [http://dx.doi.org/10.1016/0012-821X\(89\)90120-9](http://dx.doi.org/10.1016/0012-821X(89)90120-9).
- Dewey J.F., 1995. The fabrics of orogens. In: Centennial Geocongress, South African Geological Society, Extended Abstracts, vol. 1, p. 291–294.
- Dreibus G., Jagoutz E., Wänke H., 1997. Water in the Earth's mantle. *Geologiya i Geofizika (Russian Geology and Geophysics)* 38 (1), 269–275.
- England P., Houseman G., 1989. Extension during continental convergence, with application to the Tibetan Plateau. *Journal of Geophysical Research* 94 (B12), 17561–17579. <http://dx.doi.org/10.1029/JB094iB12p17561>.
- Gao Sh., Zhang B., Jin Zh., Kern H., 1999. Lower crustal delamination in the Qinling-Dabie orogenic belt. *Science in China, Series D: Earth Sciences* 42 (4), 423–433.
- Gao Sh., Zhang J.F., Xu W.L., Liu Y.Sh., 2009. Delamination and destruction of the North China Craton. *Chinese Science Bulletin* 54 (19), 3367–3378. <http://dx.doi.org/10.1007/s11434-009-0395-9>.
- Girbacea R., Frisch W., 1998. Slab in the wrong place: lower lithospheric mantle delamination in the last stage of the Eastern Carpathian subduction retreat. *Geology* 25 (7), 611–614. [http://dx.doi.org/10.1130/0091-7613\(1998\)026<0611:SITWPL>2.3.CO;2](http://dx.doi.org/10.1130/0091-7613(1998)026<0611:SITWPL>2.3.CO;2).
- Holland T.J.B., Powell R., 1998. An internally consistent thermodynamic data set for phases of petrological interest. *Journal of Metamorphic Geology* 16 (3), 309–343. <http://dx.doi.org/10.1111/j.1525-1314.1998.00140.x>.
- Houseman J.A., McKenzie D.P., Molnar P., 1981. Convective instability of a thickened boundary layer and its relevance for the thermal evolution of continental convergent belts. *Journal of Geophysical Research* 86 (B7), 6115–6132. <http://dx.doi.org/10.1029/JB086iB07p06115>.
- Jordan Th.H., 1978. Composition and development of the continental tectosphere. *Nature* 274 (5671), 544–548. <http://dx.doi.org/10.1038/274544a0>.
- Karpov I.K., Chudnenko K.V., Kulik D.A., 1997. Modeling chemical mass transfer in geochemical processes; thermodynamic relations, conditions of equilibria and numerical algorithms. *American Journal of Science* 297 (8), 767–806. <http://dx.doi.org/10.2475/ajs.297.8.767>.
- Kay R.W., Kay S.M., 1993. Delamination and delamination magmatism. *Tectonophysics* 219 (1), 177–189. [http://dx.doi.org/10.1016/0040-1951\(93\)90295-U](http://dx.doi.org/10.1016/0040-1951(93)90295-U).
- Marotta A.M., Fernandez M., Sabadini R., 1998. Mantle unrooting in collisional settings. *Tectonophysics* 296 (1), 31–46. [http://dx.doi.org/10.1016/S0040-1951\(98\)00134-6](http://dx.doi.org/10.1016/S0040-1951(98)00134-6).
- McDonough W.F., 1990. Constraints on the composition of the continental lithospheric mantle. *Earth and Planetary Science Letters* 101 (1), 1–18. [http://dx.doi.org/10.1016/0012-821X\(90\)90119-I](http://dx.doi.org/10.1016/0012-821X(90)90119-I).
- Menzies M.A., 1989. Cratonic, circumcratonic and oceanic mantle domains beneath the western United States. *Journal of Geophysical Research* 94 (B6), 7899–7915. <http://dx.doi.org/10.1029/JB094iB06p07899>.
- Menzies M.A., Bodinier J.L., Thirlwall M., Downes H., 1991. Asthenosphere-lithosphere relationships within orogenic massifs. In: Proceedings of the Fifth International Kimberlite Conference. Araxá, Brazil, p. 281–284.
- O'Reilly S.Y., Griffin W.L., Dyomani Y., 1998. Are lithosphere forever? In: Proceedings of the 7th International Kimberlite Conference. Cape Town, South Africa, p. 646–648.
- Peccerillo A., Lustrino M., 2005. Compositional variations of Plio-Quaternary magmatism in circum-Tyrrhenian area: deep versus shallow mantle processes. In: G.R. Foulger, J.H. Natland, D.S. Presnall, D.L. Anderson (Eds.), Plates, Plumes and Paradigms. Geological Society of America Special Paper, vol. 338, p. 421–434. <http://dx.doi.org/10.1130/0-8137-2388-4.421>.
- Pollack H.N., Chapman D.S., 1977. On the regional variation of heat flow, geotherms, and lithospheric thickness. *Tectonophysics* 38 (3), 279–296. [http://dx.doi.org/10.1016/0040-1951\(77\)90215-3](http://dx.doi.org/10.1016/0040-1951(77)90215-3).
- Ringwood A.E., 1966. The chemical composition and origin of the Earth. In: P.M. Harley (Ed.), Advances in Earth Science. MIT Press, Cambridge, p. 287–356.
- Ringwood A.E., Green D.H., 1969. Phase Transitions. In: P.J. Hart (Ed.), The Earth's Crust and Upper Mantle. AGU Geophysical Monograph Series, vol. 13, p. 637–649. <http://dx.doi.org/10.1029/GM013p0637>.
- Rudnik R.L., 1995. Making continental crust. *Nature* 378 (6557), 571–577. <http://dx.doi.org/10.1038/378571a0>.
- Sobolev S.V., Babeyko A.Y., 1989. Phase transformations in the lower continental crust and its seismic structure. In: R.F. Mereu, S. Mueller, D.M. Fountain (Eds.), Properties and processes of Earth's lower crust. AGU Geophysical Monograph Series, vol. 51, p. 311–320. <http://dx.doi.org/10.1029/GM051p0311>.
- Yuen D.A., Fleitout L., 1985. Thinning of the lithosphere by small-scale convection destabilization. *Nature* 313 (5998), 125–128. <http://dx.doi.org/10.1038/313125a0>.
- Zotov I.A., 1989. About sources of the transmagmaic fluids. In: Physico-chemical analysis of mineral generation. Nauka, Moscow, p. 38–45 (in Russian) [Зотов И.А. К проблеме источника трансмагматических флюидов // Физико-химический анализ процессов минералообразования. М.: Наука, 1989. С. 38–45].



Kiselev, Aleksandr I., Doctor of Geology and Mineralogy, Lead Researcher
Institute of the Earth's Crust, Siberian Branch of RAS
128 Lermontov street, Irkutsk 664033, Russia
Tel.: 8(3952)425434; ✉ e-mail: akiselev@crust.irk.ru

Киселев Александр Ильич, докт. геол.-мин. наук, в.н.с.
Институт земной коры СО РАН
664033, Иркутск, ул. Лермонтова, 128, Россия
Тел.: 8(3952)425434; ✉ e-mail: akiselev@crust.irk.ru



Ivanov, Alexei V., Doctor of Geology and Mineralogy, Lead Researcher
Institute of the Earth's Crust, Siberian Branch of RAS
128 Lermontov street, Irkutsk 664033, Russia
Tel.: 8(3952)427117; e-mail: aivanov@crust.irk.ru

Иванов Алексей Викторович, докт. геол.-мин. наук, в.н.с.
Институт земной коры СО РАН
664033, Иркутск, ул. Лермонтова, 128, Россия
Тел.: 8(3952)427117; e-mail: aivanov@crust.irk.ru



Danilov, Boris S., Candidate of Geology and Mineralogy, Researcher
Institute of the Earth's Crust, Siberian Branch of RAS
128 Lermontov street, Irkutsk 664033, Russia
Tel.: 8(3952)511680; e-mail: boris@crust.irk.ru

Данилов Борис Станиславович, канд. геол.-мин. наук, н.с.
Институт земной коры СО РАН
664033, Иркутск, ул. Лермонтова, 128, Россия
Тел.: 8(3952)511680; e-mail: boris@crust.irk.ru



<http://dx.doi.org/10.5800/GT-2015-6-2-0181>

XXVI ALL-RUSSIA YOUTH CONFERENCE “LITHOSPHERE STRUCTURE AND GEODYNAMICS”, IRKUTSK, RUSSIA, APRIL 20–25, 2015

E. V. Sklyarov, A. A. Dobrynina, A. M. Kononov

Institute of the Earth's Crust, Siberian Branch of RAS, Irkutsk, Russia

Abstract: The report presents a chronicle of the XXVI All-Russia youth conference “Lithosphere structure and Geodynamics”, dedicated to the 85th anniversary of academician Nikolai A. Logachev – outstanding geologist, specialist on the continental rifting. The major events are highlighted and a thematic review of the conference papers is given.

Key words: lithosphere, geodynamics, tectonics, magmatism, metamorphism, geochemistry, hydrogeology, engineering geology, Geographic Information Systems, geophysics, mineralogy, geomorphology.

Recommended by D.P. Gladkochub

For citation: Sklyarov E.V., Dobrynina A.A., Kononov A.M. 2015. XXVI All-Russia youth conference “Lithosphere structure and Geodynamics”, Irkutsk, Russia, April 20–25, 2015. *Geodynamics & Tectonophysics* 6 (2), 267–274. doi:10.5800/GT-2015-6-2-0181.

XXVI ВСЕРОССИЙСКАЯ МОЛОДЕЖНАЯ КОНФЕРЕНЦИЯ «СТРОЕНИЕ ЛИТОСФЕРЫ И ГЕОДИНАМИКА», ИРКУТСК, РОССИЯ, 20–25 АПРЕЛЯ 2015 Г.

Е. В. Скляр, А. А. Добрынина, А. М. Кононов

Институт земной коры СО РАН, Иркутск, Россия

Аннотация: В сообщении представлена хроника проведения XXVI Всероссийской молодежной конференции «Строение литосферы и геодинамика», посвященной 85-летию со дня рождения академика Николая Алексеевича Логачева – выдающегося геолога, специалиста по континентальному рифтогенезу. Освещены основные события и дан тематический обзор докладов конференции.

Ключевые слова: литосфера, геодинамика, тектоника, магматизм, метаморфизм, геохимия, гидрогеология, инженерная геология, геоинформационные системы, геофизика, минералогия, геоморфология.



Рис. 2. Участники конференции во время геологической экскурсии на карьер «Перевал».

Fig. 2. The group of the conference participants who took to the geological excursion to the Pereval Quarry near Slyudyanka, Irkutsk region.

ников совещания приветствовали председатель Оргкомитета Е.В. Скляр и директор ИЗК СО РАН д.г.-м.н. Д.П. Гладкочуб. С 21 по 23 апреля проводились рабочие заседания пяти научных секций, организованных в соответствии с тематикой заявленных докладов. Каждая секция открывалась пленарными докладами ведущих научных сотрудников ИЗК СО РАН. По завершении программы заседаний каждой секции проходило обсуждение представленных докладов и дискуссия по вопросам, связанным с их тематикой. Тематика секций:

Секция 1. Общая геология, тектоника, осадочная геология и палеонтология (21 апреля, утреннее заседание, конвинуеры: чл.-корр. РАН, д.г.-м.н. Е.В. Скляр, ИЗК СО РАН, д.г.-м.н. А.М. Мазабзов, ИЗК СО РАН, З.Л. Мотова, ИЗК СО РАН).

Секция 2. Геохимия, петрология, минералогия и

рудообразование (21 апреля, вечернее заседание, конвинуеры: д.г.-м.н. В.А. Макрыгина, ИГХ СО РАН, д.г.-м.н. А.В. Иванов, ИЗК СО РАН, А.В. Левин, ИЗК СО РАН).

Секция 3. Тектонофизика, современная геодинамика, неотектоника и геоморфология (22 апреля, утреннее заседание, конвинуеры: д.г.-м.н. С.И. Шерман, ИЗК СО РАН, д.г.-м.н. К.Ж. Семинский, ИЗК СО РАН, А.А. Гладков, ИЗК СО РАН).

Секция 4. Геофизика, геофизические методы исследований и геоинформатика (22 апреля, вечернее заседание, конвинуеры: д.г.-м.н. В.С. Имаев, ИЗК СО РАН, д.г.-м.н. В.И. Мельникова, ИЗК СО РАН, к.ф.-м.н. А.А. Добрынина, ИЗК СО РАН).

Секция 5. Гидрогеология, инженерная геология и нефтегенез (23 апреля, утреннее заседание, конвинуеры: д.г.-м.н. Т.Г. Рященко, ИЗК СО РАН,



Рис. 3. Рабочие моменты: геологическая экскурсия на карьер «Перевал», г. Слюдянка (член-корреспондент РАН Е.В. Скляров).

Fig. 3. During the geological excursion to the Pereval Quarry near Slyudyanka, Irkutsk region (E.V. Sklyarov, Corresponding Member of RAS).

к.г.-м.н. Е.А. Козырева, ИЗК СО РАН, В.А. Пеллинен; вечернее заседание, конвинуеры: д.г.-м.н. В.А. Скворцов, ИЗК СО РАН, д.г.-м.н. А.Г. Вахромеев, ИЗК СО РАН, к.г.-м.н. А.М. Кононов, ИЗК СО РАН).

Вечером 23 апреля состоялась стендовая секция, включавшая 27 докладов. В завершение конференции был заслушан доклад члена-корреспондента РАН Е.В. Склярова «Практические советы по подготовке публикаций и презентаций докладов», за которым последовали общая дискуссия и закрытие конференции. 24–25 апреля участники конференции выезжали в Тункинскую впадину, где были проведены следующие экскурсии:

- гидрогеологическая экскурсия «Аршан-Тункинское месторождение углекислых минерально-лечебных вод» (к.г.-м.н. Ю.И. Кустов),

- инженерно-геологическая экскурсия «Селевые потоки в окрестностях поселка Аршан 28 июня 2014 года: причины и последствия» (к.г.-м.н. А.В. Кадетова).

Тематический обзор конференции. Секция

конференции «Общая геология, тектоника, осадочная геология и палеонтология» открылась пленарным докладом директора ИЗК СО РАН, д.г.-м.н. Д.П. Гладкочуба о роли Сибирского кратона в структуре суперконтинентов докембрия. После пленарного доклада последовали выступления молодых ученых, в которых рассматривались вопросы развития отдельных тектонических структур, часть докладов была посвящена исследованию вулканогенных и вулканогенно-осадочных пород, стратиграфии и вопросам возраста терригенных отложений. Были представлены результаты применения магнитной градиентометрии при поисках золоторудных месторождений, рассматривались вопросы рациональной разработки месторождений нефти.

Секцию конференции «Геохимия, петрология, минералогия и рудообразование» открыл пленарный доклад д.г.-м.н. А.В. Иванова «Датирование цирконов U-Pb методом: TIMS, SIMS, LA-ICPMS и другие (не)понятные вещи». На секции обсуждались вопросы датирования пород различными методами, рассматривались геохимические особенности бурых суглинков и погребенных почв Приморского края и особенности состава минералов Катунинского редкометалльного и Шерловогорского олово-полиметаллического месторождений. Прозвучали доклады о результатах исследования влияния флюидного режима на мобилизацию элементов в гранитной системе и термодинамического моделирования взаимодействия толеит-базальтовой магмы с карбонатно-эвапоритовыми отложениями чехла Сибирской платформы. Были представлены исследования минералого-петрографических особенностей УНР гранатитов Кокчетавского



Рис. 4. Регистрация участников конференции.

Fig. 4. Registration of the conference participants.



Рис. 5. Открытие конференции: приветственное слово председателя Оргкомитета – члена-корреспондента РАН Е.В. Склярова.

Fig. 5. The conference opening meeting. Welcome speech by E.V. Sklyarov, Corresponding Member of RAS, Organizing Committee Chairman.

массива (Казахстан) и щелочных гранитоидов Шербахтинского массива (Западное Забайкалье). Часть докладов имела экологическую направленность и касалась вопросов исследования загрязнения ртутью снежного покрова и определения корреляционных взаимоотношений элементов в потоке рассеяния хвостохранилища, а также оценки влияния верховых пожаров на изменение геохимического фона в почвенно-растительном покрове и влияния форм нахождения химических элементов в почвах на их бионакопление.

В рамках секции «Тектонофизика, современная геодинамика, неотектоника и геоморфология» прозвучало три пленарных доклада: «О природе первичной разномасштабной делимости формирующейся и современной литосферы Земли» (д.г.-м.н.



Рис. 6. На заседании.

Fig. 6. Meeting during the conference.

С.И. Шерман), «Палеосейсмогеология Сибири: методы, опыт практического применения, перспективы и реальность» (д.г.-м.н. В.С. Имаев) и «Позднеплейстоценовое оледенение Восточного Саяна» (к.г.-м.н. С.Г. Аржанников). В докладах молодых ученых был представлен широкий спектр проблем современной геодинамики и тектонофизики – от вопросов физического и оптического моделирования и построения расчетных моделей локализации опасных геологических процессов при сильных землетрясениях до реконструкции полей тектонических напряжений структурными методами, дешифрирования космических снимков и возможностей сейсмодеформационного мониторинга. Были озвучены результаты разработки базы данных



Рис. 7. Общение коллег в неформальной обстановке.

Fig. 7. Informal communication of colleagues.



следований затухания сейсмических волн и глубинного строения Байкальского рифта и Центральной Азии.

Секция «Гидрогеология, инженерная геология и нефтегенез» была разделена на два заседания. Утреннее заседание, посвященное вопросам гидрогеологии и инженерной геологии, открылось пленарным докладом к.г.-м.н. Е.А. Козыревой «Трансформация геологической среды Сибирского региона (инженерно-геологический аспект)». Сообщения молодых ученых были посвящены моделированию физико-химических процессов в термальных источниках, оценке роли геолого-структурных условий в формировании месторождений подземных вод, исследованию соленых озер Забайкалья, а также вариациям концентраций радона в подземных водах и их связи с подготовкой и реализацией



Рис. 8, а, б. Рабочие моменты конференции: гидрогеологическая экскурсия «Аршан-Тункинское месторождение углекислых минеральнолечебных вод» (к.г.-м.н. Ю.И. Кустов).

Fig. 8, a, б. The hydrogeological excursion to the Arshan-Tunka carbonate mineral water deposit (Yu.I. Kustov, PhD).

сейсмогенных источников юга Восточной Сибири и пакета ГИС-программ для оценки пространственно-временных закономерностей проявления сейсмичности.

Секция «Геофизика, геофизические методы исследований и геоинформатика» открылась пленарным докладом д.г.-м.н. В.И. Мельниковой, посвященным проблемам очаговой сейсмологии. Доклады молодых ученых касались вопросов малоглубинной геофизики, сейсмического районирования, а также «очистки» каталога региональных землетрясений Прибайкалья от роев и афтершоков. В ряде сообщений прозвучали результаты ис-

Рис. 9. Рабочие моменты конференции: инженерно-геологическая экскурсия «Селевые потоки в окрестностях поселка Аршан 28 июня 2014 года: причины и последствия» (к.г.-м.н. А.В. Кадетова).

Fig. 9. The engineering geological excursion. Subject: Mudflows of 28 June 2014 in the vicinity of the Arshan settlement. Causes and consequences (A.V. Kadetova, PhD).

землетрясений. Кроме того, часть докладов касалась мониторинга термодинамического состояния грунтов, исследования физико-механических свойств протерозойских песчаников и химического состава снежного покрова и его связи с лесными пожарами.

Вечернее заседание секции, посвященное вопросам гидрогеологии и нефтидогенеза, началось с пленарного доклада д.г.-м.н. А.Г. Вахромеева о геологическом строении природного резервуара карбонатного рифея на Юрубчено-Тохомском НГКМ. В секционных сообщениях обсуждались вопросы уточнения геологического строения нефтяных месторождений, оценки фильтрационно-емкостных свойств нефтяных пластов, а также методы увеличения нефтеотдачи на месторождениях. Часть докладов касалась проблем гидрогеологии, в них рассматривалась систематизация источников подземных вод по содержанию радона, особенности взаимодействия техногенных вод и рассолов на месторождениях нефти и газа, а также приводились результаты анализа распределения изотопов хлора в соленых водах и рассолах Западной Якутии.

Всего по данным Оргкомитета в рамках конференции молодыми учеными было представлено **55** устных и **27** стендовых докладов.

На общей заключительной дискуссии XXVI Всероссийской молодежной конференции «Строение литосферы и геодинамика» прозвучали выступления председателя Оргкомитета, члена-корреспондента РАН Е.В. Склярова (ИЗК СО РАН), директора

ИЗК СО РАН д.г.-м.н. Д.П. Гладкочуба, зам. директора ИЗК СО РАН д.г.-м.н. К.Г. Леви, к.г.-м.н. Е.А. Козыревой (ИЗК СО РАН), к.г.-м.н. А.М. Кононова (ИЗК СО РАН), С.В. Межеловской (МГРИ-РГГРУ, г. Москва), Ю.С. Восель (ИГМ СО РАН, г. Новосибирск), д.г.-м.н. А.В. Иванова (ИЗК СО РАН) и д.г.-м.н. А.Г. Вахромеева (ИЗК СО РАН). В выступлениях старших коллег отмечался высокий научный уровень докладов молодых ученых, их хорошая подготовленность и знание вопроса. Подчеркивалась полезность конференции «Строение литосферы и геодинамика» для молодых ученых в плане представления полученных результатов, обмена мнениями и завязывания научных контактов, а также тренинга. Общей рекомендацией заседания было продолжать в дальнейшем собрания традиционной Всероссийской молодежной конференции «Строение литосферы и геодинамика».

В заключение Оргкомитет XXVI Всероссийской молодежной конференции «Строение литосферы и геодинамика» выражает благодарность всем ее участникам за активную работу, дирекции ИЗК СО РАН и Российскому фонду фундаментальных исследований – за оказанную финансовую поддержку (проект № 15-35-10075_мол-г), а также М.М. Кайсарову, зав. отделом по делам ГО и ЧС Слюдянского района, за помощь в организации геологической экскурсии на карьер «Перевал» и В.И. Сонголову, руководителю курорта «Аршан», за помощь в организации экскурсии в Тункинскую долину.



Скляров Евгений Викторович, член-корреспондент РАН, докт. геол.-мин. наук, профессор, г.н.с.
Институт земной коры СО РАН
664033, Иркутск, ул. Лермонтова, 128, Россия
Тел.: 8(3952)511665; ✉ e-mail: skl@crust.irk.ru

Sklyarov, Eugene V., Corresponding Member of RAS, Doctor of Geology and Mineralogy, Professor, Chief Researcher
Institute of the Earth's Crust, Siberian Branch of RAS
128 Lermontov street, Irkutsk 664033, Russia
Tel.: 8(3952)511665; ✉ e-mail: skl@crust.irk.ru



Добрынина Анна Александровна, канд. физ.-мат. наук, н.с.
Институт земной коры СО РАН
664033, Иркутск, ул. Лермонтова, 128, Россия
e-mail: dobrynina@crust.irk.ru

Dobrynina, Anna A., Candidate of Physics and Mathematics, Researcher
Institute of the Earth's Crust, Siberian Branch of RAS
128 Lermontov street, Irkutsk 664033, Russia
e-mail: dobrynina@crust.irk.ru



Кононов Александр Матвеевич, канд. геол.-мин. наук, заместитель директора по науке
Институт земной коры СО РАН
664033, Иркутск, ул. Лермонтова, 128, Россия
e-mail: kononov@crust.irk.ru

Kononov, Alexander M., Candidate of Geology and Mineralogy, Deputy Director
Institute of the Earth's Crust, Siberian Branch of RAS
128 Lermontov street, Irkutsk 664033, Russia
e-mail: kononov@crust.irk.ru